Appendices to AFCEE Source Zone Initiative

Final Report

CONTENTS

APPENDIX A
COLORADO STATE UNIVERSITY
LABORATORY EXPERIMENTS

APPENDIX A

INTRODUCTION

In the first year of the AFCEE Source Zone Initiative project, Colorado State University (CSU) undertook the task of performing small-scale tank experiments to test the hypotheses put forth in Section 2 of this report. The small scale allowed for greater flexibility in repeating the experiments, if needed, as well as control of more of the variables in the experiment. These variables included the contaminant used as well as the use of control tanks to eliminate many of the unknown variables.

In the second year of the AFCEE Source Zone Initiative project, CSU conducted small-scale laboratory experiments to evaluate the effects of heterogeneities on the transport of groundwater contaminants. The two main effects evaluated were (1) the effect of low transmissivity media as a contaminant sink when a primary contaminant source such as a NAPL pool is present (and later, as a source once the primary contaminant source is depleted), and (2) the geometry of such low transmissivity media. Although other sections of this work deal with similar phenomena, the small scale of the experiments described in this section allowed the study of a larger number of variables in the experimental design.

Experiments were run simultaneously on a set of six stainless steel and glass tanks filled with different porous media and fed with water containing groundwater contaminants. Combinations of sand and silt were used as the porous media, being materials representative of high and low hydraulic transmissivity media. The porous media was arranged in two main geometric configurations: one with a single high-low transmissivity interface, the second with a multiple layer configuration. Additionally, these configurations were compared to a sand-only scenario representative of homogeneous porous media. The contaminants tested as representative of relevant groundwater contaminant were MTBE, PCE, and TCE. In addition to the contaminant, the

water included bromide as a conservative tracer. The aqueous tank effluent was analyzed for the organic contaminants and bromide.

OBJECTIVES

The objectives of the first reporting period experiments include the following:

- Study the effect of the silt layer on the discharge of contaminant from the tanks.
- Evaluate how organic carbon-partitioning coefficients affect discharge of contaminant from the tanks.
- Validate theoretical models proposed by Dr. Dandy and to quantitatively measure the extent of mass storage in stagnant zones.

The general objective of the second reporting period small-scale laboratory experiments was to evaluate the effects of low permeability porous media on the transport of groundwater contaminants through high permeability media. In addition to advection through high conductivity media (a reasonably well understood process), diffusion of contaminants into low conductivity media can be a significant transport process. The following are thought to be the main variables controlling the diffusion of contaminants into such non-conductive heterogeneities:

(1) The nature of the chemical interaction of contaminants and the media (which determines the contaminant sorption into the media, and other contaminant-media interactions, such as degradation reactions), and

(2) The geometry of the heterogeneous media (i.e., the interfacial area between both types of media and the geometry of such interface).

These processes were experimentally evaluated according to the following specific objectives:

- Evaluate contaminant transport for different contaminants (with a range of transport properties) in a tank configuration with a single high transmissivity and low transmissivity interface during continuous (flow-through) experiments.

- Evaluate contaminant transport for different contaminants in a tank configuration with multiple high transmissivity and low transmissivity interfaces, using continuous (flow-through) experiments.

- Evaluate contaminant transport for different contaminants in a multiple layer configuration using modified low transmissivity media with different transport properties (sorption coefficient and higher reactivity) using continuous (flow-through) experiments.

METHODS

A.1.1 Experimental Setup

For the first reporting period, six identical tanks were constructed as detailed in Section A-4. Three of these tanks would contain a layered system of 60 percent sand and 40 percent silt; the other three would contain only sand. Each pair of sand and sand-silt tanks would contain an identical volume of perchloroethylene (PCE, a DNAPL), trichloroethylene (TCE, a DNAPL), or methyl-tertbutyl ether (MTBE, an LNAPL).

The NAPL sources were placed identically in the tanks. The water velocity through the transmissive zones would be identical (or as close as feasible) in all six tanks. Samples of the tank effluent were then taken at regular intervals. Comparisons of concentrations versus time would then be made between the sand-only tank and the sand-silt tank for each of the three contaminants. Any discrepancy could then be attributed to the presence of the silt layer.

A.1.2 Tank design, first reporting period

The tanks were designed to have an internal chamber of dimensions 100 x 50 x 2.5 cm. The internal volume is stainless steel on three sides (100 x 50 cm back and 2.5 x 50 cm top and bottom), glass on one side (100 x 50 cm front) and chemically resistant rubber on two sides (2.5 x 100 sides) as shown in Figure A-1.

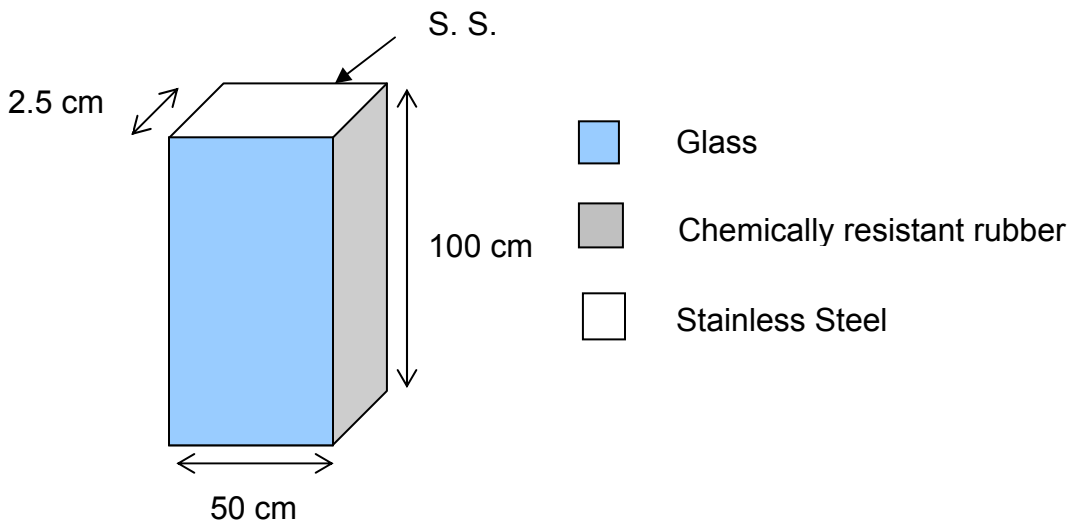

Figure A-1. Tank Dimensions and Materials.

As shown, the left and right sides of the tanks are symmetrical, as are the tops and bottoms. The tanks also contain a 2.5 cm headspace at the top and bottom. A stainless steel screen assembly protects these.

The tank frame is waterproofed using high vacuum silicone grease in combination with the chemically resistant rubber gasket surrounding the four smallest sides. The water inlet is made of standard neoprene tubing and the tank effluent is made entirely from stainless steel, glass, or Viton tubing to mitigate any adsorptive losses.

A.1.3 Tank Loading

The tanks were loaded with soil from the side in a three-person operation. One person tapped on the side of the tank approximately three times a second. The second person moved a “rainer” (a funnel with a 12 in. long x 2 in. diameter spout) across the open side of the tank. The rainer was used to ensure the soil was deposited at a nearly constant, terminal velocity. The third person fed the sand or silt into the rainer.

The sand-silt tanks were filled sand-side-first. The silt was added on top of the sand. This method allowed a thin sand barrier at the top and bottom of the tank to keep the silt from passing through the screen. Simple plastic mini-blind slats were used to separate the sand barrier from the silt as each side was filled. A diagram of the san-silt layout follows in Figure A-2.

Figure A-2. Sand-Silt Layout in the Tanks.

A.1.4 Water Flow

The tanks were run for two weeks to ensure any settling was complete before the experiment was initiated. The tank design allowed the introduction of NAPL into the tank approximately 10 cm from the bottom. Water was then forced up the column for the remainder of the experiment. Flow was drawn from 20 L glass carboys filled with de-aired tap water.

Tank effluent flow was split at the top to allow for collection of the waste product as well as periodic sampling. The sampling port was located immediately at the top of the tank through a glass “Y,” and remaining effluent was channeled through high-density polyethylene (HDPE) tubing to separate glass carboys.

A.1.5 Flow Rate

To accommodate the comparison between laboratory experiments and field data without compromising operational flexibility, a flow rate of 1 m/day was chosen. This rate is slightly faster than those typically seen in the field, but allows a reasonable amount of NAPL to be dissolved in a short time frame. It also means that the tanks are run at a rate of one pore volume per day, simplifying the data analysis. Given a porosity of 0.35 and flow areas of 2.5 x 50 cm for the sand-only tanks and 2.5 x 20 cm for the sand-silt tanks, volumetric flow rates of 3 mL/min and 1.2 mL/min, respectively, were achieved.

A.1.6 NAPL Introduction

To ensure that the NAPL did not migrate on its own, a coarse gravel inclusion was added to the sand layer (at the sand-silt interface for those tanks), which created a capillary barrier for the NAPL when it reached the much finer sand (finer than the gravel). The inclusion was approximately 1 cm in diameter and extended the full 2.5 cm depth of the tank. To this inclusion, 2 mL of NAPL (TCE, PCE, or MTBE) was added to each tank. The NAPL was added through the use of a long syringe that was pushed through a Teflon/foam rubber septa. The plunger was held in place and the syringe drawn back out of the tank to assist a uniform loading across the 2.5 cm depth.

A.1.7 De-airing procedure

To provide enough water for the duration of the experiment, it was necessary to periodically refill the carboys. Cold tap water was used to minimize the effect of dissolved solids and biological organisms. (Tap water has the advantage of being filtered and treated with biocides.) Once the carboys were refilled, a nearly 1 atm vacuum was drawn on them for approximately 4 hours. The vacuum then removed any chlorine.

A.1.8 Sampling

Samples were taken at regular intervals, with the rates being adjusted to reflect the solubility of the contaminant in each tank. MTBE is soluble to ~45,000 mg/L and the 2 mL source is very short lived. For this experiment, samples were taken every 2 hours for the duration of the two-week experiment. TCE and PCE are only soluble to ~1100 and 250 mg/L, respectively. As these sources would therefore last for weeks, sampling was performed approximately every other day for the duration of these 3-month experiments.

The tank sampling involved first drawing 2 mL to evacuate any stagnant water in the lines. A 4.5 mL sample was then taken and added to a 4.5 mL glass vial (no air above the sample) topped with a Teflon septa and capped. The sample was then labeled and refrigerated until it could be analyzed.

The following section describes the laboratory setup used for these studies conducted in the second reporting period, including the procedures used to fill the tanks with porous media and the hardware used to operate them.

A.1.9 Tank design, second reporting period

The tanks used for flow-through experiments were designed to have an internal chamber of dimensions 100 x 50 x 2.5 cm. The internal volume is confined by stainless steel on three sides (100 x 50 cm back, and 2.5 x 50 cm top and bottom), glass on one side (100 x 50 cm front) and chemically resistant rubber on two sides (2.5 x 100 sides) as shown in Figure A-3. The left and right side are symmetrical, as are the top and bottom, as indicated on the figure. The tanks also contain a 2.5 cm headspace at the top and bottom, made of stainless steel screen, to keep the porous media from clogging the influent and effluent ports.

The tank frame was waterproofed using high vacuum silicone grease in combination with the chemically resistant rubber gasket surrounding the stainless steel top, bottom, and sides. The water inlet and outlet were made of stainless steel, connected with viton fittings to glass tubing to mitigate any adsorptive

losses. Manometers were attached to both inlet and effluent ports. These allowed verification of saturated conditions within the tanks and identification of plugged lines or other flow irregularities.

All tubing and tubing fittings in contact with organic-contaminated water were made of either glass or viton. The pumps used for the feed were high precision Ismatec peristaltic pumps, used in combination with three stop high precision viton tubing (Cole-Parmer).

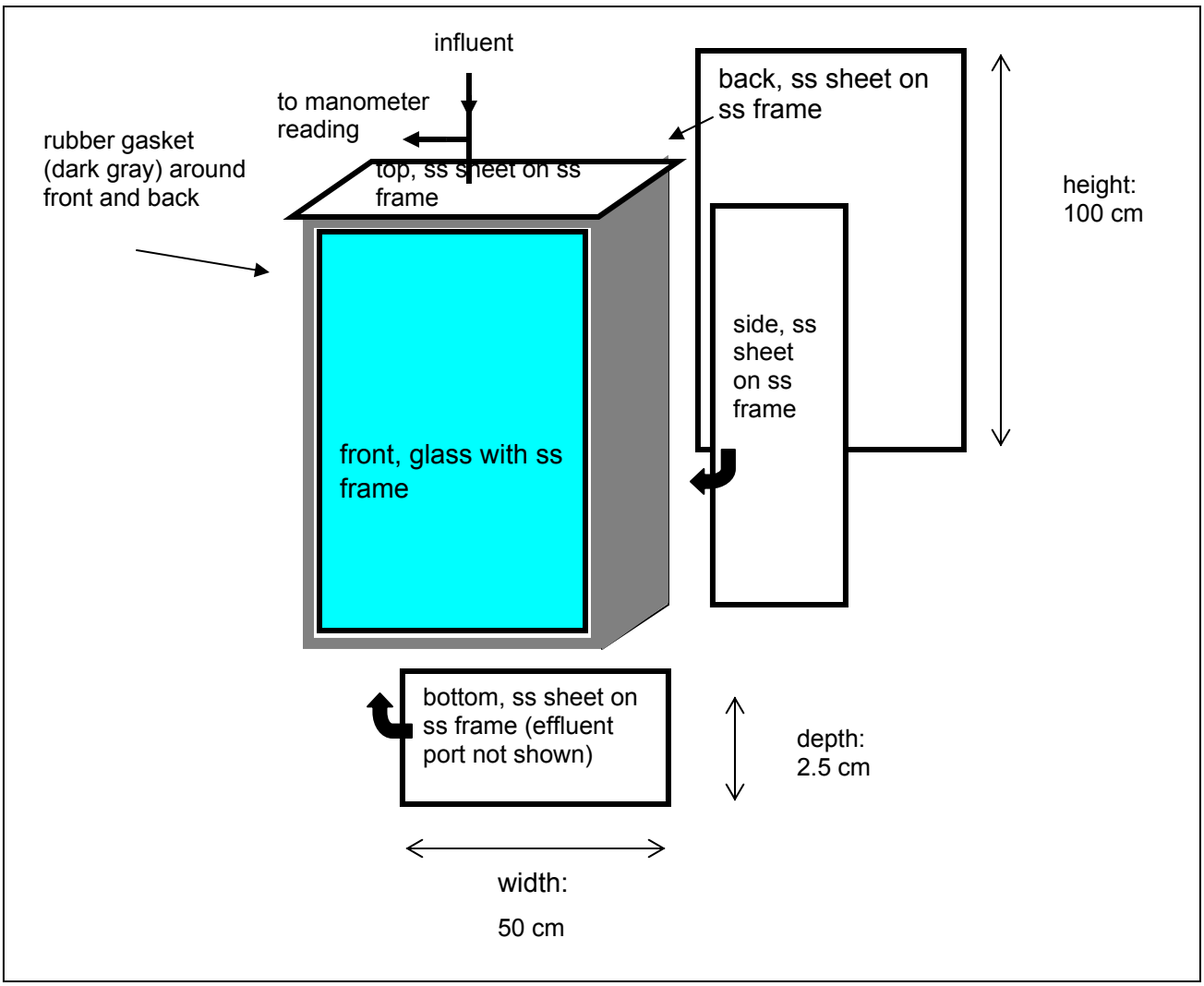

Figure A-3. Schematic diagram of tank construction. Effluent port on bottom and stainless steel left side not shown. Tank top shown attached. Glass shown in blue, stainless steel (ss) shown in white with black borders, and rubber gasket shown in dark grey. Tank Loading with Porous Media

The material used for filling the tanks was either sand or silt, according to Section A.1.12, Experimental Design. Preparation of each material is described in more detail in Section A.1.10, Materials. These porous materials were weighed before and after filling the tanks, to provide estimates of the mass loading of each type of porous media. These measurements, together with the volume of the tanks, were used to obtain porosity and bulk density of both types of porous media used.

The material was loaded with the use of a 20 in. long tube with a funnel at the end (a “rainer”), in order to add all material at terminal falling velocity. The tanks were loaded with porous media from the side in a two- or three-person operation. One person tapped on the side of the tank approximately three times a second. The second person moved the rainer across the open side of the tank. The third person fed the porous media into the rainer.

Once a tank was filled with porous media, the side was attached, and the tank was slowly filled up with degassed water, flowing upwards. The flow was reversed (downwards), to avoid potential pressure buildup within the tank due to accumulation of gas bubbles around the inlet or outlet ports, once no residual gasses were seen within the pores of the media from the glass front. The tank effluents were discharged at a higher elevation than that of the top of the tank to avoid operation under vacuum and suction of atmospheric air into the tanks.

A.1.9.1 Flow Rate

Although flow rates for tank operation were intended to mimic field conditions (with typical linear velocities around 1 ft/day), they were also limited by the capacity of the peristaltic pumps. Thus, all flow rates used in these experiments resulted in linear groundwater velocities in the range of 1 ft/day. These flow rates were initially prescribed according to the peristaltic pump calibration curve, and then measured at different times throughout the experiment.

A.1.10 Materials

This section describes the substances used in these experiments. This includes chemicals used as model groundwater contaminants, conservative tracer (bromide), porous media to fill the tanks, and the water used to simulate contaminated groundwater.

A.1.10.1 Porous Media

Porous media was obtained from the F.E Warren site. A complete description of this material and its preparation is included in Appendix F, Field Soils Characterization. Two fractions of this material, separated by sieving, were used in these experiments: sand with particle size > 450 μm, and silt with particle size < 250 μm.

A.1.10.2 Chemicals

PCE and TCE used as chlorinated organic volatile organic (CVOC) groundwater contaminants were ACS grade (99% pure), obtained from Acros (PCE) and Fisher Scientific (TCE). Methyl tertbutyl ether (MTBE), used either as a model groundwater contaminant or in the extractions of CVOCs, was analytical grade (Omni-Solve EMD). Sodium bromide (Fisher Scientific, 99% pure), used as a conservative tracer, was injected in solution with the CVOCs contaminated water.

A.1.10.3 Water Preparation

The water used as groundwater for tank feed was stored in 20-L glass carboys, which were filled up with hot tap water and subjected to a vacuum (25 psi) for at least 2 hours; this depleted both dissolved gasses and chlorine present in drinking water. The water was then left to cool to room temperature before being used as tank feed. It was necessary to periodically refill the carboys in order to provide enough water for the duration of the experiment.

A.1.11 Analytical Methods

The following section describes the methods used for the first reporting period.

A.1.11.1 Sample Preparation

Each sample is taken from the port at the top of the tank. A 4-mL glass vial is filled to capacity to eliminate any air bubbles. The vial is then capped with a Teflon coated foam rubber septa, labeled, and refrigerated. Less than two weeks

later, the sample is removed from the refrigerator. One-mL gas chromatogram (GC) vials are prepared with 4 mm of sodium sulfate crystals and labeled. The sodium sulfate is present in excess, guaranteeing that the ionization in the water is constant. One mL of each sample is added to the GC vials. Then, a standard quantity of a previously prepared internal standard solution of 1,1,1-TCA is added to the vial, which is then immediately capped and shaken for 30 seconds. This procedure is repeated for each of the samples taken from one column.

A.1.11.2 Standards

Sixteen standards are prepared for each run: two each of four concentrations spanning the upper range of concentrations (ppm range) and two each of four concentrations spanning the lower range (ppb range). For TCE, the four concentrations in the upper range are 100, 67, 33, and 1 ppm, and the four concentrations for the lower range are 1000, 667, 333, and 10 ppb. For PCE, the values are exactly half of those of TCE. For MTBE, the upper range concentrations are 5000, 1875, 703, 264, 99, 37, 14, 5 ppm; the lower range values are 1/1000th of those. The vials are then run on an Agilent series 1575 gas chromatogram with mass spectrometer.

A.1.11.3 Gas Chromatograph Setup

The first step in the setup is to purge the machine of any previous contamination. This is accomplished using a cleaning method that was developed to bake off any chemical species still present from the previous run. Next, a blank air sample is run as a baseline. The next samples run are the first set of higher concentration standards, which calibrates the machine and insures that the column is not overwhelmed. Once the standards are finished, another air sample is run. Next, all of the samples from the columns are run, with an air purge performed after every tenth sample to keep any carryover or buildup to a minimum. Finally, the second set of high concentration standards is run.

Once the sample runs have been completed, the data is analyzed. Any sample whose concentration was too low to be detected is run a second time with the machine set to a more sensitive configuration. (The same procedure is then repeated, but only for those samples and lower concentration standards.)

A.1.11.4 Data Analysis

Two peaks are detected for each sample. One of the peaks is the internal standard (1,1,1-TCA); the other is the contaminant for that particular column. It is then assumed that the internal standard should be the same for each sample. An average of the readings is taken and each sample is adjusted to that average (i.e., if the standard signal is twice the average, then the contaminant signal is divided in half).

The following sections describe the methods used for the second reporting period.

A.1.11.5 Sampling

Samples were taken from the tank effluent by a custom made flow-through zero-head-space vial cap and a 15 mL glass vial. The vials were detached from the vial cap, capped with aluminum crimp tops and Teflon-lined septa, and kept in refrigeration at 4 °C until being opened for analysis. Sampling was done daily, with few exceptions.

A.1.11.6 Organic Analysis

Chlorinated Volatile Organic Compounds (CVOCs) Analysis

The sample vials were kept in refrigeration at 4 °C until they were opened and immediately extracted with MTBE (a 1:1 volume ratio) for at least 2 minutes before separation and further injection into a GC, in accordance with EPA method 551.1 (US EPA, 1995). MTBE extractions were performed within the 2-week recommended holding time for CVOC analysis. The GC was an HP

6890, equipped with an electron capture detector (ECD) with a Ni^{63} ionization source, using a J&W Scientific DB-624 capillary column. The injector and detector temperatures were set at 250 and 300 °C, respectively, while the GC oven program consisted of an injection temperature of 40 °C, followed by a temperature ramp of 8 °C/min to a temperature of 90 °C, and then a temperature ramp of 40 °C/min to a final temperature of 185 °C (total run time of 8 min). Under these conditions, the retention times of PCE and TCE were 5.7 and 7.7 min, respectively. One MTBE blank was run for every 20 samples to evaluate potential contamination of the extraction solvent or the GC. Calibration curves for comparison of the unknown samples were run in the concentration range of 10 to 500 μg/L for both PCE and TCE, using at least six standards for each analyte. These calibration curves were linear throughout the entire concentration range. Samples with a signal outside of the linear range were run at a different dilution that resulted in a signal within the linear range.

MTBE Analysis

MTBE analysis was performed by means of purge and trap concentration of an aliquot of the aqueous sample, combined with GC using a flame ionization detector (FID) which was based on the EPA Method 8015 and used a Tekmar 2016 autosampler and a Tekmar LSC2000 Controller. The sample was preheated at 60 °C for 2 min, purged for 7 min and desorbed at 250 °C for 0.5 min. The dry purge time was 3 min, and the desorb preheat was 245 °C. The GC program consisted of an injection temperature of 35 °C, followed by a temperature ramp of 10 °C/min to a temperature of 190 °C with a hold time of 5 min (total run time 22.5 min). Under these conditions, the retention time of MTBE was 6.1 min.

Bromide Analysis

Bromide analysis was performed on the samples after the sample vials were opened and an aliquot was taken for CVOC analysis. A volume of 10 mL was drawn, adjusted for ionic strength (using 200 µL of Thermo Orion Ionic Strength

Adjustor solution for 10 mL of sample) and the bromide concentration measured with an Ion Selective Probe (Accumet, Fisher Scientific No.13-620-521), calibrated daily against standards. The reported detection limit of this analysis is 0.04 ppm.

A.1.12 Experimental Design

Two sets of experiments were run. In the first set, there was a single layer of sand (high hydraulic transmissivity porous media) and a single layer or silt (low hydraulic transmissivity porous media). For the second set of experiments, a multiple layer configuration of sand and silt was used. This section describes the experimental variables that were studied for each set of experiments, as well as particular laboratory setup requirements for each of them.

A.1.12.1 Single Layer Experiments

The purpose of these experiments was to study the simplest case of porous media heterogeneity, with one layer of high transmissivity media (sand) in contact with one layer of low transmissivity media (silt) through a single flat interface. These experiments were compared to controls including sand only as the porous media.

The contaminated groundwater feed (containing one of the CVOCs and the conservative tracer bromide) to these tanks was introduced at the interface of both porous media close to the top of the tanks (simulating a NAPL source) by means of a glass frit tube fed through a port on the stainless steel back of the tanks. The contaminated water was pumped from Tedlar gas sampling bags, representing approximately 5 percent of the total feed to the tanks. The bulk of the groundwater (uncontaminated) was introduced from the top of the tanks.

Three tanks contained two media (sand and silt, with sand filling 60 percent of the tank width and silt filling up the remainder). The other three tanks were filled up with sand only, serving as controls to allow independent evaluation of the transport processes occurring at the sand only. Each tank within a pair of sand

and sand-silt tanks (for example, Tanks 1a and 4a) was fed with the same contaminated water solution. The resulting setup for these two-layer experiments is presented in Table A-1. A diagram showing the sand and silt arrangement within each tank is shown in Figure A-4.

Table A-1. Experimental setup for the transport studies through one- and two-layer porous media. The number in the tank label is for the tank number, while the letter a indicates the first set of tank experiments.

Tank	Porous media: two-layer sand-silt	Tank	Porous media: sand only (control experiments)
1a	Contaminant: PCE	4a	Contaminant: PCE
2a	Contaminant: TCE	5a	Contaminant: TCE
3a	Contaminant: MTBE	6a	Contaminant: MTBE

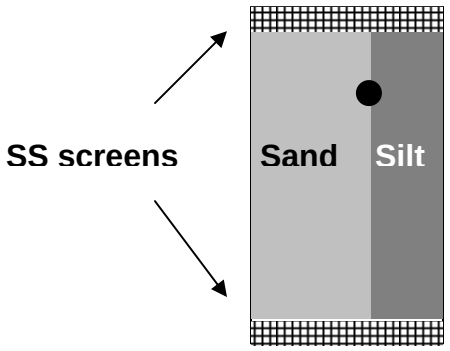

Figure A-4. Diagram of a front view of sand and silt arrangement within tanks during two-layer experiments. Light gray represents sand (30 cm thick) and dark gray represents silt (20 cm thick). Single layer experiments had an identical layout, except that silt was replaced with sand. The injection port for the contaminated groundwater is shown as a black circle. Not to scale.

A.1.12.2 Multi-Layer Experiments

The purpose of these experiments was to study a more complex geometry of porous media heterogeneity, with multiple layers of high transmissivity media (sand) alternating with multiple layers of low transmissivity media (silt).

For these experiments, five layers of sand (5 cm wide) were alternated with layers of silt of the same width. The sides of the tank were in contact with 2.5 cm wide layers of silt. The silt was used unmodified, but there were also additional treatments based on additions of 1% zero-valent iron (30 mesh, 0.589 mm) and ground/sieved (30 mesh, 0.589 mm) activated carbon to estimate the effects of reactive and highly sorptive low hydraulic transmissivity porous media, respectively. A single stream of contaminated groundwater (with bromide tracer) was fed from the top. The feed was prepared by pumping degassed water with bromide through a 22-L carboy with excess DNAPL, mixed with 200 mL/min recycling flow (using a peristaltic pump). The carboy with DNAPL was mixed for 1 week and then pumped to waste (at a flow rate equal to the groundwater flow to the tanks for one day) to avoid large feed concentration gradients due a

change in the hydrodynamic regime. The resulting setup for these multiple layer experiments is presented in Table A-2. A diagram with the layout of sand and silt layers is presented in Figure A-5.

Table A-2. Experimental setup for the multi-layer porous media experiments. The number in the tank label is for the tank number, while the letter b indicates the second set of tank experiments.

Tank	Contaminant: PCE	Tank	Contaminant: TCE
1b	Unmodified Silt	4b	Unmodified Silt
2b	Silt + 1% ZVI	5b	Silt + 1% ZVI
3b	Silt + 1% Activated Carbon	6b	Silt + 1% Activated Carbon

At the tested conditions, the feed flow rates for all experiments were in the range of 1-2 ft/day.

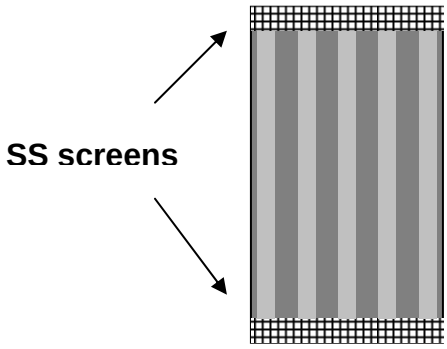

Figure A-5. Diagram of a front view of sand and silt arrangement within tanks during multiple layer experiments. Light gray represents sand (5 cm thick) and dark gray represents silt (5 cm thick, except at the sides of the tank, where it was 2.5 cm thick). Contaminated water was fed to the tanks through the top, at an injection port previous to the screen. Not to scale.

RESULTS

This section presents results from the experiments described in the preceding sections, in the form of organic contaminants and bromide concentrations in the tank effluent with respect to time, from the time the contaminated solution started being fed into each tank. Also, mass balances will be presented for each tank, for both the organic contaminant and the inorganic tracer. These mass balances will consist of cumulative contaminant mass in, cumulative contaminant mass out, and the accumulated mass (the difference between mass in and mass out) with respect to time. Results from control experiments (one-layer experiments) will be presented first, followed by two-layer experiments.

A.1.13 One-layer experiments

Table A-3 presents the results of the porous media loading on the tanks.

Table A-3. Mass loading of porous media (sand and silt) into tanks. Bulk density and porosity were calculated based on these recorded mass and tank volumes. Mean and coefficient of variation (C.V.%) values are provided for tanks loaded in a similar way.

Tank	% width filled with sand	Mass loaded (lb)		Bulk Density		Porosity	
		Sand	Silt	Sand	Silt	Sand	Silt
1	41.4%	24.4	20.5	1.969841	1.17	0.26	0.56
2	40.4%	21.0	22.6	1.732953	1.27	0.35	0.52
3	42.4%	21.4	19.2	1.68734	1.12	0.36	0.58
Mean tanks 1-3		22.3	20.8	1.80	1.18	0.32	0.55
C.V.% tanks 1-3		8.4%	8.2%	8.4%	6.4%	17.8%	5.2%
4	100%	44.8	NA	1.511891	NA	0.429	NA
5	100%	46.6	NA	1.572809	NA	0.41	NA
6	100%	47.0	NA	1.588105	NA	0.40	NA
Mean tanks 4-6		46.1	NA	1.56	NA	0.41	NA
C.V.% tanks 4-6		2.6%	NA	2.6%	NA	3.7%	NA

The recorded masses of sand and silt for each tank were used to estimate the porosity and bulk density of the porous materials loaded into the tanks. These results were later used in combination with contaminant concentrations and measured flow rates to estimate the mass balances on each tank. The measured flow rates of each tank are presented in Table A-4, together with the resulting groundwater velocity and the contaminant and tracer concentrations on the feed to each tank.

Table A-4. Measured contaminated and non-contaminated flow rates and concentrations to each tank. Data represents results from 3 different measurements for each line, taken at different times during the operation of the different pumps. Averages shown before coefficient of variation (C.V.). Resulting groundwater velocities were estimated on the total flow (mean contaminant plus mean water lines within each tank) and the sand porosity, sand width (from Table A-3), and the tank dimensions.

Parameter		Tank 1a	Tank 2a	Tank 3a	Tank 4a	Tank 5a	Tank 6a
Contaminant Lines	Mean	0.043	0.044	0.056	0.047	0.050	0.067
	C.V. %	36%	24%	17%	12%	2%	18%
Water Lines	Mean	0.307	0.285	0.309	0.642	0.901	0.708
	C.V. %	3%	8%	3%	7%	1%	18%
Resulting groundwater velocity m/day (ft/day)		0.38	0.27	0.28	0.19	0.26	0.22
		1.23	0.88	0.90	0.61	0.87	0.73
Contaminant concentration (ppm)		90	594	44,880	Same as Tank 1a	Same as Tank 2a	Same as Tank 3a
Bromide concentration (ppm)		219	225	210			

A.1.13.1 One-Layer Experiments

Figures A-6a, A-6b, and A-6c show the concentrations of the organic contaminants (PCE, TCE, and MTBE) and the conservative tracer (bromide) in the effluent of Tanks 4a, 5a, and 6a, which were completely filled up with sand.

For all of these tanks, the contaminant source being fed from the side of the tank was turned off at day 25 after the experiment startup.

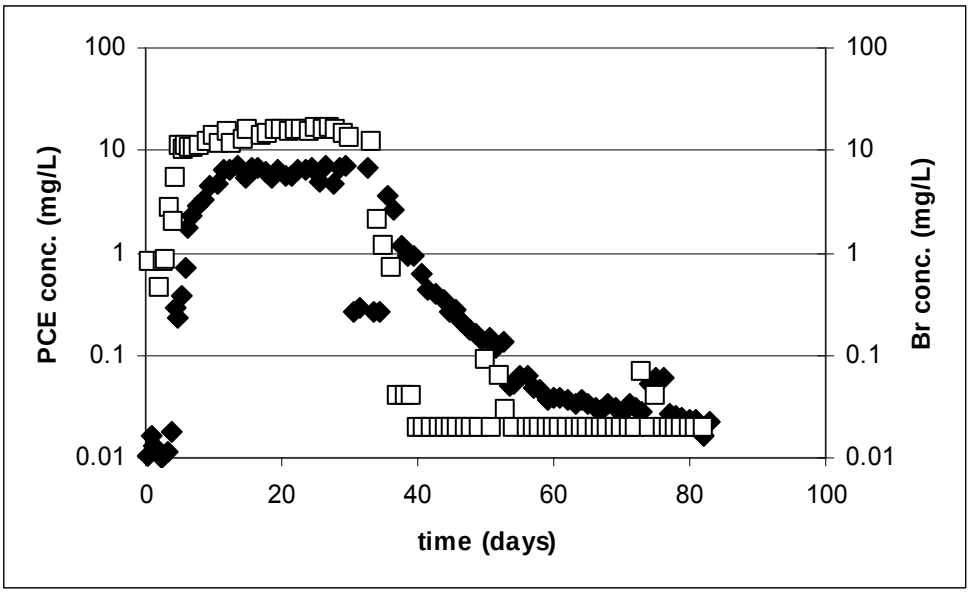

Figure A-6a. PCE (black diamonds) and bromide (open squares) concentrations in the effluent of Tank 3a. PCE contaminated water (including bromide) was fed from day 1 to day 25, after which water with neither contaminant nor bromide was fed to this tank until the end of the experiment.

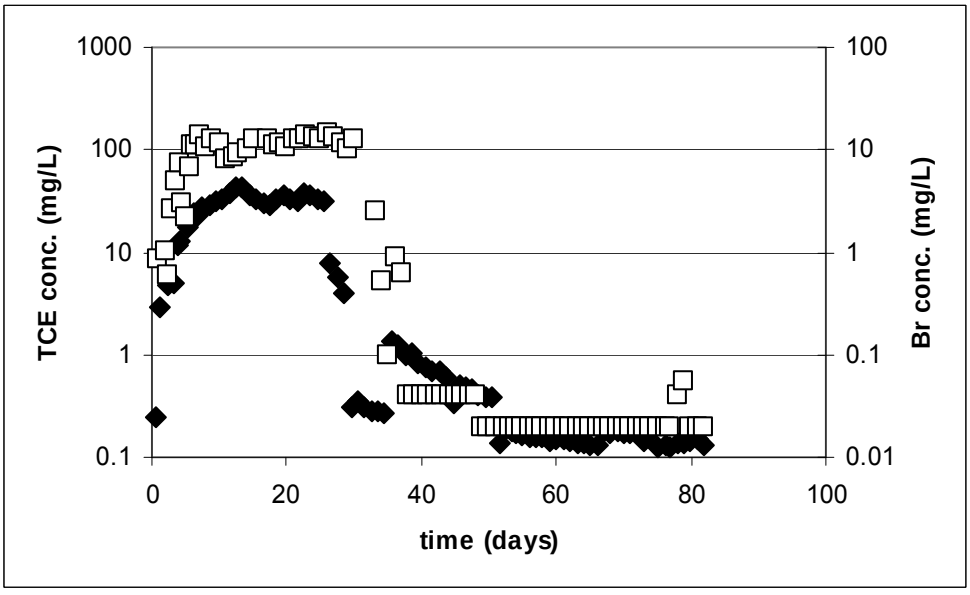

Figure A-6b. TCE (black diamonds) and bromide (open squares) concentrations in the effluent of Tank 5a. TCE contaminated water (including bromide) was fed from day 1 to day 25, after which water with neither contaminant nor bromide was fed to this tank until the end of the experiment.

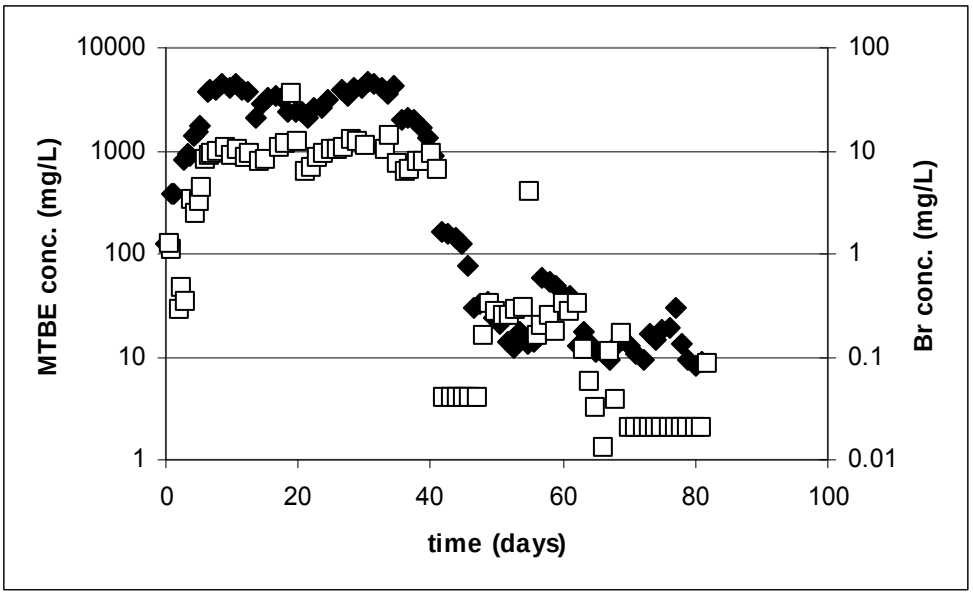

Figure A-6c. MTBE (black diamonds) and bromide (open squares) concentrations in the effluent of Tank 6a. MTBE contaminated water (including bromide) was fed from day 1 to day 25, after which water with neither contaminant nor bromide was fed to this tank until the end of the experiment.

Calculation of mass balances was based on the effluent concentrations (shown in Figures A-7a through A-7c), measured pumping rates for the groundwater feed lines and the combined contaminant/tracer, and contaminant and bromide concentrations in the contaminant feed (Table A-4). The cumulative contaminant (and tracer) mass in, out and accumulated were calculated as follows:

$$Mass_{in\ cumm,\,i} = Mass_{in\ cumm,\,i-1} + Conc_{in,\,i} * FR_{in,\,cont}$$

$$Mass_{out\ cumm,\,i} = Mass_{out\ cumm,\,i-1} + Conc_{out,\,i} * \left(FR_{in,\,cont} + FR_{in,\,groundwater}\right)$$

$$Mass_{accumulated,cumm,\,i} = Mass_{in\ cumm,\,i} - Mass_{out\ cumm,\,i}$$

in which *Mass*, *Conc*, and *FR* indicate contaminant mass, concentrations and feed flow rates, respectively. The subscript *cumm* is for cumulative mass up to a time *i*, the time period between discrete times *i* and *i-1* (when samples had been collected). The subscripts *in*, *out* and *accumulated* indicate mass (and flow rates)

into, out of, and accumulated within the tank respectively, while the subscript *cont* indicates the contaminant of interest (bromide or any of the three organics used). The subscript *groundwater* was used for the non-contaminated water flow rate.

The mass balances for the organic contaminant in one layer tanks experiments are presented in Figures A-8a, A-8b, and A-8c for the organic contaminants and Figures A-9a, A-9b, and A-9c for bromide.

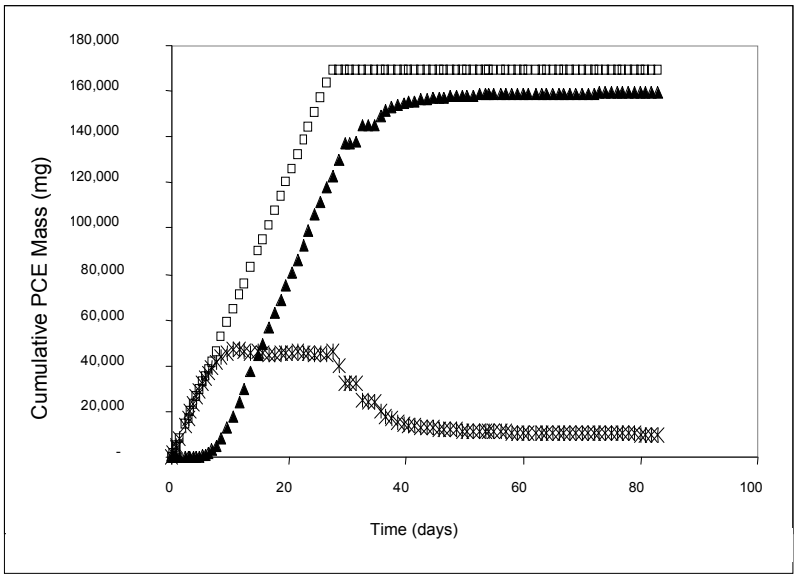

Figure A-7a. PCE mass balance for Tank 4a. Mass-in is shown as open squares, mass-out as black triangles, and the accumulation within the tank (the difference between mass-in and mass-out) as asterisks.

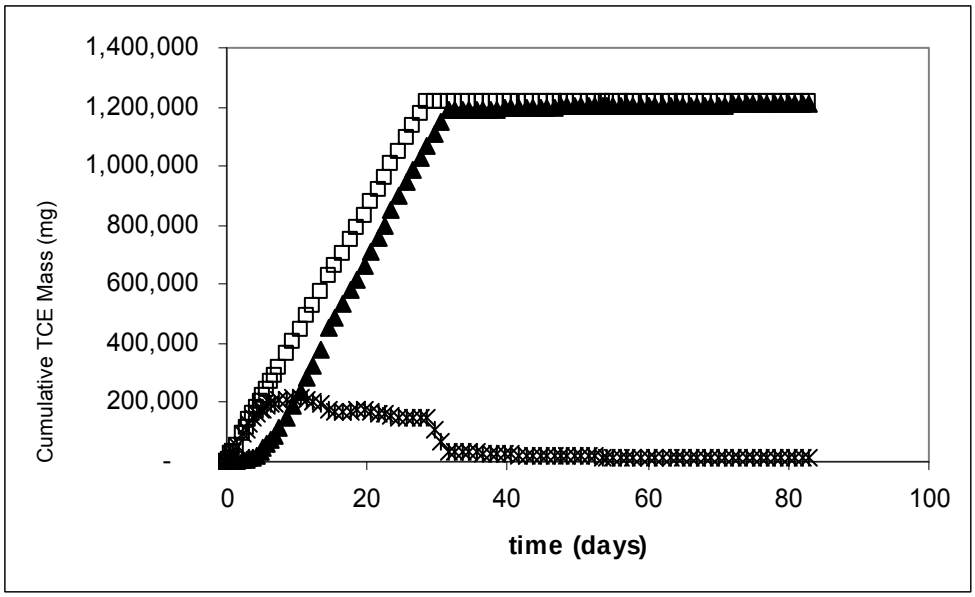

Figure A-7b. TCE mass balance for Tank 5a. Mass-in is shown as open squares, mass-out as black triangles, and the accumulation within the tank (the difference between mass-in and mass-out) as asterisks.

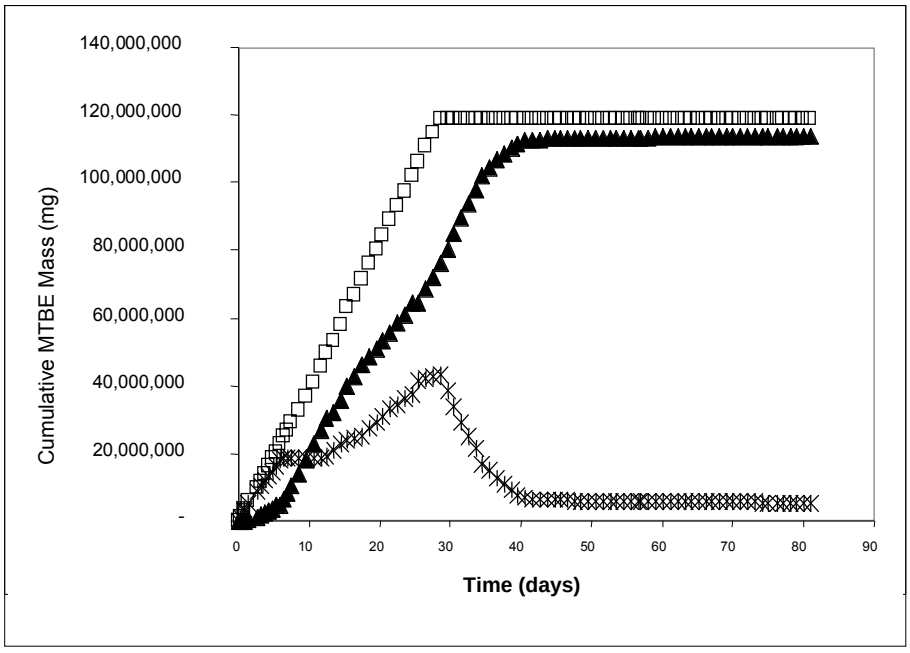

Figure A-7c. MTBE mass balance for Tank 6a. Mass-in is shown as open squares, mass-out as black triangles, and the accumulation within the tank (the difference between mass-in and mass-out) as asterisks.

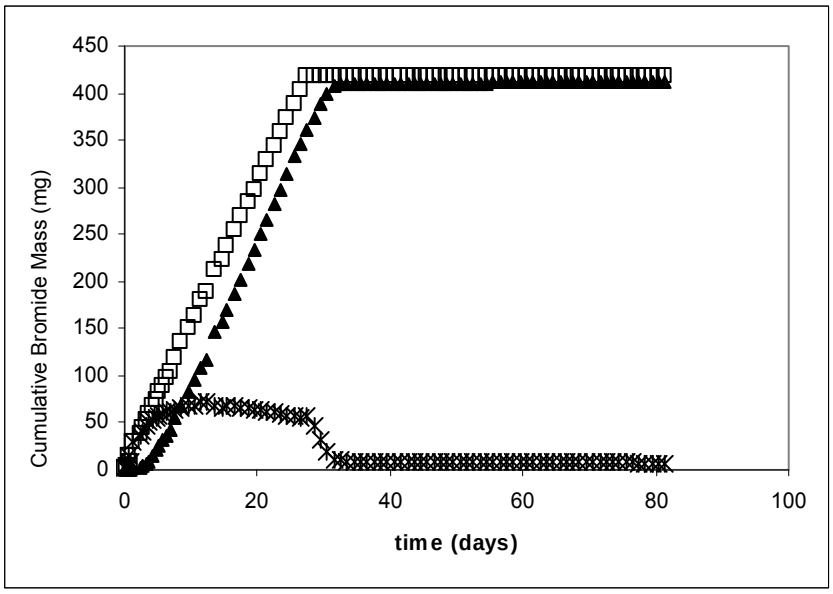

Figure A-8a. Bromide mass balance for Tank 4a. Mass-in is shown as open squares, mass-out as black triangles, and the accumulation within the tank (the difference between mass-in and mass-out) as asterisks.

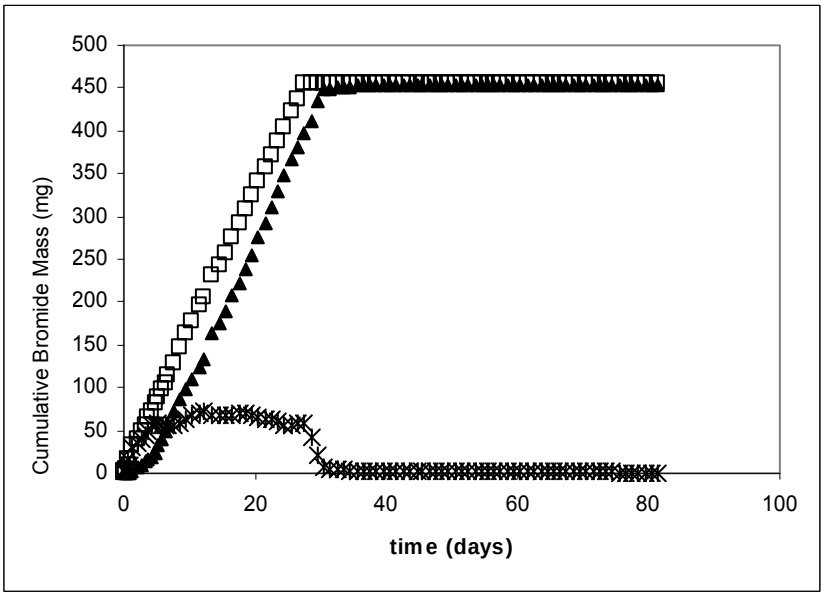

Figure A-8b. Bromide mass balance for Tank 5a. Mass-in is shown as open squares, mass-out as black triangles, and the accumulation within the tank (the difference between mass-in and mass-out) as asterisks.

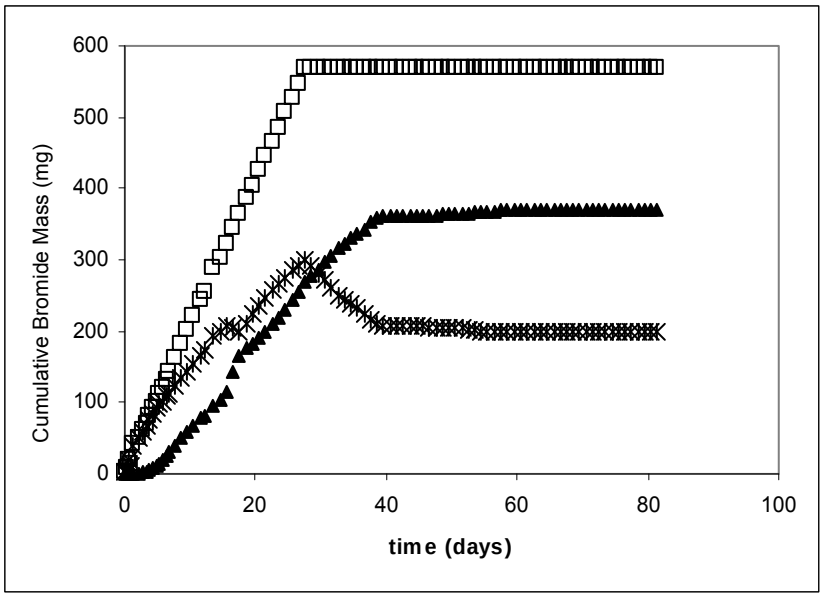

Figure A-8c. Bromide mass balance for Tank 6a. Mass-in is shown as open squares, mass-out as black triangles, and the accumulation within the tank (the difference between mass-in and mass-out) as asterisks.

A.1.13.2 Two-Layer Experiments

Figures A-10a, A-10b, and A-10c show the concentrations of organic contaminant PCE and the conservative tracer (bromide) in the effluent of Tanks 1a, 2a, and 3a. The contaminant source being fed from the side of Tanks 1a and 3a was turned off at day 25 after the experiment startup, while the source for Tank 2a was turned off at day 22 due to a contaminant feed pump failure.

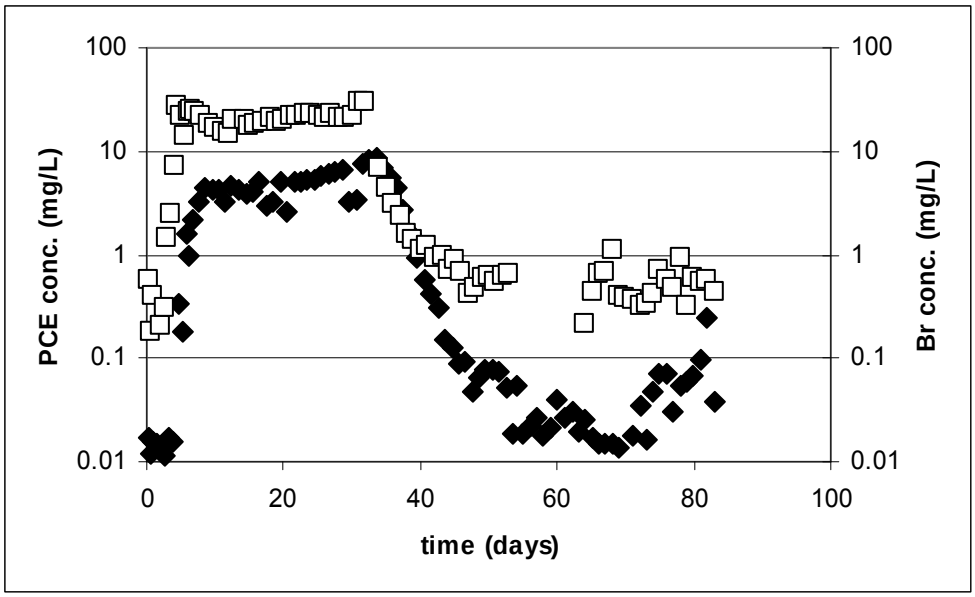

Figure A-9a. PCE (black diamonds) and bromide (open squares) concentrations in the effluent of tank 1a. PCE contaminated water (including bromide) was fed from day 1 to day 25, after which water with neither contaminant nor bromide was fed to this tank until the end of the experiment.

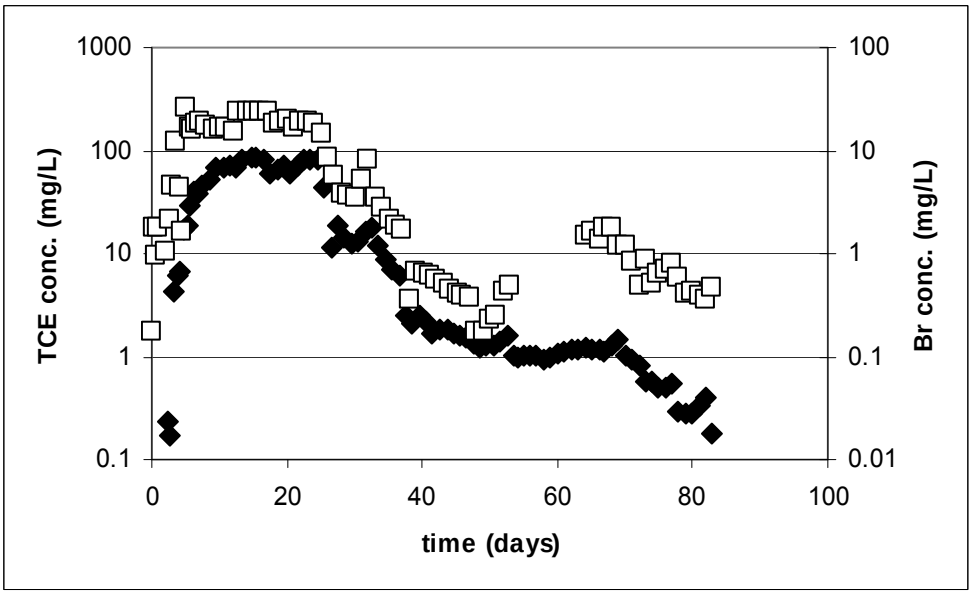

Figure A-9b. TCE (black diamonds) and bromide (open squares) concentrations in the effluent of tank 2a. TCE contaminated water (including bromide) was fed from day 1 to day 22, after which water with neither contaminant nor bromide was fed to this tank until the end of the experiment due to a pump failure.

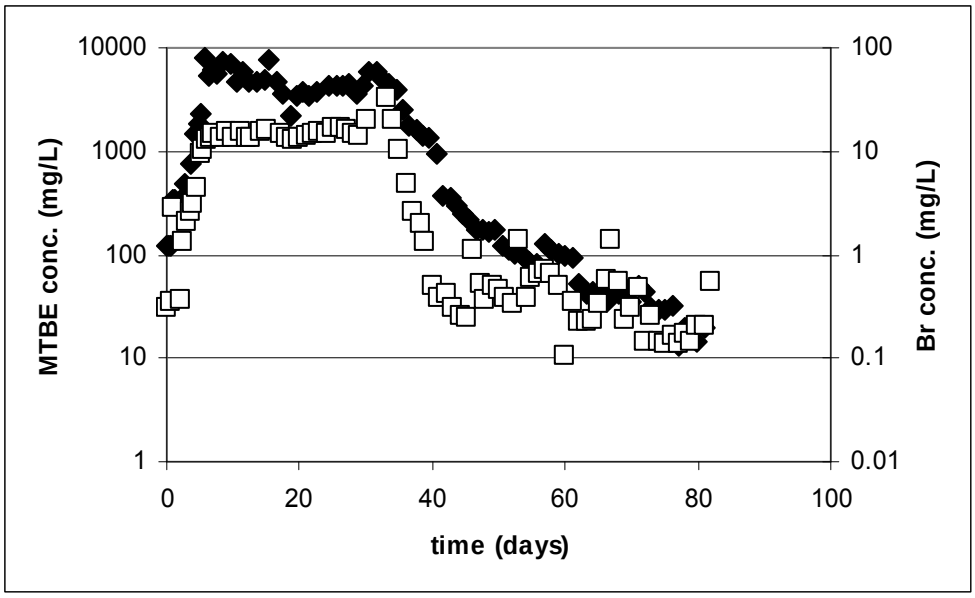

Figure A-9c. MTBE (black diamonds) and bromide (open squares) concentrations in the effluent of tank 3a. MTBE contaminated water (including bromide) was fed from day 1 to day 25, after which water with neither contaminant nor bromide was fed to this tank until the end of the experiment.

The tank effluent concentrations shown in Figures A-10a, A-10b, and A-10c were used in combination with the porous media properties (Table A-3) and the tracer and contaminant flow rates (Table A-4) to estimate the mass balances to each tank. The same formula previously described for the one-layer experiment was used for the two-layer experiments.

The mass balances for the organic contaminant two layer tanks experiments are presented in Figures A-11a, A-11b, and A-11c for the organic contaminants and Figures A-12a, A-12b, and A-12c for bromide.

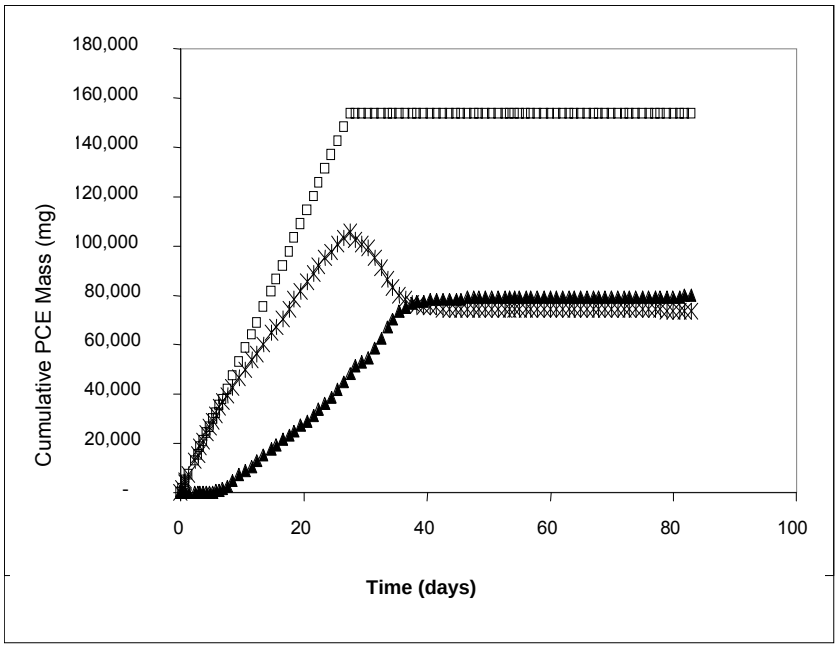

Figure A-10a. PCE mass balance for Tank 1a. Mass-in is shown as open squares, mass-out as black triangles, and the accumulation within the tank (the difference between mass-in and mass-out) as asterisks.

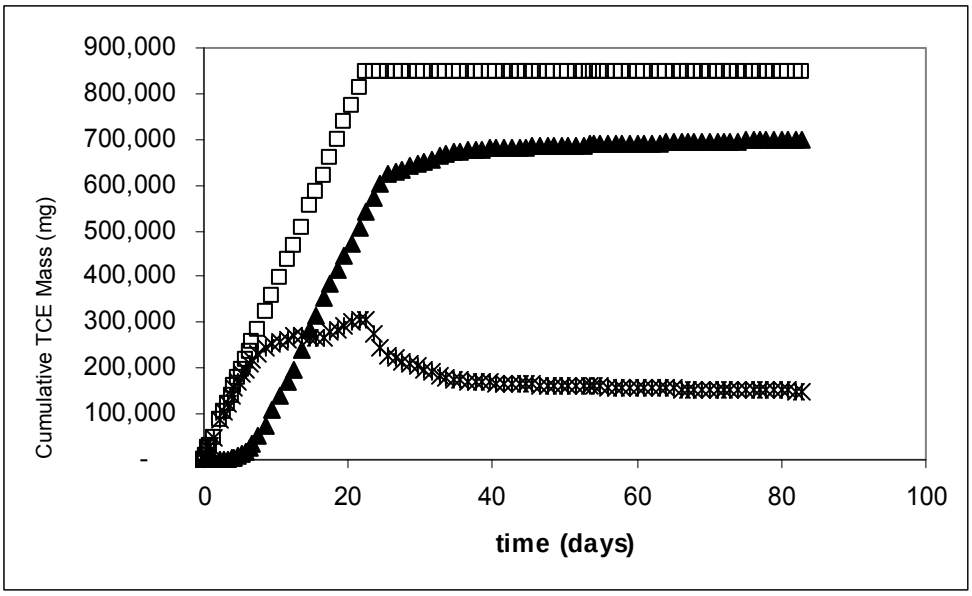

Figure A-10b. TCE mass balance for Tank 2a. Mass-in is shown as open squares, mass-out as black triangles, and the accumulation within the tank (the difference between mass-in and mass-out) as asterisks.

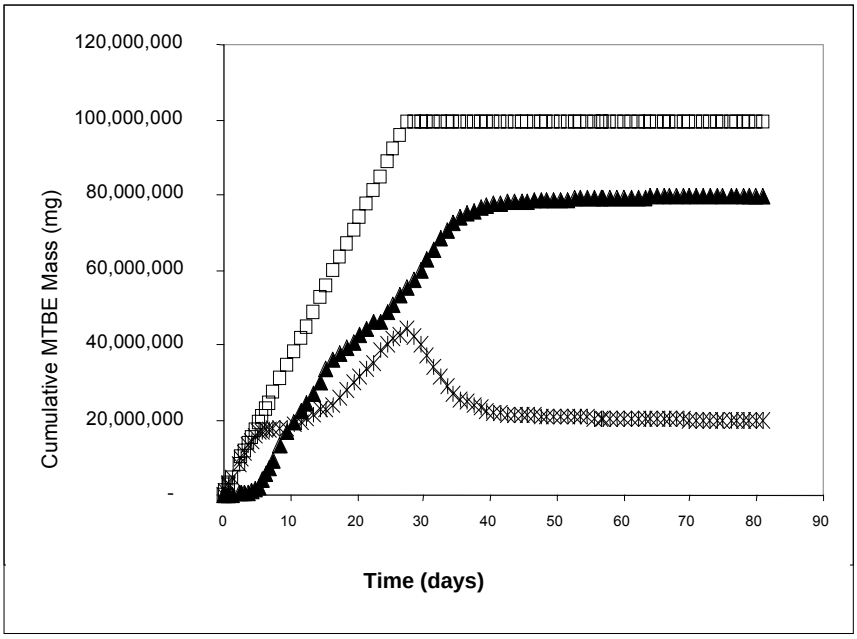

Figure A-10c. MTBE mass balance for Tank 3a. Mass-in is shown as open squares, mass-out as black triangles, and the accumulation within the tank (the difference between mass-in and mass-out) as asterisks.

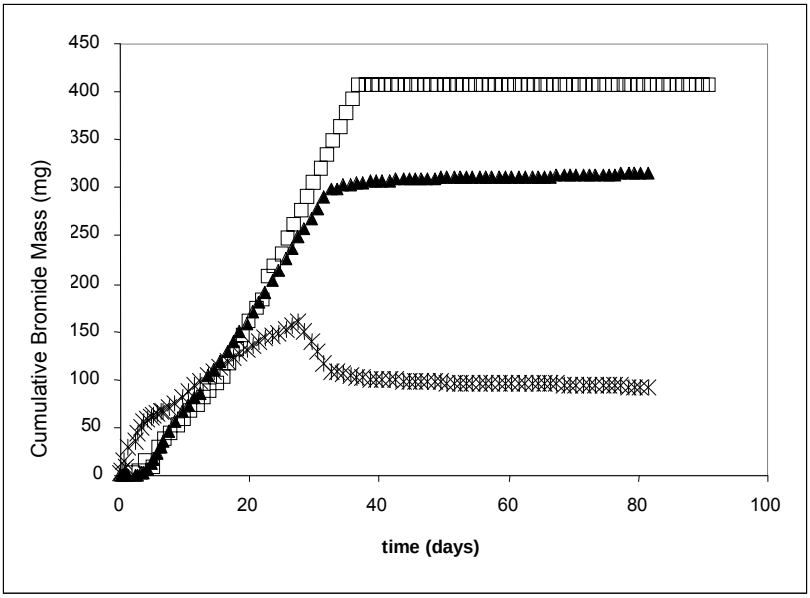

Figure A-11a. Bromide mass balance for Tank 1a. Mass-in is shown as open squares, mass-out as black triangles, and the accumulation within the tank (the difference between mass-in and mass-out) as asterisks.

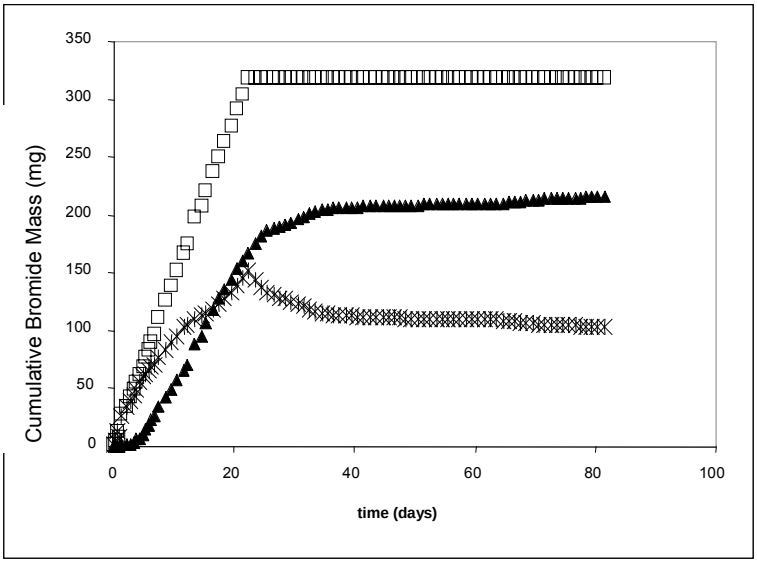

Figure A-11b. Bromide mass balance for Tank 2a. Mass-in is shown as open squares, mass-out as black triangles, and the accumulation within the tank (the difference between mass-in and mass-out) as asterisks.

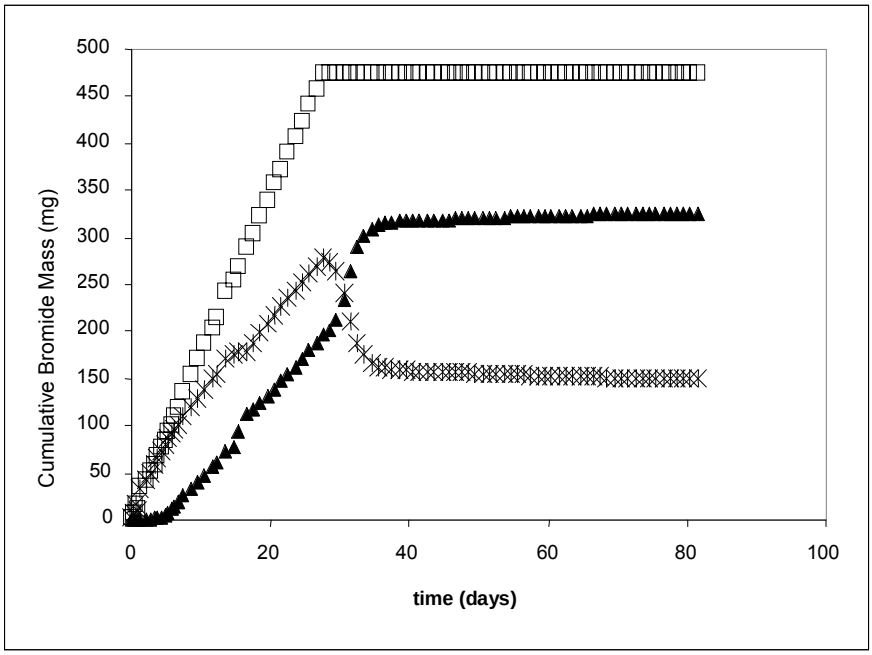

Figure A-11c. Bromide mass balance for Tank 3a. Mass-in is shown as open squares, mass-out as black triangles, and the accumulation within the tank (the difference between mass-in and mass-out) as asterisks.

A.1.14Discussion of One and Two-Layer Experiments Results

The bromide effluent concentration profiles on the one-layer experiments were obtained under identical experimental conditions: pump settings (which determined flow rates), influent bromide concentrations, and tank loading with porous media. Therefore, assuming that interaction with the organic in the feed (TCE, PCE, or MTBE) was not important, differences among these data sets are exclusively due to experimental error, given the uncertainties in the above mentioned experimental settings and/or analytical methods. These profiles are very similar for Tanks 4a, 5a, and 6a up to the shutdown time (25 days). After contaminant shutdown time, the effluent bromide concentrations in Tanks 4a and 5b show a similar pattern, decreasing sharply more than two orders of magnitude and then remaining at levels below detection limits. However, the effluent bromide concentrations in Tank 6b showed an unexpected pattern after the contaminant source was turned off, between days 50 and 63, when they became detectable in the order of 0.1 mg/L after having been non detectable (less than

0.02 mg/L) for about 10 days. These inconsistent results for Tank 6a indicate that a bromide source increased the effluent concentrations after the source probably had been depleted. This was likely due to analytical errors related to the bromide ion selective probe.

The mass balances for bromide in the one-layer experiments indicate that most of the bromide that entered the tanks left the tanks once the contaminant source was turned off, resulting in a very small net accumulation at the end of the experiment. Furthermore, with the contaminant source still on, the accumulation term leveled off early in the experiment (after approximately six days of operation from startup), indicating that these sand-only tanks were becoming mostly saturated with this chemical. This trend is very clear for Tanks 4a and 5a, while Tank 6a showed a small deviation from it. The mass balance for Tank 6a shows a constant increase in the bromide accumulation and a lack of saturation with bromide, up to the contaminant source shutdown. This trend could be explained by a non-steady source, probably related to the feed line plugging and/or high variability of the feed pump(s).

In these one-layer experiments, all three organic contaminants tested exhibited concentrations profiles similar to bromide up until the time where the contaminated source was shut down. At this point, all of them showed a smoother concentration drop than bromide, probably due to the expected stronger sorption (larger retardation) into the sand than bromide. The mass balance for PCE and TCE into single layer experiments (Figures A-8a and A-8b) indicated that these sand-only tanks became mostly saturated with the organic before the contaminant source was turned off, when the concentration dropped sharply initially and then slowly down to a near-zero net accumulation for PCE and TCE. PCE showed a larger accumulation on the long term. Considering that PCE is the most volatile of the organic compounds tested, this could have been caused by volatilization losses (which yielded lower effluent concentrations) during tank operation and/or sampling. Accumulated MTBE into the sand-only Tank 6a showed an unexpected pattern, starting to stabilize up to day 10 and

then increasing up to shutdown. This confirms the variable source of contaminant to this tank discussed previously for bromide. These unacceptable results for MTBE (and bromide) could have been caused by variability in the contaminant pump rate, plugging of the feed line, or other source of experimental error. Given the combined results for the conservative tracer bromide and MTBE, it is likely that this set of data for Tank 6a is of little value, due to experimental errors.

As in the one-layer experiments, the bromide effluent concentration profiles on the two-layer experiments were obtained under identical experimental conditions, and they can be considered replicates that are subject to differences due to experimental errors. The shutdown time for Tanks 1a and 3a was 25 days. The shutdown time for Tank 2a was 22 days because of a feed pump error (a failure shared with Tank 5a, and probably a feed error during which the common contaminant and tracer source to both tanks was not available). The bromide profiles for Tanks 1a, 2a, and 3a are very similar, leveling off at about 5 days after the experiment startup and indicating a near saturation of the tanks with bromide. After shutdown, the concentration profiles of bromide decreased sharply (with a lag time close to that of one tank bed volume), roughly one order of magnitude for approximately 10 days, and then stabilized at a concentration higher than the concentrations achieved in the one layer tanks at similar times. These results suggest that the low permeability layers in the two layer tanks behaved as a long-term source of tracer after the source was shutdown, sustaining much higher concentrations (up to two orders of magnitude) on the long term operation than those without the low-permeability zones (one-layer experiments).

The mass balances for bromide in the two-layer experiments (Figures A-12a through A-12c) show two major differences with respect to the one-layer experiments: (a) with the bromide source on, the near saturation of the one layer tanks observed in Figures A-9a and A-9b (Tanks 4a and 5a) is not apparent; the accumulation of the two tanks increased steadily until the tanks were shutdown, and (b) upon source shut down, after a sharp decrease in the accumulated

contaminant within the tank (probably due to flushing of the high hydraulic conductivity sand layer), all two layer tanks showed a net accumulation of bromide, even at sixty days after bromide source shutdown. This suggests that the low permeability layers worked as a long term source of bromide, slowly releasing bromide accumulated before the source was shut down.

In these two-layer experiments, the profiles of all three organic contaminants tested showed a slower decrease after the contaminant source was shutdown than seen in single layer experiments, Further, the long-term contaminant concentrations for TCE and MTBE were larger than in the single-layer experiments, even though the water velocity was significantly faster (see Table A-4), which would dampen this effect. The concentration profile for PCE was very similar in both the single and two-layer experiments, although the results are not directly comparable because the groundwater velocities are different. Mass balances are corrected for this difference in velocity between one- and two-layer tanks and thus represent a more objective comparison.

As in the case of bromide, the mass balances for organic contaminants show long-term accumulation of the organic contaminants with significant, irreversible accumulation of the organics in the two-layer tanks (of similar magnitude to the accumulation of bromide), suggesting the accumulation of organics in the low permeability zones. Associated with this is an observable lack of media saturation, shown by the continuous growth of the accumulation term until the primary contaminant source was shut down, coupled with a prolonged release of the stored contaminant once the primary contaminant source was depleted. For Tanks 3a and 6a (one and two-layer tanks with a common contaminant reservoir), a sudden increase was apparent around day 20, indicating problems with the common bromide and contaminant source for both tanks. This confirms inconsistency of these data for Tanks 3a and 6a in comparison to the data from other tanks, and such inconsistency makes the results from Tanks 3a and 6a questionable.

A.1.15 Multi-Layer Experiments

The results of the porous media loading on the tanks are shown in Table A-5. The recorded masses of sand and silt for each tank were used to estimate the porosity and bulk density of the porous materials loaded into the tanks. These results were later used in combination with contaminant concentrations and measured flow rates to estimate the mass balances on each tank. Table A-6 presents measured flow rates to each tank, together with the resulting groundwater velocity and the contaminant and tracer concentrations on the feed to each tank.

Table A-5. Mass loading of porous media (sand and silt) into multi-layer tanks. Bulk density and porosity were calculated based on these recorded mass and tank volumes. Mean and coefficient of variation (C.V.%) values are provided for all multi-layer tanks for which measurements were available. The data on 2b, 5b, and 6b was not measured due to experimental omission.

Tank	Height (cm)	Silt layers width		Width of all layers (cm)		Loading (lb)		Bulk Density		Porosity	
		mean	c v%	Total	Sand	Silt Mass	Sand Mass	Silt	Sand	Silt	Sand
1b	93	4.9	9%	24.3	25.3	24.3	21.7	1.5	1.6	0.42	0.38
2b	95	4.7	11%	23.5	26.0	Not measured					
3b	80	5.0	10%	24.8	24.8	22.4	17.9	1.4	1.8	0.46	0.32
4b	93	4.9	13%	24.6	24.9	23.6	18.6	1.3	1.6	0.51	0.39
5b	94	5.0	5%	24.9	24.6	Not measured					
6b	95	4.6	8%	23.1	26.4	Not measured					
							Mean	1.4	1.7	0.46	0.36
							cv%	9%	6%	10%	10%

Table A-6. Measured feed flow rates and contaminant concentrations to each tank. Data represents results from 6 different measurements for each line, taken at different times during the operation of the pumps (averages and coefficient of variation, C.V. %). Resulting groundwater velocities were estimated on the total flow (mean contaminant plus mean water lines within each tank) and the sand porosity, sand width (from Table A-5), and the tank dimensions. Contaminant and bromide concentrations shown next to the date measured (in parenthesis).

Tank	Feed line flow rate (mL/min)		Ground water velocity (ft/day)	Contaminant Concentrations (mg/L)	Bromide Concentrations (mg/L)
	mean	C.V. (%)			
1b	0.62	13%	1.07	683 (11/24/2004) 84 (12/1/2004 85 (12/2/2004) 123 (12/3/2004) 146 (12/10/2004) 0 (12/23/2004 and after)	6-11/24/2004 9-12/9/2004 0-12/23/2004 and after
2b	0.59	16%	1.03		
3b	0.59	14%	1.23		
4b	0.55	12%	0.948	147(11/24/2004) 91 (12/1/2004) 94 (12/2/2004) 85 (12/3/2004) 76 (12/10/2004) 0 (12/23/2004 and after)	
5b	0.54	12%	0.994		
6b	0.48	15%	0.823		

Figure A-12 shows the effluent TCE concentrations from Tanks 1b, 2b, and 3b. Tank 1b is considered a control, since the silt used for it was unmodified, whereas silt modified with 1% powder activated carbon (AC) was used in Tank 2b and zero-valent iron (ZVI) was used in Tank 3b. The contaminant source was turned off at day 29 after the experiment startup. Figure A-13 shows the effluent bromide concentrations for the same tanks (1b and 3b) during the same experiment.

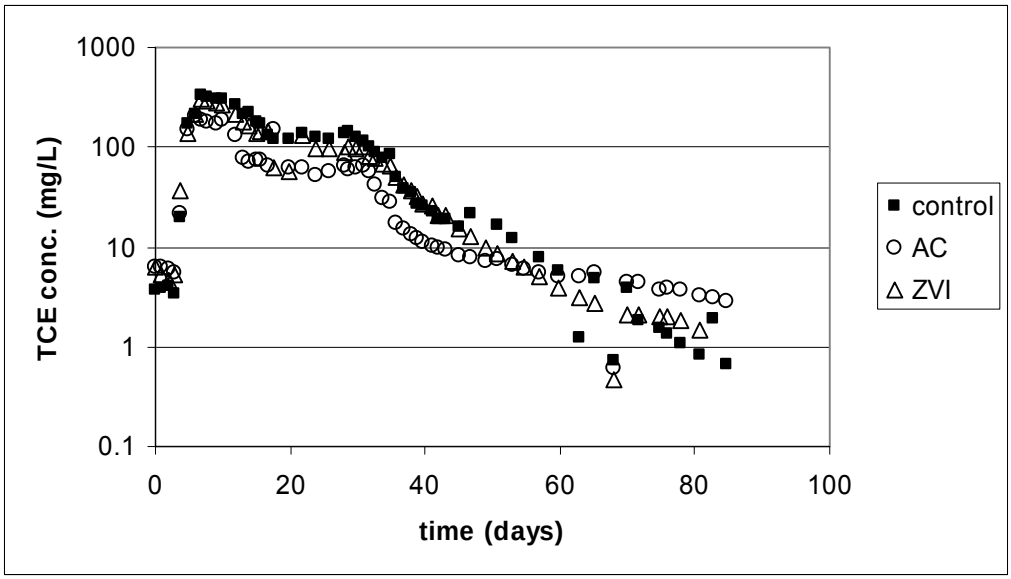

Figure A-12. TCE effluent concentrations for Tanks 1b and 3b. Control (tank with unmodified silt) TCE concentrations are shown as black squares. Tanks with activated carbon (AC)- and zero-valent iron (ZVI)- modified silt are shown as open circles and open squares, respectively.

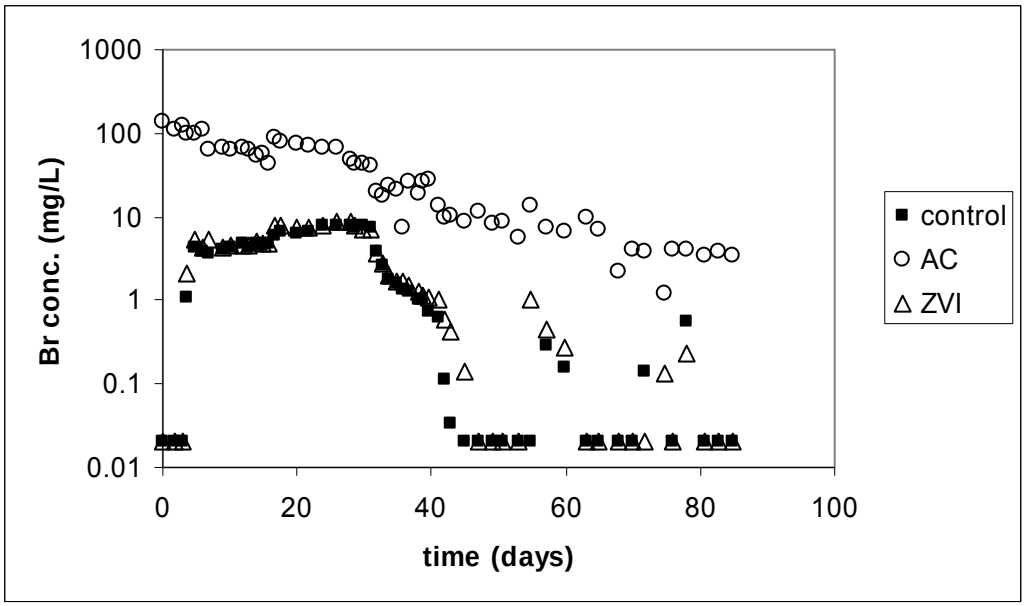

Figure A-13. Bromide effluent concentrations for Tanks 1b and 3b. Control (tank with unmodified silt) TCE concentrations are shown as black squares. Tanks with activated carbon (AC)- and zero-valent iron (ZVI)- modified silt are shown as open circles and open squares, respectively.

For the one- and two- layer experiments, calculation of mass balances was based on the effluent concentrations shown in Figures A-12 and A-13, measured pumping rates for the groundwater feed lines and the combined contaminant/tracer, and contaminant and bromide concentrations in the contaminant feed (Table A-6). Organic concentrations in the feed varied widely because the source of contaminant was prepared continuously (with free NAPL being stirred).

Mass balances for TCE in these multi-layer tank experiments are shown in Figures A-14a through A-14c. Bromide mass balances for the unmodified silt and zvi-modified silt were performed during these same experiments and are shown in Figures A-15a and A-15b, respectively. The mass balance for the activated carbon-modified silt was not calculated, since the activated carbon showed very large background bromide concentrations, as presented on Figure A-13.

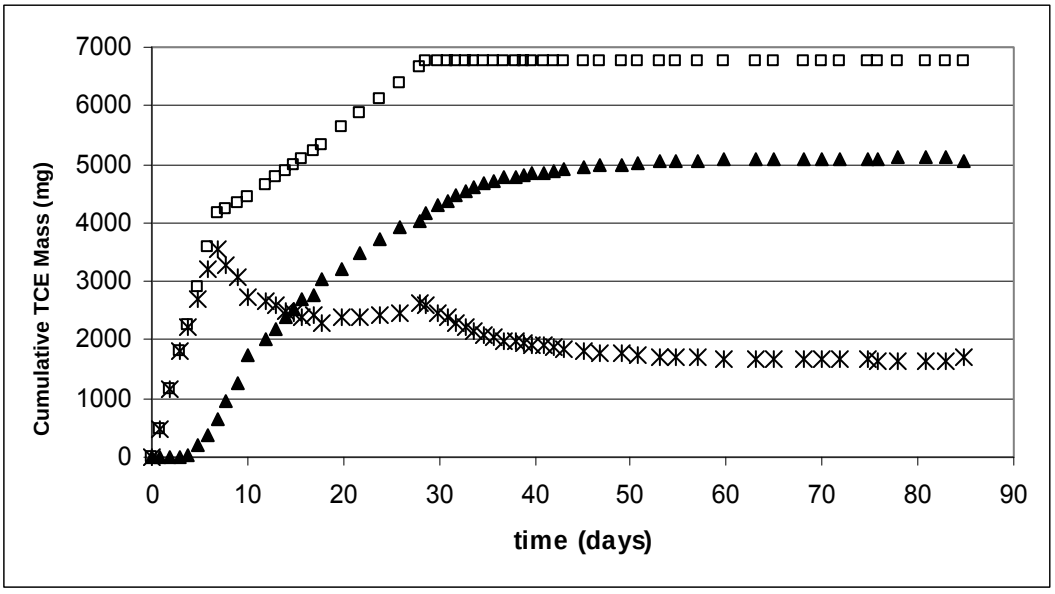

Figure A-14a. TCE mass balance for Tank 1b. Mass-in is shown as open squares, mass-out as black triangles, and the accumulation within the tank (the difference between mass-in and mass-out) as asterisks.

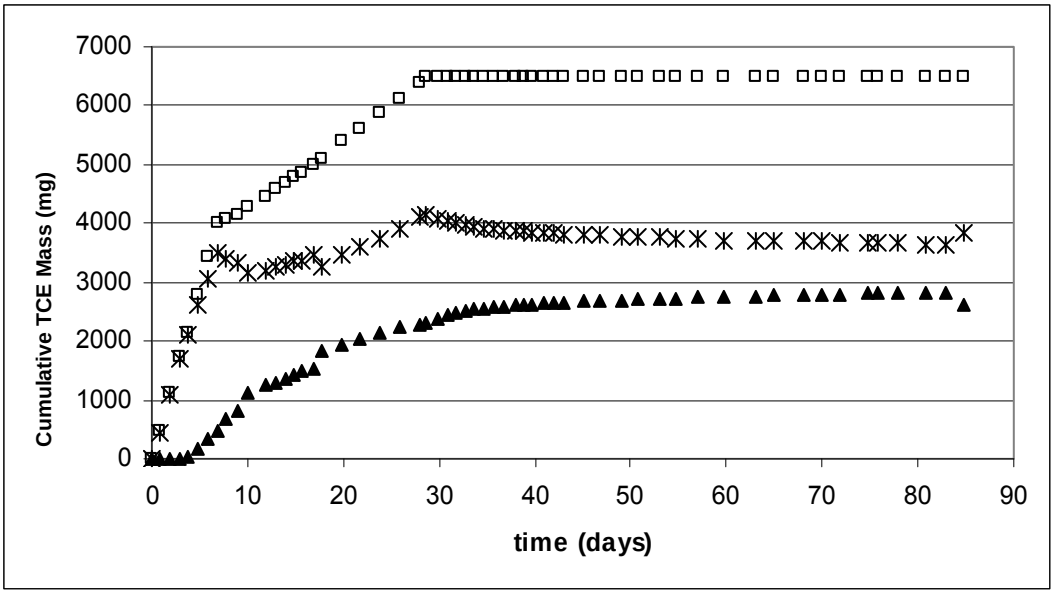

Figure A-14b. TCE mass balance for Tank 2b. Mass-in is shown as open squares, mass-out as black triangles, and the accumulation within the tank (the difference between mass-in and mass-out) as asterisks.

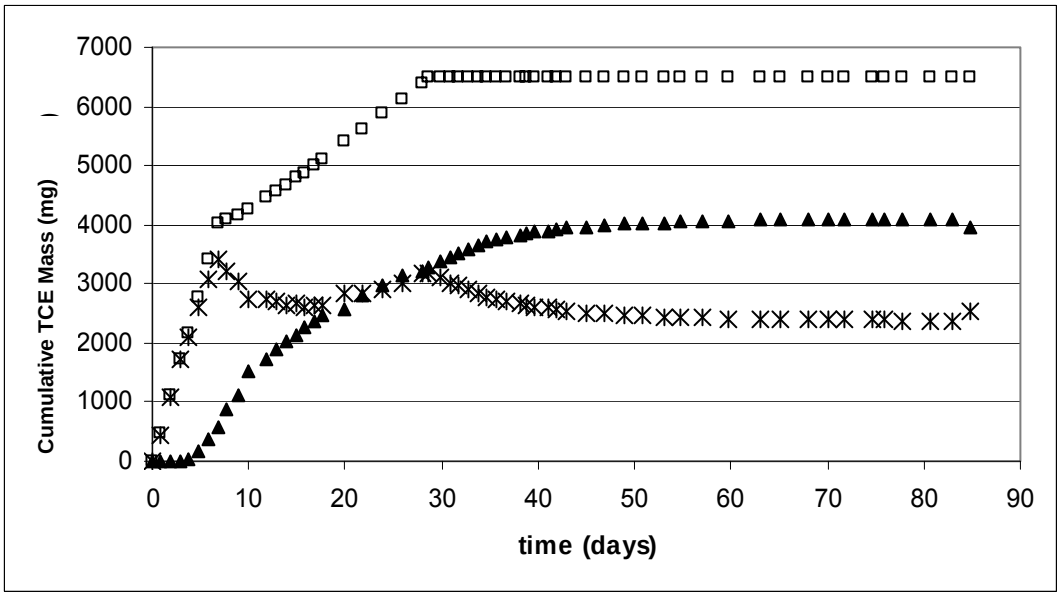

Figure A-14c. TCE mass balance for Tank 3b. Mass-in is shown as open squares, mass-out as black triangles, and the accumulation within the tank (the difference between mass-in and mass-out) as asterisks.

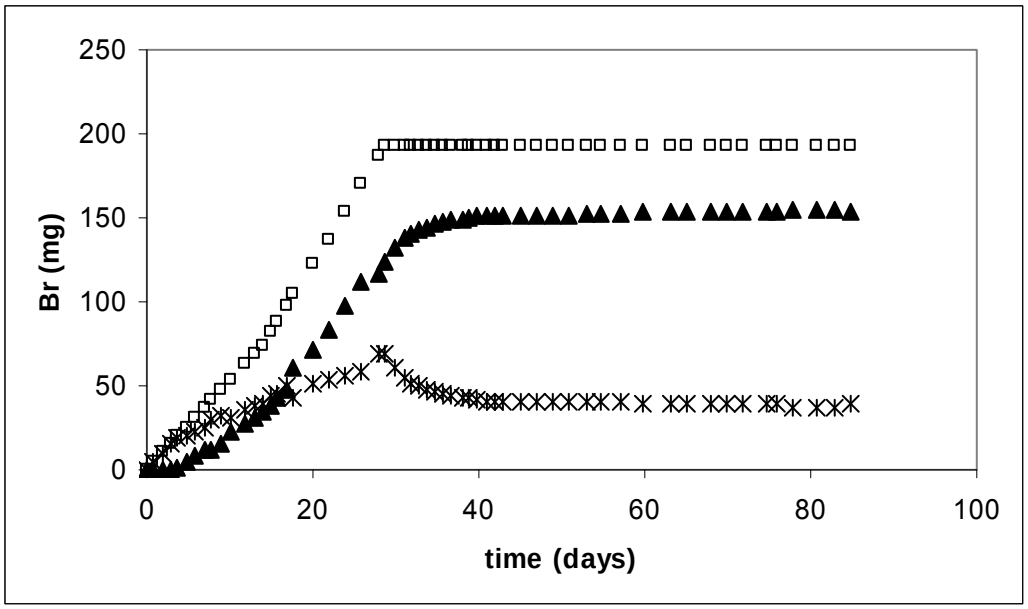

Figure A-15a. Bromide mass balance for Tank 1b. Mass-in is shown as open squares, mass-out as black triangles, and the accumulation within the tank (the difference between mass-in and mass-out) as asterisks.

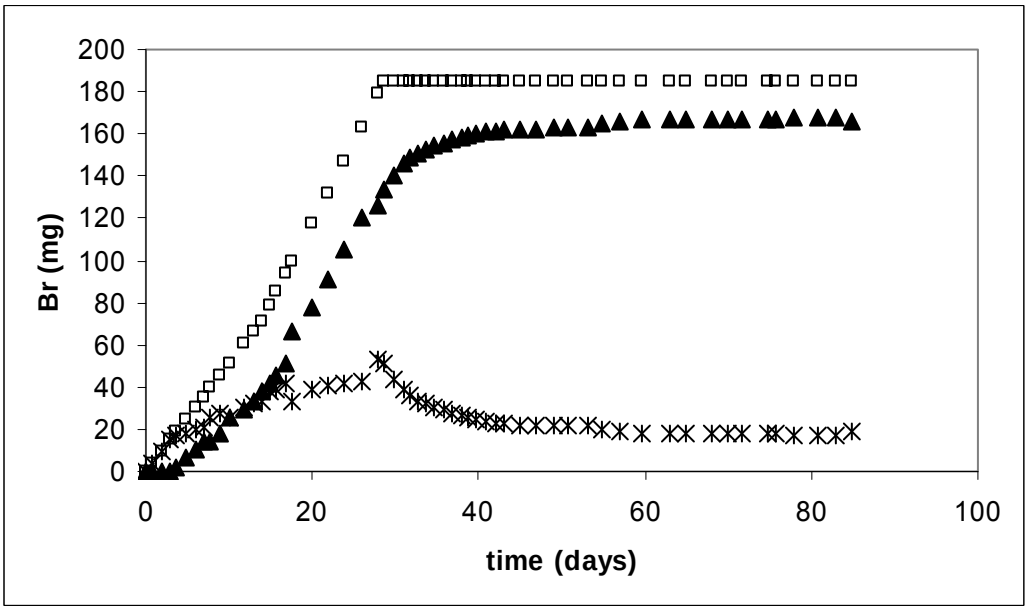

Figure A-15b. Bromide mass balance for Tank 3b. Mass-in is shown as open squares, mass-out as black triangles, and the accumulation within the tank (the difference between mass-in and mass-out) as asterisks.

Figure A-16 shows the effluent PCE concentrations from Tanks 4b, 5b, and 6b. Tank 4b used unmodified silt, whereas Tank 5b used silt modified with 1% powder activated carbon (AC) and Tank 6b used zero-valent iron (ZVI). The contaminant source was turned off at day 29 after the experiment startup. Figure A-17 shows the effluent bromide concentrations performed during the same experiment for Tanks 4b and 6b.

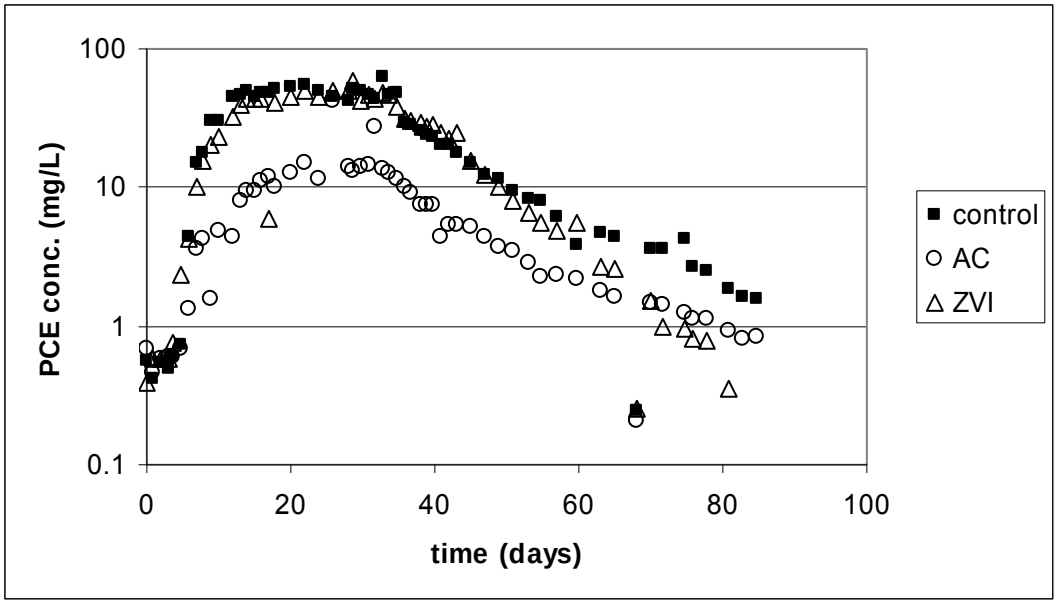

Figure A-16. PCE effluent concentrations for Tanks 4b and 6b. Control (tank with unmodified silt) PCE concentrations are shown as black squares, while tanks with activated carbon (AC)- and zero-valent iron (ZVI)- modified silt shown as open circles and open squares, respectively.

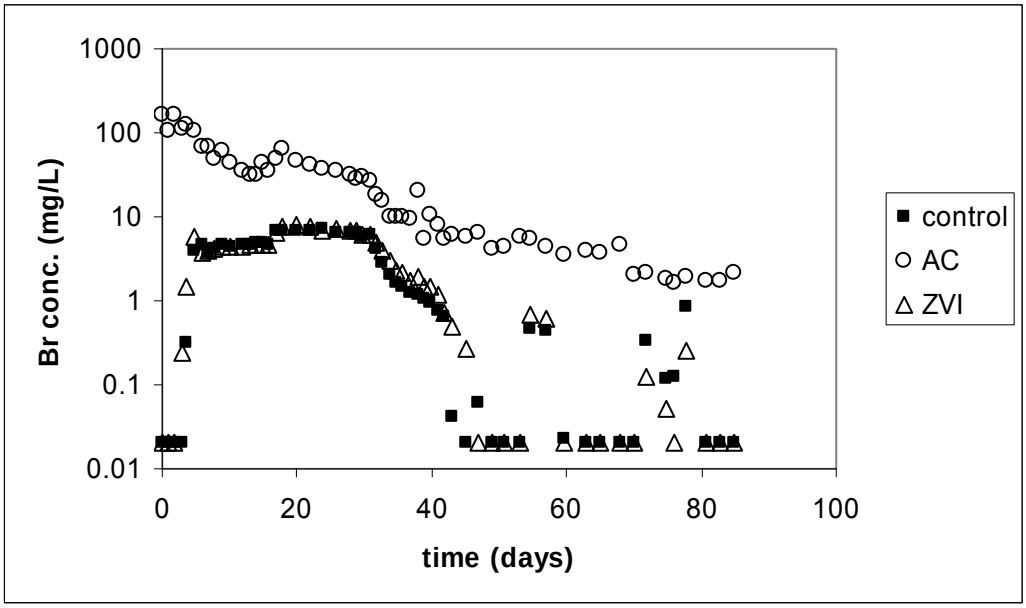

Figure A-17. Bromide effluent concentrations for Tanks 4b and 6b. Control (tank with unmodified silt) bromide concentrations are shown as black squares, while tanks with activated carbon (AC)- and zero-valent iron (ZVI)- modified silt are shown as open circles and open squares, respectively.

The mass balances for PCE in the multi-layer tank experiments are shown in Figures A-18a through A-18c. Bromide mass balances for the unmodified silt and zvi-modified silt were performed during these same experiments and are shown in Figures A-19a and A-19b, respectively. The mass balance for the activated carbon-modified silt was not calculated, since the activated carbon showed very large background bromide concentrations, as shown on Figure A-17.

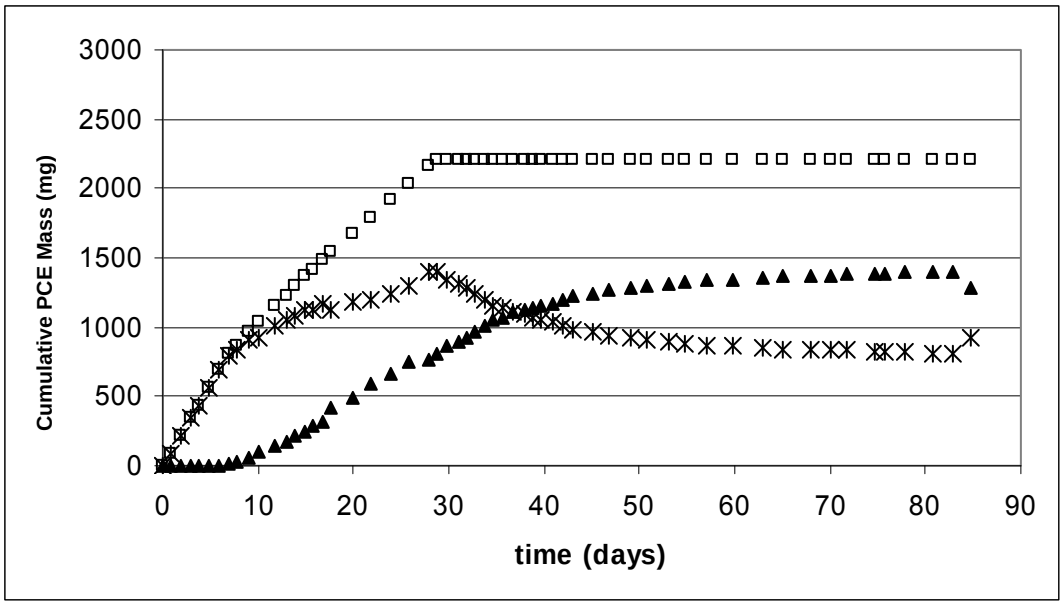

Figure A-18a. PCE mass balance for Tank 4b. Mass-in is shown as open squares, mass-out as black triangles, and the accumulation within the tank (the difference between mass-in and mass-out) as asterisks.

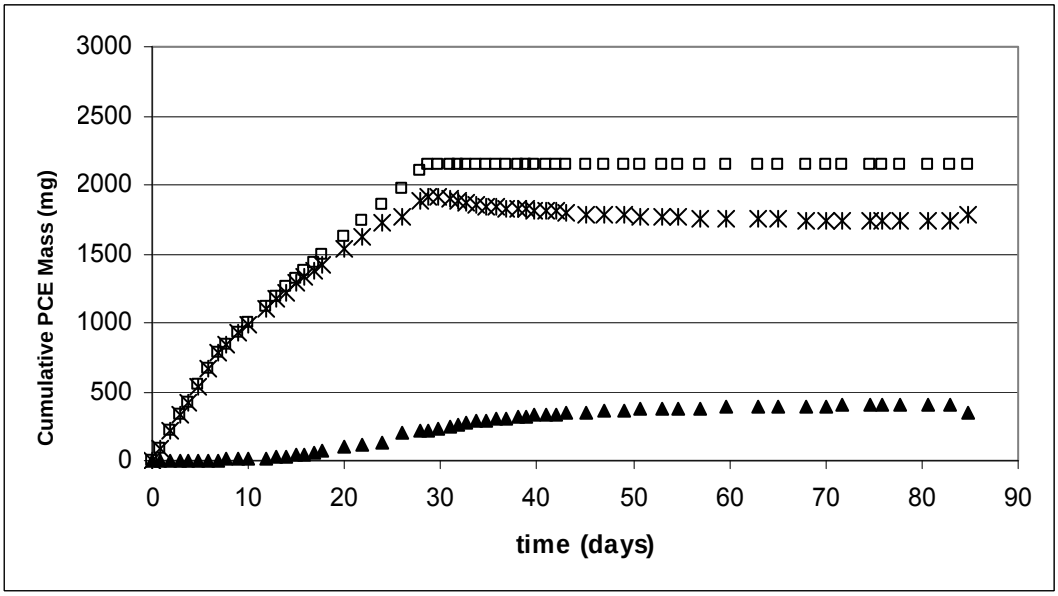

Figure A-18b. PCE mass balance for Tank 5b. Mass-in is shown as open squares, mass-out as black triangles, and the accumulation within the tank (the difference between mass-in and mass-out) as asterisks.

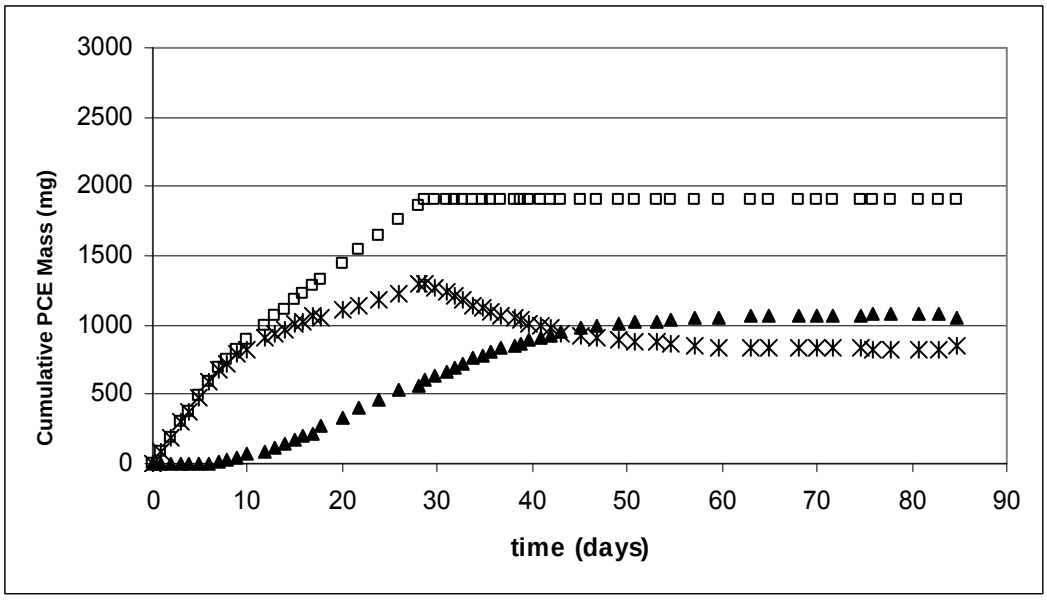

Figure A-18c. PCE mass balance for Tank 6b. Mass-in is shown as open squares, mass-out as black triangles, and the accumulation within the tank (the difference between mass-in and mass-out) as asterisks.

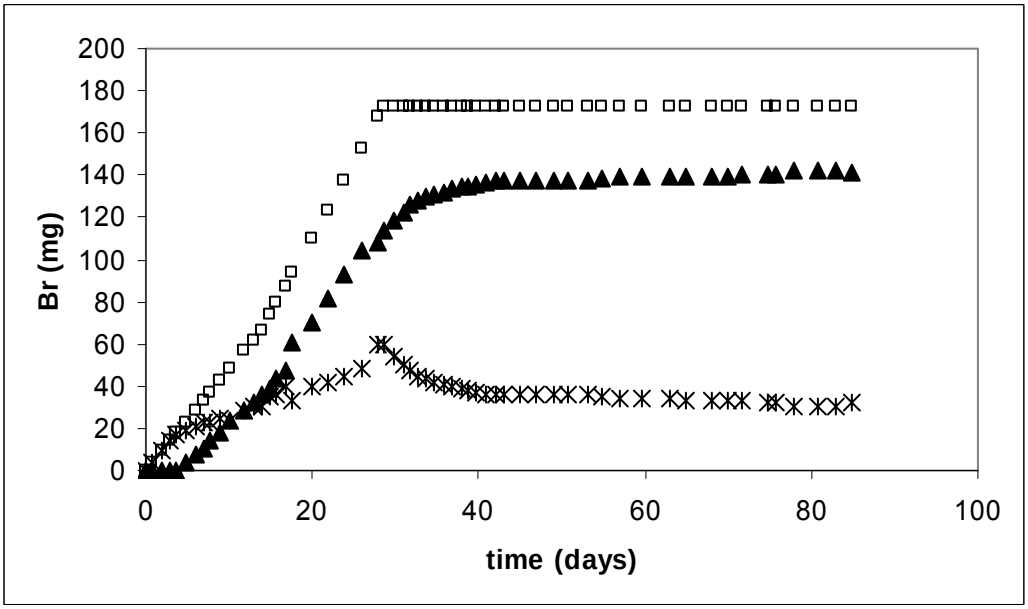

Figure A-19a. Bromide mass balance for Tank 4b. Mass-in is shown as open squares, mass-out as black triangles, and the accumulation within the tank (the difference between mass-in and mass-out) as asterisks.

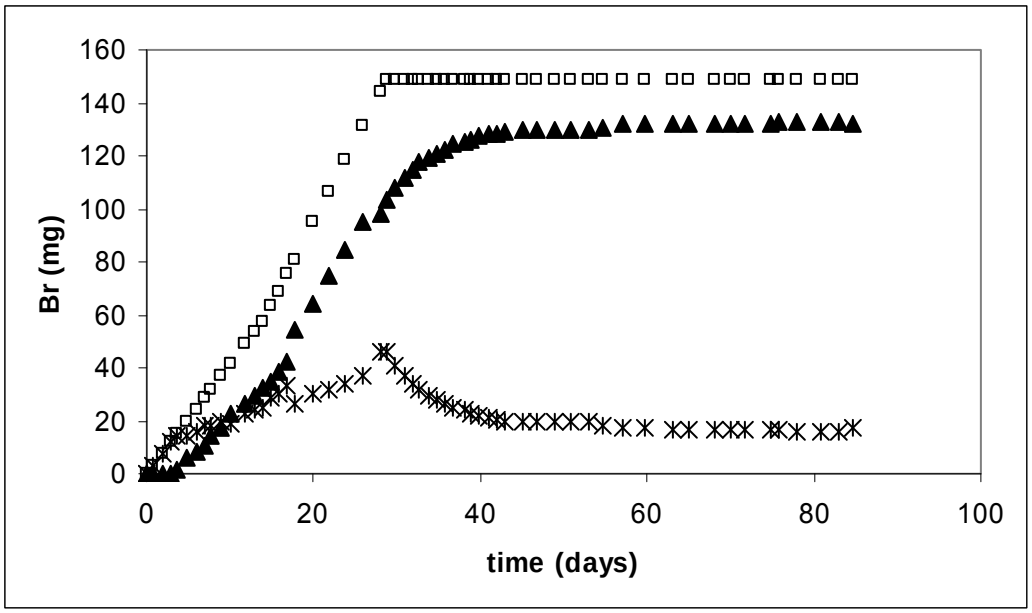

Figure A-19b. Bromide mass balance for Tank 6b. Mass-in is shown as open squares, mass-out as black triangles, and the accumulation within the tank (the difference between mass-in and mass-out) as asterisks.

A.1.15.1 Discussion of Experiments Results

For the first reporting period, concentrations of contaminants discharged from the tanks were determined as a function of time. Results from the MTBE tanks are shown in Figure A-20. Concentration on the y-axis was plotted as a function of time on arithmetic and log scales. Observed concentrations from the sand-only tank breakthrough sooner and attain higher values, reflecting the absence of the silt layer that attenuates MTBE concentrations in the sand. Due to reverse diffusion from the silt, effluent concentrations from the silt-sand tanks are sustained for a far longer time, illustrating the role of mass storage in stagnant zones.

MTBE Tank Experiments

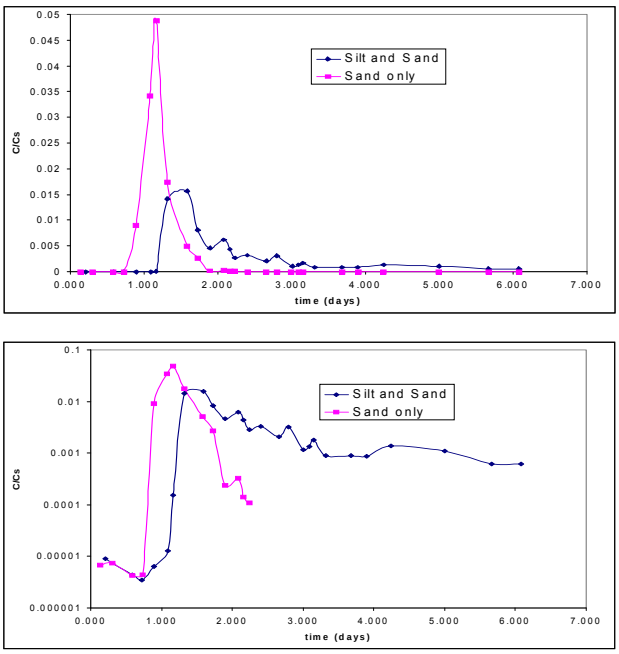

Figure A-20. MTBE results.

Unfortunately, results from our mass balances on the TCE and PCE experiments were unacceptable. The methods of analysis were changed and the experiments were repeated for the second reporting period.

For the second reporting period, the bromide effluent concentration profiles for the three pairs of tanks—Tanks 1b and 4b, Tanks 2b and 5b, and Tanks 3b and 6b—were obtained under identical experimental conditions—pump settings (which determined flow rates), influent bromide concentrations, and tank loading with porous media— and can be considered duplicates. Therefore, assuming that interaction with the organic in the feed (TCE or PCE) was not important, differences within each tank pair are exclusively due to experimental error, caused by uncertainties in the above mentioned experimental settings and/or analytical methods.

The Tank 2b and 5b pair showed initial bromide concentrations exceeding those of the feed by a factor of 10 or more. Analysis of activated carbon aqueous leachate (at a 1:1 weight:volume ratio) detected very high bromide

concentration—in excess of 100 mg/L. Thus, the bromide data set for this pair could not be used.

Bromide effluent concentrations for Tanks 1b and 4b (unmodified silt) were very similar to each other (Figures A-13 and A-17). After contaminant source shutdown at day 29, these concentration profiles showed a nearly steady decrease for 14 days, when bromide concentrations became non detectable. For non detectable concentrations, concentrations were assumed to be 50% of the detection limit of 0.04 mg/L reported by the manufacturer (although a reasonable value might be higher than that, as discussed later in Section A.11.3, Quality Assurance/Quality Control). Within those 14 days, the reduction in the bromide concentrations, with respect to pre-contaminant source shutdown levels, had fallen by slightly over one order of magnitude. Because concentrations became lower than detection limits only two weeks after contaminant shutdown, longer term conclusions cannot be drawn from these data. Therefore, the following observations are only valid for the short time after contaminant source shutdown (up to 14 days after contaminant source shutdown), when bromide concentrations were still measurable.

The bromide data for Tanks 3b and 6b were very similar to each other and also similar to the unmodified silt (see Figures A-13 and A-17). Thus, the presence of ZVI in the silt layer did not have large effects in the bromide transport with respect to unmodified silt. At the point of contaminant source shutdown (29 days after experiment startup) mass balances for bromide in both types of tanks using unmodified and ZVI-modified silt show accumulation between 25 to 30% of the total mass-in (Figures A-15a, A-15b, A-19a, and A-19b). Upon contaminant source shutdown, bromide accumulation began to decrease at a much slower rate than in the two-layer experiments (Figures A-11a, A-11b, and A-11c).

The concentration profiles up to the source shutdown time for TCE in multi-layer experiments using unmodified silt and ZVI (Tanks 1b and 3b) were very similar (Figure A-12), whereas the effluent concentrations of AC-modified silt showed

significantly lower concentrations. Upon contaminant shutdown, all of these concentrations decreased at much slower rates than those observed in the two-layer experiments (Figure A-9b). Tank 2b, having used AC-modified silt, could sustain higher concentrations than Tank 1b (unmodified silt) after 40 days of contaminant shutdown, despite the fact that the effluent concentrations of Tank 2b were smaller than Tank 1b before contaminant source shutdown. The similar concentration profiles of Tanks 1b (unmodified silt) and 3b (ZVI-modified silt) might indicate very small reactivity of TCE towards ZVI.

Mass balances for TCE in Tanks 1b and 3b (unmodified silt and ZVI-modified silt, Figures A-14a and A-14c, respectively) show that long term accumulation of TCE within the tank was of the same order of magnitude (about 2000 mg after approximately 15 days after contaminant source shutdown) and remained near that level until the end of the experiment (about 40 days later, at 55 days after contaminant source shutdown). This confirms the small reactivity of TCE towards ZVI, and also emphasizes the significant role of the silt in sustaining high contaminant concentrations in the effluent on the long term. TCE accumulation in the AC-modified tank (Figure A-14b) was nearly 50% higher than in the unmodified (and ZVI-modified) silt (Figures A-14a and A-14c), indicating that the effluent contaminant concentrations are very sensitive to the contaminant sorption to the low permeability media.

The concentration profiles for PCE in multilayer experiments (Figure A-16) show that, after contaminant source shutdown, all of these concentrations decreased at much slower rate than in the two-layer experiments (Figure A-9a). Up until contaminant source shutdown, the concentration profiles for PCE in multi-layer experiments using unmodified silt and ZVI-modified silt (Tanks 4b and 6b) were very similar, while the effluent concentrations in the tank with AC-modified silt (Tank 5b) were much smaller. Upon contaminant source shutdown, the PCE concentrations in the ZVI-modified tank (Tank 6b) dropped at a slightly faster rate than at the tank with the unmodified silt. After contaminant source shutdown, effluent concentrations in the AC-modified silt (Tank 5b) dropped at a similar rate

to the one observed in the unmodified silt Tank 4b. However, mass balances for these tanks indicate that, at the end of the experiment, accumulation in the AC-modified tank (Tank 5b, Figure A-18b) was nearly 80% of the cumulative mass fed into this tank, while the PCE accumulation at the end of the experiment on Tank 4b using unmodified silt (Figure A-18a) was approximately 40%, half the long term accumulation in the AC-modified Tank 5b. As in the case of TCE, these results underline the importance of the sorptive processes within the low permeability media on the effluent contaminant concentrations. The mass balance for the ZVI-modified tank 6b (Figure A-18c) showed very small differences in respect to the unmodified silt Tank 4b. This is probably a result of the limited effects of reactivity of the ZVI on the overall mass balance (although there seems to be a small effect on the effluent concentrations, as shown on Figure A-16).

It must be noted that these experiments did not have the capability to differentiate between true accumulation in the tanks with ZVI-modified silt (Tanks 3b and 6b) and a more likely sink term. Differentiating these terms would require actual analysis of the low permeability porous media, which was not conducted.

A.1.16 Quality Assurance /Quality Control

For every 20 samples collected for chlorinated organics analysis (PCE and TCE), one MTBE blank was run to evaluate potential contamination of the extraction solvent or the GC. Calibration curves for comparison of the unknown samples were run in the concentration range of 10 to 500 μg/L for both PCE and TCE, using at least 6 standards for each analyte, and were linear throughout the entire concentration range. Samples with a signal outside of the linear range were run at a different dilution that resulted in a signal within the linear range. The reported detection limit for this method is 0.0002 μ/L for both PCE and TCE (US EPA, 1995) and the reported analytical error is less than 3%: the relative standard deviation of replicate samples (US EPA, 1995). Triplicate analyses of a single sample showed a coefficient of variation of 5%.

For every 15 samples collected for MTBE analysis, a blank was run to estimate background measurable concentrations in the water used for dilutions before the purge and trap sample processing. The estimated detection limit for the GC/FID method used for MTBE is about 10 mg/L, a limit based on low aromatic diesel (US EPA, 2003). Blank analysis showed a measurable peak close to the retention time of MTBE, probably due to a poor selection of the chromatography column. This situation showed analytical issues with the measurement of low MTBE concentrations.

The bromide ion selective probe was calibrated daily. The reported error of this analysis is less than 2% at concentrations higher than 1 mg/L, and up to 12% at concentrations of 0.5 mg/L (US EPA, 1996). The reported detection limit is 0.2 mg/L (US EPA, 1996), although the ion selective probe manufacturer claimed a detection limit of 0.04 mg/L. It was found in our laboratory than measurements of concentrations below 0.5 mg/L were unreliable, since the reading value took a long time to stabilize. Measurements were taken at 2.0 min after inserting the probe in the aliquot being tested.

REFERENCES CITED

US EPA. 1995. Method 551.1. “Determination of Chlorination Disinfection Byproducts, Chlorinated Solvents and halogenated pesticides/herbicides in Drinking water by liquid-liquid extraction and gas chromatography with electron capture detector.” Revision 0. United States Environmental Protection Agency.

US EPA. 1996. Method 9211. “Potentiometric Determination of Bromide in Aqueous Samples with Ion-Selective Electrode.” Revision 0. United States Environmental Protection Agency.

US EPA. 2003. Method 8015D. “Nonhalogenated Organics Using GC/FID.“ Revision 4. United States Environmental Protection Agency.

APPENDIX B
COLORADO SCHOOL OF MINES
LABORATORY EXPERIMENTS

APPENDIX B

EXPERIMENTAL OBJECTIVES AND SETUP

This section provides detailed descriptions of the experiments that were performed at the Colorado School of Mines, including the objectives of each experiment and the design and implementation of the experimental equipment for five small tanks, two intermediate tanks and three large tanks.

B.1.1 Large Tank (16 ft.)

B.1.1.1 Large Tank Objectives

There are three primary objectives to the large tank experiments. The first objective of the large tank experiments will be to further study the effects of Fluxes 1, 2, 3 and 4, as discussed in the conceptual model in the main body of this report. Specifically, the large tank will enable the study of these concepts at larger scales of both time and space. The second objective of the large tank experiment will be to determine whether there are more factors to the conceptual model (other than Fluxes 1, 2, 3 and 4), and/or whether one process is more dominant than another. A third and final objective of the large tank experiments is to provide data to valid a numerical model that will be simulating these processes.

B.1.1.2 Large Tank Materials

A 16-ft-long tank was developed to further study the time and scaling factors related to matrix diffusion. A longer length was selected to create a test domain that captures the matrix diffusion both in the source zone and within the dissolved plume downgradient of the source. The tank walls consisted of four separate sections, each measuring 8 ft in length $\times$ 4 ft in height $\times$ 4 in. in width. The frame of each wall section consisted of 4 ft $\times$ 4.0 in. $\times$ 0.5 in. pieces of aluminum spaced on 1 ft centers. Each frame was fastened to a 0.75 in. thick piece of polycarbonate measuring 8 $\times$ 4 ft. The tank end and bottom plates were

constructed out of 0.5 in. thick × 1.0 ft wide aluminum plates. The plates were purchased in 16-ft lengths and were then cut into 4-ft sections for the end plates. The bottom plate consisted of a 12-ft section butted up against a 4-ft section.

The tank walls were lined with plate glass to prevent DNAPL chemically interacting with the polycarbonate wall surface. Four pieces of 4 × 8 ft × 3/16 in. pieces of plate glass were attached to the polycarbonate surfaces using silicone. Silicone was also applied at each of the fastener holes located on the polycarbonate surfaces, to the bottom of the tank, and to the end plates prior to fastening. The entire tank was then bolted together with 1/4 in. machine grade bolts and nuts. Four aluminum plates were fastened perpendicular to the top of the tank in order to prevent the tank from “bowing out” when filled with soil.

Each 8-ft section of the tank was cleaned, and had a panel of plate glass installed. After the plate glass installation, two of the 8-ft sections were bolted together to make the adjoining 16 ft walls of the tank. One wall, with the glass side up, was then turned upside down with the bottom facing up. The other wall was flipped in the same manner and positioned 2 in. across from the other wall. Four pieces of 2-in-thick R15 styrofoam insulation were placed as a barrier between the wall sections.

Once the two wall sections were aligned along the bottom and sides, the bottom plates for the tank were C-clamped in place. A number of 1/4 in. holes (64) were then drilled in-place into the bottom plate. Once the holes were drilled, 1/4 in. machine grade bolts were used to fasten the bottom plate in place, following a modest application of silicone between the aluminum plates. With the help of approximately 15 volunteers, the tank was then laid over and pushed back up, thereby righting itself back into its correct orientation.

The inlet and outlet holes were drilled approximately 2 ft up from the bottom of the tank on each end plate. The holes were tapped and 1/4 in. brass ball valves were installed to control the flow in and out of the tank. End filters for the tank were then constructed out of aluminum screen and fiberglass. A 7.5 in. × 4 ft

piece of aluminum screen was folded into thirds. A very thin piece of fiberglass insulation was then pulled into a thickness of approximately 2 to 3 mm. The fiberglass piece was then placed into the aluminum screen, which was subsequently folded onto itself. After three months of construction, the tank was leak tested and patched in order to maintain a watertight seal.

B.1.1.3 Large Tank Methods

The 16 ft tank was packed (from the bottom to the top) with a 12 in. layer of the field soil collected from the Naval Air Station Fort Worth (NASFtW), Air Force Plant 4 (AFP4) site, a 28-in. layer of #30 laboratory sand, and 2 in. of bentonite clay. Compacting the soil material in 3 in. lifts with a metal rod achieved uniform packing. As discussed previously, the tank has two constant head reservoirs at each end, and a clay layer at the top was established to simulate confined aquifer conditions. The initial source zone consisted of a 2 in. x 2 in. x 2 in. coarse inclusion of #16 laboratory sand. A thin (1 mm ID) piece of Teflon tubing was glued to 5 in. of 1. 5 mm ID thin-wall glass tubing with epoxy: the glass-tubed end of this tubing was allowed to rest on the surface of the #16 sand to provide an injection point for the DNAPL.

Based on the results from the 2-ft tank studies (described in the Section B.1.3), the source zone will be excavated and repacked to mimic the conditions of the 2-ft tank source architecture. Also, the source zone is being repacked to capture the dissolution of the DNAPL from the source zone using X-ray analysis. The size of the large tank prevents it from fitting into the frame of the X-ray equipment. A gamma-ray instrument will be available to analyze prescribed points within the source zone, so that validate the correlation of data from the X-ray measurements.

Thin diameter glass monitoring wells will also be installed at locations downstream of the source zone to monitor migration of the downstream DNAPL plume both spatially and temporally. Liquid samples will be taken both from the sampling wells and the effluent. Upon completion of the experiment, the 16-ft

tank will be destructively sampled in place using a split spoon sampler that has been developed that will allow soil samples to be cored and frozen in-situ using liquid nitrogen. Soil sample cores will be analyzed to complete the mass balance of the DNAPL within the tank domain.

B.1.2 Intermediate Tank (8 ft)

B.1.2.1 Intermediate Tank Objectives

The large experiments allow for the representation of test domains at larger scales to study the matrix diffusion in both the source zone (where the DNAPL is entrapped in free phase) and in the plume. However, there were a number of factors that required the research team to limit the number of large tank experiments. The first is that the large tank experiments were difficult to set up and time consuming. Also, as real contaminants are used, these tests produce large volumes of contaminated soils that require disposal. Another limitation was associated with the testing method available to measure the source zone DNAPL saturation. Two methods are used to measure DNAPL saturation in the laboratory: the first uses gamma energy attenuation, and the second uses X-ray attenuation. In our past work, we have shown that the X-ray methods provide more accurate measurements compared to gamma. The available space allows for the placement of much smaller test tanks in the X-ray test platform. Hence, more accurate source zone characterization could only be done in smaller test tanks. A set of experiments was conducted in intermediate scale test tanks placed on the X-ray test platform.

The objective of these intermediate scale tank experiments was to evaluate the phenomenon of matrix diffusion in a smaller test domain than the Large Tank, thereby allowing more experiments to be executed in less time, with less generation of waste, and with more accurate source zone characterization. Also, the Intermediate Tank size allowed for sufficient soil volume downgradient of the NAPL source zone so that the effects of matrix storage could be observed. The observations from the Intermediate Tank will be used during packing and

execution of the Large Tank to maximize the productiveness of the Large Tank experiments. Additionally, the Intermediate Tank allowed for the calibration of a numeric model to be used for subsequent Large Tank experiments.

B.1.2.2 Intermediate Tank Design

The dimensions of the tank were 244 cm in length × 60 cm in height × 5 cm in width. The bottom of the tank consisted of an aluminum plate. The sides of the tank were formed by affixing clear polycarbonate walls on top of the aluminum plate at a distance from each other that created the 5 cm width of the tank. One-eighth in. glass was adhered to the walls of the polycarbonate sides to prevent any sorption of the source contaminant to the polycarbonate. Stainless steel sheets reinforced by particleboard backing formed the endplates of the tank. In order to prevent leaking, GE Silicone II silicone caulk was applied to all areas of contact between any two sections of the tank, prior to contact. The pieces were then held in place by the tightening of 52 bolts placed at regular intervals along the bottom and along the four sides of the tank. For rigidity, two small aluminum plates spanning the width of the tank were bolted across the top.

Brass fittings were inserted through the stainless steel endplates to allow for flow in and out of the tank. To keep the soil from washing out of the tank via the brass fittings, filters consisting of fiberglass wrapped in a stainless steel wire mesh attached to aluminum channels by small screws were designed for each end. Many holes were drilled into the aluminum channels to minimize flow restrictions. A filter was inserted into the tank near both the influent and effluent ends, which produced a space between the end of the tank and the soil of approximately 1.25 cm. Upon saturation of the tank with water, this space created small reservoirs at both ends of the tank that enabled uniform flow for the entire length of the tank.

The flow of water into and out of the tank was controlled by custom constant head devices. These constant head devices were comprised of an aluminum plate roughly 6 × 4 in. with two holes drilled through it. Brass nozzles were

threaded into the holes of the plate from underneath. A PVC cylinder 4 in. tall and slightly larger in diameter than the holes in the plate was glued to the top of the plate over the hole nearer the center of the plate. A second PVC cylinder 3 in. tall and wide enough to fit over both holes in the plate was glued to the top of the plate as well. For the influent constant head device, vinyl tubing was used to connect the inner brass nozzle to the inlet of the tank. During execution, de-aired tap water was pumped to the inner PVC cylinder at a rate that kept the cylinder full and produced a small amount of overflow. The overflow was retained by the outer PVC cylinder. The outer hole in the aluminum plate allowed for the overflow to escape via additional vinyl tubing and return to the supply of de-aired tap water. For the effluent constant head device, the inner nozzle was attached to the outlet of the tank. The water from the filled tank supplied the effluent constant head device via this connection. The overflow from the inner PVC cylinder was captured and measured in order to ascertain a flow rate for the tank. The head of each constant head device was adjusted by raising or lowering the devices separately. For the experiments performed, a head drop of 2.5 cm over the 244 cm tank was selected to emulate field conditions at the NAS Forth Worth site.

B.1.2.3 Intermediate Tank Packing

The tank was filled with water to ensure that there were no leaks. After the tank was drained, the process of packing it with sand began. The first packing was a simple-layered heterogeneous architecture. This packing configuration represented a situation where the DNAPL accumulated at the interface of a coarse and a fine sand layer. The bottom one-third of the tank was packed with F140 sand: a very fine sand that is used in sandblasting applications. Due to its fine texture, F140 sand has a permeability of 432 cm/day (as determined via constant head test performed as part of this research), which is similar to field silts. This was the desired trait because the bottom layer in the packing was intended to behave like an aquitard, or layer of relatively low permeability. The top two-thirds of the tank was packed with F30 sand. This is a fairly coarse sand

with a much higher permeability: 12,500 cm/day (Illangasekare et al., 1995) than the F140 sand. Thus, the F30 sand represented the aquifer atop the aquitard.

The desired placement for the NAPL was at the interface of the two sands near the inlet side of the tank. In order to best achieve this placement, a small coarse inclusion was created at the interface of the sands and 43 cm from the influent end of the tank. The coarse inclusion consisted of F16 sand in the shape of a $1 \times 1 \times 5$ cm block that ran the entire width of the tank. The coarse inclusion was constructed by placing two small metal spacers that were attached to a wooden beam into the tank at the desired location along the F140/F30 sand interface. Once the metal spacers were in position, F16 sand was dropped into the space until the desired height of 1 cm was reached. During this procedure, a 0.2 cm inner diameter glass tube was held in place such that one end of the tube was in the coarse inclusion and the other end rose above the height of the tank. This tube served as the pathway for the NAPL during injection. The spacers were removed once enough F30 sand layer had been packed to ensure that the F16 coarse inclusion did not fall to the sides. The glass tube was held in place throughout the F30 packing.

Once the F30 was completely packed, a 2-inch-thick layer of wet bentonite was pressed on top of the F30 sand. This created a virtually impermeable layer on top of the aquifer. When the constant head devices were raised so that their heads were greater than the lower elevation of the bentonite, the aquifer became a confined aquifer. This was a desired characteristic that promoted uniform, horizontal flow.

For each of the sands, a homogeneous packing was attempted through a procedure wherein approximately three in. of sand were placed in the tank and then a small-diameter rod was used to push and mix the sand from the top into previously laid layers.

After the tank was fully packed in dry conditions, flow was allowed to enter the tank slowly. To minimize entrapped air, the head was brought up slowly, which

forced the air to exit via the reservoir at the effluent end of the tank. Following full saturation, flow was allowed to continue for two weeks prior to NAPL injection to remove any remaining entrapped air.

B.1.2.4 Intermediate Tank – NAPL Injection

The injection of the NAPL was a critical procedure for all of the experimental tank studies. Due to the nature of the experiment, any mishap in the NAPL injection that resulted in unknown NAPL mass being introduced in the tank would delay the experiment until sufficient time had passed to allow for the NAPL to dissolve and to be recovered in the effluent. Therefore, extreme care was taken during the NAPL injection.

The NAPL was dyed with Sudan IV red dye at a ratio of 0.0005 mg Sudan IV to 1.0 mg NAPL. The NAPL was then withdrawn into a gastight syringe. A three-way valve was fitted to the syringe and the mass of the apparatus was observed. Next, a second syringe with a few milliliters of de-aired tap water was fitted to the three-way valve. Then, the entire apparatus was moved into position directly over the glass tube that jutted out from the top of the tank. The third connection on the three-way valve was attached to a needle that had been previously fitted via epoxy to the end of the glass tube. Once the apparatus was tightly connected to the needle on the glass tube, the air in the glass tube was extracted by withdrawing the water syringe slightly and slowly. After visual inspection determined that the air had been removed from the glass tube, the desired amount of NAPL was infused from the gastight syringe. Next, to avoid volatilization losses of the NAPL to the air, a small amount of water was infused into the glass tube such that the NAPL was forced lower into the tube and nearer the source zone. Finally, the mass of the apparatus was observed again after the water syringe was removed and the needle affixed to the glass tube was disconnected. The difference in masses was equal to the mass of NAPL injected.

B.1.3 Small Tank (2 ft.)

B.1.3.1 Small Tank Objectives

The specific objective of the small tank work was to examine how the degree of DNAPL saturation in the source zone affected the mass transfer into the low permeability layer (Process 2) relative to the mass transfer via dissolution into the aquifer (Process 1). The smaller tank enabled more detailed study of the factors affecting matrix storage near the source zone because multiple experiments could be performed in a shorter period of time with different soil types and different levels of DNAPL saturation in the source zone. In addition to the decreased size of the tank, the size of the source zone was increased from the intermediate scale experiments. This provided enhanced resolution of the source zone, thereby enabling testing of the hypothesis that DNAPL saturation levels, both initially and over time as dissolution occurs, in the source zone impact the mass transfer rate into the zone of lower permeability. Also, utilization of the small tank removed the unwanted downgradient effects of matrix storage from the experiments.

B.1.3.2 Small Tank Design

The design and construction of the Small Tanks closely followed that of the Intermediate Tank. Both had an aluminum bottom and polycarbonate walls with glass lining. The end filters were the same, as were the brass plumbing fittings at the ends. The constant-head devices were also identical for the tanks. The only difference in construction materials between the Small Tank and the Intermediate Tank was in the endplates. Whereas the Intermediate Tank had stainless steel endplates reinforced with particleboard, the Small Tanks had aluminum endplates reinforced with polycarbonate. This change was due to the easier machining capabilities of the aluminum versus the stainless steel. The main differences from the Intermediate Tank were the dimensions of the Small Tank. The Small Tank was 60 cm in length, 40 cm in height, and 2.5 cm in width.

EXPERIMENTAL METHODS OF OBSERVATION

This section describes the experimental methods of observation that were used for all of the tank studies.

B.1.4 X-ray Photon Attenuation

The Center for Experimental Study of Environmental Processes (CESEP) X-ray system is based upon an automated positioning frame, an X-ray tube, and a photon detector. The positioning frame moves the source and the detector in a horizontal-vertical (XZ) plane. At all times, the X-ray source and detector are kept in a co-linear arrangement. As shown in Figure B-1, the frame allows for precise and repeatable positioning over an area roughly 10 feet long $\times$ 4 feet high, with an internal clearance for objects up to 14 in. wide.

Custom LabVIEW software has been developed to provide automated movements synchronized for data collection. Experience has shown that typical movement times are less than twenty seconds with sub-millimeter positioning accuracy and repeatability.

Figure B-1. CESEP X-ray system.

The X-ray source is a Pantak model HF100 tube: an industrial unit originally designed for high-photon-flux applications such as the characterization of cracks in welds and castings. (More details can be found at www.ndt.agfa.com.) With a maximum operating range of 100 kV potential, 3 kW power, and a variable collimation, the unit is capable of saturating the photon detector under all reasonable operating conditions. Thus, the system is “detector flux rate limited” and the detector electronics and the motor positioning speeds, not the photon production rate, largely determine measurement times.

The third component of the X-ray system is a high-performance Germanium (HPGe) detector manufactured by Princeton Gamma-Tech (www.pgt.com). Like most modern HPGe models, the unit has high (>90%) quantum efficiencies for photons under 100 keV, and is capable of total photon observation rates approaching 100,000 events per second. However, control on the X-ray source and filtering must be implemented to remain within a linear response regime and limit total photon fluxes at the detector to less than 50,000 events per second: the “detector flux rate limited” situation.

B.1.4.1 Methods

The chosen experimental strategy for X-ray analysis is straightforward and makes best use of the CESEP lab's unique X-ray capabilities. By measuring both the effluent concentrations and the DNAPL persistence within each tank’s source zone, inferences can be made regarding the nature of the source of observed down-stream contaminants. In addition, X-ray measurement has the following benefits:

(1) It does not in any way disturb the flow field, so one cannot claim that contaminants are unnaturally driven into the low-permeability regions by sampling or other flow-field disturbances.

(2) It is a relatively direct observational approach that allows for certain mass-balance consistency checks.

(3) The direct measurement of DNAPL presence shows the actual rate of dissolution (a process that is very difficult to estimate *a priori*) and makes it easier to infer the source conditions.

(4) The relatively large size of the tanks helps to overcome scaling problems inherent with smaller (i.e., column-based) experiments.

X-ray analysis has the following drawbacks:

(1) The procedure requires relatively long observation times (weeks to months) to monitor a relatively small source zone.

(2) The limited size of the X-ray framing precludes the setup of many simultaneous experiments.

(3) The aforementioned size, space, and time requirements make it difficult to quickly replicate individual experiments.

Unlike natural gamma sources, the X-ray system provides minutely tune-able spectra through the selection of tube voltages, currents, and filters. This capability means that X-ray spectra can be produced that maximizes the information gathered per measurement time. For the experiments described here, relatively broad (30 to 70 keV) spectra were produced with the help of Samarium and Erbium filters placed within the source cabinet. Using the tuning variables previously discussed, the overall system was configured as a balance between two conflicting goals:

(1) Minimization of the total measurement time required at each location to observe numerous locations (and thereby infer spatial DNAPL distributions with some level of detail), and

(2) Maximization of the overall accuracy/precision of each individual measurement.

As described in Hill et al. (2002), counting times and accuracy are inversely related, so a trade-off between the two is necessary. After much trial-and-error, a configuration that appeared to give good overall results was chosen:

(1) A 2-mm diameter collimated beam;

(2) Spectral filters composed of varying path lengths of samarium, erbium, and aluminum;

(3) A tube voltage of 70 kV and a tube amperage of 10 mA; and

(4) Measurement (or “live”) times between 5 and 10 seconds and

The above configuration was used for all the X-ray experiments presented here.

B.1.4.2 Results

Figure B-2 presents the X-ray data from the 8 ft tank source zone, showing TCE dissolution in 10 to 11 days.

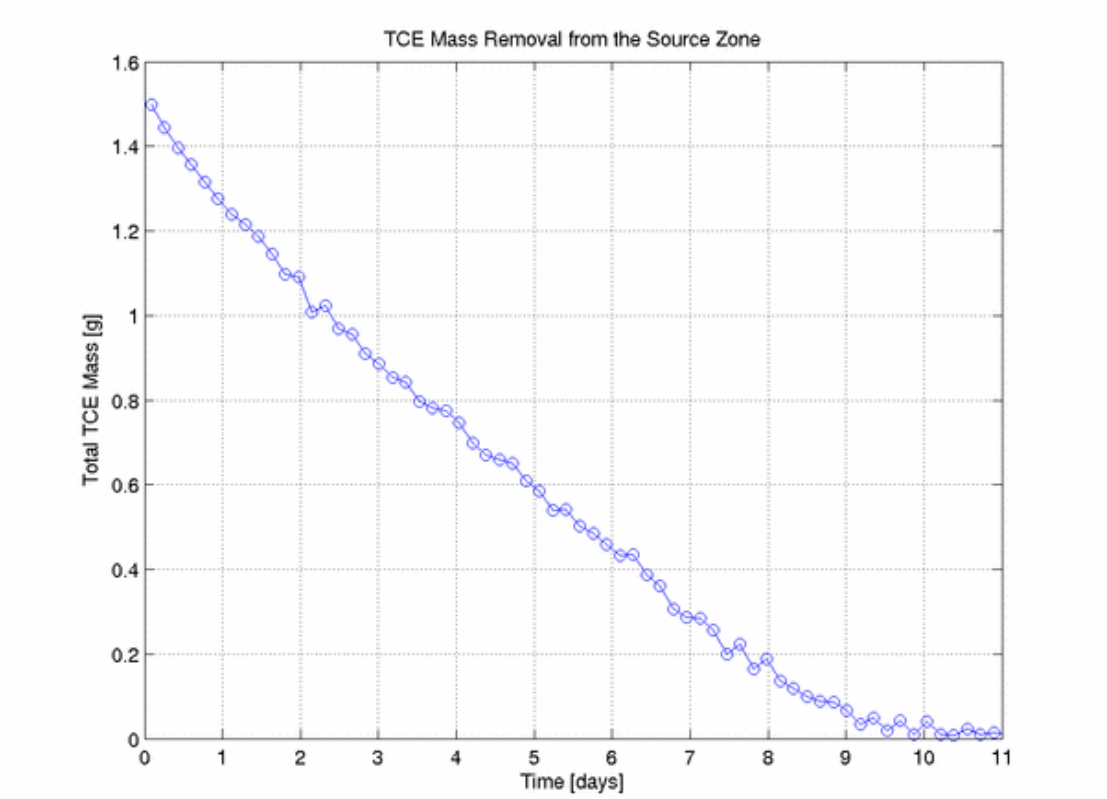

Figure B-2. TCE Source Dissolution as Measured by X-ray Analysis.

The X-ray data from the 8-ft tank in Figure B-3 shows 1,1,2-TCA dissolution in 7 to 8 days.

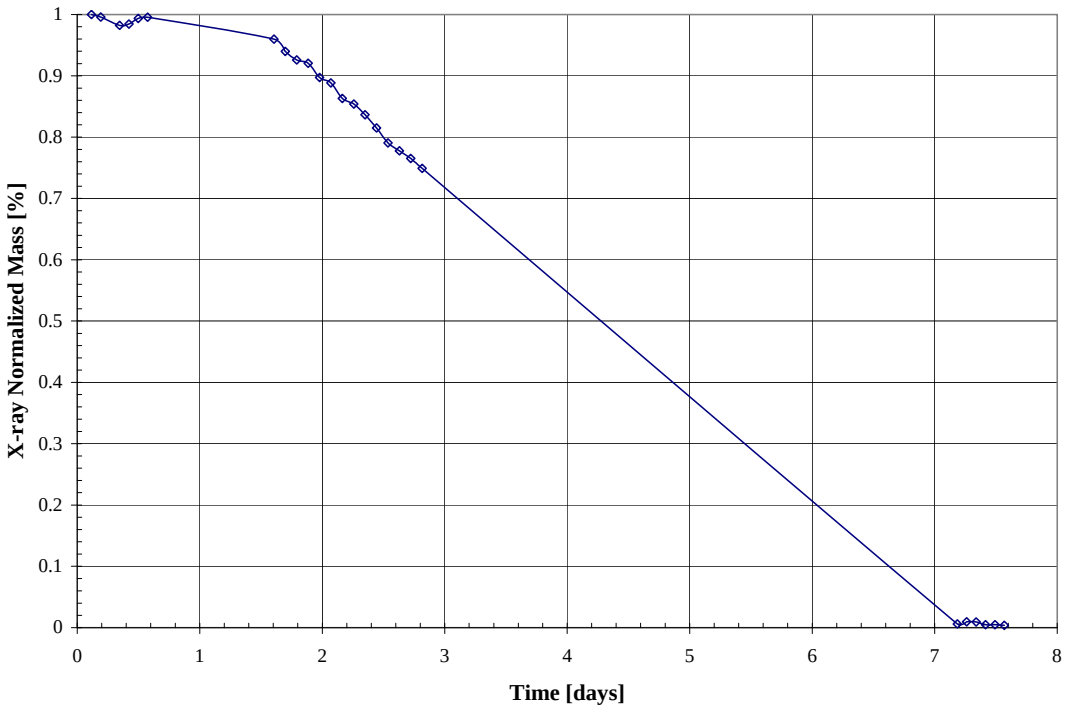

Figure B-3. 1,1,2-TCA Source Dissolution as Measured by X-ray Analysis.

Based upon the measurement data, the standard deviations for DNAPL path lengths are in the range of 0.05 to 0.2 mm. For the TCE experiment, the initial mass injected (as determined by gravimetric procedures) was 1.53 +/- 0.02 g and the mass measured by the X-ray during the first full scan (4 hours data) was 1.498 +/- 0.025 g, resulting in a 2% mass balance error. For the 1,1,2-TCA experiment, the initial mass injected (as determined by gravimetric procedures) was 4.24 +/- 0.02 g. A sub-component equipment failure of the X-ray at day 3 made the determination of an accurate mass balance impossible. However, after the X-ray was repaired and restarted, it was seen that the 1,1,2-TCA mass had completely dissolved from the source zone at approximately day 7.

B.1.4.3 Conclusions

Our results suggest that at our scale of observation (centimeters), dissolution of common DNAPL contaminants proceeded in a relatively quick and nearly linear fashion. The data suggest that DNAPL blobs or pools are not particularly long-lived and thus are not a long-term source of DNAPL contamination.

In spite of the relatively quick (<10 days) decimation of the DNAPL pools and residuals, downstream concentrations remained well above USEPA maximum contaminant levels (MCLs) for weeks to months. The disconnect between relatively quick DNAPL dissolution and long downstream tails is best explained by matrix storage, which may be the most significant storage/source mechanism and thus deserves consideration at field sites.

B.1.5 Effluent Sampling and Measurement

Obtaining the data needed to evaluate effluent aqueous concentration versus time from the NAPL injection and to calculate the NAPL mass that had dissolved and migrated out of the tank required collecting many samples of the effluent. Moreover, since the focus of the research was on the matrix storage capability of the experimental tank setups, each experiment was performed for many weeks to capture the data necessary to evaluate the significance of this process as represented by a long, low level tail of the effluent concentration.

Once injection of the NAPL source occurred, effluent sampling began. Initially, a sample was taken every 20 minutes. This frequency continued for several days and was performed so that the initial breakthrough curve of the dissolved contaminant could be well characterized. After the initial breakthrough curve was captured, sampling frequency decreased over a period of seven to ten days until samples were only taken two or three times a day. The low sampling frequency was sufficient to capture the slow, relatively steady effluent concentrations that were observed during the long process of the release of the contaminant mass that had been stored in the low permeability region of the soil matrix.

Each sample was analyzed via a GC. The first Intermediate Tank experiment used 1,1,2-TCA as the injected NAPL and hexane extraction for the sampling protocol. A known volume of hexane was infused into a sealed vial. A known volume of the effluent sample was then added to the vial. Due to the hydrophobicity of the 1,1,2-TCA and its relative affinity for the hexane, the 1,1,2-TCA partitioned into the hexane. After a minimum of three hours had elapsed, the hexane was extracted into a vial that was subsequently evaluated on the GC using the Electron Capture Detector (ECD). The GC provided the 1,1,2-TCA concentration in the hexane. Since the mass of hexane and the mass of effluent in the original vial were known, the concentration provided by the GC was used to calculate the concentration in the effluent. Therefore, effluent concentration versus elapsed time could be plotted and evaluated.

The hexane extraction technique required many manual steps: dispensing the hexane, measuring the mass of the hexane in the sample vial, measuring the mass of the effluent in the sample vial, and extracting the hexane into another vial ready for the GC. As switching to a protocol using aqueous samples directly on the GC would reduce the manual labor required for each experiment, a method using the Flame Ionization Detector (FID) was developed. The FID is capable of analyzing aqueous samples; the ECD is not. A study to compare the accuracy of the two sampling protocols was performed using additional samples from the Intermediate Tank effluent. Consecutive samples were obtained using alternating techniques (first hexane extraction and then direct aqueous sampling). The samples were then evaluated using their respective methods on the GC. The results indicated less than a 10 percent difference between the two sampling protocols on average. Therefore, hexane extraction was abandoned for later experiments and direct aqueous sampling was used.

The effluent concentrations were also used to determine the total mass that had been recovered in the effluent. This was achieved via numerical integration of the area under the curve of the effluent concentration versus effluent volume plot using the Trapezoid Method approximation, consisting of the following formula:

$$(Conc(t = x) + Conc(t = x + \Delta t)) * (x + \Delta t - x)/ 2$$

B.1.6 Flow Rate Measurement

To obtain the flow rate of the groundwater in the tanks, the effluent was captured in a 5-gallon bucket and its mass was observed and calculated by subtracting the mass of the empty bucket. The effluent was then disposed into an approved waste container for subsequent removal from the lab. By recording the elapsed time at each effluent mass observation, a flow rate of the groundwater in the tank was determined.

B.1.7 Soils Acquisition and Properties: NAS Forth Worth/AFP4

B.1.7.1 Experimental materials and methods

In November of 2002, eleven 55-gallon barrels of soil were collected from a NAS Fort Worth mound excavated as a result of a reactive barrier installation at the site. Care was taken to collect only soil from below the topsoil; organic material was avoided where possible. Once the soil was returned to the lab it was prepared for testing in a three-step process. First, the soil was laid out and allowed to air dry at room temperature. After 24 to 48 hours, the soil was hand ground in preparation to be sieved in a mechanical shaker. The mechanical sieve was constructed as shown in Table B-1.

Table B-1. Mechanical Sieve Apparatus.

Screen Location	Sieve #	Sieve Size
Top	18	1.0 mm/0.0394 in.
Middle	40	425 um/0.0165 in.
Bottom	50	300 um/0.0117 in.

The purpose of the mechanical sieve was to separate the field soil into two primary fractions: 1) a silty-sand and 2) a silt. Several physical and chemical

analyses were then performed on the field soil fractions and on the #140 laboratory sand obtained from Manley Bros. of Indiana. This section of the report presents the results of the grain size distribution analysis.

B.1.7.2 Results

The results of a grain-size-distribution test on the field silty-sand fraction, performed in accordance with ASTM-D-422, are shown in Figure B-4. The following sieve sizes were used in accordance with ASTM-D-422: #200 (0.075 mm), #140 (0.106 mm), #60 (0.250 mm), #40 (0.425 mm), #20 (0.850 mm), #10 (2.000 mm), #4 (4.750 mm) and a 3/8 in. (9.50 mm).

The results of the grain-size distribution performed on the #140 laboratory sand are depicted on Figure B-5. The properties of #140 laboratory sand are anticipated to be similar to that of the field silt. As is seen in Figures B-4 and B-5, the D_{50} of the field sand is 0.38 mm and the D_{50} of the #140 sand is 0.1 mm.

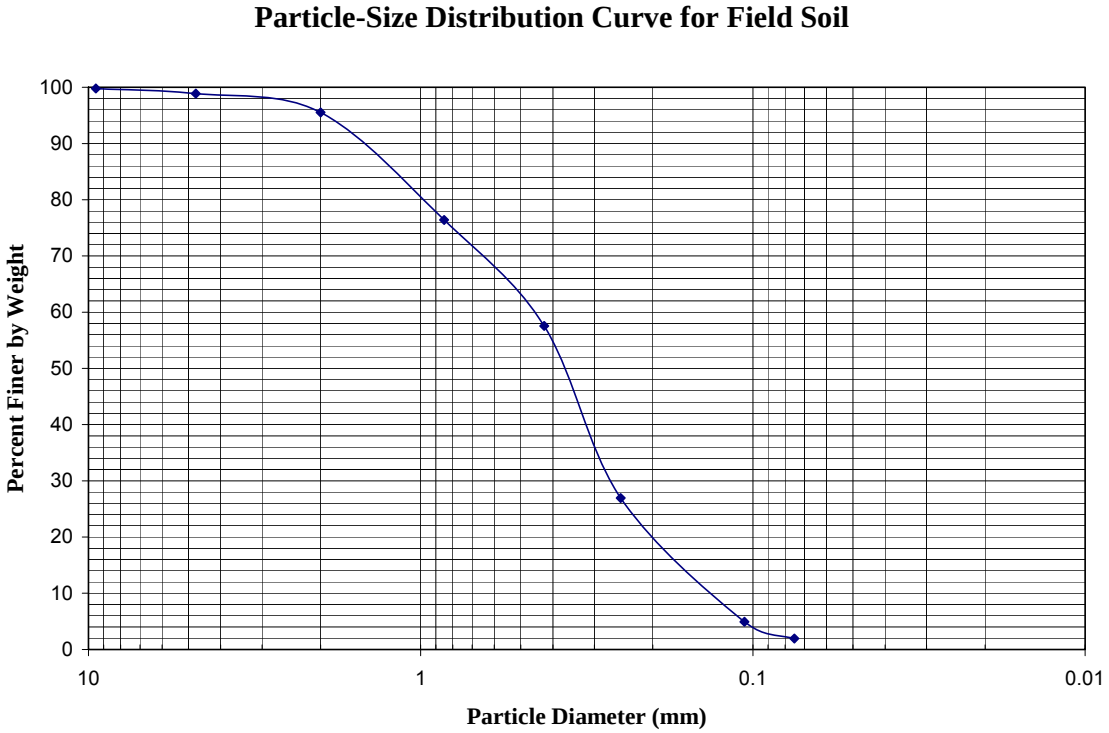

Figure B-4. Grain-size distribution for the field sand.

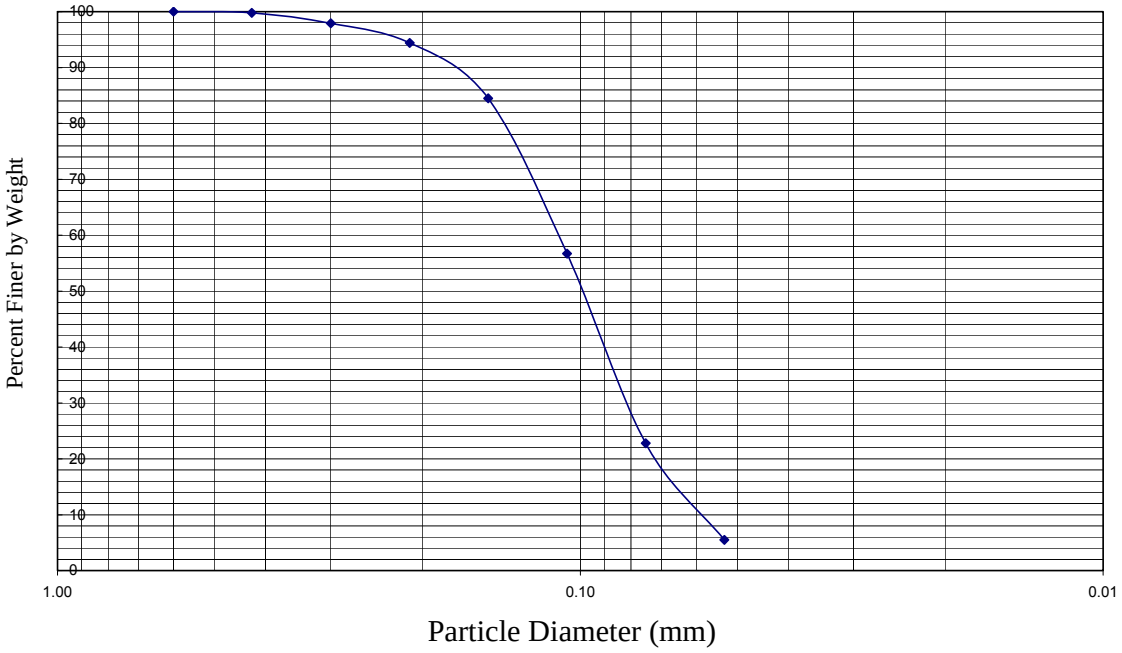

Figure B-5. Grain-size distribution for the #140 sand.

A mechanical analysis was performed on the field sand and field silt according to ASTM-D-422. The results of these analyses are shown in Table B-2.

Table B-2. Mechanical analysis results of field soil.

	% silt (0.074 to 0.005 mm)	**% clay (less than 0.005 mm)**	**% sand (>0.074 mm)**
field silt	76	24	0
field sand	1.4	0.5	98.1*
*fractionation of sand component	Coarse (2.00 to 4.75 mm)	medium (0.425 to 1.99 mm)	Fine (0.075 to 0.424 mm)
	4.5 %	38 %	55.6 %

EXPERIMENTAL PARAMETERS AND RESULTS

This section describes the experimental parameters that were recorded during each of the tank experiments performed. All experiments were performed at room temperature, which ranged from 65-73°F. Observed results are also included for each experiment.

B.1.8 Large Tank

B.1.8.1 Large Tank #1

The goal of the first intermediate-scale experiment was to test the first hypothesis of this research study. The first hypothesis states (see Section 3) that the generation of a contaminant plume in a textural heterogeneous system from the source zone is affected by (1) transverse advection from the DNAPL to the transmissive zone, (2) transverse diffusion into the silt layer through the pool, (3) longitudinal advection and (4) transverse diffusion into the silt from the plume. The simple layered system constructed for this experiment consisted of a #30 white silica sand obtained from Unimin Corporation in Emmett, ID overlying a field soil obtained from the NAS Ft. Worth Site. The properties of the materials are shown in Table B-3.

Table B-3. Soil properties.

Media Type	Hydraulic conductivity (cm/day)	Retardation Factor	Mean grain size (mm)	Uniformity Coefficient
#30	15,000	1.0	0.49	1.5
Field	2,000	1.4	0.38	3.0

The tank was packed (from the bottom to the top) with a 5.1 cm bentonite layer, a 30.5 cm layer of the field soil, a 71.1-cm layer of #30 sand and 5.1 cm of bentonite clay (obtained from Wyo-Ben, Inc. in Billings, MT) was packed at the

top of the tank to establish confined aquifer conditions and to prevent volatilization of contaminants. Uniform packing was achieved by compacting the soil material in 7.6-cm lifts with a metal rod. The tank had constant head reservoirs at each end of the tank to establish the hydraulic gradient across the tank. The emplaced source zone consisted of a 5.1 cm x 5.1 cm x 5.1 cm coarse inclusion of #16 silica sand. A thin (1 mm ID) piece of Teflon tubing was epoxyed to 12.7 cm of 1. 5 mm ID thin-wall glass tubing and the end with the glass tubing was allowed to rest on the middle surface of the #16 sand to provide an injection point for the DNAPL. The remaining sections of glass and plastic tubing were packed into the soil layers, respectively.

Since the preliminary tank experiment was located in the main bay of the laboratory (located outside of the X-ray room) a separate small tank was packed and injected with 1,1,2-TCA in order to determine the 1,1,2-TCA dissolution rate for the dissolved mass leaving the source zone. Further discussion on the details of the small tank experiment may be found in Section 5 under Task 2. At the conclusion of the small tank experiment, the intermediate tank experiment was started.

After achieving steady-state flow conditions in the intermediate scale tank, approximately 14.82 g of Sudan IV dyed 1,1,2-TCA was injected into the source zone. The 1,1,2-TCA saturation in the source zone was calculated to be 34%. Liquid samples were collected from the effluent end of the tank and analyzed on a gas chromatograph (GC) using a flame ionization detector (FID) for 1,1,2-TCA. After approximately 40 days, tailing in the breakthrough curve for observed. The tailing was allowed to continue for an additional 40 days, until it was assumed that no further change in concentration would occur in the effluent. Flow to the tank was then stopped and the field soil was cored and approximately 400 samples were analyzed using a hexane extraction method on the GC using the electron capture detector (ECD). Upon completion of the soil core analysis, a complete mass balance for the tank was calculated.

Due to a problem encountered during the X-ray analysis of the small tank experiment, results of the small-tank experiments performed by (Wilking 2004) were interpolated to assume that the source zone had completely dissolved after approximately 14 days. Liquid samples collected from the effluent end of the tank are shown in Figure B-6. The figure displays long tailing, indicating non-ideal behavior. It is also interesting to note that even at 80 days, the 1,1,2-TCA concentration leaving the tank are still at 8 ppm, which is significantly higher than the maximum contaminant level (MCL) for 1,1,2-TCA of 5 ppb.

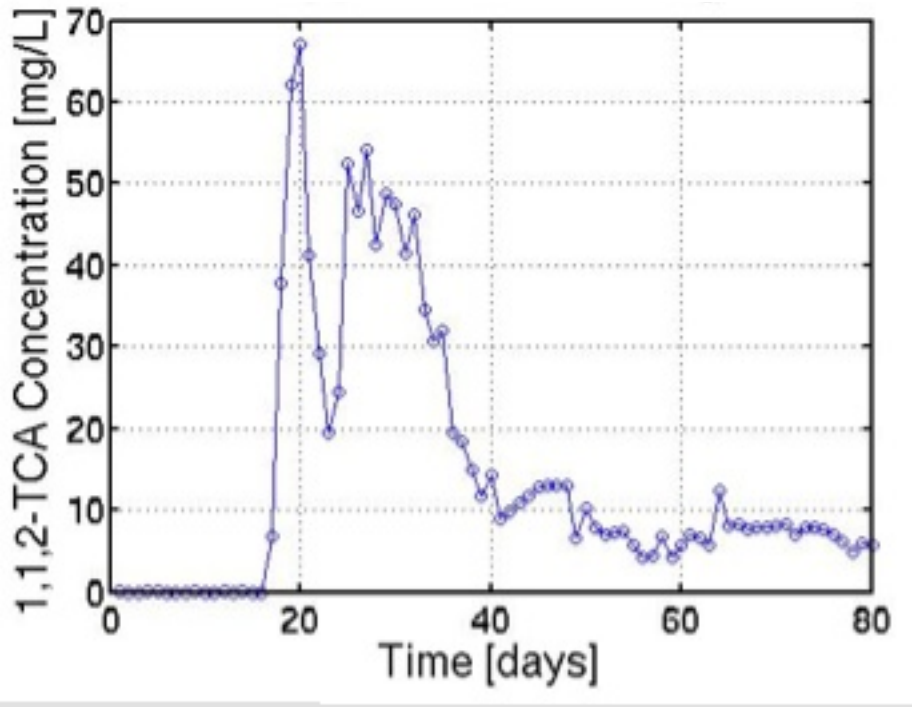

Figure B-6. Tank #1 1,1,2-TCA effluent curve.

As is shown in Figure B-7, at 80 days, 80% of the 1,1,2-TCA mass has been removed from the system, but 20% is unaccounted for. The results of the soil cores analysis are shown in Figure B-8.

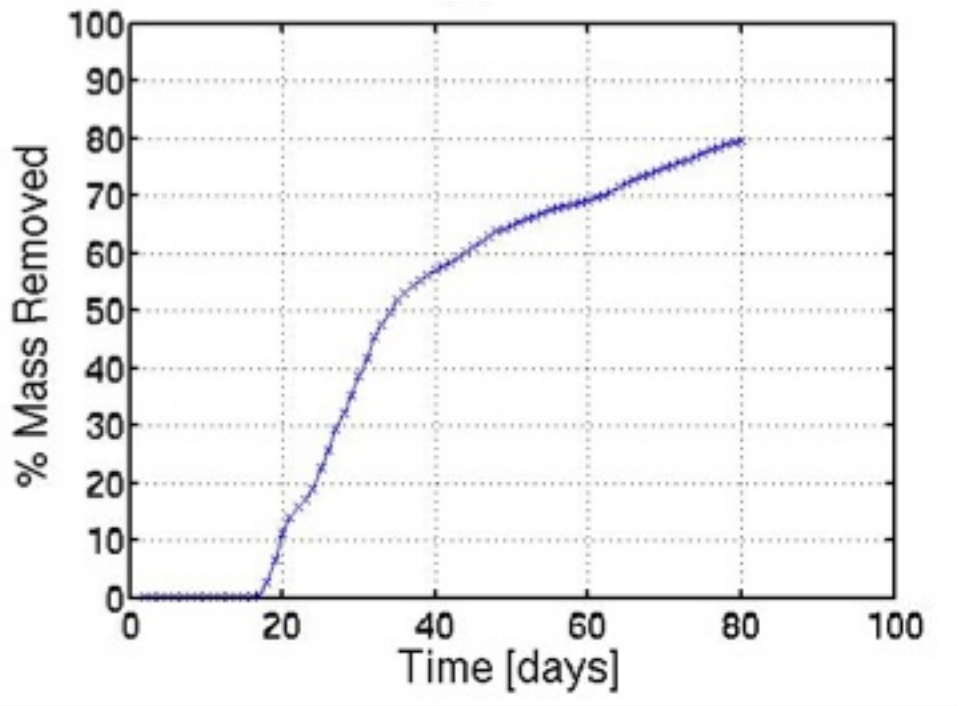

Figure B-7. Tank #1 1,1,2-TCA mass removed from tank.

Figure B-8 shows that the majority of the dissolved 1,1,2-TCA mass is contained in the field soil layer. This figure also supports the hypothesis that at greater length and time scales in a system containing orders of magnitude in difference in hydraulic conductivity, the lower conducting layer will act as a new contaminant source acting over the length of the entire layer. This may explain why contamination in groundwater wells at field sites is still observed, even after the source is known to have been depleted or removed.

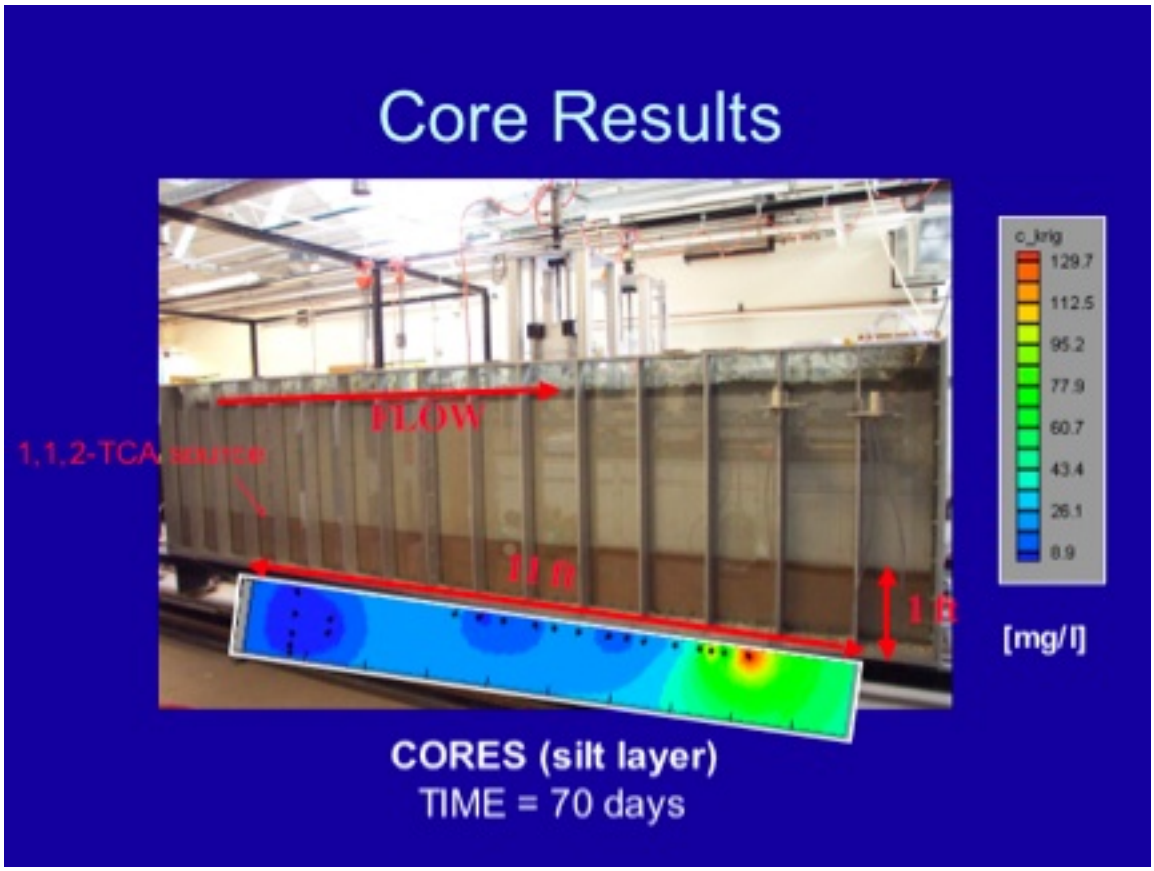

Figure B-8. Tank #1 1,1,2-TCA soil core results.

B.1.8.2 Large Tank #2

The second intermediate-tank experiment was conducted in the same tank as the first intermediate-scale tank experiment. The domain of this experiment included a low-permeability mound (field soil) embedded in a high permeability matrix (#50 sand) packed on a low permeability #140 sand layer. The source zone was packed with #16 sand. The material properties are shown below in Table B-4.

Table B-4. Soil properties.

Media Type	Hydraulic conductivity (cm/day)	Retardation factor	Mean grain size (mm)	Uniformity coefficient
#140 sand	400	1.0	0.10	1.86
#50 sand	3,500	1.0	0.31	1.94
#16 sand	51,000	1.0	0.96	1.73
Field soil	2,000	1.0	0.38	3.0

The primary objective of the second intermediate-scale experiment was to create a system that would have solute transported by both advective transport and by transverse diffusion. It was hypothesized that the mound would both affect the flow pattern through the tank, resulting in an attenuated breakthrough curve; as well as having dissolved mass going into the mound and then back diffusing into the system. This effect would also cause the breakthrough curve to be attenuated.

The tank was packed in the same manner as what was done for the first experiment. The flow in the tank was allowed to reach steady-state conditions prior to injection. Approximately, 59.6 g of 1,1,2-TCA were injected into the same dimension source zone as was used for the first experiment. The resulting 1,1,2-TCA saturation was calculated to be 42%. A second small-tank experiment was not used to determine the rate of dissolution from the source zone, as the data provided by Wilking (2004) was used again. Liquid samples were collected from the effluent and analyzed using the FID on the GC. Figure B-9 shows the breakthrough curve after approximately 80 days of analysis. As compared to the breakthrough curve obtained in the first experiment, the curve in Figure B-9 shows high attenuation of the dissolved mass, thought to be a direct result of the mound.

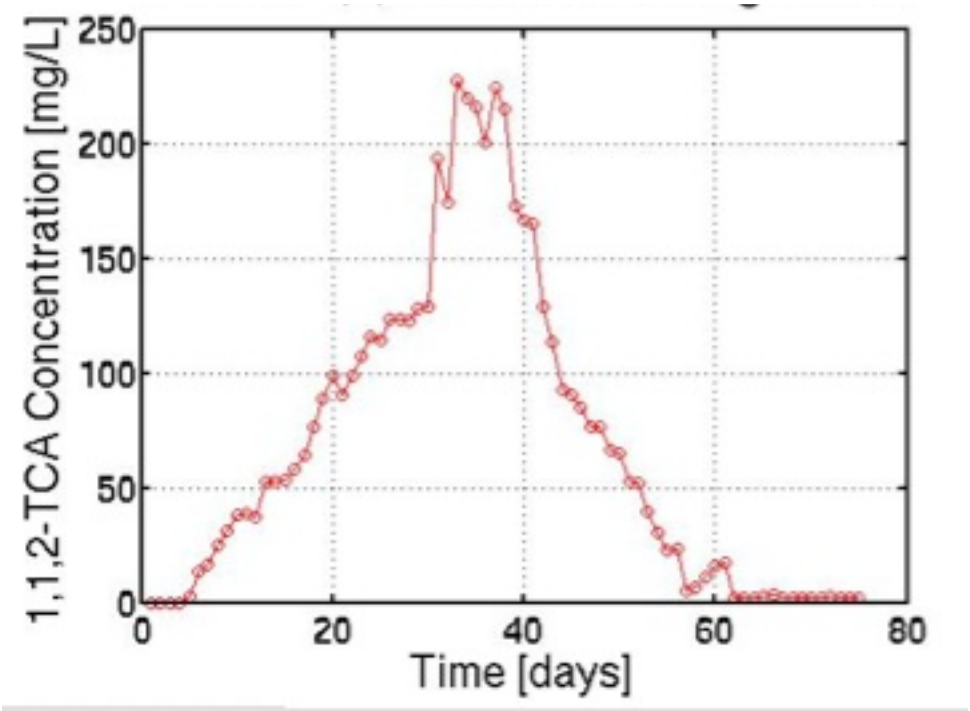

Figure B-9. Tank #2 1,1,2-TCA effluent curve.

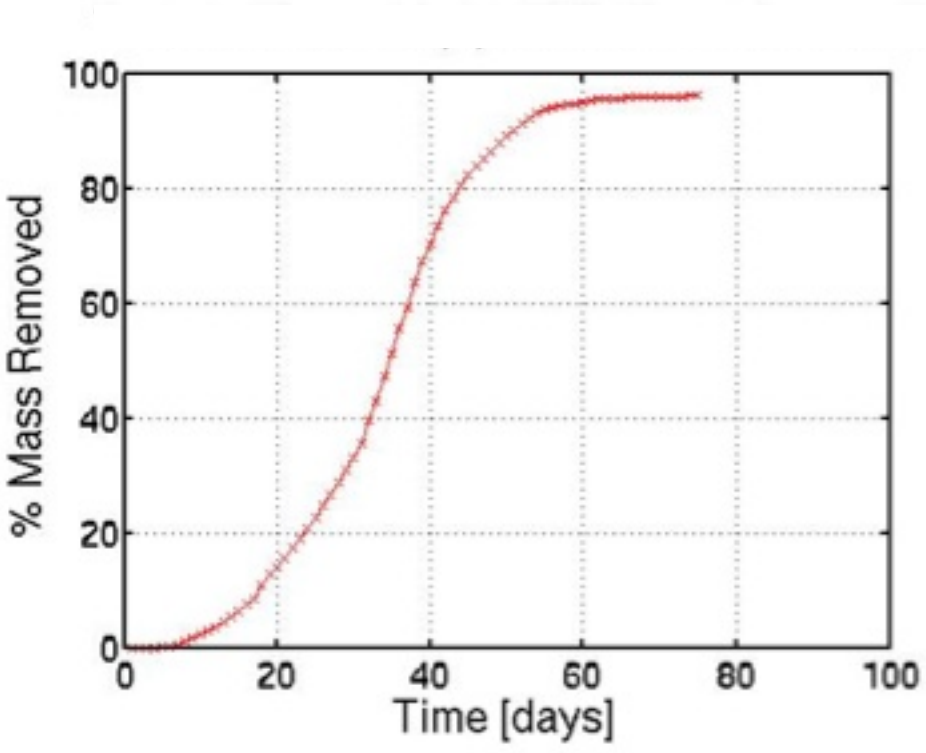

Figure B-10. Tank #2 1,1,2-TCA mass removed from tank.

Figure B-10 shows almost 97% mass removal from the system at the completion of the experiment. This experiment was thought to have greater mass recovery, because when compared to the first experiment, the available surface area of the field soil is only 550 cm^2 when compared to 1680 cm^2 of the first experiment. Almost three times as much surface area of field soil was available for mass to back diffuse in the first experiment as compared to the second experiment. In summary, this experiment showed that even a small amount of low-conductivity material could affect both the advective transport and transverse diffusion of a system.

B.1.8.3 Large Tank #3

For the final intermediate-scale tank experiment, a second tank was constructed in the frame of the X-ray machine. The major advantage of having the tank in the X-ray frame was to allow direct monitoring of the source during dissolution. The domain of this experiment included an inclined low permeability layer (field soil)

beneath a high-permeability (#30 sand) layer. The soil properties were the same as for what was described in Section 2. The objective of this experiment was the same as for the second experiment (advective transport and transverse diffusion dominated), but in addition a complex flow regime was added with the inclined plane. The field soil was packed at a 12% incline from the input of the tank to the output. The #30 sand was packed on top of the incline, with a #16 coarse sand inclusion for the source.

After achieving steady-state conditions in the tank, approximately 35.43 g of 1,1,2-TCA was injected into the tank. The 1,1,2-TCA saturation in the source zone was calculated to be 22%. Immediately after injecting the 1,1,2-TCA into the tank, the X-ray scans were started. For approximately 26 days (24 hours a day, 7 days a week), the source was scanned over 750 points. The source was not completely dissolved at 26 days, but the X-ray system had to be stopped due to a leaking roof near the X-ray power supply. After reviewing the data, it was assumed that the source was near complete dissolution and would have probably been completely dissolved in 28 days. For further discussion of the X-ray analysis, see Section 5.4.4. The effluent liquid data analyzed with the FID on the GC yielded the data shown in Figure B-11. The mass removed is shown in Figure B-12. To date, approximately 95% of the mass has been removed. It is interesting to note the amount of attenuation that has occurred due to the inclined plane in comparison with the first two experiments. The field soil has been cored and the analysis is in progress.

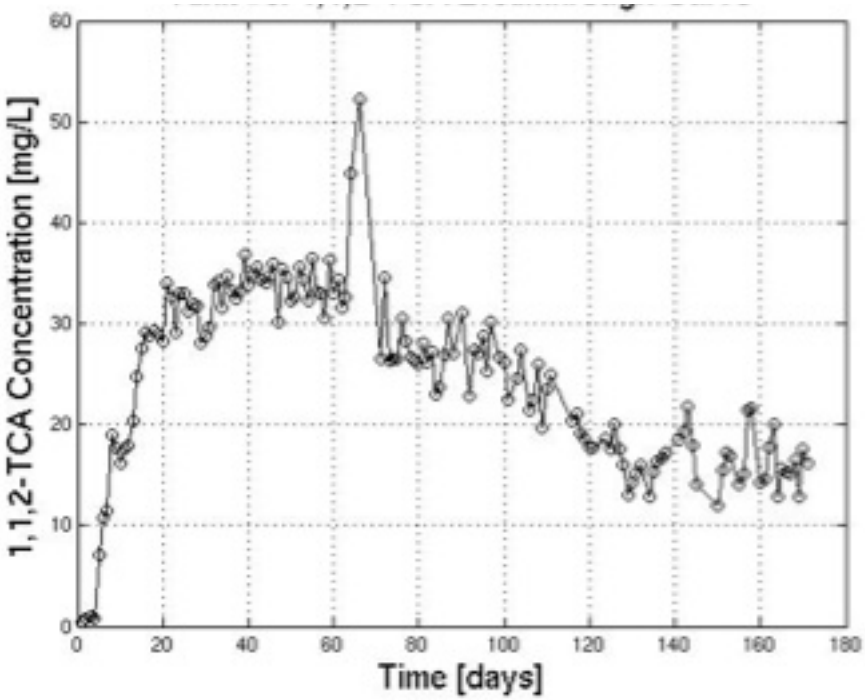

Figure B-11. Tank #3 1,1,2-TCA effluent curve.

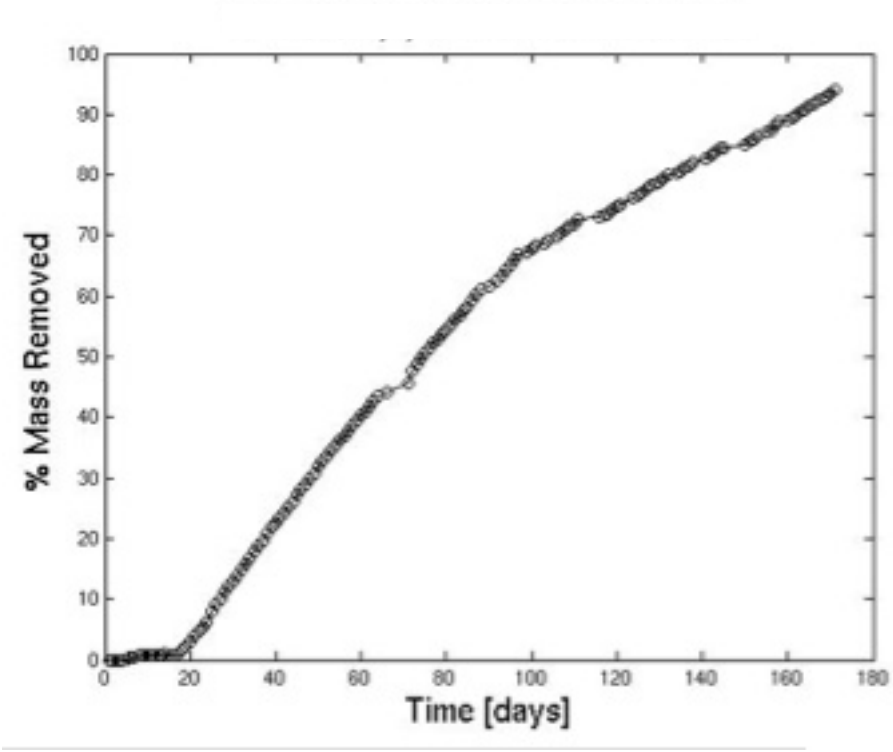

Figure B-12. Tank #3 1,1,2-TCA mass removed from tank.

B.1.9 Intermediate Tank

B.1.9.1 Intermediate Tank Experiment #1

Prior to NAPL injection, the coarse inclusion was scanned repeatedly using the X-ray system to provide pre-injection path-length data. Then, 4.24 grams of 1,1,2-TCA was injected into the coarse inclusion. The X-ray system was again used to scan the coarse inclusion post-injection. The intent was to scan the coarse inclusion continuously until the NAPL had completely dissolved. However, after two days of scanning, a hardware failure on the X-ray system caused system downtime until 7 days after the injection. Therefore, there was a gap in the X-ray data from day 2 until day 7. The data from day 7.5 clearly indicated complete depletion of the NAPL in the coarse inclusion source zone.

Effluent sampling using hexane extraction began immediately after the injection of the 1,1,2-TCA. Sampling continued for 61 days, at which time the 1,1,2-TCA

concentrations in the effluent were not detectable by the GC. Figure B-13 depicts the breakthrough of the aqueous 1,1,2-TCA in the effluent versus elapsed time from the NAPL injection. Figure B-14 illustrates the depletion of the NAPL in the source zone, as well as the 1,1,2-TCA mass recovered in the effluent. As can be seen in Figure B-14, 102 percent of the 1,1,2-TCA injected in the source zone was recovered in the effluent. The mass recovered was greater than the mass injected because of the errors in the hexane extraction sampling protocol. Hexane is highly volatile and therefore, some of the hexane will be lost to the air. Following Raoult's Law, when very small amounts of the 1,1,2-TCA partitioned into the hexane, the losses of the organic mixture to the air were over 99 percent hexane. Thus, the 1,1,2-TCA concentration in the hexane became greater as the hexane volatilized. These slightly overstated concentrations resulted in the observation of slightly more mass being recovered than was actually injected.

During the course of the experiment, the flow rate was measured to range between 15.0 and 16.5 L/day.

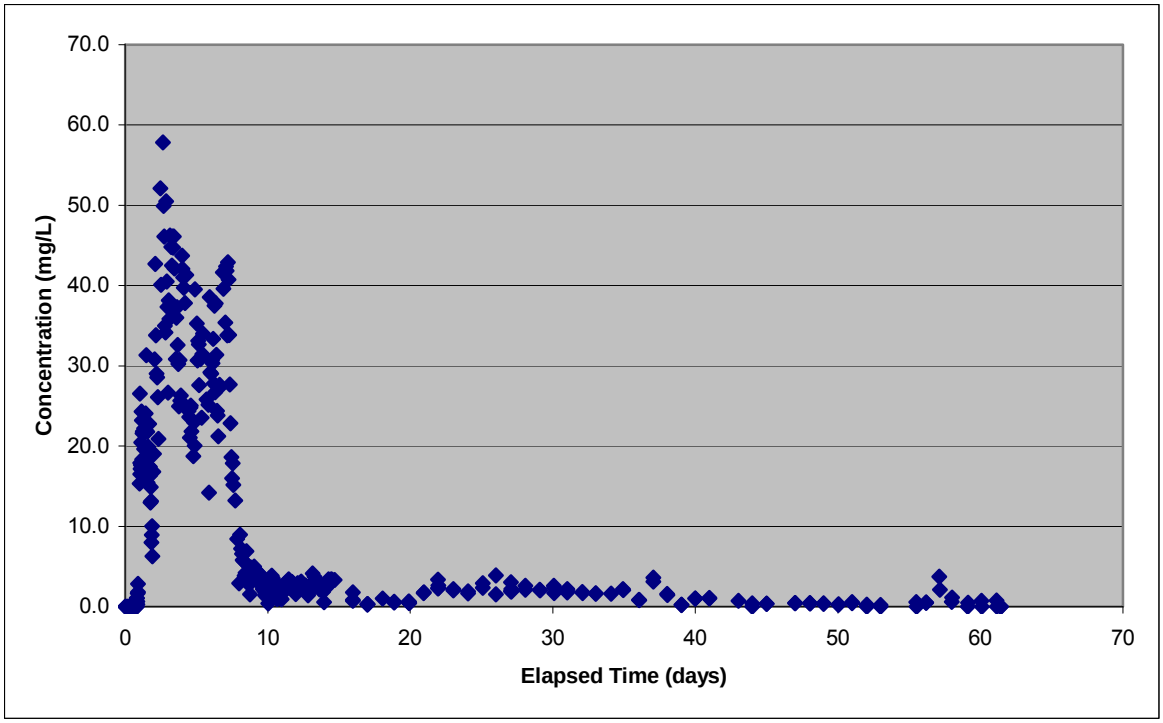

Figure B-13. 1,1,2- TCA Concentration in Effluent For Intermediate Tank Experiment #1.

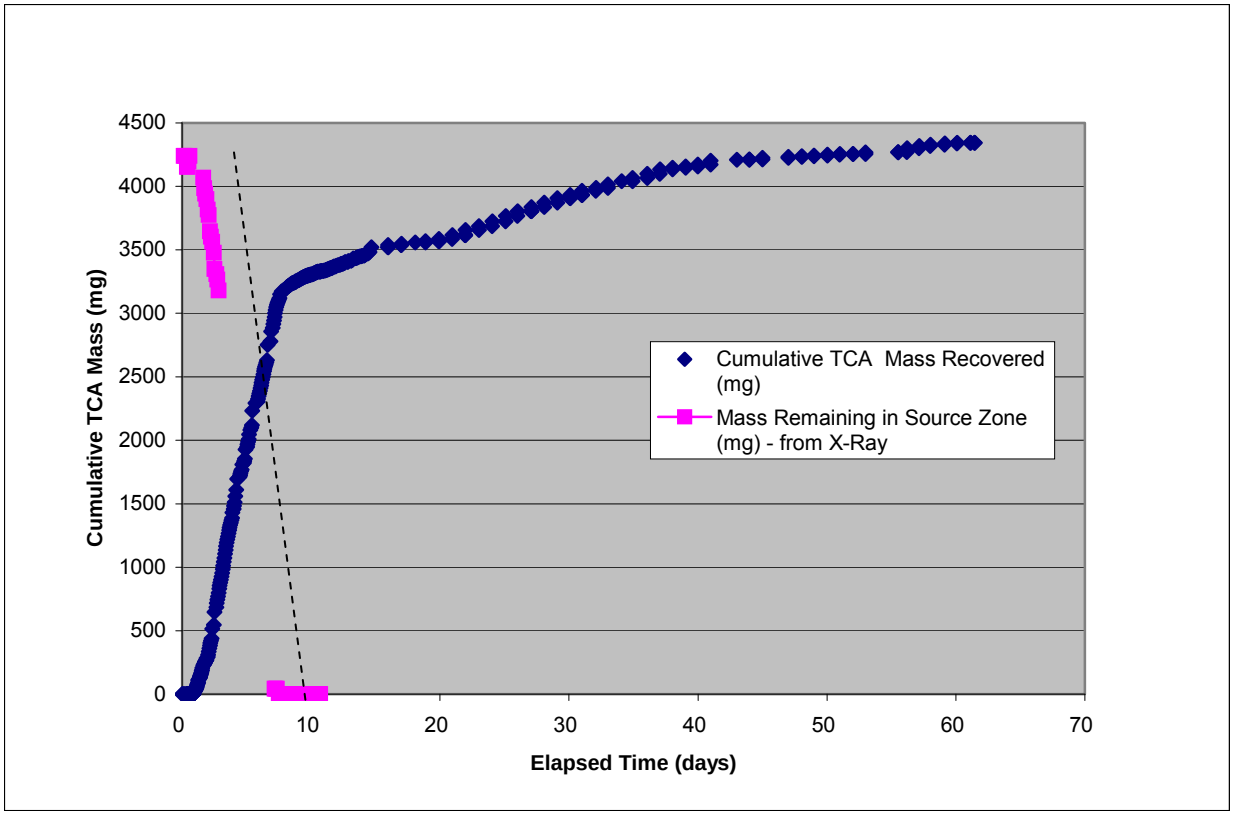

Figure B-14. Cumulative 1,1,2-TCA Mass Removed/ Recovered For Intermediate Tank Experiment #1.

B.1.9.2 Intermediate Tank Experiment #2

Again, the X-ray system was used to scan the coarse inclusion source zone multiple times before the NAPL was injected to obtain the baseline condition for later analysis. For this experiment, TCE was selected as the NAPL to eliminate the issue of residual mass from Intermediate Tank Experiment #1 contributing to the mass observed during this experiment.

Due to the lower solubility of TCE than 1,1,2-TCA, a smaller amount of mass (1.53 grams) was injected into the source zone. After the injection occurred, the X-ray system was used to scan the source zone continuously until the NAPL was fully depleted. Complete dissolution of the NAPL was observed after 11 days.

Figure B-15 shows the dissolution of the TCE versus time. For this source zone architecture, the dissolution followed a nearly linear dissolution rate.

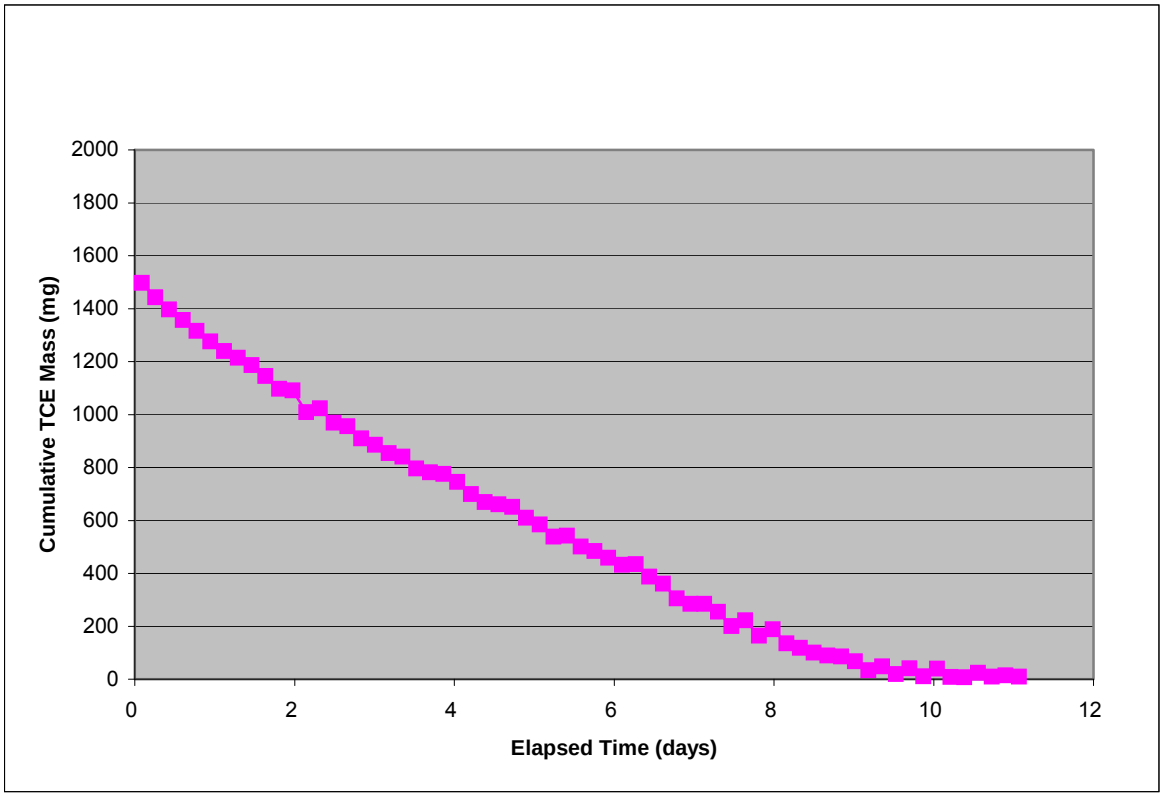

Figure B-15. TCE Remaining in Source Zone Based Upon X-ray Analysis For Intermediate Tank Experiment #2.

The effluent was sampled and directly measured in the aqueous phase by the FID on the GC. However, two issues arose that prevented the development of the effluent contaminant breakthrough versus time curve. First, the sampling protocol allowed for the sealed sample vials to be exposed to the air via a thin-gauge needle used for venting purposes. This enabled the loss of TCE to the air and reduced the observed concentrations to a level much below the anticipated concentrations. A separate study was performed to quantify the effects of the air exposure, and it was determined that up to 70 percent of the TCE mass could be lost due to partitioning to the air for the normal sample sitting time of 12 to 24 hours.

Second, the filters in the tank became clogged and the flow rate dropped dramatically to approximately one-third of the original flow rate. As the flow rate was not measured on a daily basis during this experiment, the effects of the flow rate change on the dissolution and migration of the TCE in the tank could not be determined.

For these two reasons, the effluent data from this experiment could be used and are not presented here.

B.1.9.3 Selection of DNAPLs Used for Experimental Tank Studies

These experiments were initially intended to be executed using dichloromethane (DCM) as the injected NAPL. DCM was chosen because of its relatively high solubility (20,000 mg/L) compared to other NAPLs (1,1,2-TCA ~ 4400 mg/L and TCE ~ 1100 mg/L) (Lucius et al., 1992). However, DCM was replaced with 1,1,2-TCA and TCE for two reasons. First, the measurement of aqueous phase DCM concentrations via the GC proved to be difficult. Although multiple attempts were made to obtain a high quality calibration curve, consistent results could not be achieved, and a piece line calibration curve had to be used. Secondly, the DCM is highly volatile. This caused handling losses to such an extent that the effort to obtain a reasonable mass balance during the experiment was thwarted. Therefore, DCM was abandoned as the source NAPL.

B.1.9.4 Small Tank Experiments

B.1.9.4.1 Small Tank Experiment (Tank 1)

The following sections describe five sets of experiments being formed in two identically constructed small tanks. The tanks are identified as BST1, BST2, BST3, BST4 and BST5 in the title of each section in order to differentiate them from each other. The small tank design section is common to both tanks.

In Small Tank 1, 7.47 grams of TCE were injected into the coarse inclusion. Unfortunately, the same issues relating to losses of TCE that hindered BLT2

were also present here, causing an erratic breakthrough curve with large variations in concentrations between aqueous samples. This experiment, which was the last one to use TCE, was continued for 144 days before a pump failure caused termination.

B.1.9.4.2 Small Tank Experiment (Tank 2)

This experiment used Small Tank 2, which is a large tank that has been converted to a small tank. The flow rate in the tank was maintained at 5.7 L/day. The DNAPL (1,1,2-TCA) injection procedure was slightly modified from previous injections. The goal of the injection was to create a known saturation profile in the vertical direction that was homogeneous in the horizontal direction. By doing so, a one dimensional saturation profile would be developed that would provide data essential to understanding how the degree of DNAPL saturation affected the net mass flux into the fine layer. In support of this goal, the DNAPL injection procedure was modified such that DNAPL was injected until the entire source zone was fully saturated (as determined by visual inspection). Then, DNAPL was withdrawn from the source zone back into the syringe at a slow rate. This continued until the fluid being removed contained distinct sections of DNAPL intermixed with sections of water. Once this occurred, the injection syringe was removed from the tank and X-ray scans commenced. This resulted in 13.6 grams of 1,1,2-TCA being injected. The resulting DNAPL saturation distribution within the source zone, as depicted in contours via X-ray analysis, is shown in Figure B-16.

In Figure B-16, the contours represent the length of DNAPL material that was encountered by the photons of the X-ray system. The vertical axis represents a vertical distance 0.5 cm greater than the height of the source zone, and the horizontal axis is 0.5 cm greater than the lateral extent of the source zone material. The vertical axis is exaggerated by a factor of five. The zero position on the vertical axis represents the interface between the coarse inclusion and the fine layer. For this experiment, a maximum DNAPL saturation (path length divided by the product of tank width and porosity) of 0.55 was observed near the

right edge of the source zone. However, Figure B-16 also shows substantial variations in levels of DNAPL saturation in both horizontal and vertical directions. Therefore, it is valuable to examine specific sections of the source zone to assess the degree of heterogeneity in saturation levels that occur.

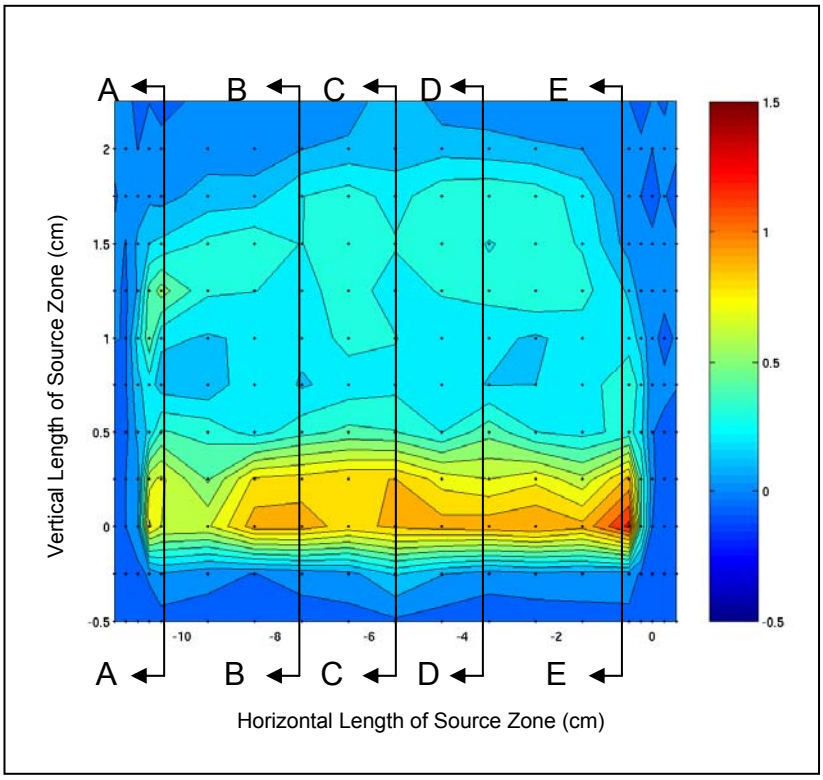

Figure B-16. DNAPL distribution after injection during BST2.

X-ray scanning continued throughout the duration of DNAPL dissolution. Effluent sampling was performed beginning after the DNAPL injection, and continuing until 2.6 days after the DNAPL source had been depleted. The breakthrough curve is shown in Figure B-17.

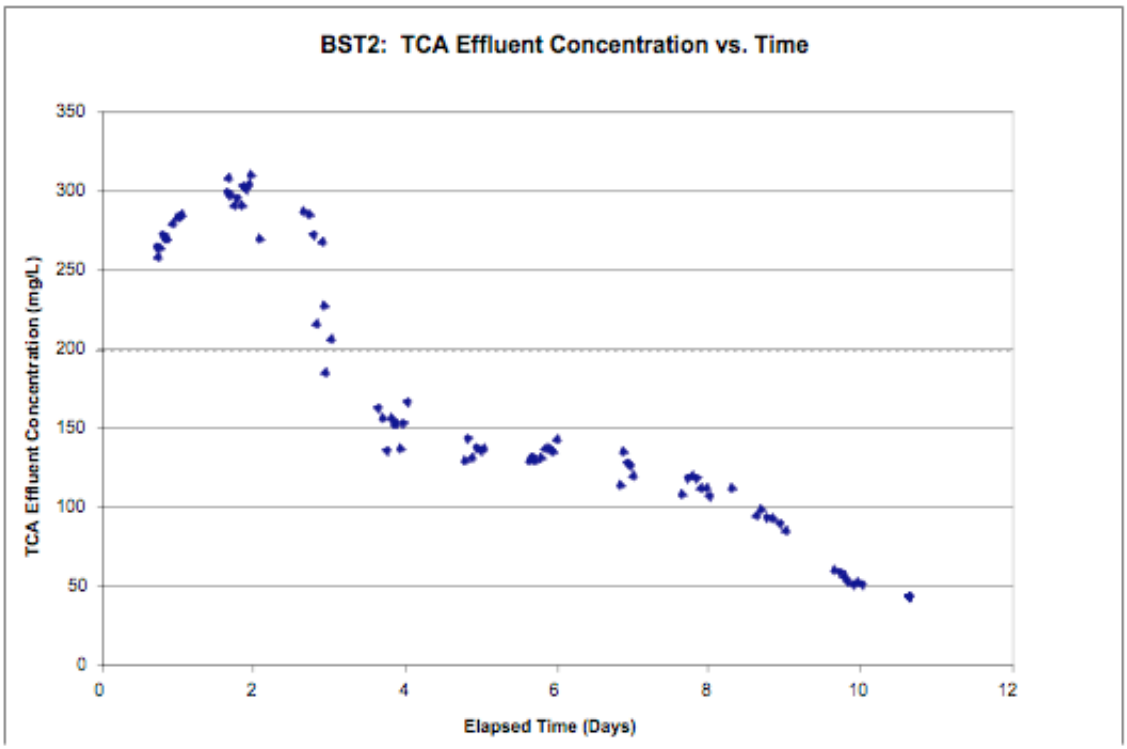

Figure B-17. Contaminant breakthrough in effluent versus time for BST2.

Although the mass recovery of the 1,1,2-TCA only totaled 67 percent of the injected mass, the majority of the losses is assumed to have occurred in the excavation procedure, as explained later. It is unlikely that any significant degree of handling loss was incurred during the effluent sampling, as this procedure was used for all small tank experiments including those with excellent mass recovery percentages. Therefore, since these losses likely occurred after the effluent sampling stopped, the results shown in Figure B-17 are assumed valid.

Figure B-17 shows several interesting occurrences in the breakthrough curve. For instance, there is a peak concentration of approximately 300 mg/L observed at two days of elapsed time from the DNAPL injection. Then, there is a noticeable, abrupt drop in concentration at three days elapsed time. After the sharp drop, the concentration declines very slowly until eight days have elapsed. Finally, after eight days, the concentration decreases again at a more rapid pace. A closer examination of Figure B-16 and Figure B-17 reveals a relationship

between the DNAPL distribution in the source zone and the occurrences in the breakthrough curve. The DNAPL saturation levels near the bottom of the source zone are sufficiently high to reduce the aqueous phase relative permeability such that only limited flow occurs in this area. The flow bypasses this area in favor of a more permeable zone, which is located in the upper sections of the source zone, so the upper part of the source zone has an increased rate of flow through it. Therefore, the dissolution of the DNAPL during the first three days occurs primarily from the upper source zone area.

Since the level of DNAPL saturation is low and does not vary widely in this section (less than 0.15 except for section AA), flow occurs throughout all areas of the upper source zone. This produces the peak concentration at Day 2 as shown in Figure B-17. Once the DNAPL in the upper area of the source zone has been depleted via dissolution (Day 3 in Figure B-17), the only remaining DNAPL source available to contribute to the effluent concentration is in the lower portions of the source zone. However, as the levels of DNAPL saturation in that part of the source zone remain high enough to encourage flow bypassing, only the edges of the lower area of the source zone contribute to the dissolution of DNAPL. This slows the rate of dissolution in the source zone, causing lower concentrations than observed during the first three days. Additionally, the concentration declines very slowly during this period (between 3 and 8 days), because the interfacial area of DNAPL and water declines very slowly. Finally, as shown in Figure B-18, analysis of X-ray data shows the DNAPL has completely dissolved after 8.3 days. The effluent concentrations correspond to this by declining more sharply after day 8, since there is no longer a DNAPL source.

In addition to the effluent results, this experiment yielded other data that are important to understanding the processes that govern matrix storage. These data were acquired during the excavation and coring of the tank that occurred 2.5 days after complete DNAPL dissolution. The distribution of the dissolved contaminant is shown in Table B-5 and Figure B-19. Because the laboratory quartz sands were used for this experiment, no measurable sorption to soil

particles occurred. Therefore, the concentrations obtained through the coring procedure were a result of only aqueous phase contaminant.

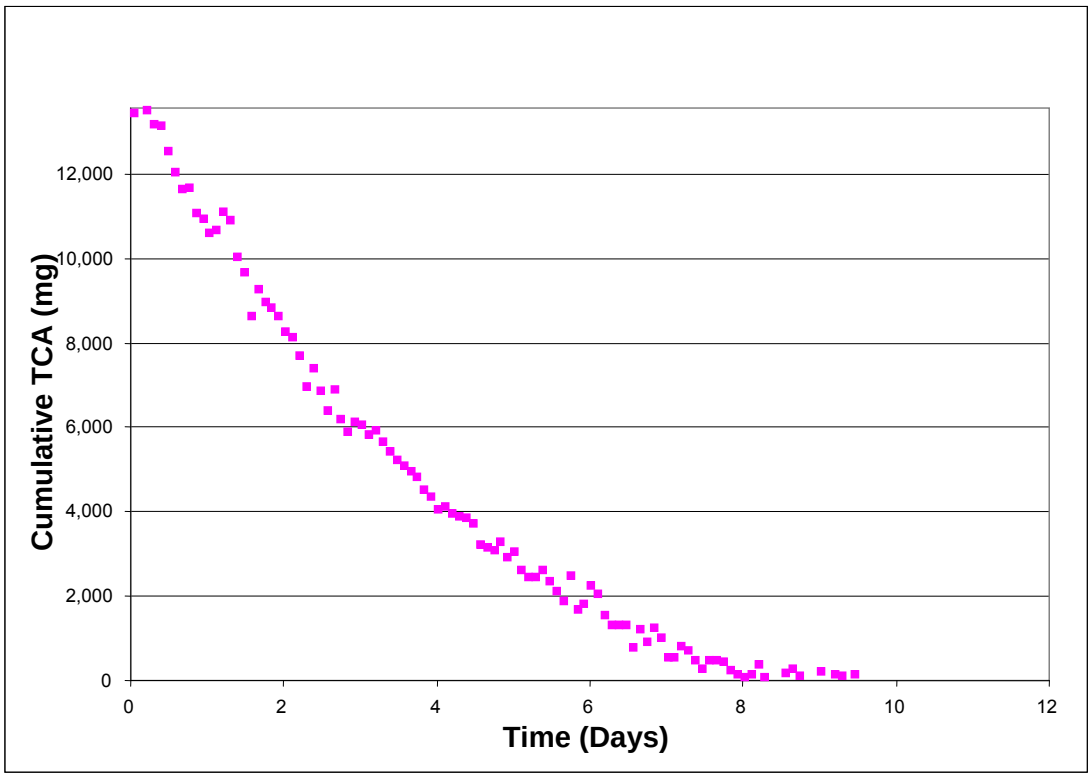

Figure B-18. Results of DNAPL dissolution for BST2 as depicted by X-ray.

This was the first attempt for the coring procedure. Although good data were obtained for a small volume of the low permeability layer, the cores did not cover the full lateral or vertical extent of the tank. Specifically, the cores covered only 22.2 cm laterally and only 6 cm vertically in the low permeability layer. The lack of data for such a large area of the tank was a key contributor to the handling losses mentioned above. For subsequent tanks, steps were taken to ensure full coverage of the low permeability layer was obtained.

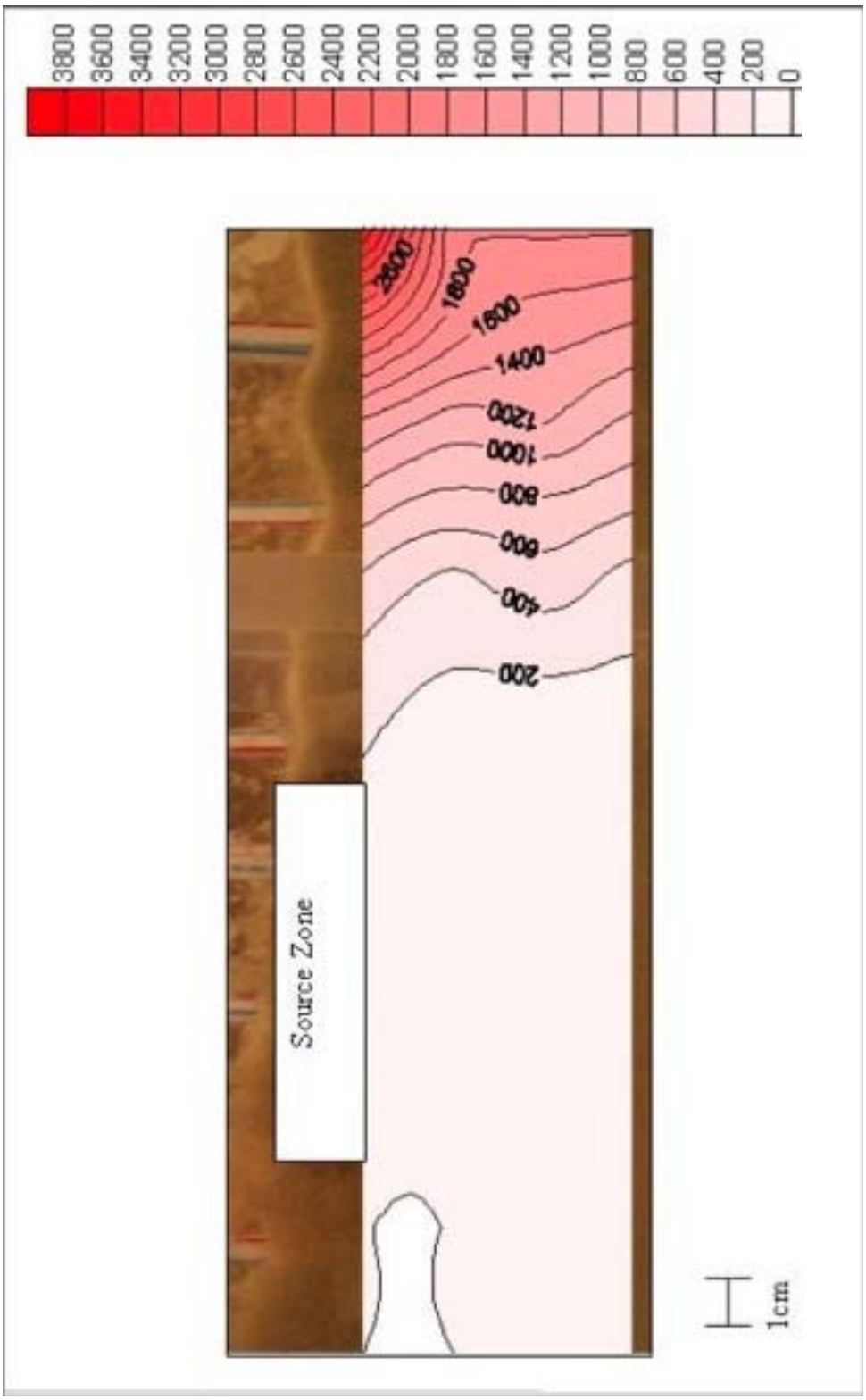

Figure B-19. Distribution of the dissolved TCA contaminant for BST2.

Table B-5. Distribution of dissolved 1,1,2-TCA (mg/L) within soil solution of low permeability layer for BST2.

Depth below interface (cm)	Horizontal distance from leading edge of coarse inclusion (cm)							
	-1.9	**0.6**	**5.1**	**7.6**	**10.8**	**13.3**	**16.5**	**20.3**
0 - 1	N/A	N/A	18.0	78.2	N/A	540.6	1373.9	3621.3
1 - 2	N/A	N/A	13.5	62.7	133.2	368.3	1098.1	1846.7
2 -4	N/A	N/A	9.9	46.6	119.6	295.5	1229.7	1846.0
4-6	N/A	N/A	5.0	41.0	112.1	292.5	951.8	1826.3

Although the coring did not provide full coverage of the #140 sand in the tank, the results revealed an important observation. The highest concentrations (nearly 3000 mg/L) were observed at the top of the #140 sand layer. This suggests that the primary mode of contaminant transport into the #140 sand layer was diffusion from the source zone and the coarse layer above. The peak concentrations were also downgradient from the source zone. This was due to the small degree of advection that occurred in the #140 sand layer. Since the cores were taken 2.5 days after DNAPL dissolution ceased, the highest concentrations had been transported toward the downgradient section of the tank.

B.1.9.4.3 Small Tank Experiment 3 (BST3)

This experiment also used Small Tank 2, as well as #30 sand and #140 sand. The flow rate in the tank was maintained at 5.1 L/day. The DNAPL injection procedure followed the procedure outlined in the previous section. The injection resulted in 14.2 grams of 1,1,2-TCA being placed in the coarse inclusion. The DNAPL distribution within the source zone, as depicted via X-ray analysis, is shown in Figure B-20.

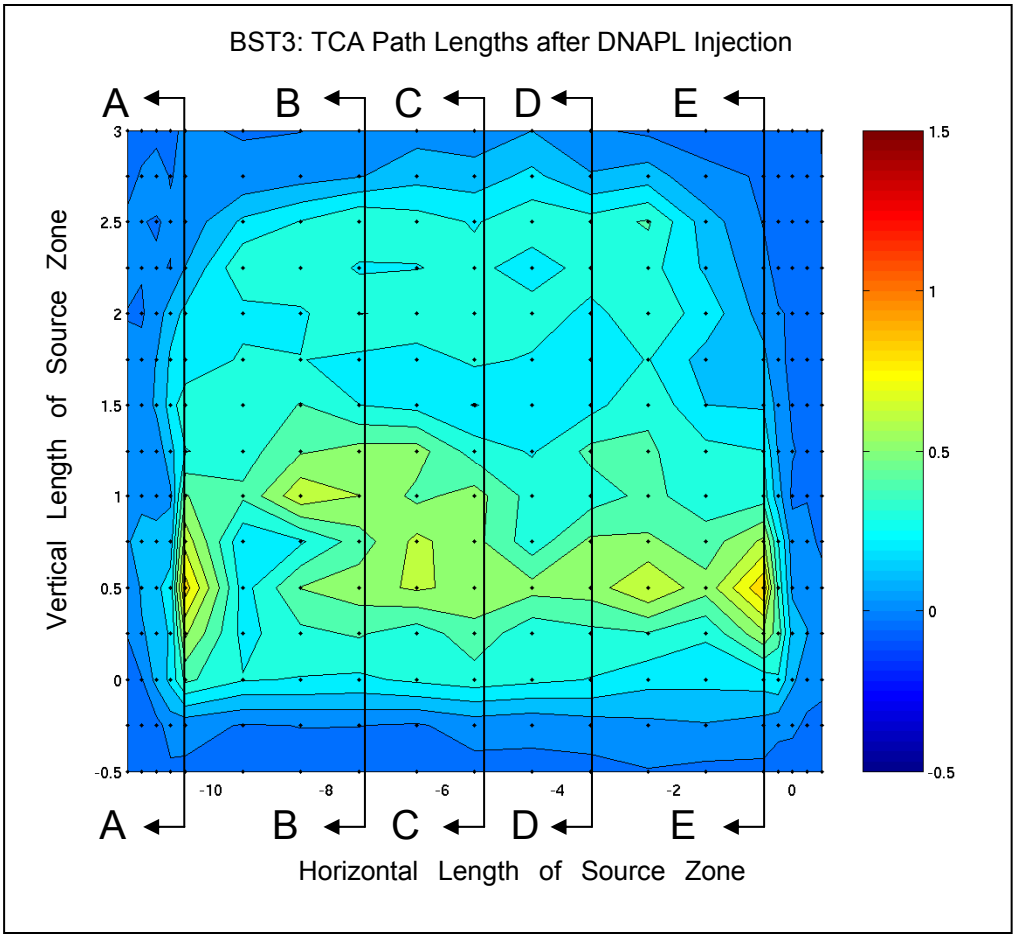

Figure B-20. DNAPL distribution after injection during BST3.

Figure B-20 shows some heterogeneity in the levels of DNAPL saturation through the source zone, although it is less pronounced than for BST2. The maximum DNAPL saturation level is 0.40 - 0.42 for section E and section A and less than 0.30 for all other sections. Additionally, due to the DNAPL withdrawal procedure, the maximum DNAPL saturation level is observed at 0.5 cm above the interface with the low-permeability layer.

The experiment was performed for 9 days. Effluent sampling and soil coring for BST3 achieved recovery of 94 percent of the 1,1,2-TCA mass injected into the tank. This is shown in Figure B-21, which also shows that the analysis of X-ray data indicated that the DNAPL had completely dissolved after 5.5 days. The effluent contaminant breakthrough curve is shown in Figure B-22.

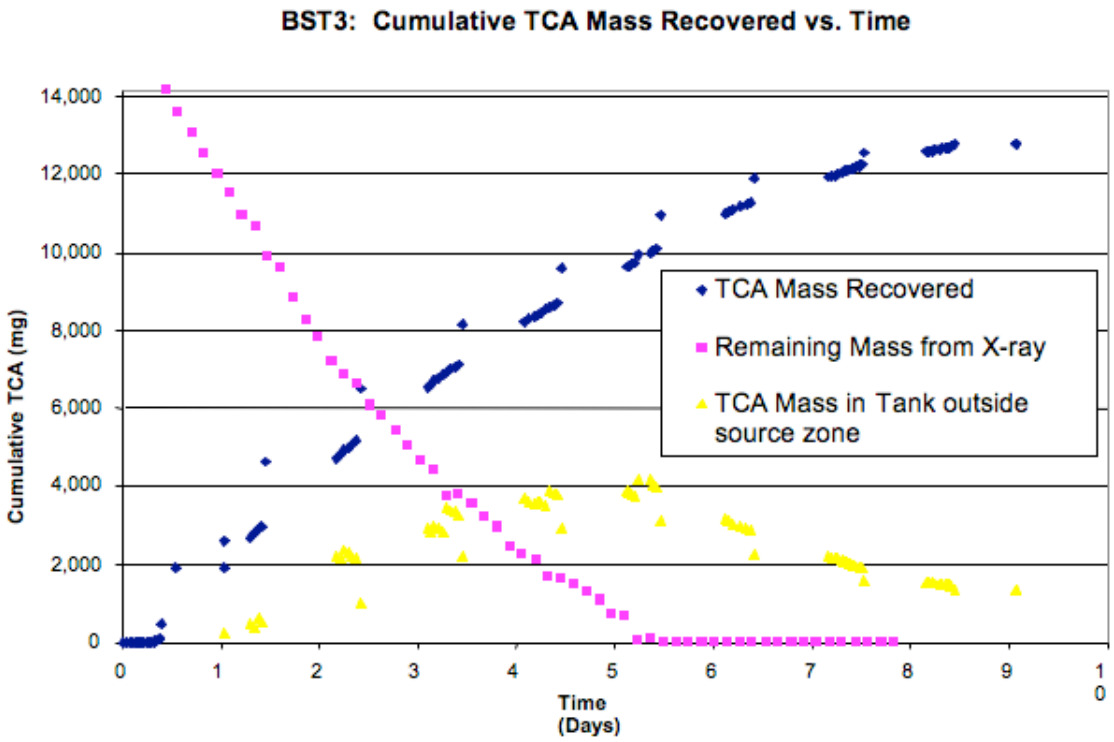

Figure B-21. Distribution and recovery of TCA mass for BST3.

A comparison of Figure B-22 and Figure B-17 (the breakthrough curve for BST2) identifies three differences between the two curves. First, the peak concentration for BST2 was approximately 300 mg/L, but the peak concentration for BST3 was greater than 500 mg/L. Second, after the initial peak, BST2 displayed an abrupt drop in concentration that was not present in the same magnitude in BST3. Third, a greater amount of DNAPL (14.2 grams) was injected during BST3 compared to 13.6 grams for BST2, yet BST3 dissolved in a shorter period of time (5.5 days compared to 8.3 days).

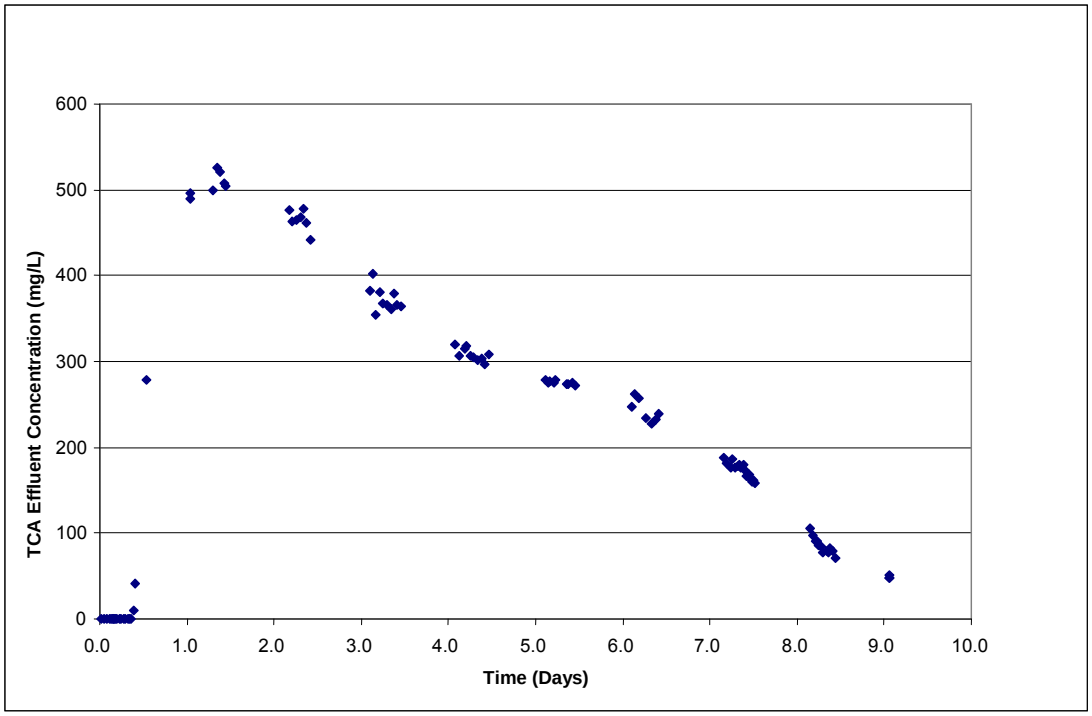

Figure B-22. Contaminant breakthrough in effluent versus time for BST3.

These differences demonstrate that different phenomena were controlling the dissolution and/ or the solute transport during the experiments. The flow rate was similar between the two experiments (5.1 L/day for BST3 versus 5.7 L/day for BST2). The tank packing for BST3 closely approximated the packing of BST2. The only major difference between the two tanks was the distribution of the DNAPL in the source zones. BST3 did not contain a highly saturated area near the bottom of the source zone. Additionally, it did not contain as wide a range of levels of DNAPL saturation as BST2. These factors caused a different flow field to develop through the source zone within BST3. BST3 did not exhibit the degree of flow bypassing that occurred in BST2. Therefore, the entire source zone experienced flow through it that enabled dissolution of DNAPL from all parts of the source zone to occur throughout the duration of the experiment. This hypothesis is supported by the breakthrough curves. The DNAPL in BST3 was more exposed to the flow, which increased the dissolution rate and generated higher peak concentrations. Also, because flow bypassing was minimal in BST3, the abrupt drop after the initial peak seen in BST2 was not present in BST3.

Moreover, the DNAPL in BST3 dissolved more quickly because of the enhanced flow throughout the source zone whereas DNAPL in the lower area of the BST2 source zone had minimal exposure to the water causing a lower dissolution rate.

Coring of the low permeability layer upon termination of the experiment was performed over the entire lateral distribution of the tank. Additionally, the cores were driven into the low permeability layer to a maximum depth ranging from 9 to 14 cm. This provided comprehensive coverage of the distribution of the dissolved contaminant mass in the low permeability layer at 3.5 days after dissolution had ended. Table B-6 lists the measured values for each soil core. Figure B-23 shows a contour plot of the aqueous concentrations that were observed in the low permeability layer. As with BST2, no appreciable sorption to the quartz sands occurred.

Table B-6. Soil Cores Results for BST3.

Depth below interface (cm)	Horizontal distance from leading edge of coarse inclusion (cm)																	
	0	2.5	6	8.2	11	13.2	15.7	18.7	21.8	24	27	29.5	32.5	34.5	37	39.5	42.5	45.5
0 - 1.35	ND	ND	ND	ND	ND	ND	ND	0	0	8	9	9	3	18		12	37	9
1.35 - 2.70	ND	ND	ND	ND	ND	ND	ND	0	0	9	17	26	47	81	264	104	173	82
2.70 - 4.05	ND	ND	ND	ND	ND	ND	ND	0	0	9	20	45	100	208	476	325	508	369
4.05 - 5.40	ND	ND	ND	ND	ND	ND	ND	ND	0	8	13	46	112	267	456	569	837	786
5.40 - 6.75	ND	ND	ND	ND	ND	ND	ND	ND	0	4	29	34	123	212	323	655	841	986
6.75 - 8.10	ND	ND	ND	ND	ND	ND	ND	ND	ND	4	6	19	74	151	222	546	647	687
8.10 - 9.45	ND	ND	ND	ND	ND	ND	ND	ND	ND	ND	4	8	29		130	330	374	
9.45 - 10.80	ND	ND	ND	ND	ND	ND	ND	ND	ND	ND	6	5	19		55	176	162	
10.80 - 12.15	ND	ND	ND	ND	ND	ND	ND	ND	ND	ND	9	4	9					
12.15 - 13.50											7	3						

ND = Non-detect

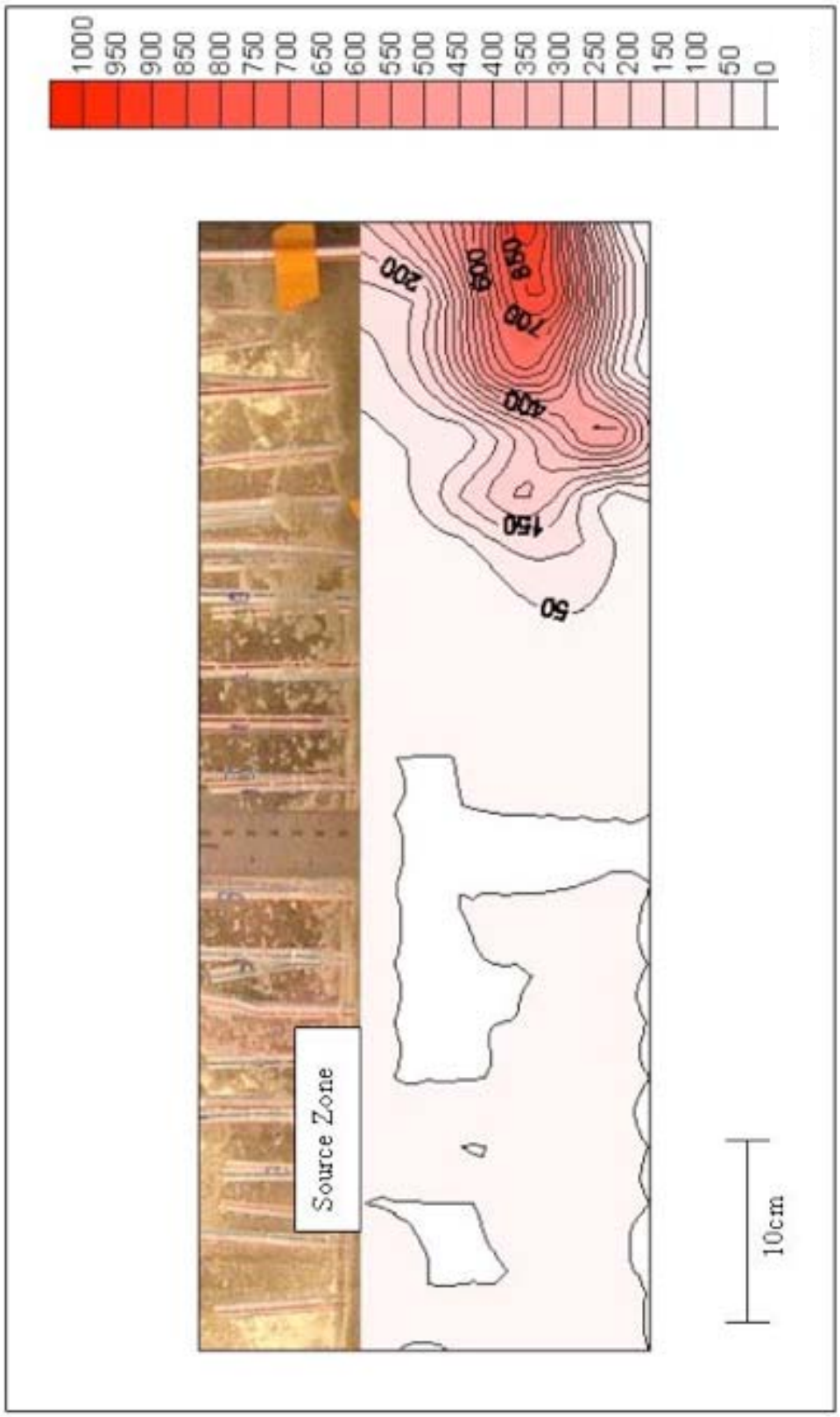

Figure B-23. TCA concentrations that were observed in the low permeability layer.

The peak concentrations were once again downgradient of the former source zone because of the small degree of advection in the #140 sand layer. However, the depth of the peak concentration was from 5.5 to 7.0 cm below the interface of the two soils, whereas the peak concentration in BST2 was at the interface of the soils. This result suggests that diffusion was not the key transport mechanism for contaminant mass into the #140 sand layer. Instead, a vertical component of the flow field had been introduced, causing advective transport into the low-permeability layer. Inspection of the source zone from Figure B-20 suggests that DNAPL distribution caused aqueous phase relative permeability changes. As a result, the flow field was modified in the source zone and became two-dimensional. Additionally, since the level of DNAPL saturation at the interface was not as high as 0.5 cm above the interface, flow was encouraged downward toward the low permeability layer. As water flowed through the source zone, it reached dissolved-phase concentrations near or at the maximum solubility. Thus, when it entered the low-permeability layer, it was laden with contaminant mass. The vertical flow was met by the horizontal flow within the low-permeability layer, and eventually the vertical component was stopped from transporting flow any deeper into the low-permeability layer. After this point, the mass was transported horizontally downgradient in the low-permeability layer.

It is important to note that, although diffusion did not dominate the contaminant transport in this experiment, its effects were still seen. Detectable concentrations were observed at depths up to 13 cm from the soil interface. Thus, while advection transported the highest concentrations 5.5 to 7.0 cm deep into the low-permeability layer, diffusion was responsible for transporting the contaminant deeper. Depths greater than 13 cm may have been reached if the DNAPL had persisted for a longer period of time.

B.1.9.4.4 Small Tank Experiment 4 (BST4)

The objective of BST4 and BST5 was to perform a pair of experiments that repeated BST2 and BST3, but used a different material as the low-permeability

layer. BST4 and BST5 used the NAS Ft. Worth field silt in place of the #140 sand.

The desired flow rate for this experiment was 5.1 L/day because that was the actual flow rate from BST3. However, due to partial clogging of the fiberglass filters at the ends of the tank, a constant flow rate could not be obtained. The head gradient was adjusted three times during the experiment to attempt to return the flow rate to its desired value, but a constant flow could not be achieved. The flow rate was monitored daily, and it is shown in Figure B-24 along with the effluent breakthrough curve.

The DNAPL injection procedure from BST3 was duplicated for this experiment. However, during the injection process a small hole developed at the interface of the Teflon tubing and the glass tube. This prevented any of the DNAPL from being withdrawn from the source zone back into the syringe. This resulted in a much greater DNAPL mass (56.76 grams) than desired. However, the experiment was continued because the governing processes of matrix storage still applied. The only negative was that the duration of the experiment was extended to six weeks from two weeks.

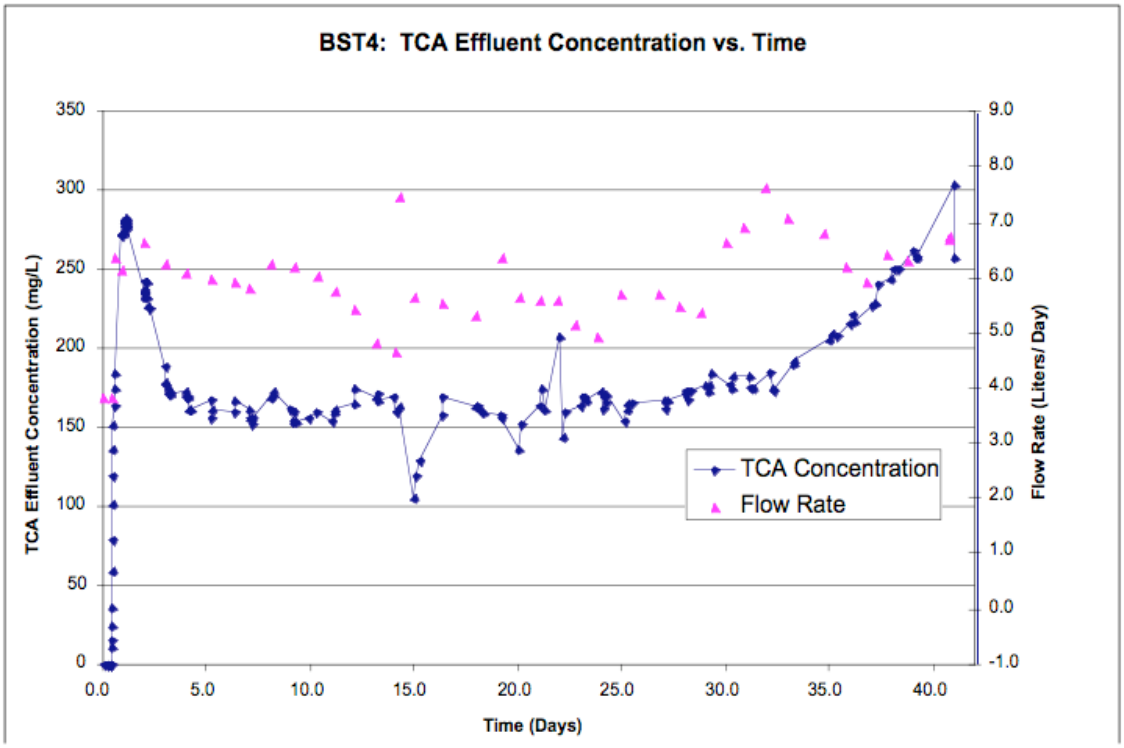

Figure B-24. Contaminant breakthrough and water flow rate for BST4.

The DNAPL distribution within the source zone, as depicted via X-ray analysis, is shown in Figure B-25. The highest levels of DNAPL saturation were in the bottom portion of the source zone. The excess DNAPL in the source zone caused higher saturation levels than for the other small-tank experiments.

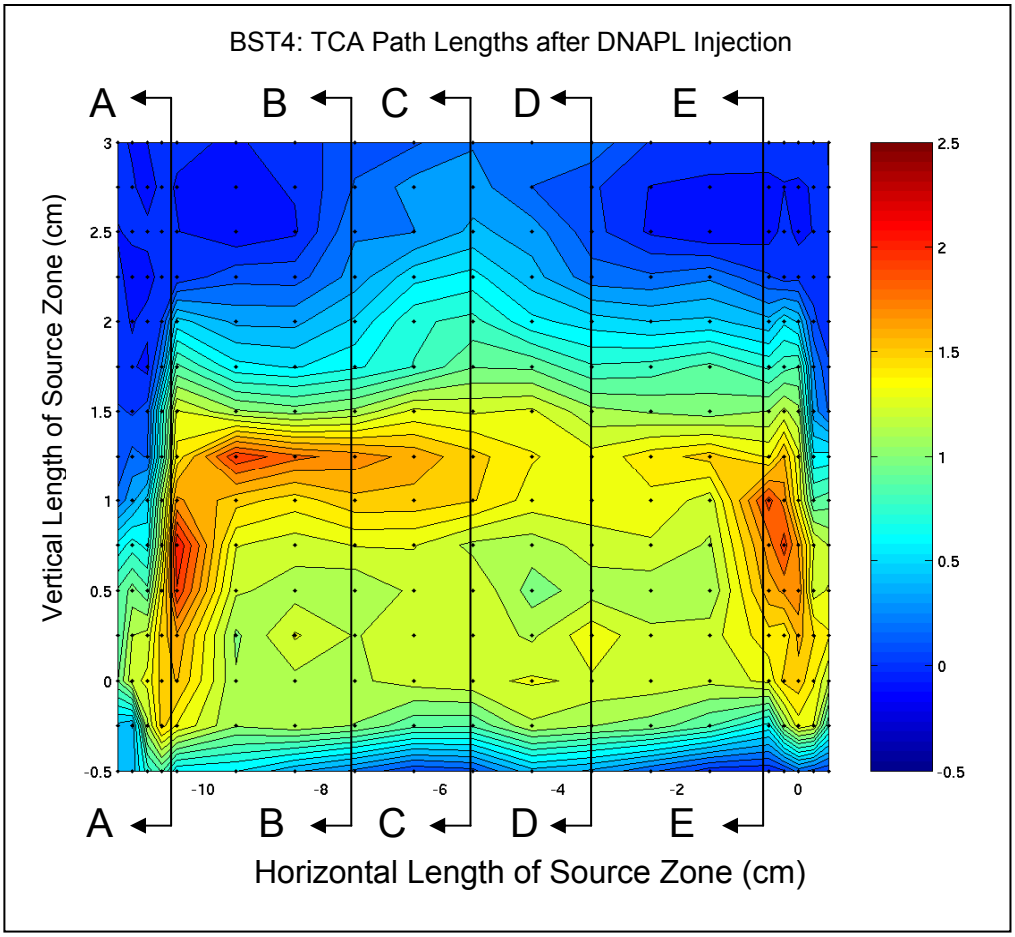

Figure B-25. DNAPL distribution after injection during BST4.

The experiment was conducted for 41 days. Effluent sampling and soil coring for BST4 achieved recovery of 87 percent of the 1,1,2-TCA mass injected into the tank. This is shown in Figure B-26, which also shows that the analysis of X-ray data indicated that the DNAPL had completely dissolved after 40 days. Due to the extended duration of the experiment, X-ray scanning was discontinued during days 14 through 36, resuming from day 37 until day 41, when the analysis showed that the DNAPL had dissolved.

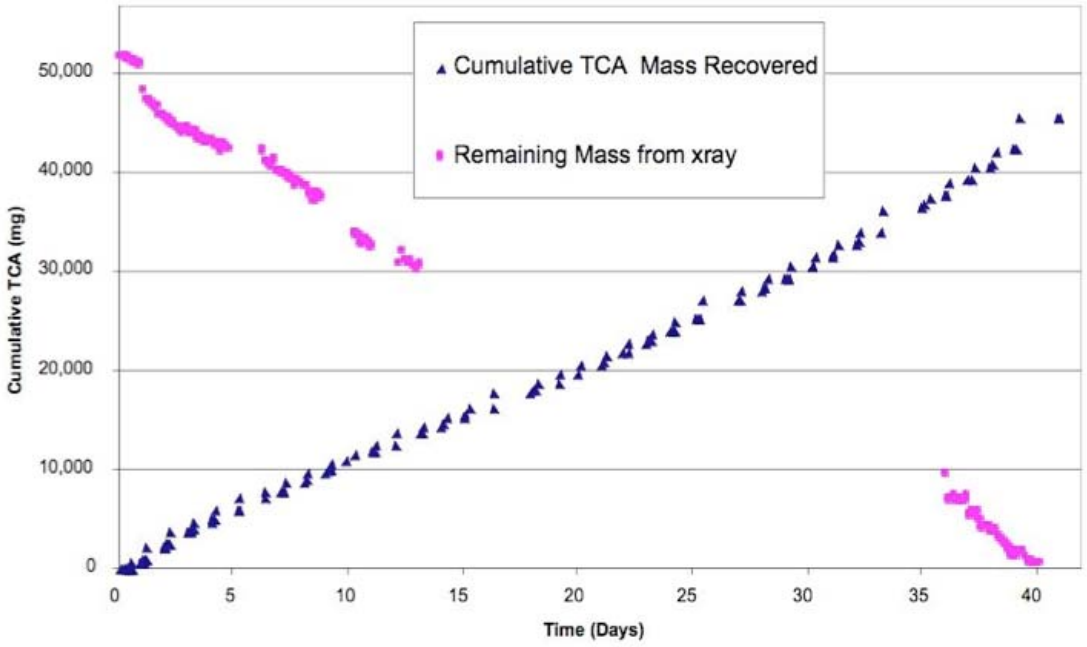

Figure B-26. DNAPL and recovered TCA versus time for BST4.

The breakthrough curve (shown earlier in Figure B-24) indicated that the expected initial peak, which occurred at 1.2 days of elapsed time, was followed by a sharp decline in concentration from two to four days of elapsed time. Then, a period of constant concentrations was observed from four days to 26 days. This followed the pattern previously observed in BST2. This correlation was logical when the DNAPL distribution in the source zones for both experiments was compared. The higher levels of DNAPL saturation on the bottom of the source pool forced flow bypassing. Thus, after the dissolution of the upper section of the source zone, only dissolution from the edges of the lower section of DNAPL occurred, thereby lowering the effluent concentration significantly. (Note in Figure B-24 that the outlying data points taken at 15 days elapsed time correspond to the high flow rate of 7.46 L/day observed at 14.3 days. The flow velocity was sufficiently high that dissolution became rate limited. Since equilibrium between the DNAPL and dissolved phases was not reached, the concentrations in the effluent were lower than for other flow rates).

Unlike BST2, though, the breakthrough curve of BST4 indicates a rebounding effect after day 26 that continued until the experiment was terminated. The highest concentration observed at any time during the experiment was seen on the last day of sampling. This was unexpected. A possible explanation is that sufficient DNAPL from the lower portion of the source zone had dissolved to allow channels of flow to occur through it. Thus, the depressed concentrations observed during the middle of the experiment correspond to dissolution from the edges of a highly saturated zone, and the rebound in concentration at the end of the experiment was due to enhanced dissolution caused by flow through the highly saturated zone. This is one hypothesis for the observed phenomenon, and further research should be done in this area to validate it.

After the experiment was terminated, the tank was excavated and soil cores were taken and analyzed. The results of the coring procedure are shown in Table B-7 and Figure B-27. During batch testing, the field silt was observed to exhibit appreciable sorptive characteristics. Its sorption coefficient was measured to be 0.6. Thus, the observed concentrations from the soil coring include both dissolved and sorbed phases.

Due to the extended duration of the experiment, the residence time of DNAPL exposure to the low permeability layer was much longer than in previous experiments. The elongated residence time is the primary reason why the contaminant has reached a greater lateral and vertical extent than in previous experiments. Also, the hydraulic conductivity of the NAS Ft. Worth silt is only one-third of the #140 sand. Thus, the decreased flow allowed for dissolved contaminant within the silt layer to diffuse into a larger portion of the layer. Concentrations reaching 200 mg/L were observed at the extreme upgradient edge of the tank signifying that diffusion rivaled advection in the low permeability layer.

An examination of the peak concentration shows that the greatest concentrations remained near the interface of the two soils. This suggests that transport into the

low permeability layer was dominated by diffusion. Also, because of the small flow velocity that existed in the low permeability layer and because the cores were taken after DNAPL dissolution was complete, advection had carried the peak concentrations downgradient. As with BST2, the heavy levels of DNAPL saturation near the soil interface had occluded flow from that region. Thus, flow bypassing had occurred into the upper section of the source zone. Since there was no flow between the two soil layers, diffusion was the key transport mechanism for contaminant mass into the low permeability layer. The highest saturation levels occurred between 0.75 cm and 1.5 cm above the soil interface. This contradicts the results from BST3 where this distribution of DNAPL seemed to encourage flow into the low permeability layer. However, the absolute values of the levels of DNAPL saturation at the soil interface were very different between BST3 and BST4. BST3 saturation levels ranged from 0.1 – 0.2, but BST4 levels ranged from 0.55 – 0.72. This suggests that the absolute level of DNAPL saturation at the soil interface is important to determining the transport mechanism into the low permeability layer as well as the relative levels of DNAPL saturation throughout the source zone.

Table B-7. Soil Core Results for BST4.

	Horizontal distance from leading edge of coarse inclusion (cm)																					
Depth below interface (cm)	-6	-2.5	-0.2	2.7	6	9.8	12	14.1	16.5	20	23.1	25.6	27.2	29.2	31.5	33.9	36.3	38.8	41	41.8
0 - 1.13	41	N/A	N/A	N/A	N/A	237	281	308	563	432	530	521	785	787	842	757	967	1117	1007	383
1.13 - 3.40	30	N/A	45	82	N/A	110	409	134	427	310	288	377	565	744	673	682	849	1029	728	863
3.40 - 5.67	24	N/A	21	90	95	33	403	63	221	187	159	250	400	577	124	554	700	889	528	705
5.67 - 7.94	19	N/A	12	137	83	11	171	26	122	102	121	180	291	421	812	407	503	686	377	572
7.94 - 10.21	20	N/A	6	112	59	4	75	10	58	55	0	121	280	313	491	311	418	552	241	491
10.21 - 12.48	30	66	1	41	15	2	27	4	23	26	57	81	149	213	357	220	341	414	338	461
12.48 - 14.75	35	39	10	15	9	9	16	6	27	24		39	72	144	254	121	253	292		423
14.75 - 17.02														77			135			302

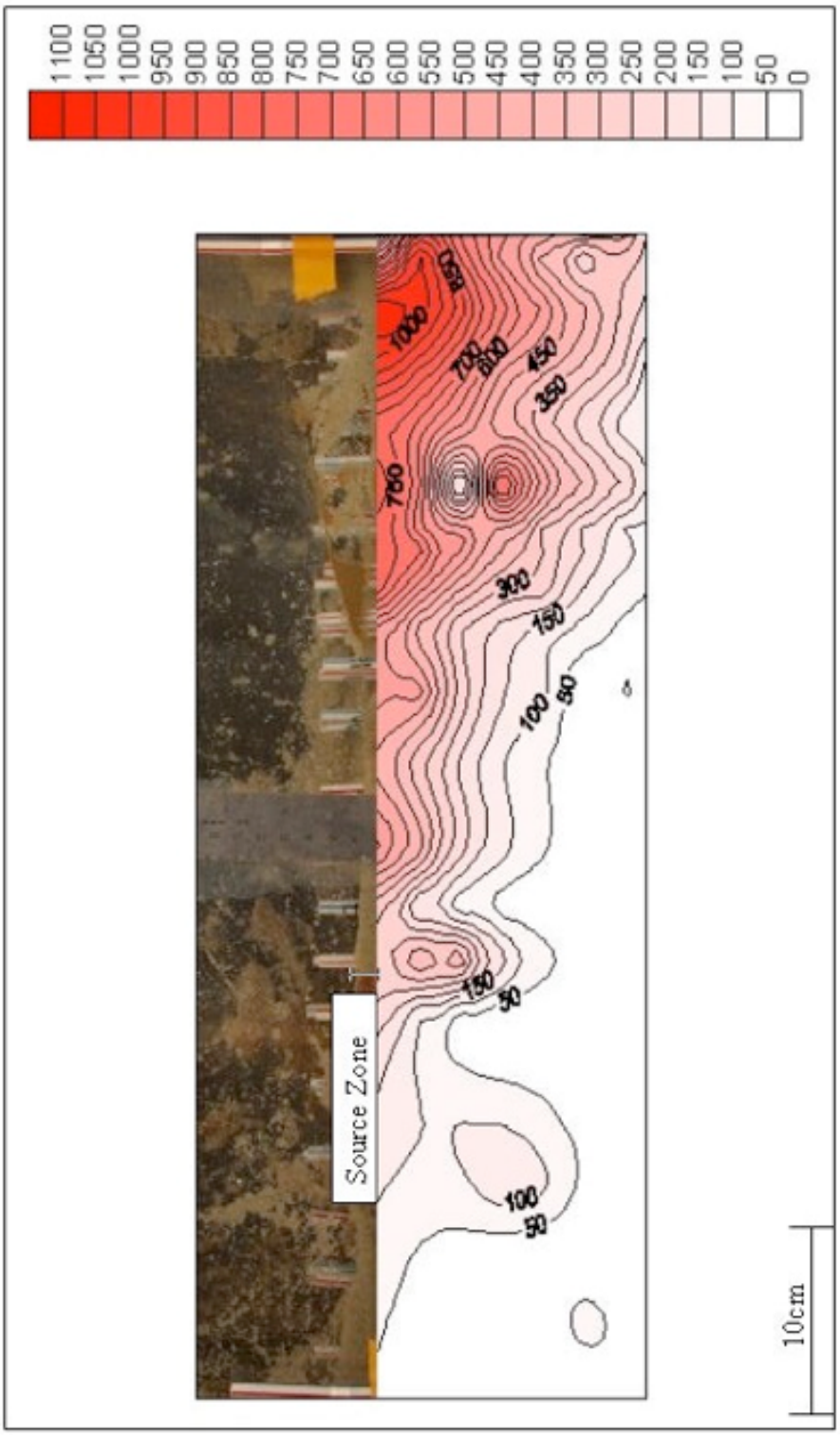

Figure B-27. Results of TCA Coring for BST4.

B.1.9.4.5 Small-Tank Experiment 5 (BST5)

BST5 used the same packing configuration and soil types as BST4. The goal of this experiment was to create a different distribution of DNAPL in the source zone, and then compare the results to BST4. A constant flow rate was desired. However, similar filter clogging issues as occurred with BST4 made this unattainable. Figure B-28 shows the flow rate and effluent concentration versus elapsed time. Between three days and seven days after DNAPL injection, the flow rate varied from 3.43 L/day to 11.25 L/day. The head gradient was adjusted during this time to compensate for the clogging. Unfortunately, the adjustments to the head gradient over compensated for the clogging issue causing the wide range of flow velocities observed during this time. After seven days, the flow rate remained steady. The experiment was conducted for 14 days. Effluent sampling and soil coring for BST5 achieved recovery of 86 percent of the 1,1,2-TCA mass injected into the tank.

The DNAPL infusion and withdrawal procedure resulted in 19.32 grams of 1,1,2 TCA being injected in the tank. The DNAPL distribution within the source zone, as depicted via X-ray analysis, is shown in Figure B-29. The level of saturation at the soil interface (between 0.40 – 0.54) was much greater than in the upper sections of the source zone.

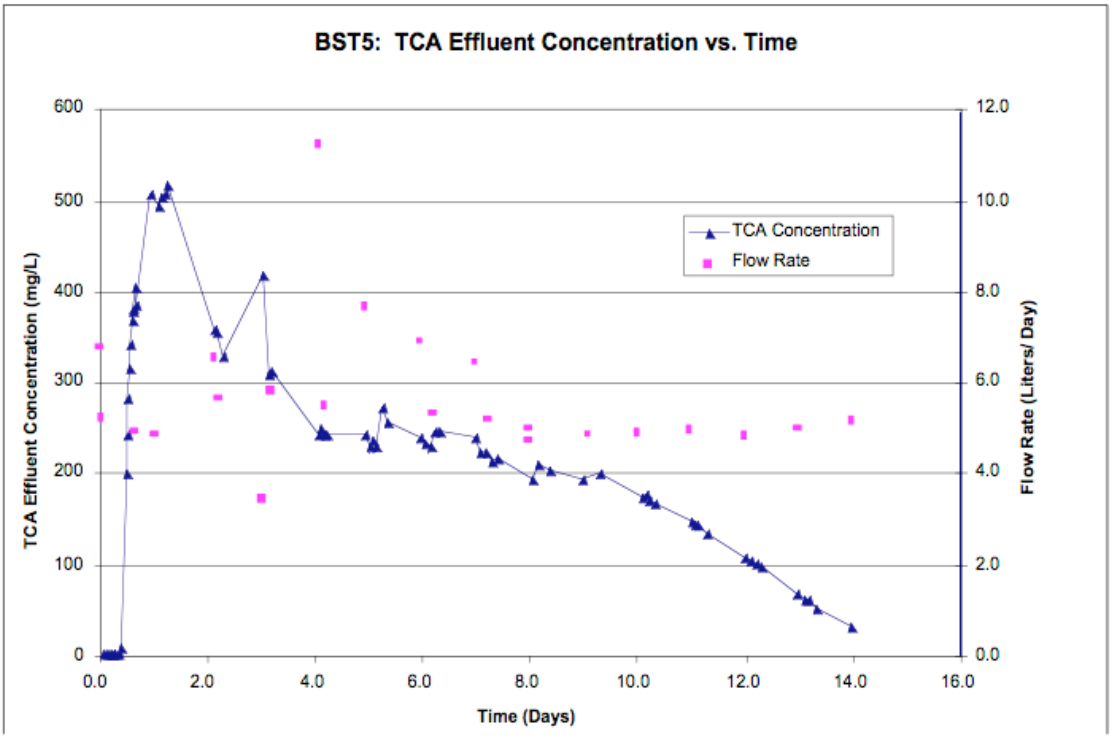

Figure B-28. Contaminant breakthrough and water flow rate for BST5.

The short transition zone between high levels of saturation and low levels of saturation suggests that flow bypassing of the lower source zone area may have been encouraged in this experiment. Indeed, that is what is shown in Figure B-28, where the effluent concentrations reached an initial peak during the bypassing of flow into the upper source zone area causing an enhanced dissolution rate. Then, after the upper source zone area was depleted of DNAPL, the effluent concentrations declined quickly until day four when a slow decrease in concentration occurred. At day nine, the concentrations dropped more rapidly again signaling the approach of complete dissolution of DNAPL in the tank. For BST5, due to X-ray equipment problems, only an initial scan of the tank was performed. In order to determine when the DNAPL had dissolved completely, the breakthrough curve was examined as mentioned previously.

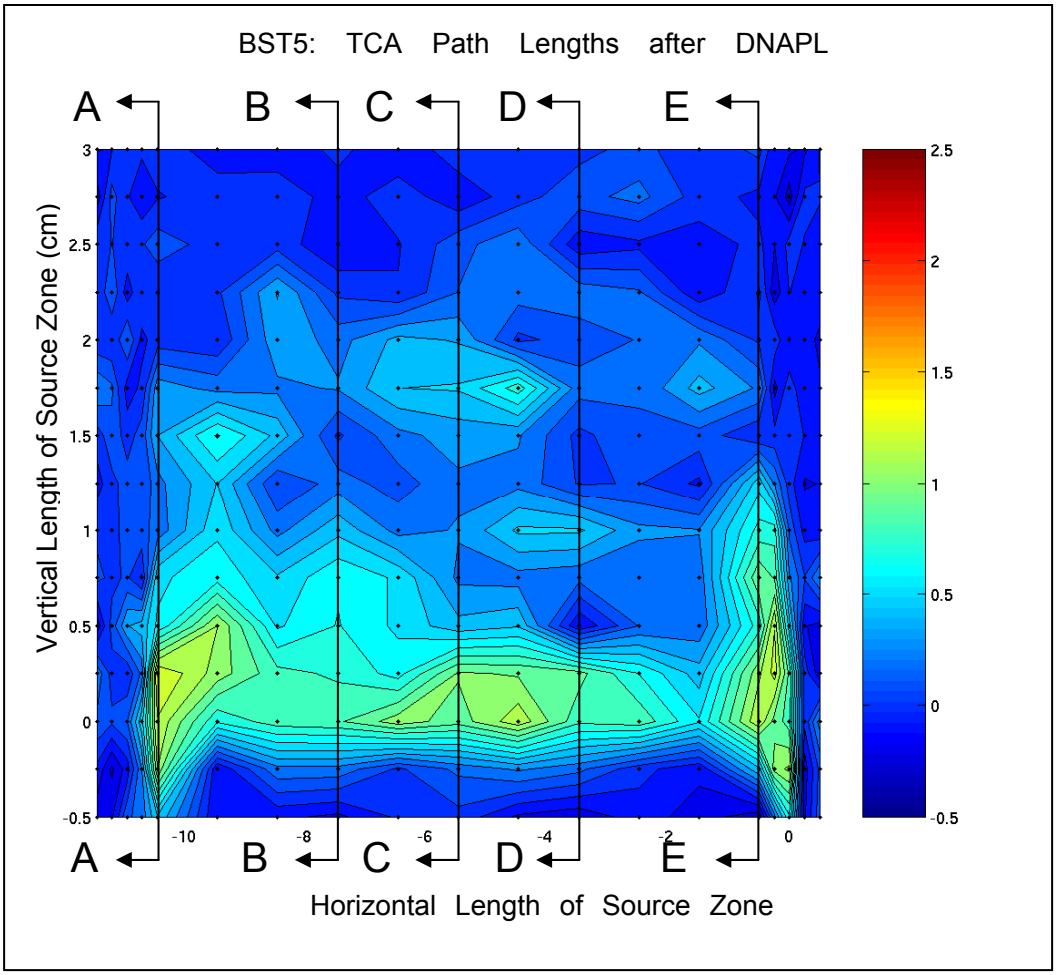

Figure B-29. DNAPL distribution after injection during BST5.

The DNAPL distribution for BST5 showed similarities to BST2 and BST4 with respect to the highest levels occurring at the bottom of the source zone and a wide range of saturation levels from top to bottom. However, BST5 also showed similarities to BST3 regarding the absolute levels of DNAPL saturation in the tank being lower than in BST2 and BST4. In order to analyze how both the relative and absolute levels of DNAPL saturation affected matrix storage, soil cores were taken. The results of the coring are shown in Table B-8 and Figure B-30.

The highest concentrations were seen at depths from 4.4 – 6.6 cm below the soil interface. This suggests that advection from the source zone into the low-permeability layer played a key role in the contaminant transport. This is a similar observation to BST3. Therefore, this data suggest that the absolute levels of

DNAPL saturation controlled the flow from the source zone into the low-permeability layer. While the relative levels of DNAPL saturation were important regarding the flow field through the source zone, if high enough levels of saturation occurred at the soil interface, flow was not permitted to enter the low-permeability layer. This was observed in BST2 and BST4.

Additionally, it is noted that the penetration depth within the low-permeability layer of the peak concentration was lower (4.4 to 6.6 cm) in BST5 than in BST3 (5.5 to 7.0 cm). This may correspond to the lower permeability of the silt used in BST5 than the #140 sand used in BST3. However, the DNAPL distribution was complex and tank specific, so it is difficult to isolate and quantify the causes of the differences in vertical flow velocities through the source zone. Thus, only qualitative assessments can be made about the role of the hydraulic conductivities of the soils. However, the expected result was observed.

Table B-8. Soil Core Results for BST5.

Depth below interface (cm)	-6.0	-3.8	-0.8	1.9	5.1	8.3	11.5	14.4	16.9	19.5	22.0	24.5	27.0	30.0	32.5	35.3	38.2	40.8	44.0
0.0-2.2	0.0	0.0	0.0	0.7	3.1	19.1	53.5	117.2	109.8	192.7	287.3	208.2	186.3	215.2	244.9	246.5	476.6	147.0	42.2
2.2-4.4	0.0	0.0	0.5	1.1	1.6	18.9	81.4	170.7	220.0	320.2	418.0	444.9	379.8	351.0	473.4	462.9	583.7	409.6	100.7
4.4–6.6	0.0	0.0	0.0	0.0	1.4	16.0	57.0	139.3	196.5	299.3	327.5	415.8	482.3	453.2	472.4	488.7	488.3	488.7	325.0
6.6-8.8	0.0	0.5	0.0	0.0	0.8	7.2	27.5	100.4	146.7	182.4	213.0	397.9	376.1	397.8	433.6	421.0	396.1	512.8	518.0
8.8-11.0	0.0	0.5	0.0	0.0	0.8	3.2	8.8	37.9	87.0	113.0	137.1	267.1	265.2	362.5	308.0	292.4	252.9	497.5	556.5
11.0-13.2	0.0	0.7	0.6	0.0	0.0	1.5	2.8	14.5	49.7	62.8	81.9	153.2	171.9	234.0	193.4	207.1	137.4	314.9	442.7
13.2-15.4	0.0	1.0	0.6	0.0	0.8	0.9	1.7		24.3	20.0	44.2	90.4	88.9	134.7	74.1	94.5	44.5	176.7	294.9
15.4-		0.7		0.0	1.2	1.2	1.3		9.4	7.2	13.5	36.5	27.0					112.4	146.1

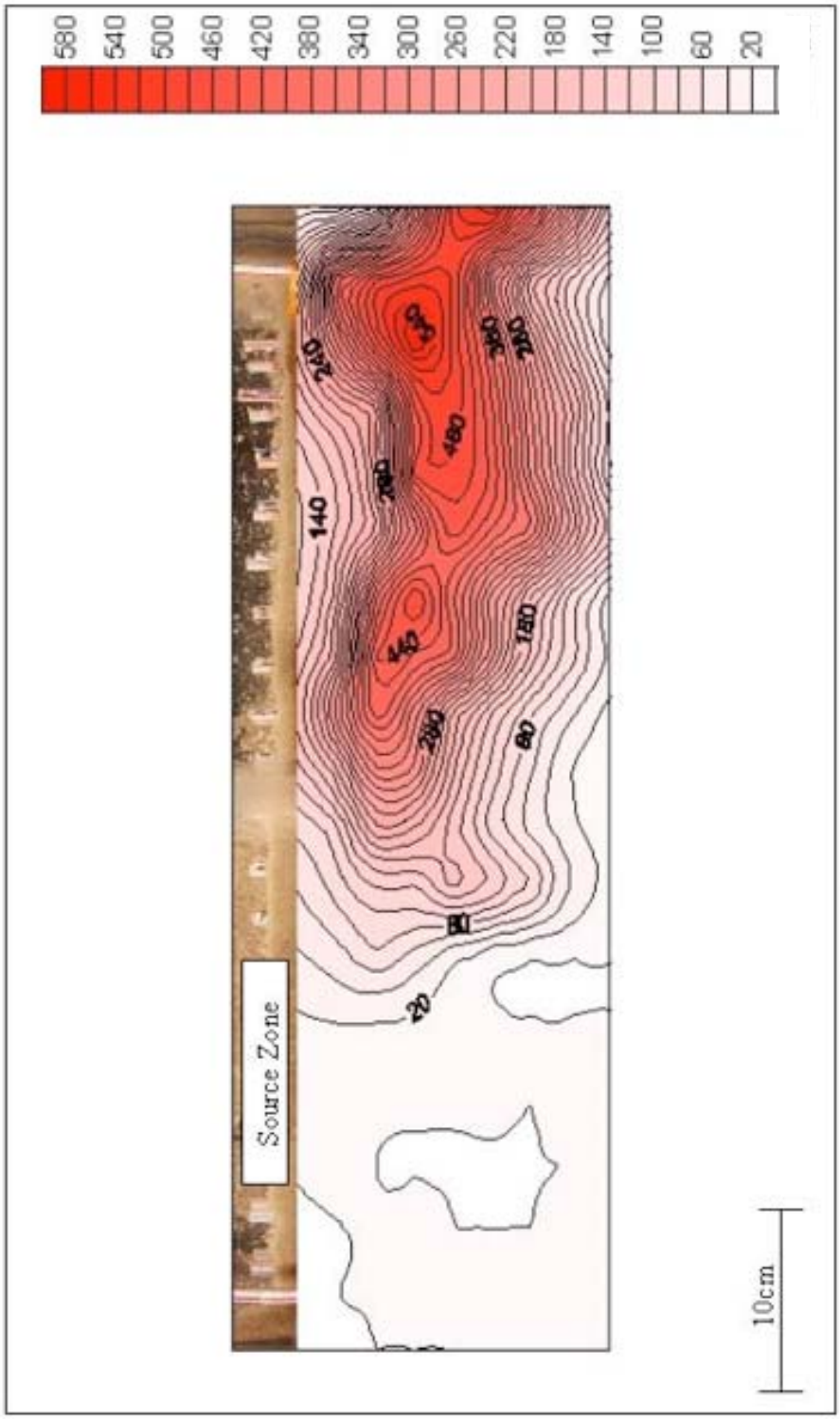

Figure B-30. Results of TCA Coring for BST5.

B.1.10 Contaminant Transport Retardation Analysis

Based on the experimental tank studies, values of retardation of the contaminant transport due to soil sorption must be obtained to calibrate the numerical model. These parameters cannot be independently determined based upon tank results alone. A separate study is required to ascertain the retardation properties of the experimental soils.

B.1.10.1 Hypothesis

The retardation of contaminant transport can be estimated by

$$R = 1 + (\text{Bulk Density} * K_d)/ \text{Porosity} \qquad (R1)$$

where R is the retardation factor and K_d is the sorption coefficient. Porosity can be assumed to be 0.40 for the laboratory soils (F140, F30) and 0.35 for the NASFtW field soils. Bulk density and K_d can be independently determined through batch scale studies that are described below.

B.1.10.2 Method: Bulk Density Determination

The following procedure was used to obtain the bulk density of each of the four soils used in the AFCEE project at CSM. The procedure was performed in triplicate on each of the four soils.

Known amounts of soil mass were placed in a vial, and the soil was oven dried for 39 hours at 107°C. After removal from the oven, the soil mass was again recorded. Tap water was added to a replicate vial (empty) until the meniscus reached the same height as the soil in the original vial. The mass of the water was recorded and was assumed to be equivalent to the bulk volume of the soil. Next, the mass of the soil was divided by the volume of the soil to obtain the bulk density. The results are shown in Table B-9.

Table B-9. Summary of results of bulk density study. [Values in bold were used as input to the numerical model].

Soil Type	Vial	Mass of Dried Soil (g)	Volume of water to match soil volume (ml)	Bulk Density (kg/L)
F140	a	7.81	5.59	1.40
F140	b	7.12	5.29	1.35
F140	c	7.68	5.55	**1.38**
F30	a	8.32	5.26	1.58
F30	b	7.79	5.08	1.53
F30	c	7.34	4.76	**1.54**
NAS Mix	a	7.60	5.43	1.40
NAS Mix	b	7.31	5.07	1.44
NAS Mix	c	7.80	5.46	**1.43**
NAS Silt	a	7.55	5.41	**1.40**
NAS Silt	b	7.17	5.10	1.41
NAS Silt	c	7.09	5.10	1.39

B.1.10.3 Method: Sorption Coefficient Determination

The following methodology was used to perform a 10-day sorption study of aqueous phase 1,1,2-TCA and TCE for each of the four soils being used in the AFCEE project at CSM. While the protocol is based upon the work of Ball and Roberts (1991), several deviations from the Ball method were made due to equipment and time issues. As the goal of this sorption study was to provide a retardation parameter to a numerical model, a close approximation of the actual sorption was satisfactory. Thus, the deviations from Ball were deemed to be insignificant in this context.

Known amounts of 1,1,2- TCA and TCE were introduced into a capped glass container with de-aired tap water taken from the same source as the experimental tank influent. To allow for aqueous phase equilibration of the NAPL mixture, the container was then placed on a shaker table for 10 days. During this time, several actions were taken to prepare for the ensuing study. Specifically, 75 10-mL centrifuge vials were obtained (15 vials for each of the 4 soils and 15 blanks) and the vial masses were recorded. Then, 12 grams of soil were added to each of the 15 vials for each soil. Next, de-aired tap water was added to the vials with the soil to fully saturate the soil such that the meniscus was approximately 1 mm above the top of soil. Finally, the mass and volume of water required for the previous saturating step were recorded and the vials were capped.

After the 10-day equilibration period, 3 samples of the aqueous phase from the 1,1,2-TCA/ TCE solution were taken, and the 1,1,2-TCA and TCE concentrations were measured using the FID on the GC. These samples provided a reference point for the expected concentrations in the rest of the vials.

Next, aqueous 1,1,2-TCA/TCE solution and de-aired tap water was added to all 15 vials for each of the four soils such that no headspace remained, and then the vials were capped. The details for each of the 15 vials for one soil type are listed in Table B-10. A range of five concentrations was selected to produce enough data points to fit a sorption coefficient. For each of the five concentrations in the range, sample vials were prepared in triplicate.

Table B-10. The expected TCE and 1,1,2-TCA concentrations added to the NAS Ft. Worth Silt. The concentrations listed are those that would have been expected if no sorption occurred.

Vial #	TCE Expected Concentration (mg/L)	1,1,2-TCA Expected Concentration (mg/L)
Q1	0.66	2.76
Q2	0.63	2.65
Q3	0.65	2.73
R1	3.00	12.5
R2	2.97	12.4
R3	2.99	12.5
S1	23.0	96.2
S2	27.2	114
S3	29.5	123
T1	225	941
T2	232	972
T3	223.	934

Additionally, de-aired tap water and 1,1,2-TCA/ TCE solution were added to the blanks such that the range of concentrations used in the vials with soil was approximately replicated in triplicate. The blanks were then capped. The vials with soil were placed in a tumbler and tumbled along their longitudinal axis for 10 days at approximately 0.25 rpm. The blanks were not placed in the tumbler. Instead, the blanks were placed on their side to simulate the position of the soil vials during tumbling and to normalize the sorptive effects of the Teflon cap of the vials. Once a period of 10 days had passed, the vials with soil were removed from the tumbler, centrifuged, and placed in GC-ready vials.

Aqueous concentrations were obtained using the FID on the GC. The data were used as input into the following procedure to calculate sorption coefficients.

First, using the data from the blanks, percentage difference between the expected blank concentration based upon the solubility samples and the observed concentrations was determined. This percentage was used to eliminate the effects of the Teflon cap sorption and handling losses, and to allow for calibration issues of the compounds on the GC. Next, the expected soil sample concentrations were multiplied by 1 minus the blank percentage. This step allowed for comparison of the observed concentrations with the expected concentrations such that the only difference should be due to soil sorption.

After the normalization calculations were performed, the observed soil sample concentrations were subtracted from the expected concentrations and multiplied by the bulk density. The result was the sorbed concentration in mg/kg. The data were evaluated to discard any outliers within each group of triplicates. For the remaining data, charts were produced plotting normalized expected aqueous concentration versus observed sorbed concentrations. This was done for each of the four soils and for both 1,1,2-TCA and TCE. The slope of the plots represents the sorption coefficient, K_d. Figure B-31 presents a Sample Plot:

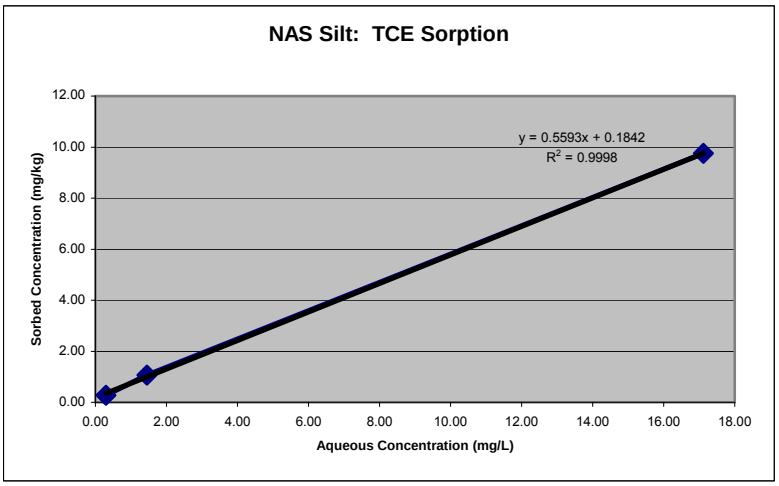

Figure B-31. Sample experimental sorption isotherm.

As a linear isotherm was selected, K_d values for the soil and contaminant pair were obtained by averaging the K_d from each of the three individual plots, provided that the plot represented a linear approximation. If a plot showed a severely non-linear curve, it was discarded. The results of the study are summarized in Table B-11.

Table B-11. Summary of results from 10-day sorption study.

	K_d				Retardation			
	NAS Mixed	**NAS Silt**	**F140**	**F30**	**NAS Mixed**	**NAS Silt**	**F140**	**F30**
TCE	0.35	0.6	0.01	0.02	2.43	3.39	1.03	1.08
TCA	0.12	0.19	0.04	0.00	1.49	1.76	1.14	1.00

B.1.10.4 Conclusions

Several conclusions were drawn from the results of these studies,. First, TCE sorbs more strongly to the soils than the 1,1,2-TCA. Second, the laboratory soils (F140, F30) exhibited virtually no sorptive capability. This was expected, given the assumption that little to no organic carbon existed in these soils. Third, the NASFtW field soils exhibited stronger sorptive capabilities than the laboratory soils, with the NASFtW Silt being more sorptive than the NASFtW Mixed. This was expected because the NASFtW Mixed included a sand fraction that was not present in the NASFtW Silt.

CONCLUSIONS FROM EXPERIMENTAL TANKS

This section describes the conclusions drawn from the observed data for each experiment.

B.1.11 Large Tanks

The large scale tanks provided experimental data based on dominant subsurface site conditions that show the significance of mass storage into low-permeability

zones as it affects the longevity of the dissolved plume. All three tanks experiments had the source zone dissolve in 14 to 27 days, while the tails of the breakthrough curves extended on for 70 to 170 days depending on the textural heterogeneity of the experimental domain. In addition, all three tanks continued to be orders of magnitude higher than the regulatory limit of 5 ppb for 1,1,2-TCA in groundwater. The significance of each large-tank experiment will now be discussed.

The simple layering of the large tank #1 experiment provided a large surface area of low-permeability material for dissolved mass to 1) transverse diffuse into during the first passage of the contaminant plume and 2) back diffuse from the low-permeability layer back into the transmissive zone at later times. Dissolved mass was also being advectively transported through the low-permeability layer, albeit at very slow rates. The significance of the back diffusion from the low permeability is that it may explain why sustained contaminant concentrations persist in downgradient monitoring wells, even after the contaminant source was thought to have been removed. Depending on the textural heterogeneities of the subsurface, the new contaminant sources may be from small-interspersed interbedded layers of low-permeability materials, or may be from large low-permeability layers, e.g., a layer of clay.

The second large tank experiment provided data for a system that consisted of a high-permeability layer over a low-permeability layer with a mound of field soil downstream, placed on top of the low-permeability layer. The data from this experiment showed the effects of the field soil layer attenuating the shape of the breakthrough curve by dissolved mass being advectively transported into the field layer, as well as around the mound. The dissolved mass that was transported into the field soil layer may be compared to the analogy of a “roach motel.” The mass gets transported into the field soil later, but the dissolved mass does not come out for a very long-time duration, if at all. In addition, similar to the first large-tank experiment, there is a large region of surface area provided by the field soil mound for dissolved mass diffusion into and out of the mound.

The third large-tank experiment was similar to the first large tank experiment; except that the field soil layer was at a 12% incline. The incline provided a complex flow field as compared to the simple layered system. The source in this experiment was completely dissolved in 27 days, as measured by X-ray analysis. Although, after 171 days of flow through the tank, dissolved mass was still being produced from the field soil layer at concentrations well above the MCL. The shape of the breakthrough curve showed an initial breakthrough, but then slow back diffusion from the incline plane for time greater than 40 days. As was the case for the first two experiments, this slow back diffusion from a low-permeability layer would result in extended cleanup times in the field, as well as creating further complications when trying to define these downstream areas that are the “new” source zones for the resulting dissolved phase plume.

B.1.12 Intermediate Tank

The intermediate-scale tank provided experimental evidence that mass storage in the low-permeability zone of the soil matrix can have a significant effect on the longevity of groundwater contamination at a site. Under simplified heterogeneous conditions, the injected DNAPL dissolved in seven days, but effluent concentrations of 1 ppm (over two orders of magnitude greater than the MCL of 0.005 ppm) persisted until sampling was stopped at 61 days after the injection of the DNAPL. Independent batch and column sorption studies supported the hypothesis that no appreciable sorption to solid particles was occurring in the tank. Thus, the extended duration of the release of the contaminant mass was attributed to storage in the low-permeability zone. These experimental data support field data from F.E. Warren Air Force Base and NAS Ft Worth that suggests the position that contaminated conditions may exist at a site many decades after the DNAPL source has been depleted or removed. This assessment is dependent upon the volume of the DNAPL spill and its distribution in the subsurface. Additionally, the longevity of the dissolved phase contamination is a function of the age of the DNAPL spill and the types of DNAPL remediation schemes that were attempted at the site.

The MCL for 1,1,2-TCA is 0.005 ppm; the same value for more commonly spilled TCE and PCE. Thus, 1,1,2-TCA can be viewed as a surrogate for these common DNAPLs. However, there are important differences that may cause each chemical to act in a unique manner. For example, PCE and TCE have different aqueous solubilities than 1,1,2-TCA that will cause different rates of dissolution. Also, TCE and PCE will sorb to the soil matrix a in similar, but not equal, manner as the 1,1,2-TCA. These differences must be included in any analysis that attempts to extrapolate the results of this study for use with other chemicals.

B.1.13 Small Tanks

Powers et al. (1991) determined that the assumption of local equilibrium is valid for DNAPL dissolution except under high flow velocities. In the small-tank studies, the flow velocity in the layer of low permeability near the source zone was much less than in the coarse layer of the tank. Thus, for the small flow velocities in the low-permeability layer, it can be concluded that the local equilibrium assumption was valid for the dissolution of DNAPL from the source zone into the layer of low permeability. An extension of this assumption is that the aqueous phase in the layer of low permeability at the interface with the source zone maintained a level of maximum solubility during the period of DNAPL persistence regardless of the DNAPL distribution in the source zone. Therefore, although the four small tank experiments exhibited different DNAPL distributions, maximum solubility in the aqueous phase was achieved for all of them. Excluding differences in DNAPL depletion times and the #140 sand versus the NAS Ft. Worth silt, this condition of universal maximum solubility should have led to equivalent distributions of dissolved contaminant in the layer of low permeability for each of the four experimental tanks.

However, the small tank studies provided experimental evidence that the distribution of DNAPL within the source zone impacted both the amount of contaminant mass that entered the low permeability zone and the distribution of

the contaminant mass within the zone. Thus, it can be concluded that another transport process, advection, contributed to the distribution of the mass. Figure B-32 shows the same observed concentrations in the low permeability layer for BST3 that were observed after 5.5 days of 1,1,2-TCA dissolution. The observed concentrations were taken from soil cores that were extracted three days after DNAPL depletion and from a vertical plane 39.5 cm downgradient from the leading edge of the source zone (since horizontal advection transported the contaminant within the low permeability layer).

The observed concentrations deviated substantially from the diffusion-only points due to the presence of advection into the low permeability layer. For BST3, the highest concentrations were observed 5.5 – 7.0 cm below the soil interface. At this depth, the observed concentrations were 5-6 times greater than the predicted values providing additional verification that advection was occurring in the tank. At greater depths, diffusion was the controlling transport mode for both datasets. The observed concentrations were still much higher than the predicted values because the increased concentrations at middle depths for the observed data produced a higher concentration gradient than for the hypothetical data.

Moreover, the significance of advection into the zone of low permeability was influenced by the distribution of DNAPL in the source zone. The changes in aqueous phase relative permeability in the source zone caused by the presence of the DNAPL influenced the flow fields through the source zone. The flow fields created unique situations within each tank that encouraged advection differently.

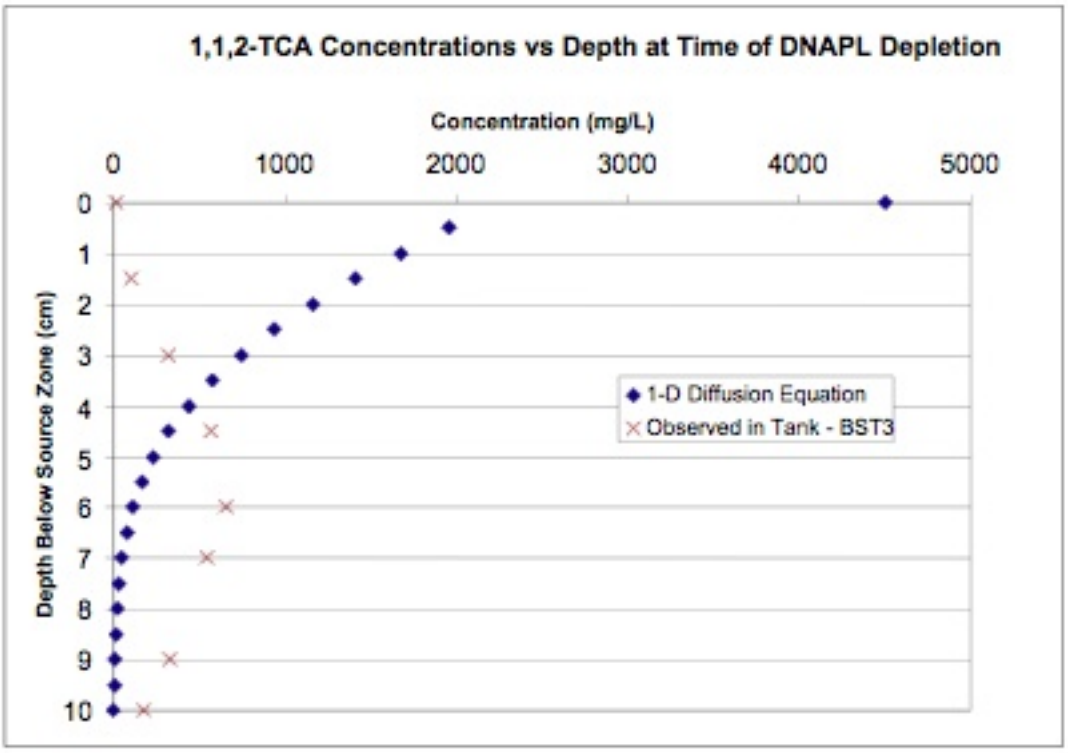

Figure B-32. Comparison of concentrations in low-permeability layer for diffusion transport only versus observed results from one of the small tank experiments.

Areas of high levels of DNAPL saturation prohibited flow through them and caused flow bypassing to occur. This resulted in decreased dissolution rates. Additionally, it precluded flow between the source zone and the zone of low permeability resulting in transport into the low-permeability zone primarily by diffusion. Conversely, a source zone that did not contain an area with sufficiently high levels of DNAPL to discourage flow through it, resulted in increased dissolution rates and advective transport of contaminant mass into the low-permeability zone.

The significance of advective transport into the layer of low permeability was also limited by the hydraulic conductivity of that layer. The NAS Ft. Worth silt had a hydraulic conductivity of approximately one-third of the #140 sand. Thus, it was more difficult for advection to transport contaminant as deeply into the silt as into the #140 sand. This was validated by a comparison of the BST3 and BST5 soil coring data. From Figure B-23, the BST3 (#140 sand experiment) presented its

highest concentrations 1.0 – 2.0 cm deeper in the low-permeability zone than BST5 (NAS Ft. Worth silt experiment, see Figure B-30). Therefore, the hydraulic conductivity of the low-permeability layer is a key factor in the distribution of the dissolved contaminant. Zones with extremely low hydraulic conductivities such as clays or bedrock may prohibit advective transport even when the DNAPL distribution in the source zone promotes a vertical component of advection. Conversely, fine sands or silts may allow for increased advection to occur, and thus may present a different dissolved mass distribution. Additional factors, such as desorption rates and size and distribution of fractures would need to be considered also.

It was beyond the scope of this study to quantify the effects of the downstream back diffusion. Liu and Ball (2002) provided some similar data that frames the significance of this effect. In that study, plots similar to Figure B-32 were presented that depicted sorbed concentrations of PCE versus depth for soil cores taken from two locations. One core showed no back diffusion effects, and the highest concentrations were observed at the interface with the aquifer. The other core displayed the effects of back diffusion. The peak concentrations in that core were observed at 10 cm below the interface with the coarse layer. However, at the NAS Ft Worth, where the study was performed, the DNAPL source had been excavated 10 years prior to the coring procedure. The peak concentrations had only shifted from the interface to a depth of 10 cm over a period of 10 years. In the research presented here, only three days had elapsed from DNAPL depletion to soil coring. Therefore, it is unlikely that back diffusion played a substantial role in the effluent contamination of the small tank experiments with the exception of the contaminant contained within the uppermost millimeters of the low-permeability layer. This is reinforced by the results of BST2 and BST4 where the peak concentrations were observed at the soil interface.

REFERENCES CITED

Ball, W.P., and P.V. Roberts. 1991. “Long-Term Sorption of Halogenated Organic Chemicals by Aquifer Material. 1. Equilibrium.” *Environmental Science. Technology.* Vol. 25, No 7. pp. 1223-1237,

Hill III, E.H., L.L. Kupper, and C.T. Miller, 2002. Evaluation of Path-Length Estimators for Characterizing Multiphase Systems Using Polyenergetic X-Ray Absorpiometry. Soil Science, 167(11): 703-719.

Illangasekare, T.H., and Armbruster E.J, III. 1995. “Non-Aqueous-Phase Fluids in Heterogeneous Aquifers-Experimental Study.” *Journal of Environmental Engineering*, August, Vol. 121, No. 8.

Liu, C., and W. P. Ball, 2002. Back diffusion of chlorinated solvent contaminants from a natural aquitard to a remediated aquifer under well-controlled field conditions: predictions and measurements. Groundwater, 40(2): 175-184.

Powers, S. E., C. O. Loureiro, L. M. Abriola, and W. J. Weber Jr., 1991. Theoretical study of the significance of nonequilibrium dissolution of nonaqueous phase liquids in subsurface systems. Water Resour. Res., 27(4): 463–477.

Wilking, B. 2004. Factors Controlling Matrix Storage during DNAPL Mass Depletion in Heterogeneous Porous Media, Master’s Thesis, Colorado School of Mines.

APPENDIX C
ANALYTICAL SOLUTION DEVELOPMENT

Flux 1 Derivation

Additional insights into mass transfer constraints can be realized by considering the rate at which dissolved chemical can be transported away from the DNAPL by the processes of dispersion and advection. The concept of mass transfer into a flowing aqueous phase adjacent to a DNAPL subzone is illustrated in Figure 6. Distribution of solute concentration in the aqueous phase is the result of advection, longitudinal dispersion, and transverse dispersion. Laboratory studies pertaining to transport about DNAPL subzones have focused on pools and columns constructed in flumes containing uniform granular porous media. Work regarding pools is reported by Schwille (1988); Voudrias et al. (1994); Whelan et al. (1994); Pearce et al. (1994). Transport from column shaped subzones oriented parallel and perpendicular to flow are reported by Gellar and Hunt (1993) and Anderson et al. (1992), respectively.

Figure 6 - Conceptualization of mass transfer into a flowing aqueous phase adjacent to a DNAPL subzone

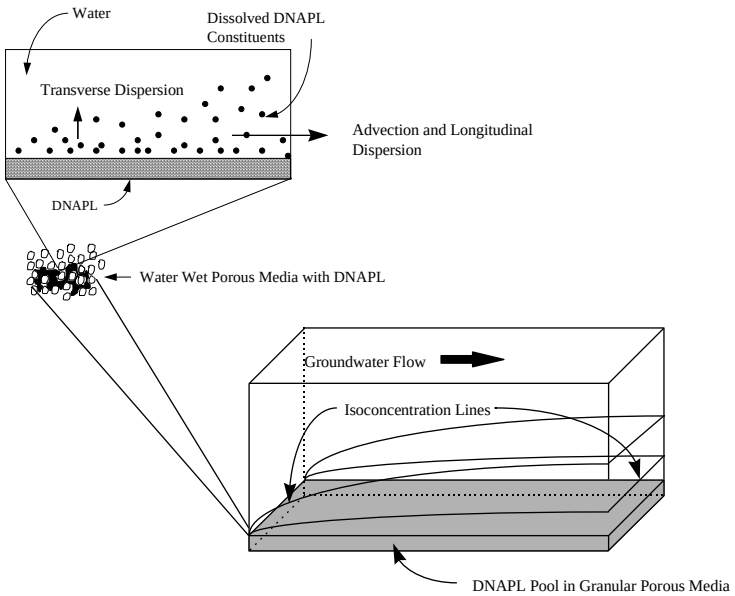

Pool studies performed by Evangelos et al. (1994); Whelan et al. (1994); and Pearce et al. (1994) involved point measurements of aqueous concentration about DNAPL pools. These data show 1) order of magnitude changes in aqueous concentrations over distances of a few centimeters above pools, 2) steep concentration gradients at the influent end of a pool which lessen with distance along a pool, and 3) aqueous concentrations approaching effective solubility along the interface of the NAPL subzone. Laboratory studies reported by Schwille (1988) and Gellar and Hunt (1993) report whole-flume effluent concentrations on the order of 1 and 10 percent of effective solubility, respectively.

Following the methods of Bird et al., (1960) for diffusion into a flowing liquid film, as modified by Hunt et al., (1988) for porous media, the governing equation for two-dimensional transport with one-dimensional flow is

$$V_w \frac{dC_a}{dx} = D_T \frac{d^2 C_a}{dz^2} \tag{7}$$

The variables x and z are the distance along the pool in the direction of flow and above the pool, respectively. D_T is the transverse dispersion coefficient (L^2/T). A key assumption implicit in (7) is that longitudinal dispersion is negligible relative to advective transport. Relevant boundary conditions for a semi-infinite plane source located at $x \geq 0$ and $z = 0$ are:

$$C_a = C_s \text{ for } x < 0,\ z = 0 \tag{8}$$

$$C_a = 0 \text{ for } x = 0 \tag{9}$$

$$C_a = 0 \text{ for } z = \infty \tag{9a}$$

Solving (7) subject to (8), (9), and (9a)

$$C_a(x,z) = C_s(1 - erf(\frac{z}{2\sqrt{D_T x/V_w}})) \tag{10}$$

The mass flux from the pool surface as a function of distance along the pool is obtained by computing the concentration gradient in the z-direction at the pool surface for use in the mass flux equation. This results in

$$J(x) = -\phi D_T \left.\frac{\partial C}{\partial Z}\right|_{x=0} = C_s \phi \sqrt{V_w D_T / x\pi} \qquad (11)$$

where $J(x)$ (M/(T-L^2)) is the mass flux from the pool into the flowing aqueous phase. Figures 7 and 8 plot results obtained from (10) and (11) with C_s = 1000 mg/l, V_w = 1 E-6 m/sec, and D_T = 1 E-9 m^2/sec.

Figure 7 - Normalized concentration above a DNAPL pool

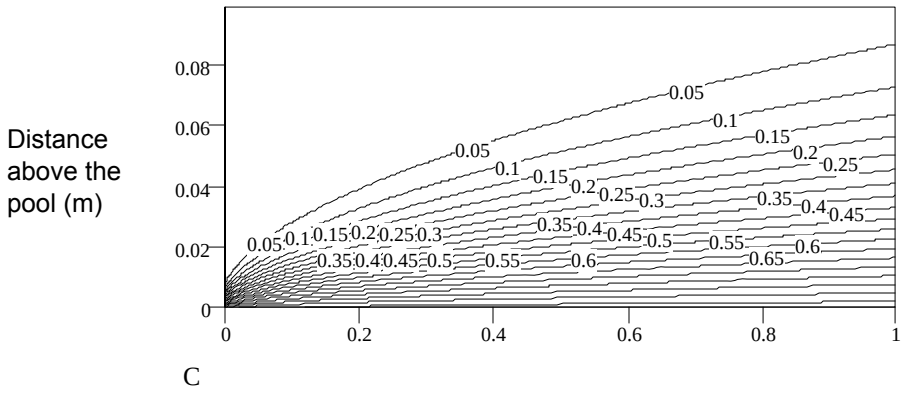

Figure 8 - Mass transfer flux along a DNAPL pool

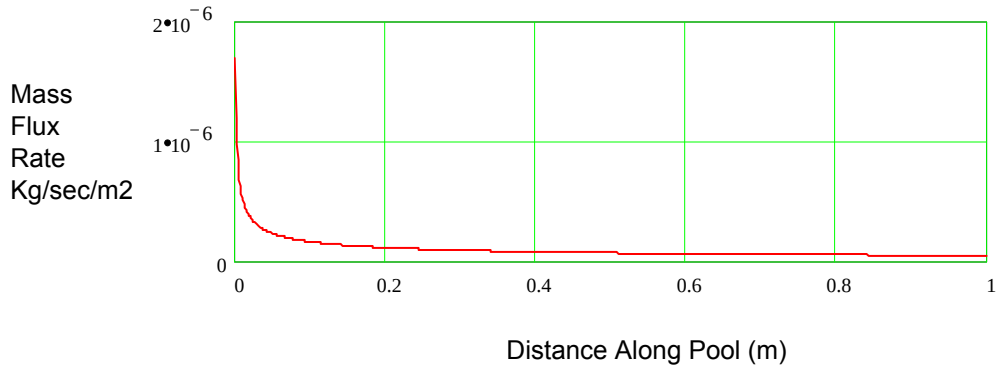

Finally, the total mass transfer rate per unit width of the pool can be estimated by integrating (11) with respect to *x* from *x*=0 to *x*=*L*. This results in

$$\dot{M}_W = 2\phi C_s \sqrt{\frac{LV_w D_T}{\pi}} \qquad (12)$$

where $\dot{M}_W$ is the bulk mass transfer rate per unit width of pool (M/(TL)).

Flux 2 Derivation

Following Miller et al. (1990) analysis of steady-state non-reactive transport in a semi-infinite column results in the following governing equation

$$\frac{D_L \partial^2 C_a}{\partial^2 x} - \frac{K_l (C_s - C_a)}{\phi} = \frac{V_w \partial C_a}{\partial x} \qquad (3)$$

The variable *x* is the distance into a semi-infinite DNAPL zone in the direction of flow, D_L is the longitudinal dispersion coefficient (L^2/T), and V_w is the seepage velocity (L/T). Boundary conditions considered by Miller et al. (1990) are

$$C_a = 0 \qquad \text{at } x=0 \qquad (4)$$

$$\frac{dC_a}{dx} = 0 \qquad \text{at } x = \infty \qquad (5)$$

Solving (3) subject to (4) and (5) results in

$$C_a(x) = C_s(1 - \exp((\frac{x}{2D_L})(V_w - \sqrt{V_w^2 + \frac{4D_l K_l}{\phi}}))) \qquad (6)$$

Substitution of (6) into (1) allows estimation of mass transfer as a function of distance into a semi-infinite DNAPL zone. Figure 9 plots mass transfer rate and normalized concentration as a function of distance into a semi-infinite uniform DNAPL zone. Conditions considered include an effective solubility of 1000 mg/l, a longitudinal dispersion coefficient D_L =10E-8 m^2/sec, a porosity ϕ=0.3, and a seepage velocity V_w =

10E-6 m/sec. The range of K_l (100 to 1000 days^{-1}) is based on results reported by Miller et al. (1990) and Imhoff et al. (1993).

Figure 9 - Mass transfer rate and normalized concentration as a function of distance along a flow path into a semi-infinite DNAPL subzone

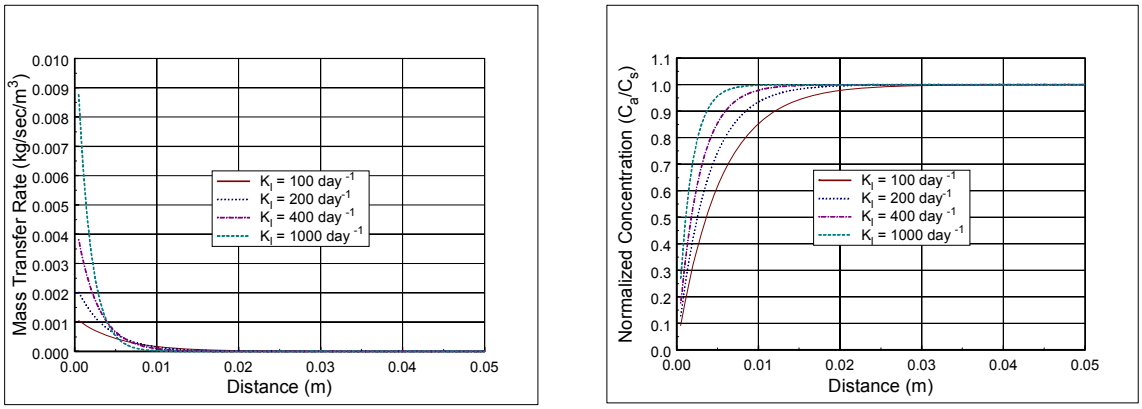

Figure 9 indicates decreasing rates of mass transfer between 0 and 0.02 m. This reflects that the difference in chemical potential driving mass transfer (C_s-C_a) rapidly approaches zero as aqueous concentrations approach effective solubility. At distances greater than 0.02 m, rates of mass transfer are essentially zero for all values of K_l. Based on Figure 9 it is noted that K_l effects the distribution of mass transfer rates at distances less than 0.02 m. On the other hand, bulk mass transfer, the product of the Darcy velocity and the aqueous concentration, is largely independent of K_l when distances greater than 0.02 m are considered. This leads to the observation that the dependence of the bulk mass transfer rate on K_l is a function of the scale being considered.

The implication of large initial rates of mass transfer is that mass transfer within DNAPL objects will occur primarily at the edges of the object. Due to near equilibrium conditions along the remainder the flow path, rates of interphase mass transfer approach zero. It is concluded that the dimensions of DNAPL subzones will decrease with time as mass is removed. This phenomena is demonstrated in laboratory data presented by Imhoff et al. (1993). Measurement of trichloroethene saturation in a column after 25, 75, and 120 pore volumes of water indicate an active dissolution interval at the leading edge of the DNAPL zone ranging from 0.011 to 0.021 m. Little to no active dissolution appears to be occurring in the remainder of the column.

Finally it is noted that rapid attainment of equilibrium within DNAPL zones provides no explanation for observed concentrations orders of magnitude below effective solubility within field-scale DNAPL zones. To resolve this issue it is necessary to consider how advective-dispersive transport about DNAPL subzones constrains concentration deficits ($C_s - C_a$) and overall rates of interphase mass transfer.

Subsurface Solute Transport

1. Steady source derivation

The domain of interest is shown in Fig. 1. It is assumed that the domain is infinite in extent in x, and sufficiently large in y that the solute cannot reach the upper sand boundary or the lower silt boundary during the time of interest.

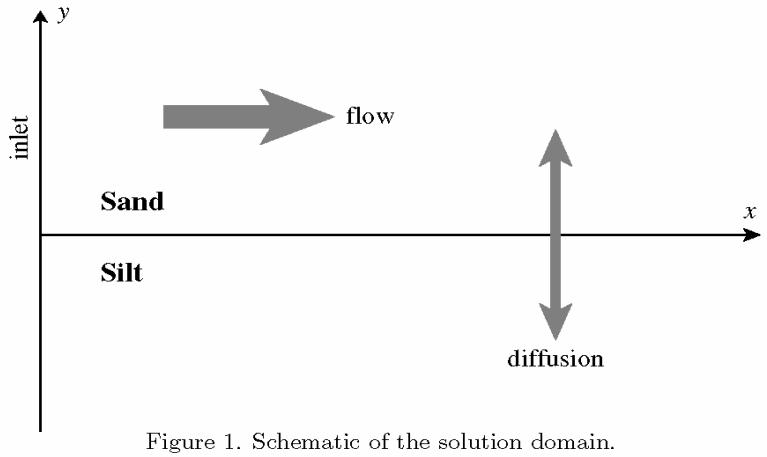

Figure 1. Schematic of the solution domain.

A number of assumptions are built into the analysis. First, it is assumed that the system is unreactive so that the retardation factor is zero. Second, it is assumed transport in the x-direction within the sand is dominated by convection. Third, it is assumed the permeability of the silt layer is small enough that the only transport within that phase is molecular. With these assumptions, the familiar forms of the species conservation equations may be written in the two phases.

Sand

The concentration of solute (contaminant) within the aqueous phase in the sand, $c(x, y, t)$, is described by a convection/diffusion equation:

$$\frac{\partial c}{\partial t} + v \frac{\partial c}{\partial x} = D_t \frac{\partial^2 c}{\partial y^2}, \tag{1}$$

where v is the groundwater velocity, and D_t is the transverse diffusion coefficient given by

$$D_t = \alpha_t v + D^*,$$

where α_t is the transverse dispersivity of the sand and D^* is an effective molecular diffusion coefficient. The associated initial condition and boundary conditions are

$$\begin{aligned} c(x, y, 0) &= 0 && \text{(IC)} \\ c(0, y, t) &= f_o(y) && \text{(BC 1)} \\ c(x, y \to \infty, t) &= 0 && \text{(BC 2)} \\ n D_t \frac{\partial c}{\partial y}(x, 0, t) &= n' D^* \frac{\partial c'}{\partial y}(x, 0, t) && \text{(BC 3)} \end{aligned}$$

The expression in BC 3 represents the flux matching boundary condition at the sand-silt interface; it contains the solute concentration within the aqueous phase in the silt, $c'(x,y,t)$, the sand porosity n, and the silt porosity n'.

Silt

Contaminant transport within the silt layer is described by an equation similar to Eq. (1), but without forced convection. The equation for c' is

$$\frac{\partial c'}{\partial t} = D^* \frac{\partial^2 c'}{\partial y^2}. \tag{2}$$

The boundary conditions associated with Eq. (2) are given by

$$\begin{aligned} c'(x,y,0) &= 0 && \text{(IC)} \\ c'(x,0,t) &= c(x,0,t) && \text{(BC 1)} \\ c'(x,y\to-\infty,t) &= 0 && \text{(BC 2)} \end{aligned}$$

Inlet boundary condition

The form for $f_o(y)$ must be specified before proceeding. Given the restrictive assumption that the contaminant source is steady, it's desirable to at least incorporate the finite size of the source in the model. The simplest way to do this using a continuous function is to assume that

$$c(0,y,t) = c_o e^{-by} \qquad (y \geq 0),$$

where c_o is the strength of the source at $y = 0$, and $b > 0$ (m^{-1}) is the decay constant of the source.

Solution

For the sets of equations, initial conditions, and boundary conditions listed above, the resulting expression for the solute concentration in the sand layer is given by

$$\begin{aligned} \frac{c}{c_o} = {} & \frac{1}{2} e^{b^2 x/\phi^2} \left[e^{by} \operatorname{erfc}\left(\frac{b}{\phi}\sqrt{x} + \frac{\phi\, y}{2\sqrt{x}} \right) + e^{-by} + e^{-by} \operatorname{erf}\left(-\frac{b}{\phi}\sqrt{x} + \frac{\phi\, y}{2\sqrt{x}} \right) \right] \\ & - \frac{\phi\,\gamma}{\pi} e^{by} \sqrt{t - x/v} \int_0^x \frac{e^{b^2\xi/\phi^2}}{\sqrt{x-\xi}} \left[\frac{\operatorname{erfc}\left(\frac{b}{\phi}\sqrt{\xi} + \frac{\phi\, y}{2\sqrt{\xi}} \right)}{\gamma^2(x-\xi) + \phi^2(t - x/v)} \right] d\xi, \end{aligned} \tag{3}$$

where this expression is valid for $y \geq 0$ and $t > x/v$ and

$$\phi = \sqrt{\frac{v}{D_t}} \qquad \text{and} \qquad \gamma = \frac{n'\sqrt{D^*}}{n\, D_t}.$$

The concentration of solute in the silt layer is given by (for $t > x/v$)

$$\frac{c'}{c_o} = \frac{1}{\sqrt{\pi}} \int_0^x \frac{I}{\sqrt{x-\xi}} \left[\frac{1}{\sqrt{\pi\,\xi}} - \frac{b}{\phi} e^{b^2\xi/\phi^2} \operatorname{erfc}\left(\frac{b}{\phi}\sqrt{\xi} \right) \right] d\xi, \tag{4}$$

where the term I in Eq. (4) is given by

$$I = \operatorname{erfc}\left(\frac{y/\sqrt{D^*}}{2\sqrt{t-x/v}}\right) - \frac{\gamma \operatorname{erfc}\left(\frac{\gamma y/\sqrt{D^*}}{2(t-x/v)\sqrt{\gamma^2/(t-x/v)+\phi^2/(x-\xi)}}\right)}{\sqrt{t-x/v}\sqrt{\gamma^2/(t-x/v) + \phi^2/(x-\xi)}\,\exp\left(\frac{\phi^2 y^2/D^*}{4[\gamma^2(x-\xi)+\phi^2(t-x/v)]}\right)}. \quad (5)$$

The expression for c' in Eqs. (4) and (5) is based on a variable transformation such that $y \geq 0$ in those equations. Thus, even though the schematic in Fig. 1 indicates that $y \leq 0$ in the silt, the variable denoted as y in Eqs. (4) and (5) must be ≥ 0.

The concentration profile in Eq. (3) can be used to evaluate the flux at the sand-silt boundary, $y = 0$. Defining the flux q_y of solute *out* of the sand and into the silt as positive,

$$q_y = -n\,D_t \frac{\partial c}{\partial y}(x,0,t),$$

the expression in Eq. (3) can be differentiated and evaluated at $y = 0$ to obtain

$$q_y = \frac{n'\,c_o}{\sqrt{\pi}}\sqrt{v\,D^*/D_t}\sqrt{t-x/v}\left\{\frac{1}{\sqrt{\gamma^2\,x(t-x/v)+\phi^2(t-x/v)^2}} + \frac{b}{\sqrt{\pi}}\int_0^x \frac{e^{b^2\xi/\phi^2}}{\sqrt{x-\xi}}\left[\frac{\operatorname{erfc}\left(\frac{b}{\phi}\sqrt{\xi}\right)}{\gamma^2(x-\xi) + \phi^2(t-x/v)}\right]d\xi\right\}. \quad (6)$$

2. Transient source derivation

The governing equations (1) and (2) for $c(x,y,t)$ and $c'(x,y,t)$ remain the same, as do most of the boundary and initial conditions. The only condition that does change is BC 1 for Eq. (1), and it is modified to model the source behavior observed in earlier experiments. That boundary condition becomes

$$c(0,y,t) = f_o(y)\,[1 - H(t-\tau)] \qquad \text{(BC 1)},$$

where H is the Heaviside step function and

$$H(t-\tau) = \begin{cases} 0, & \text{if } t \leq \tau \\ 1, & \text{if } t > \tau. \end{cases}$$

The general behavior of the inlet condition is shown in Fig. 2. The form of BC 1 assumes that the source has a constant strength (which can vary with y), until it abruptly disappears at time $t = \tau$. As with the steady case it is assumed that $f_o(y) = c_o\,e^{-by}$ for $y \geq 0$.

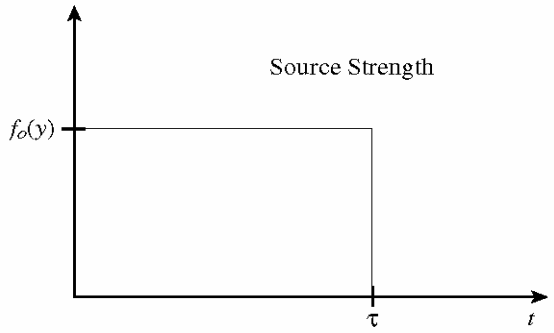

Figure 2. The inlet source is assumed to behave like a step function.

Solution

The forms of the governing equations and boundary conditions lead to solutions for c and c' applicable to three distinct time ranges.

1. $t \le x/v$: Convection dominated transport in the x direction requires that $c(x,y,t) = 0$ and $c'(x,y,t) = 0$ when $x/v \ge t$.

2. $x/v < t \le \tau + x/v$: The expressions for c and c' are the same as for the steady source, namely,

$$\frac{c}{c_o} = \frac{1}{2} e^{b^2 x/\phi^2} \left[e^{by} \operatorname{erfc}\left(\frac{b}{\phi}\sqrt{x} + \frac{\phi\, y}{2\sqrt{x}} \right) + e^{-by} + e^{-by} \operatorname{erf}\left(-\frac{b}{\phi}\sqrt{x} + \frac{\phi\, y}{2\sqrt{x}} \right) \right]$$
$$- \frac{\phi\,\gamma}{\pi} e^{by} \sqrt{t - x/v} \int_0^x \frac{e^{b^2\xi/\phi^2}}{\sqrt{x-\xi}} \left[\frac{\operatorname{erfc}\left(\frac{b}{\phi}\sqrt{\xi} + \frac{\phi\, y}{2\sqrt{\xi}} \right)}{\gamma^2(x-\xi) + \phi^2(t - x/v)} \right] d\xi, \tag{7}$$

where this expression is valid for $y \ge 0$ and

$$\phi = \sqrt{\frac{v}{D_t}} \qquad \text{and} \qquad \gamma = \frac{n'\sqrt{D^*}}{n\, D_t},$$

and

$$\frac{c'}{c_o} = \frac{1}{\sqrt{\pi}} \int_0^x \frac{I_1}{\sqrt{x-\xi}} \left[\frac{1}{\sqrt{\pi\,\xi}} - \frac{b}{\phi} e^{b^2\xi/\phi^2} \operatorname{erfc}\left(\frac{b}{\phi}\sqrt{\xi} \right) \right] d\xi, \tag{8}$$

where the term I_1 in Eq. (8) is given by

$$I_1 = \operatorname{erfc}\left(\frac{y/\sqrt{D^*}}{2\sqrt{t - x/v}} \right)$$
$$- \frac{\gamma \operatorname{erfc}\left(\frac{\gamma y/\sqrt{D^*}}{2(t-x/v)\sqrt{\gamma^2/(t-x/v) + \phi^2/(x-\xi)}} \right)}{\sqrt{t-x/v}\sqrt{\gamma^2/(t-x/v) + \phi^2/(x-\xi)}\, \exp\left(\frac{\phi^2\, y^2/D^*}{4[\gamma^2(x-\xi) + \phi^2(t-x/v)]} \right)}. \tag{9}$$

As with the steady solution, the expression for c' in Eqs. (8) and (9) is based on a variable transformation such that $y \ge 0$ in those equations. Thus, even though the schematic in Fig. 1 indicates that $y \le 0$ in the silt, the variable denoted as y in Eqs. (8) and (9) must be ≥ 0.

If we again adopt the convention that solute flux q_y ($\mathrm{kg\,m^{-2}\,s^{-1}}$) from sand to silt is positive, we find that, at $y = 0$,

$$q_y = \frac{n'\,c_o}{\sqrt{\pi}}\sqrt{v\,D^*/D_t}\sqrt{t - x/v}\left\{\frac{1}{\sqrt{\gamma^2\,x(t-x/v)+\phi^2(t-x/v)^2}} + \frac{b}{\sqrt{\pi}}\int_0^x \frac{e^{b^2\xi/\phi^2}}{\sqrt{x-\xi}}\left[\frac{\operatorname{erfc}\left(\frac{b}{\phi}\sqrt{\xi}\right)}{\gamma^2(x-\xi)\;+\;\phi^2(t-x/v)}\right]d\xi\right\}. \quad (10)$$

3. $t > \tau + x/v$: Once the source is exhausted the concentration of solute at any point in the sand or silt will be determined by diffusive transport. The concentration in the sand is given by

$$\frac{c}{c_o} = -\frac{\phi\,\gamma}{\pi}e^{by}\left\{\sqrt{t-x/v}\int_0^x \frac{e^{b^2\xi/\phi^2}}{\sqrt{x-\xi}}\left[\frac{\operatorname{erfc}\left(\frac{b}{\phi}\sqrt{\xi}+\frac{\phi\,y}{2\sqrt{\xi}}\right)}{\gamma^2(x-\xi)\;+\;\phi^2(t-x/v)}\right]d\xi - \sqrt{t-\tau-x/v}\int_0^x \frac{e^{b^2\xi/\phi^2}}{\sqrt{x-\xi}}\left[\frac{\operatorname{erfc}\left(\frac{b}{\phi}\sqrt{\xi}+\frac{\phi\,y}{2\sqrt{\xi}}\right)}{\gamma^2(x-\xi)\;+\;\phi^2(t-\tau-x/v)}\right]d\xi\right\}. \quad (11)$$

In the silt, the concentration profile is given by

$$\frac{c'}{c_o} = \frac{1}{\sqrt{\pi}}\int_0^x \frac{I_1 - I_2}{\sqrt{x-\xi}}\left[\frac{1}{\sqrt{\pi\,\xi}} - \frac{b}{\phi}e^{b^2\xi/\phi^2}\operatorname{erfc}\left(\frac{b}{\phi}\sqrt{\xi}\right)\right]d\xi, \quad (12)$$

where I_1 is given by Eq. (9) and I_2 is

$$I_2 = \operatorname{erfc}\left(\frac{y/\sqrt{D^*}}{2\sqrt{t-\tau-x/v}}\right) - \frac{\gamma\operatorname{erfc}\left(\frac{\gamma y/\sqrt{D^*}}{2(t-\tau-x/v)\sqrt{\gamma^2/(t-\tau-x/v)+\phi^2/(x-\xi)}}\right)}{\sqrt{t-\tau-x/v}\sqrt{\gamma^2/(t-\tau-x/v)\;+\;\phi^2/(x-\xi)}\,\exp\left(\frac{\phi^2\,y^2/D^*}{4[\gamma^2(x-\xi)+\phi^2(t-\tau-x/v)]}\right)}. \quad (13)$$

The flux q_y at $y = 0$ is found to be

$$q_y = \frac{n'\,c_o}{\sqrt{\pi}}\sqrt{v\,D^*/D_t}\left\{\frac{\sqrt{t-x/v}}{\sqrt{\gamma^2 x(t-x/v)+\phi^2(t-x/v)^2}} - \frac{\sqrt{t-\tau-x/v}}{\sqrt{\gamma^2 x(t-\tau-x/v)+\phi^2(t-\tau-x/v)^2}} + \frac{b}{\sqrt{\pi}}\sqrt{t-x/v}\int_0^x \frac{e^{b^2\xi/\phi^2}}{\sqrt{x-\xi}}\left[\frac{\operatorname{erfc}\left(\frac{b}{\phi}\sqrt{\xi}\right)}{\gamma^2(x-\xi)\;+\;\phi^2(t-x/v)}\right]d\xi \quad (14)$$
$$- \frac{b}{\sqrt{\pi}}\sqrt{t-\tau-x/v}\int_0^x \frac{e^{b^2\xi/\phi^2}}{\sqrt{x-\xi}}\left[\frac{\operatorname{erfc}\left(\frac{b}{\phi}\sqrt{\xi}\right)}{\gamma^2(x-\xi)\;+\;\phi^2(t-\tau-x/v)}\right]d\xi\;\right\}.$$

Retardation factor

When sorption processes are accounted for, the concentration of solute (contaminant) within the aqueous phase in the sand, $c(x, y, t)$, is described by the convection/diffusion equation

$$\frac{\partial c}{\partial t} + v \frac{\partial c}{\partial x} = D_t \frac{\partial^2 c}{\partial y^2} - \frac{\rho_b}{n} \frac{\partial C^*}{\partial t}, \tag{1}$$

where v is the average linear groundwater velocity, D_t is the transverse diffusion coefficient, C^* is the mass of solute sorbed per dry unit weight of solid, ρ_b is the bulk density of the porous medium, and n is the porosity. If a linear sorption isotherm is assumed, such that

$$C^* = K_d c,$$

where K_d is the distribution coefficient, then Eq. (1) may be rewritten as

$$R \frac{\partial c}{\partial t} + v \frac{\partial c}{\partial x} = D_t \frac{\partial^2 c}{\partial y^2}, \tag{2}$$

where the retardation factor R is given by

$$R = 1 + \frac{\rho_b}{n} K_d. \tag{3}$$

We can then define

$$v_c = \frac{v}{R},$$

where v_c is the average velocity of the solute front where the concentration is one-half of the original. Equation (2) then becomes

$$\frac{\partial c}{\partial t} + v_c \frac{\partial c}{\partial x} = \frac{D_t}{R} \frac{\partial^2 c}{\partial y^2}. \tag{3}$$

Through a similar process we arrive at an expression for the concentration of solute in the silt, c',

$$\frac{\partial c'}{\partial t} = \frac{D^*}{R'} \frac{\partial^2 c'}{\partial y^2}, \tag{4}$$

where the retardation factor in the silt, R', is

$$R' = 1 + \frac{\rho_b'}{n'} K_d',$$

and the primed quantities denote silt properties.

The bottom line is that, mathematically, the governing equations and boundary conditions are identical to those used to derive the steady state and transient solutions.

Multilayer model: solution for sand and silt

Sand

The governing equation for solute transport in the sand phase is

$$\frac{\partial c}{\partial t} + v_c \frac{\partial c}{\partial x} = \hat{D}_t \frac{\partial^2 c}{\partial y^2} - \hat{k}\, c,$$

where

$$\begin{aligned} v_c &= v/R \\ \hat{D}_t &= D_t/R \\ \hat{k} &= k/R \end{aligned}$$

and R is the retardation factor, and k is the reaction rate constant in the sand. The domain under consideration is shown in the figure below. It's assumed that the sand and silt phases alternate in a continuous manner, and that the thickness of each phase—$2B$ for silt and $2A$ for sand—is constant.

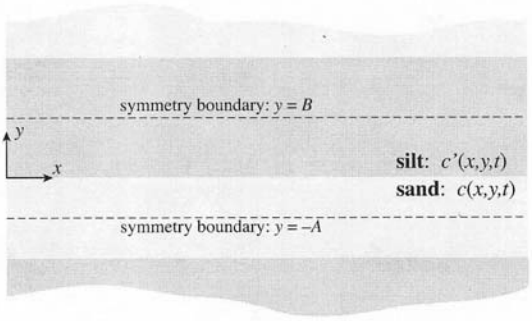

The initial and boundary conditions for the sand and silt are

$$\begin{aligned}
c(x,y,0) &= 0, \quad 0 \le x < \infty, \ -A \le y \le 0 && \text{(IC 1)} \\
c(0,y,t) &= c_o, \quad -A \le y \le 0, \ t > 0 && \text{(BC 1)} \\
c(x,0,t) &= c'(x,0,t), \quad 0 \le x < \infty, \ t > 0 && \text{(BC 2)} \\
\frac{\partial c}{\partial y}(x,-A,t) &= 0, \quad 0 \le x < \infty, \ t > 0 && \text{(BC 3)} \\
c'(x,y,0) &= 0, \quad 0 \le x < \infty, \ 0 \le y \le B && \text{(IC 2)} \\
n' D^* \frac{\partial c'}{\partial y}(x,0,t) &= n D_t \frac{\partial c}{\partial y}(x,0,t), \quad 0 \le x < \infty, \ t > 0 && \text{(BC 4)} \\
\frac{\partial c'}{\partial y}(x,B,t) &= 0, \quad 0 \le x < \infty, \ t > 0 && \text{(BC 5)}
\end{aligned}$$

1

For the special case where there is *no* homogeneous solute decay reaction occurring in the silt phase (i.e., $k' = 0$), the solution for the solute concentration in the sand phase is (for $t > x/v_c$)

$$\begin{aligned}\frac{c}{c_o} \;=\; e^{-kx/v}\Bigg\{1 \;-\; \frac{4\,\gamma}{\pi^2 B}\Bigg[\int_0^\infty\!\!\int_0^\infty \frac{\epsilon}{\omega\mathcal{D}}\Bigg\{\frac{\epsilon^2}{2}T_1\sum_{m=0}^{\infty}\left(\frac{e^{-\zeta_m(t-x/v_c)}}{\zeta_m^2+\epsilon^4/4}\right) \;-\; T_2\sum_{m=0}^{\infty}\left(\frac{\zeta_m\, e^{-\zeta_m(t-x/v_c)}}{\zeta_m^2+\epsilon^4/4}\right) \;+\; \frac{1}{2}T_3\sum_{m=0}^{\infty}\left(\frac{\zeta_m\, e^{\zeta_m x/v_c}}{\zeta_m^2+\epsilon^4/4}\right)\\ \;-\; \frac{\epsilon^2}{4}T_4\sum_{m=0}^{\infty}\left(\frac{e^{\zeta_m x/v_c}}{\zeta_m^2+\epsilon^4/4}\right)\Bigg\}d\epsilon\, d\omega\\ \;-\; \frac{2}{\pi}\sum_{n=0}^{\infty}\frac{(-1)^n}{2n+1}\cos\Big[\pi(n+1/2)\Big(\frac{A+y}{A}\Big)\Big]\;\times\\ \int_0^\infty\!\!\int_0^\infty \frac{\omega\,\epsilon}{\mathcal{D}\,(\kappa_n^2+\omega^4/4)}\Bigg\{\frac{\epsilon^2}{2}YT_5\sum_{m=0}^{\infty}\left(\frac{e^{-\zeta_m(t-x/v_c)}}{\zeta_m^2+\epsilon^4/4}\right) \;+\; T_6\sum_{m=0}^{\infty}\left(\frac{\zeta_m\, e^{-\zeta_m(t-x/v_c)}}{\zeta_m^2+\epsilon^4/4}\right)\\ \;+\; T_7\sum_{m=0}^{\infty}\left(\frac{\zeta_m\, e^{\zeta_m x/v_c}}{\zeta_m^2+\epsilon^4/4}\right) \;+\; \frac{\epsilon^2}{2}T_8\sum_{m=0}^{\infty}\left(\frac{e^{\zeta_m x/v_c}}{\zeta_m^2+\epsilon^4/4}\right)\Bigg\}d\epsilon\, d\omega\;\Bigg]\Bigg\},\end{aligned}$$

where $\gamma = n'D^*/nD_t$ and ζ_m is defined below. The terms appearing in the above expression are

$$\begin{aligned}\mathcal{D} \;&=\; \left[(E_R+H_R)^2+(Y-\Omega)^2\right]\left[(E_R+H_R)^2+(Y+\Omega)^2\right]\\
T_1 \;&=\; \left[(E_R+H_R)^2+Y^2-\Omega^2\right]Y\sin(F_x) \;+\; 2(E_R+H_R)Y\Omega[1-\cos(F_x)]\\
T_2 \;&=\; (E_R+H_R)\left[(E_R+H_R)^2+Y^2+\Omega^2\right]\sin(F_x) \;+\; \left[(E_R+H_R)^2+\Omega^2-Y^2\right]\Omega[1-\cos(F_x)]\\
T_3 \;&=\; \left[(E_R+H_R)^2+(Y-\Omega)^2\right]\left[(E_R+H_R)\sin(F_x+F_t)-(Y+\Omega)\cos(F_x+F_t)\right]\\
&\quad+\; \left[(E_R+H_R)^2+(Y+\Omega)^2\right]\left[(E_R+H_R)\sin(F_x-F_t)+(Y-\Omega)\cos(F_x-F_t)\right]\\
&\quad+\; 2\Omega\left[(E_R+H_R)^2+\Omega^2-Y^2\right]\cos(F_t) \;+\; 4(E_R+H_R)Y\Omega\sin(F_t)\\
T_4 \;&=\; \left[(E_R+H_R)^2+(Y-\Omega)^2\right]\left[(E_R+H_R)\cos(F_x+F_t)+(Y+\Omega)\sin(F_x+F_t)\right]\\
&\quad+\; \left[(E_R+H_R)^2+(Y+\Omega)^2\right]\left[(Y-\Omega)\sin(F_x-F_t)-(E_R+H_R)\cos(F_x-F_t)\right]\\
&\quad+\; 4(E_R+H_R)Y\Omega\cos(F_t) \;-\; 2\Omega\left[(E_R+H_R)^2+\Omega^2-Y^2\right]\sin(F_t)\\
T_5 \;&=\; \omega^2 e^{-\kappa_n x}(E_R+H_R)\Omega \;-\; \kappa_n e^{-\kappa_n x}\left[(E_R+H_R)^2+Y^2-\Omega^2\right]\\
&\quad+\; \kappa_n\Big[\Big((E_R+H_R)^2+Y^2-\Omega^2\Big)\cos(F_x)+2(E_R+H_R)\Omega\sin(F_x)\Big]\\
&\quad+\; \frac{\omega^2}{2}\Big[\Big((E_R+H_R)^2+Y^2-\Omega^2\Big)\sin(F_x)-2(E_R+H_R)\Omega\cos(F_x)\Big]\\
T_6 \;&=\; -\frac{\omega^2}{2}e^{-\kappa_n x}\Omega\left[(E_R+H_R)^2+\Omega^2-Y^2\right] \;+\; \kappa_n e^{-\kappa_n x}(E_R+H_R)\left[(E_R+H_R)^2+Y^2+\Omega^2\right]\\
&\quad-\; \kappa_n\Big[(E_R+H_R)\Big((E_R+H_R)^2+Y^2+\Omega^2\Big)\cos(F_x) \;+\; \Omega\Big((E_R+H_R)^2+\Omega^2-Y^2\Big)\sin(F_x)\Big]\\
&\quad+\; \frac{\omega^2}{2}\Big[\Omega\Big((E_R+H_R)^2+\Omega^2-Y^2\Big)\cos(F_x) \;-\; (E_R+H_R)\Big((E_R+H_R)^2+Y^2+\Omega^2\Big)\sin(F_x)\Big]\end{aligned}$$

$$
\begin{aligned}
T_7 \;=\; & \frac{\omega^2}{2} e^{-\kappa_n x}\Big[\Big((E_R+H_R)^2+\Omega^2-Y^2\Big)\Omega\cos(F_t) \;+\; 2(E_R+H_R)Y\Omega\sin(F_t)\Big] \\
& -\; \kappa_n e^{-\kappa_n x}\Big[(E_R+H_R)\Big((E_R+H_R)^2+Y^2+\Omega^2\Big)\cos(F_t) + \Big((E_R+H_R)^2+Y^2-\Omega^2\Big)Y\sin(F_t)\Big] \\
& +\; \kappa_n\Big[(E_R+H_R)\Big((E_R+H_R)^2+Y^2+\Omega^2\Big)\cos(F_x)\cos(F_t) \;+\; \Big((E_R+H_R)^2+\Omega^2-Y^2\Big)\Omega\sin(F_x)\cos(F_t) \\
& \qquad +\; \Big((E_R+H_R)^2+Y^2-\Omega^2\Big)Y\cos(F_x)\sin(F_t) \;+\; 2(E_R+H_R)Y\Omega\sin(F_x)\sin(F_t)\Big] \\
& +\; \frac{\omega^2}{2}\Big[-\Big((E_R+H_R)^2+\Omega^2-Y^2\Big)\Omega\cos(F_x)\cos(F_t) \;-\; 2(E_R+H_R)Y\Omega\cos(F_x)\sin(F_t) \\
& \qquad +\; (E_R+H_R)\Big((E_R+H_R)^2+Y^2+\Omega^2\Big)\sin(F_x)\cos(F_t) \\
& \qquad +\; \Big((E_R+H_R)^2+Y^2-\Omega^2\Big)Y\sin(F_x)\sin(F_t)\Big] \\
T_8 \;=\; & \frac{\omega^2}{2} e^{-\kappa_n x}\Big[\Big((E_R+H_R)^2+\Omega^2-Y^2\Big)\Omega\sin(F_t) \;-\; 2(E_R+H_R)Y\Omega\cos(F_t)\Big] \\
& +\; \kappa_n e^{-\kappa_n x}\Big[\Big((E_R+H_R)^2+Y^2-\Omega^2\Big)Y\cos(F_t) \;-\; (E_R+H_R)\Big((E_R+H_R)^2+Y^2+\Omega^2\Big)\sin(F_t)\Big] \\
& +\; \kappa_n\Big[(E_R+H_R)\Big((E_R+H_R)^2+Y^2+\Omega^2\Big)\cos(F_x)\sin(F_t) \;-\; \Big((E_R+H_R)^2+Y^2-\Omega^2\Big)Y\cos(F_x)\cos(F_t) \\
& \qquad +\; \Big((E_R+H_R)^2+\Omega^2-Y^2\Big)\Omega\sin(F_x)\sin(F_t) \;-\; 2(E_R+H_R)Y\Omega\sin(F_x)\cos(F_t)\Big] \\
& +\; \frac{\omega^2}{2}\Big[-\Big((E_R+H_R)^2+\Omega^2-Y^2\Big)\Omega\cos(F_x)\sin(F_t) \;+\; 2(E_R+H_R)Y\Omega\sin(F_x)\cos(F_t) \\
& \qquad +\; (E_R+H_R)\Big((E_R+H_R)^2+Y^2+\Omega^2\Big)\sin(F_x)\sin(F_t) \\
& \qquad -\; \Big((E_R+H_R)^2+Y^2-\Omega^2\Big)Y\sin(F_x)\cos(F_t)\Big].
\end{aligned}
$$

In the expressions above for T_1 through T_8,

$$
F_x \;=\; \frac{\omega^2 x}{2} \qquad \text{and} \qquad F_t \;=\; \frac{\epsilon^2 t}{2}.
$$

Also,

$$
\begin{aligned}
E_R &= \frac{\phi\,\omega}{2}\left[\frac{\sinh(\phi A\omega)-\sin(\phi A\omega)}{\cosh(\phi A\omega)+\cos(\phi A\omega)}\right] \\
H_R &= \frac{\gamma^*\,\epsilon}{2}\left[\frac{\sinh(B^*\epsilon)-\sin(B^*\epsilon)}{\cosh(B^*\epsilon)+\cos(B^*\epsilon)}\right] \\
Y &= \frac{\gamma^*\,\epsilon}{2}\left[\frac{\sinh(B^*\epsilon)+\sin(B^*\epsilon)}{\cosh(B^*\epsilon)+\cos(B^*\epsilon)}\right] \\
\Omega &= \frac{\phi\,\omega}{2}\left[\frac{\sinh(\phi A\omega)+\sin(\phi A\omega)}{\cosh(\phi A\omega)+\cos(\phi A\omega)}\right] \\
\kappa_n &= \left(\frac{\pi(n+1/2)}{\phi\,A}\right)^2 \\
\zeta_m &= \left(\frac{\pi(m+1/2)}{B^*}\right)^2
\end{aligned}
$$

And in these expressions,

$$\gamma^* = \frac{n'\sqrt{R'D^*}}{n\,D_t}$$

$$B^* = \frac{B}{\sqrt{\hat{D}^*}} = B\sqrt{\frac{R'}{D^*}}$$

$$\phi = \sqrt{\frac{v}{D_t}}$$

Silt

For the special case where $k' = 0$, the equation governing solute transport in the silt phase is

$$\frac{\partial c'}{\partial t} = \hat{D}^* \frac{\partial^2 c'}{\partial y^2},$$

where $\hat{D}^* = D^*/R'$. The solution of this equation, subject to the boundary conditions shown on the first page, is

$$\begin{aligned}\frac{c'}{c_o} = \frac{4}{\pi^2 A} e^{-kx/v} \Bigg\{ & \int_0^\infty \int_0^\infty \sum_{n=0}^{\infty} \left[\frac{\omega}{\epsilon\,\mathcal{D}} \left(\frac{1}{\kappa_n^2 + \omega^4/4} \right) \left(-\frac{1}{2} T_1' + T_2' \right) \right] d\epsilon\, d\omega \\ & + \frac{2}{\pi} \sum_{m=0}^{\infty} \frac{(-1)^m}{2m+1} \cos\left[\pi(m+1/2) \left(\frac{B-y}{B} \right) \right] \times \\ & \int_0^\infty \int_0^\infty \sum_{n=0}^{\infty} \left[\frac{\epsilon\,\omega}{(\kappa_n^2 + \omega^4/4)(\zeta_m^2 + \epsilon^4/4)\mathcal{D}} \left(\frac{1}{2} e^{\zeta_m x/v_c} \left[\frac{\epsilon^2}{2} T_1' + \zeta_m T_3' \right] \right. \right. \\ & \left. \left. - e^{-\zeta_m (t - x/v_c)} \left[\frac{\epsilon^2}{2} T_2' + \zeta_m T_4' \right] \right) \right] d\epsilon\, d\omega \Bigg\}\end{aligned}$$

In this expression for c', ζ_m, κ_n, and $\mathcal{D}$ are the same as defined above, and

$$\begin{aligned} T_1' = {} & \kappa_n \Big[\Big((E_R + H_R)^2 + (Y - \Omega)^2 \Big) \Big((Y + \Omega)\cos(F_x + F_t) - (E_R + H_R)\sin(F_x + F_t) \Big) \\ & + \Big((E_R + H_R)^2 + (Y + \Omega)^2 \Big) \Big((E_R + H_R)\sin(F_x - F_t) + (Y - \Omega)\cos(F_x - F_t) \Big) \Big] \\ & + \frac{\omega^2}{2} \Big[\Big((E_R + H_R)^2 + (Y - \Omega)^2 \Big) \Big((Y + \Omega)\sin(F_x + F_t) + (E_R + H_R)\cos(F_x + F_t) \Big) \\ & + \Big((E_R + H_R)^2 + (Y + \Omega)^2 \Big) \Big((Y - \Omega)\sin(F_x - F_t) - (E_R + H_R)\cos(F_x - F_t) \Big) \Big] \\ & + 2\kappa_n e^{-\kappa_n x} \Big[(E_R + H_R) \Big((E_R + H_R)^2 + Y^2 + \Omega^2 \Big) \sin(F_t) - Y \Big((E_R + H_R)^2 + Y^2 - \Omega^2 \Big) \cos(F_t) \Big] \\ & + \omega^2 e^{-\kappa_n x} \Big[2(E_R + H_R) Y \Omega \cos(F_t) - \Big((E_R + H_R)^2 + \Omega^2 - Y^2 \Big) \Omega \sin(F_t) \Big] \\ T_2' = {} & \kappa_n \Big[\Big((E_R + H_R)^2 + Y^2 - \Omega^2 \Big) Y \cos(F_x) + 2(E_R + H_R) Y \Omega \sin(F_x) \Big] \\ & + \frac{\omega^2}{2} \Big[\Big((E_R + H_R)^2 + Y^2 - \Omega^2 \Big) Y \sin(F_x) - 2(E_R + H_R) Y \Omega \cos(F_x) \Big] \\ & - \kappa_n e^{-\kappa_n x} Y \Big((E_R + H_R)^2 + Y^2 - \Omega^2 \Big) + \omega^2 e^{-\kappa_n x} (E_R + H_R) Y \Omega \end{aligned}$$

$$
\begin{aligned}
T_3' \;=\; & -\kappa_n\Big[\Big((E_R+H_R)^2+(Y-\Omega)^2\Big)\Big((Y+\Omega)\sin(F_x+F_t)\;+\;(E_R+H_R)\cos(F_x+F_t)\Big)\\
& \quad +\;\Big((E_R+H_R)^2+(Y+\Omega)^2\Big)\Big((E_R+H_R)\cos(F_x-F_t)\;-\;(Y-\Omega)\sin(F_x-F_t)\Big)\Big]\\
& -\frac{\omega^2}{2}\Big[\Big((E_R+H_R)^2+(Y-\Omega)^2\Big)\Big((E_R+H_R)\sin(F_x+F_t)\;-\;(Y+\Omega)\cos(F_x+F_t)\\
& \quad +\;\Big((E_R+H_R)^2+(Y+\Omega)^2\Big)\Big((E_R+H_R)\sin(F_x-F_t)\;+\;(Y-\Omega)\cos(F_x-F_t)\Big)\Big]\\
& +\;2\kappa_n e^{-\kappa_n x}\Big[Y\Big((E_R+H_R)^2+Y^2-\Omega^2\Big)\sin(F_t)\;+\;(E_R+H_R)\Big((E_R+H_R)^2+Y^2+\Omega^2\Big)\cos(F_t)\Big]\\
& -\;\omega^2 e^{-\kappa_n x}\Big[\Omega\Big((E_R+H_R)^2+\Omega^2-Y^2\Big)\cos(F_t)\;+\;2(E_R+H_R)Y\Omega\sin(F_t)\Big]\\
T_4' \;=\; & -\kappa_n\Big[\Omega\Big((E_R+H_R)^2+\Omega^2-Y^2\Big)\sin(F_x)\;+\;(E_R+H_R)\Big((E_R+H_R)^2+Y^2+\Omega^2\Big)\cos(F_x)\Big]\\
& -\frac{\omega^2}{2}\Big[(E_R+H_R)\Big((E_R+H_R)^2+Y^2+\Omega^2\Big)\sin(F_x)\;-\;\Omega\Big((E_R+H_R)^2+\Omega^2-Y^2\Big)\cos(F_x)\Big]\\
& +\;\kappa_n e^{-\kappa_n x}(E_R+H_R)\Big((E_R+H_R)^2+Y^2+\Omega^2\Big)\;-\;\frac{\omega^2}{2}e^{-\kappa_n x}\Omega\Big((E_R+H_R)^2+\Omega^2-Y^2\Big)
\end{aligned}
$$

The terms F_x, F_t, Y, Ω, E_R, and H_R are defined above.

REFERENCES CITED

Bird, R, B., W.E. Stewart, and E.N. Lightfoot. 1960. *Transport Phenomena*. John Wiley and Sons, Inc.

Gellar, J.T., and J.R. Hunt. 1993. “Mass Transfer From Nonaqueous Phase Organic Liquids in Water Saturated Porous Media.” *Water Resources Research*, Vol. 29, No. 4, pp. 833-845.

Schwille, F. 1988. *Dense Chlorinated Solvents in Porous and Fractured Media*. Translated by J. F. Pankow. Lewis Publishers, Boca Raton, Florida.

APPENDIX D
ANALYTICAL CALCULATIONS

APPENDIX D: ANALYTICAL CALCULATIONS

SIMPLE CASE FLUXES 1 THROUGH 3

Developed 3/16/03 - Revised 8/7/03

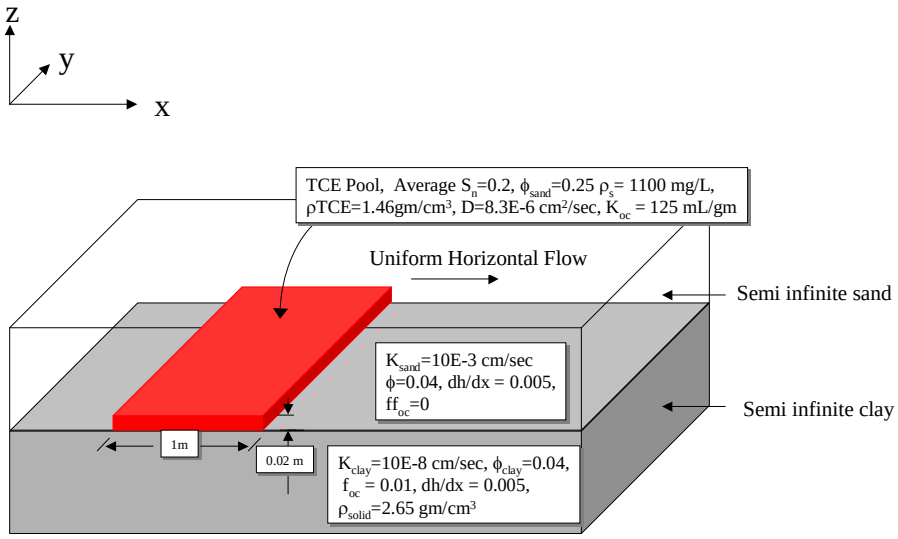

Inputs

$\rho_s := 1100 \cdot \frac{mg}{L}$ $S_n := 0.2$ $D := 8.3 \cdot 10^{-6} \cdot \frac{cm^2}{sec}$ $K_{oc} := 125 \cdot \frac{mL}{gm}$ $\rho_{solid} := 2.65 \cdot \frac{gm}{cm^3}$

$h_{pool} := 0.02 \cdot m$ $L_{pool} := 1 \cdot m$ $\rho_{TCE} := 1.46 \cdot \frac{gm}{cm^3}$ $\phi_{sand} := 0.25$ $K_{sand} := 10^{-3} \cdot \frac{cm}{sec}$

$i_{sand} := 0.005$ $foc_{sand} := 0$ $\phi_{clay} := 0.4$ $K_{clay} := 10^{-8} \cdot \frac{cm}{sec}$ $i_{clay} := 0.005$

$foc_{clay} := 0.01$

1) Calculate, for the sand and the clay, a) the seepage velocity (vw) b) the effective diffusion coefficients (De), c) the retardation factors (R):

$$v_{wsand} := \frac{K_{sand} \cdot i_{sand}}{\phi_{sand}} \qquad v_{wsand} = 2 \times 10^{-7} \frac{m}{s} \qquad v_{wsand} = 20.707 \frac{ft}{yr}$$

$$v_{wclay} := \frac{K_{clay} \cdot i_{clay}}{\phi_{clay}} \qquad v_{wclay} = 1.25 \times 10^{-12} \frac{m}{s} \qquad v_{wclay} = 1.294 \times 10^{-4} \frac{ft}{yr}$$

$$D_{esand} := D \cdot \phi_{sand}^{\frac{1}{3}} \qquad D_{esand} = 5.229 \times 10^{-10} \frac{m^2}{s}$$

$$D_{eclay} := D \cdot \phi_{clay}^{\frac{1}{3}} \qquad D_{eclay} = 6.115 \times 10^{-10} \frac{m^2}{s}$$

$$R_{clay} := 1 + \frac{\left[K_{oc} \cdot foc_{clay} \cdot \rho_{solid} \cdot \left(1 - \phi_{clay}\right)\right]}{\phi_{clay}} \qquad R_{clay} = 5.969$$

$$R_{sand} := 1 + \frac{\left[K_{oc} \cdot foc_{sand} \cdot \rho_{solid} \cdot \left(1 - \phi_{sand}\right)\right]}{\phi_{sand}} \qquad R_{sand} = 1$$

2) Estimate the steady state rate of contaminant discharge (kg/sec/m of pool width) due to flow through the pool. Assume the relative permeability to the wetting phase in the pool is 0.1.

$$k_{rw} := 0.1 \qquad M_{Through} := K_{sand} \cdot k_{rw} \cdot i_{sand} \cdot h_{pool} \cdot \rho_s \qquad M_{Through} = 1.1 \times 10^{-10} \frac{kg}{ms}$$

3) Estimate the steady state rate of contaminant discharge (kg/sec/m of pool width) due to transverse diffusions into groundwater flowing in the sand above the pool.

$$M_{sand} := 2 \cdot \phi_{sand} \cdot \rho_s \cdot \sqrt{\frac{L_{pool} \cdot v_{wsand} \cdot D_{esand}}{\pi}} \qquad M_{sand} = 3.173 \times 10^{-9} \frac{kg}{ms}$$

4) Accounting for adsorption, estimate the rate of contaminant mass discharge (kg/sec/m of pool width) into the clay layer at 1, 10, 100, and 1000 days. Assume 1) the footprint of the pool is constant and 2) $\rho s = \rho TCE$ at the sand-clay contact, remain constant.

$$M_{clay}(R, t) := \phi_{clay} \cdot \rho_s \cdot \sqrt{\frac{D_{eclay} \cdot R}{\pi \cdot t}} \cdot 1 \cdot m$$

$$M_{clay}(R_{clay}, 1 \cdot day) = 5.102 \times 10^{-8} \frac{kg}{ms}$$

$$M_{clay}(R_{clay}, 10 \cdot day) = 1.614 \times 10^{-8} \frac{kg}{ms}$$

$$M_{clay}(R_{clay}, 100 \cdot day) = 5.102 \times 10^{-9} \frac{kg}{ms}$$

$$M_{clay}(R_{clay}, 1000 \cdot day) = 1.614 \times 10^{-9} \frac{kg}{ms}$$

5) Using the values calculated in 2-4 estimate, the percent of total mass discharge attributable to flow through the pool, transverse diffusion into the sand above the pool, and diffusion into the clay below the pool at 1, 10, 100, and 1000

days. Assume all of the pool properties remain constant through time. Plot the data on a semi log plot (linear % [y axis] and log time [x axis]).

$$M_{Total}(t) := M_{Through} + M_{sand} + M_{clay}(R_{clay}, t)$$

$t_i :=$

$1 \cdot day$
$10 \cdot day$
$100 \cdot day$
$1000 \cdot day$

$$\%_{Through}(t) := 100 \cdot \frac{M_{Through}}{M_{Total}(t)} \qquad \%_{Above}(t) := 100 \cdot \frac{M_{sand}}{M_{Total}(t)}$$

$$\%_{Diff}(t) := 100 \cdot \frac{M_{clay}(R_{clay}, t)}{M_{Total}(t)}$$

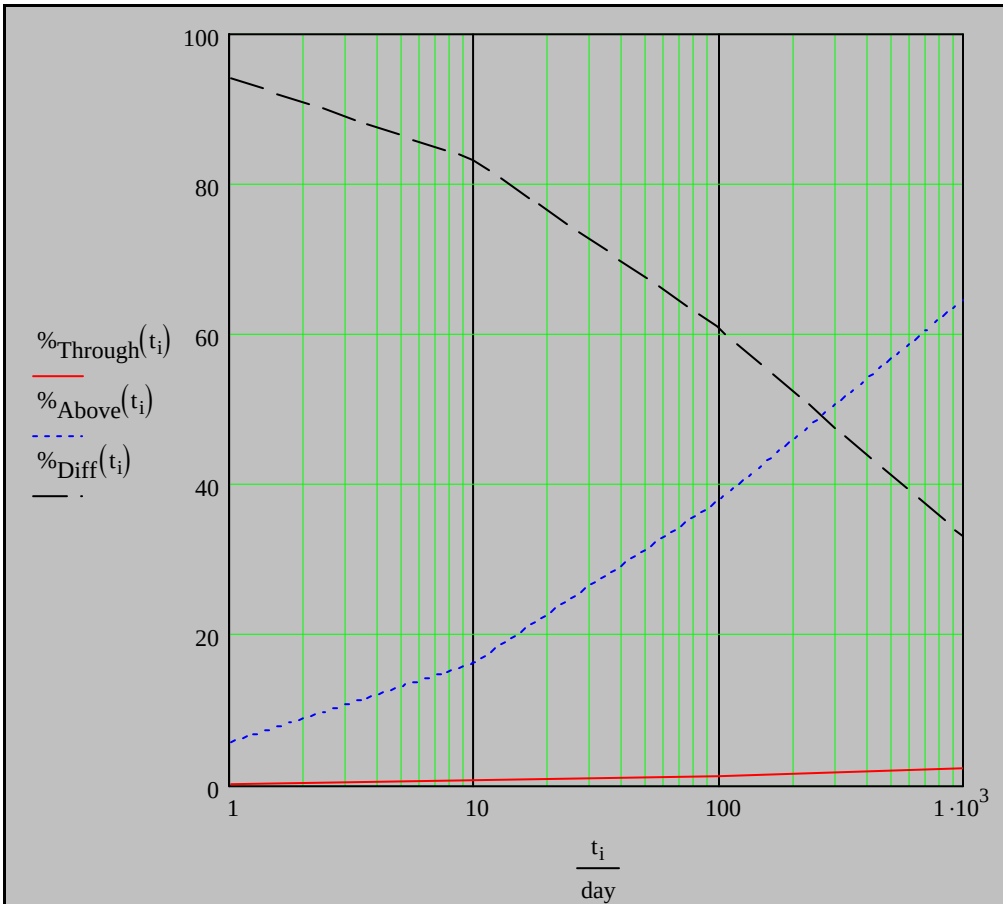

6) Calculate a) the total mass initially present in the pool, b) the percent depleted after 1000 days.

$$Mass_{Source} := 1 \cdot m \cdot h_{pool} \cdot \phi_{sand} \cdot S_n \cdot \rho_{TCE} \qquad Mass_{Source} = 1.46 \frac{kg}{m}$$

$$Mass_{Total} := \int_{0 \cdot day}^{1000 \cdot day} M_{Total}(t)\, dt \qquad Mass_{Total} = 0.562 \frac{kg}{m}$$

$$\%Depleted := 100 \cdot \frac{Mass_{Total}}{Mass_{Source}} \qquad \%Depleted = 38.527$$

7) Estimate the cumulative mass discharges to the sand above (1), silt below (2) and sand downstream (3).

$$t := 1 \cdot day, 2 \cdot day .. 1000 \cdot day$$

$$M_1(t) := 2 \cdot \phi_{sand} \cdot \rho_s \cdot t \cdot \sqrt{\frac{L_{pool} \cdot v_{wsand} \cdot D_{esand}}{\pi}} \qquad M_2(t) := 1 \cdot m \cdot 4 \cdot \phi_{clay} \cdot \rho_s \cdot \sqrt{\frac{R_{clay} \cdot D_{eclay} \cdot t}{\pi}}$$

$$M_3(t) := v_{wsand} \cdot \phi_{sand} \rho_s \cdot h_{pool} \cdot t \qquad M_T(t) := M_1(t) + M_2(t) + M_3(t)$$

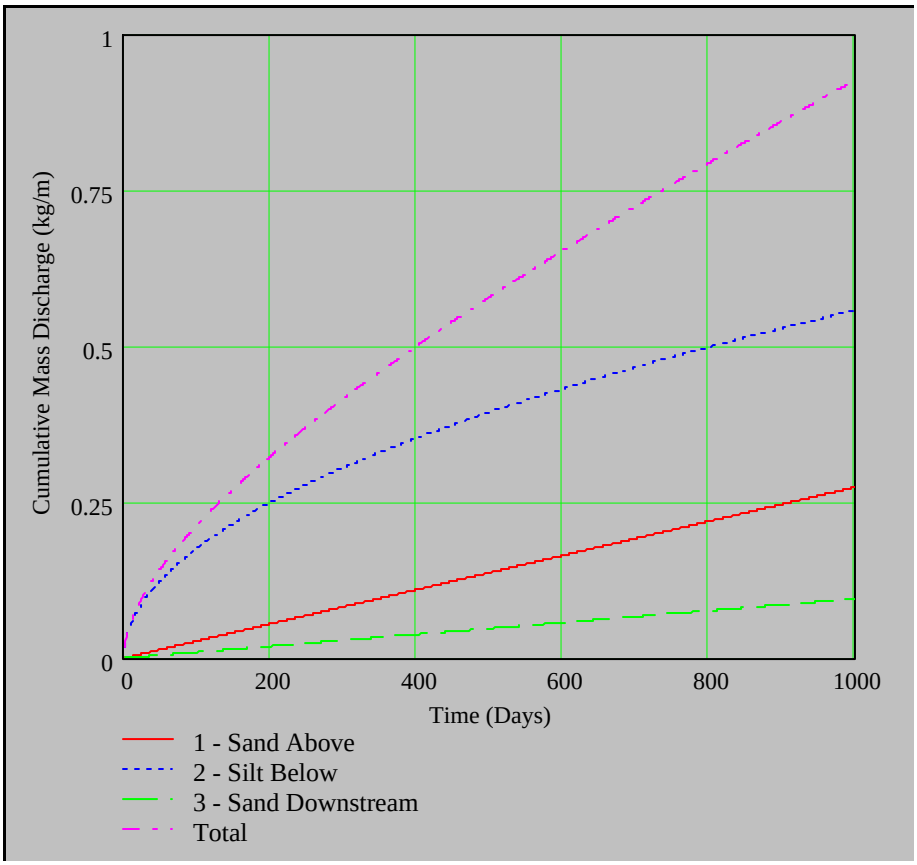

8) What Fraction of pool depleted as a function of time?

$$\frac{M_T(1000\cdot day)}{Mass_{Source}} = 0.635 \qquad \frac{M_T(1881\cdot day)}{Mass_{Source}} = 1$$

9) Estimate mass loading to the sand after the DNAPL is depleted

$t' := 1000\cdot day$ $\qquad$ $t := 1001\cdot day, 1002\cdot day .. 2000\cdot day$

$$M_2(t,t') := M_2(1000\cdot day) - \left[1\cdot m\cdot 4\cdot \phi_{clay}\cdot \rho_s\cdot\left[\sqrt{\frac{R_{clay}\cdot D_{eclay}\cdot t}{\pi}} - \sqrt{\frac{R_{clay}\cdot D_{eclay}\cdot (t-t')}{\pi}}\right]\right]$$

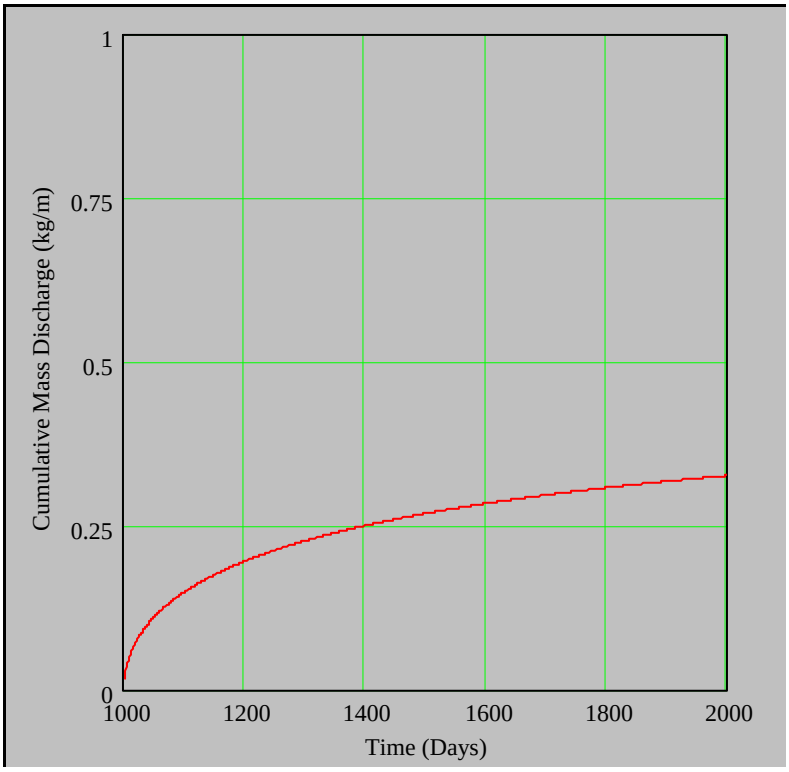
Cumulative Mass Discharge (kg/m)
1
0.75
0.5
0.25
0
1000
1200
1400
1600
1800
2000
Time (Days)

TEST OF THE ANALYTICAL SOLUTION

The following is a test of the analytical solution developed by Dave Dandy for the AFCEE Project.

Test Conditions

$v := 1 \cdot \frac{ft}{day}$ seepage velocity

$n := 0.25$ sand porosity

$n' := 0.4$ silt porosity

$b := 0.1 \cdot mm^{-1}$ source characteristic

$D_{aq} := 8.3 \cdot 10^{-6} \cdot \frac{cm^2}{sec}$ $D_t := n^{\frac{1}{3}} \cdot D_{aq} + 0.01 \cdot cm \cdot v$ $D_t = 8.756 \times 10^{-10} \frac{m^2}{s}$

$D' := n^{\frac{1}{3}} \cdot D_{aq}$ $D' = 5.229 \times 10^{-10} \frac{m^2}{s}$ $\phi := \sqrt{\frac{v}{D_t}}$

$\phi = 63.473 \frac{1}{m^{0.5}}$ $\gamma := \frac{n' \cdot \sqrt{D'}}{n \cdot D_t}$ $\gamma = 4.178 \times 10^4 \frac{s^{0.5}}{m}$

Inlet Boundary Condition

$c(y, b, c_o) := c_o \cdot e^{-b \cdot y}$ $y := 0 \cdot mm, 0.1 \cdot mm .. 100 \cdot mm$

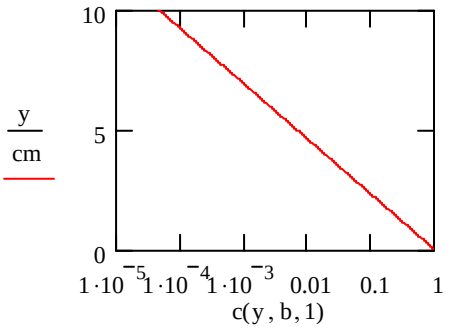

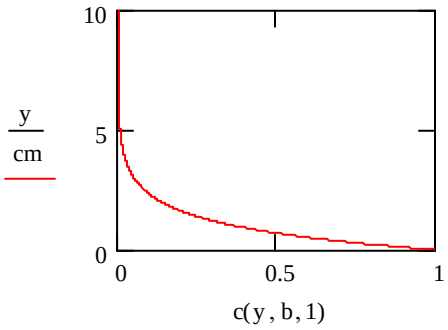

Sand

$$c'_{sand}(x,y,t) := \left[\frac{1}{2}\cdot e^{\frac{b^2\cdot x}{\phi^2}}\cdot\left(e^{b\cdot y}\cdot \operatorname{erfc}\left(\frac{b}{\phi}\cdot\sqrt{x}+\frac{\phi\cdot y}{2\cdot\sqrt{x}}\right)+e^{-b\cdot y}+e^{-b\cdot y}\cdot \operatorname{erf}\left(\frac{-b}{\phi}\cdot\sqrt{x}+\frac{\phi\cdot y}{2\cdot\sqrt{x}}\right)\right)\ldots \right.$$
$$\left. +\frac{-\phi\cdot\gamma}{\pi}\cdot e^{b\cdot y}\cdot\sqrt{t-\frac{x}{v}}\cdot\int_{0\cdot m}^{x}\frac{e^{\frac{b^2\cdot\xi}{\phi^2}}}{\sqrt{x-\xi}}\cdot\left[\frac{\operatorname{erfc}\left(\frac{b}{\phi}\cdot\sqrt{\xi}+\frac{\phi\cdot y}{2\sqrt{\xi}}\right)}{\gamma^2(x-\xi)+\phi^2\cdot\left(t-\frac{x}{v}\right)}\right]d\xi \right]$$

Silt

$$I(x,y,t,\xi) := \left[\operatorname{erfc}\left(\frac{\frac{y}{\sqrt{D'}}}{2\cdot\sqrt{t-\frac{x}{v}}}\right)\ldots \right.$$
$$\left. +-\left[\gamma\cdot\frac{\operatorname{erfc}\left[\frac{\frac{\gamma\cdot y}{\sqrt{D'}}}{2\cdot\left(t-\frac{x}{v}\right)\cdot\sqrt{\frac{\gamma^2}{\left(t-\frac{x}{v}\right)}+\frac{\phi^2}{x-\xi}}}\right]}{\sqrt{t-\frac{x}{v}}\cdot\sqrt{\frac{\gamma^2}{t-\frac{x}{v}}+\frac{\phi^2}{x-\xi}}\cdot\exp\left[\frac{\frac{\phi^2\cdot y^2}{D'}}{4\left[\gamma^2\cdot(x-\xi)+\phi^2\cdot\left(t-\frac{x}{v}\right)\right]}\right]}\right] \right]$$

$$c'_{silt}(x,y,t) := \frac{1}{\sqrt{\pi}} \cdot \int_{0 \cdot m}^{x} \frac{I(x,y,t,\xi)}{\sqrt{x-\xi}} \cdot \left(\frac{1}{\sqrt{\pi \cdot \xi}} - \frac{b}{\phi} \cdot e^{\frac{b^2 \cdot \xi}{\phi^2}} \cdot \operatorname{erfc}\left(\frac{b}{\phi} \cdot \sqrt{\xi} \right) \right) d\xi$$

Flux at the sand-silt boundary

$$M_{dot\_y}(x,t) := \frac{n'}{\sqrt{\pi}} \cdot \sqrt{v \cdot \frac{D'}{D_t}} \cdot \sqrt{t - \frac{x}{v}} \cdot \left[\frac{1}{\sqrt{\gamma^2 \cdot x \cdot \left(t - \frac{x}{v} \right) + \phi^2 \cdot \left(t - \frac{x}{v} \right)^2}} \ldots + \frac{b}{\sqrt{\pi}} \cdot \int_{0 \cdot m}^{x} \frac{e^{\frac{b^2 \cdot \xi}{\phi^2}}}{\sqrt{x-\xi}} \cdot \left[\frac{\operatorname{erfc}\left(\frac{b}{\phi} \cdot \sqrt{\xi} \right)}{\gamma^2 \cdot (x-\xi) + \phi^2 \cdot \left(t - \frac{x}{v} \right)} \right] d\xi \right]$$

Deal with condition that t<x/v C=0

$$C''_{sand}(x,y,t) := \left| \begin{array}{l} X \leftarrow c'_{sand}(x,y,t) \quad \text{if } \frac{x}{v} < t \\ X \leftarrow 0 \quad \text{otherwise} \\ X \end{array} \right. \qquad C''_{silt}(x,y,t) := \left| \begin{array}{l} X \leftarrow c'_{silt}(x,y,t) \quad \text{if } \frac{x}{v} < t \\ X \leftarrow 0 \quad \text{otherwise} \\ X \end{array} \right.$$

Sand Layer

$$AAA_{sand}(\Delta x, \Delta y, t) := \left| \begin{array}{l} n \leftarrow 0 \\ \text{for } i \in 0..40 \\ \quad \text{for } j \in 0..20 \\ \quad\quad n \leftarrow n + 1 \\ \quad\quad XX_{n,1} \leftarrow \frac{\Delta x \cdot i}{m} + 0.0001 \\ \quad\quad XX_{n,2} \leftarrow \frac{\Delta y \cdot j}{m} + 0.0001 \\ \quad\quad XX_{n,3} \leftarrow C''_{sand}(i \cdot \Delta x + 0.0001 \cdot m, j \cdot \Delta y + 0.0001 \cdot m, t) \\ XX \end{array} \right.$$

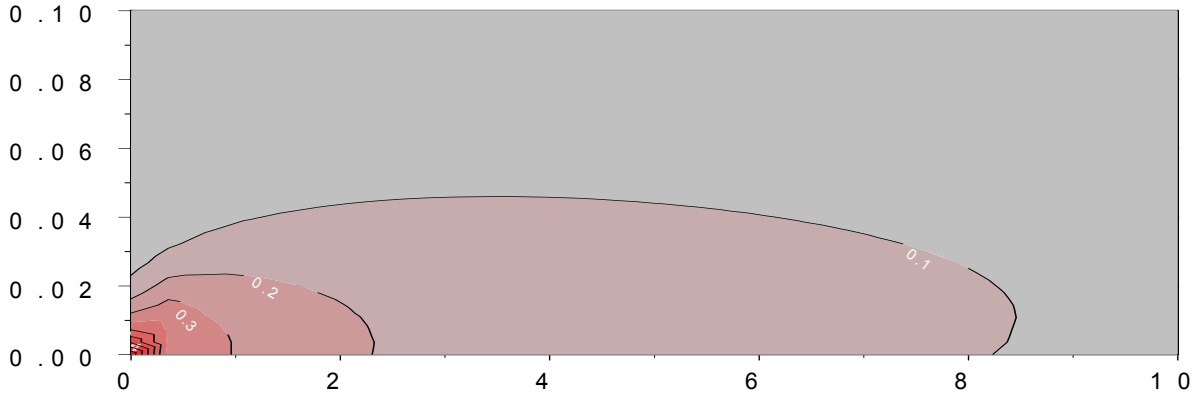

$AAA_{sand}(25\,cm, 0.5\,cm, 1000\,day)$

Silt Layer

$$AAA_{silt}(\Delta x, \Delta y, t) := \left| \begin{array}{l} n \leftarrow 0 \\ \text{for } i \in 0..40 \\ \quad \text{for } j \in 0..40 \\ \quad\quad \left| \begin{array}{l} n \leftarrow n + 1 \\ XX_{n,1} \leftarrow \frac{\Delta x \cdot i}{m} + 0.0001 \\ XX_{n,2} \leftarrow \frac{-1 \cdot \Delta y \cdot j}{m} - 0.0001 \\ XX_{n,3} \leftarrow C''_{silt}(i \cdot \Delta x + 0.0001 \cdot m, j \cdot \Delta y + 0.0001 \cdot m, t) \end{array} \right. \\ XX \end{array} \right.$$

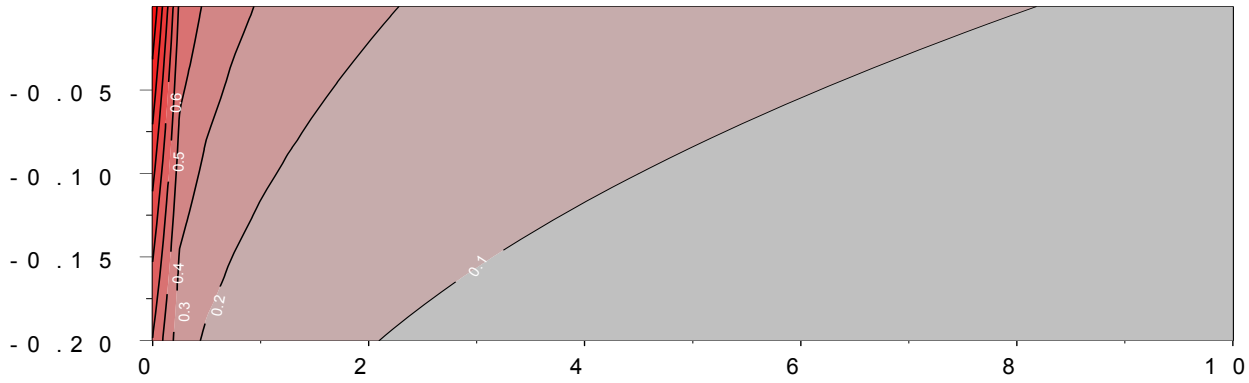

$AAA_{silt}(25\,cm, 0.5\,cm, 1000\,day)$

Both Layers

$$AAA_{sand\_silt}(\Delta x, \Delta y, t) := \left| \begin{array}{l} n \leftarrow 0 \\ \text{for } i \in 0..40 \\ \quad \text{for } j \in 0..20 \\ \quad\quad n \leftarrow n + 1 \\ \quad\quad XX_{n,1} \leftarrow \frac{\Delta x \cdot i}{m} + 0.0001 \\ \quad\quad XX_{n,2} \leftarrow \frac{\Delta y \cdot j}{m} + 0.0001 \\ \quad\quad XX_{n,3} \leftarrow C''_{sand}(i \cdot \Delta x + 0.0001 \cdot m, j \cdot \Delta y + 0.0001 \cdot m, t) \\ \text{for } i \in 0..40 \\ \quad \text{for } j \in 0..40 \\ \quad\quad n \leftarrow n + 1 \\ \quad\quad XX_{n,1} \leftarrow \frac{\Delta x \cdot i}{m} + 0.0001 \\ \quad\quad XX_{n,2} \leftarrow \frac{-1 \cdot \Delta y \cdot j}{m} - 0.0001 \\ \quad\quad XX_{n,3} \leftarrow C''_{silt}(i \cdot \Delta x + 0.0001 \cdot m, j \cdot \Delta y + 0.0001 \cdot m, t) \\ XX \end{array} \right.$$

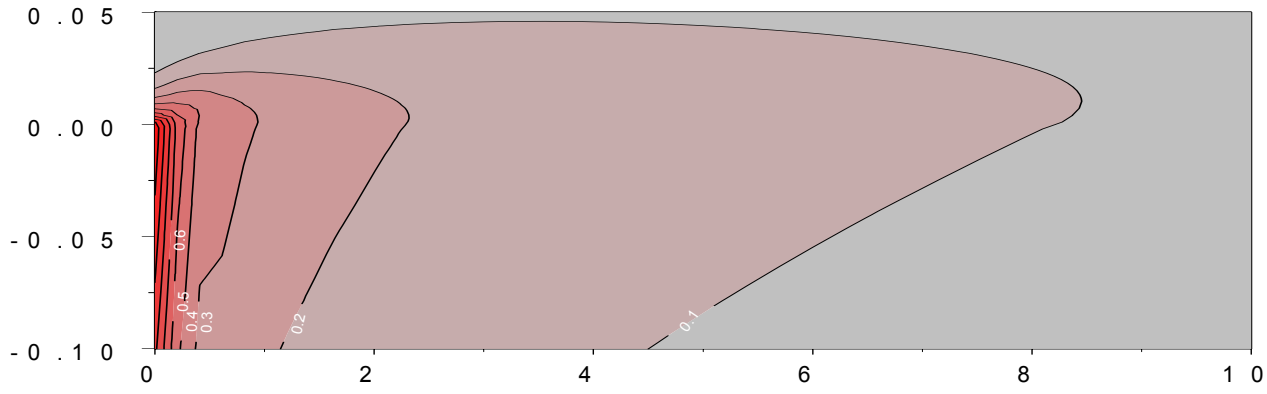

$AAA_{sand\_silt}(25 \cdot cm, 0.25cm, 1000day)$

Superposition in Time

t = total time

t' = time source ended

$$Cx''_{sand}(x,y,t,t') := \begin{| X \leftarrow C''_{sand}(x,y,t) \quad \text{if } t \le t' \\ X \leftarrow C''_{sand}(x,y,t) - C''_{sand}(x,y,t-t') \quad \text{otherwise} \\ X}$$

$$Cx''_{silt}(x,y,t,t') := \begin{| X \leftarrow C''_{silt}(x,y,t) \quad \text{if } t \le t' \\ X \leftarrow C''_{silt}(x,y,t) - C''_{silt}(x,y,t-t') \quad \text{otherwise} \\ X}$$

$$AAAx_{sand\_silt}(\Delta x,\Delta y,t,t') := \begin{| n \leftarrow 0 \\ \text{for } i \in 0..40 \\ \quad \text{for } j \in 0..20 \\ \quad\quad \begin{| n \leftarrow n+1 \\ XX_{n,1} \leftarrow \frac{\Delta x \cdot i}{m} + 0.0001 \\ XX_{n,2} \leftarrow \frac{\Delta y \cdot j}{m} + 0.0001 \\ XX_{n,3} \leftarrow Cx''_{sand}(i\cdot\Delta x + 0.0001\cdot m, j\cdot\Delta y + 0.0001\cdot m, t, t') \\ \text{for } i \in 0..40 \\ \quad \text{for } j \in 0..40 \\ \quad\quad \begin{| n \leftarrow n+1 \\ XX_{n,1} \leftarrow \frac{\Delta x \cdot i}{m} + 0.0001 \\ XX_{n,2} \leftarrow \frac{-1\cdot\Delta y \cdot j}{m} - 0.0001 \\ XX_{n,3} \leftarrow Cx''_{silt}(i\cdot\Delta x + 0.0001\cdot m, j\cdot\Delta y + 0.0001\cdot m, t, t') \\ XX}$$

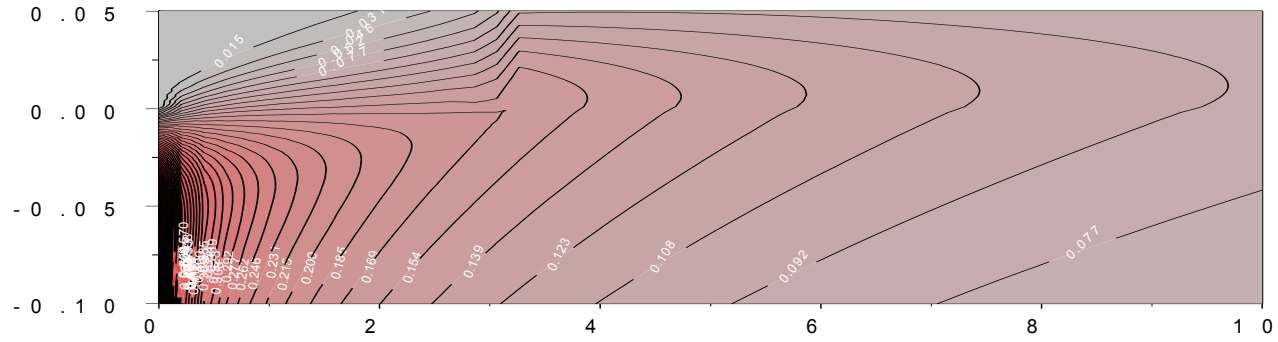

$AAAx_{sand\_silt}(25\,cm, 0.25cm, 1010day, 1000day)$

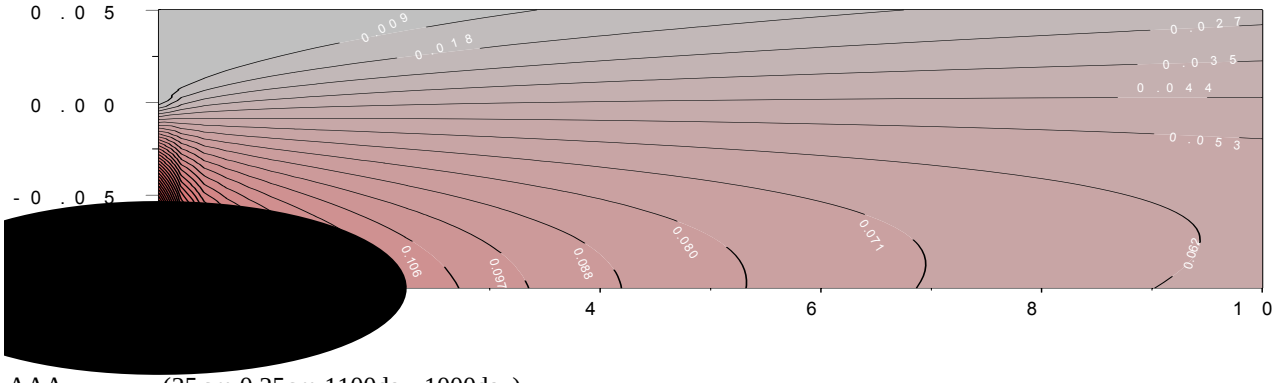

$AAAx_{sand\_silt}(25\,cm, 0.25cm, 1100day, 1000day)$

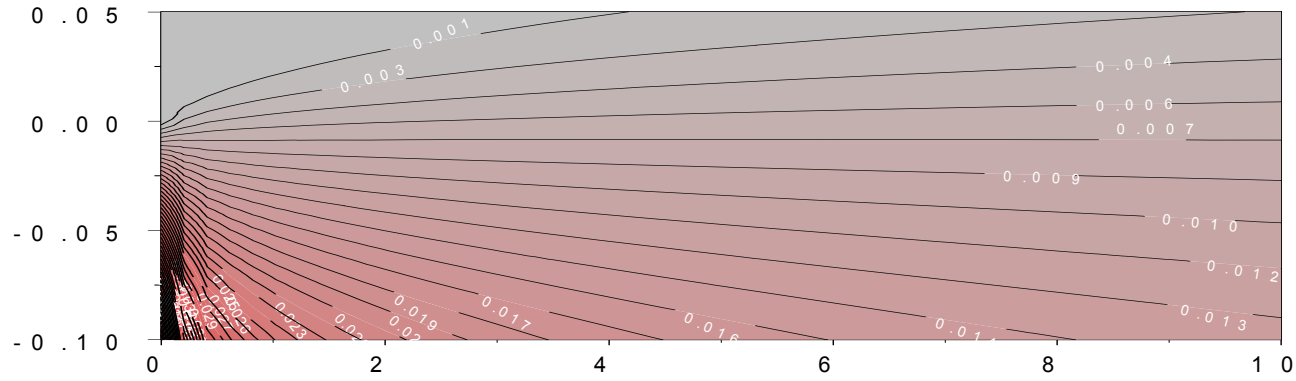

$AAAx_{sand\_silt}(25\,cm, 0.25cm, 2000day, 1000day)$

Integrating over space

$$ZZZ(t, C_o) := 1\cdot m\cdot C_o\cdot \int_{0\cdot ft}^{20\cdot ft}\int_{0\cdot ft}^{2\cdot ft} C''_{sand}(x, y, t)\, dy\, dx$$

$$ZZZ\left(10\cdot day, 1100\cdot \frac{mg}{L}\right) = 20.985 gm$$

$$TTT(t, C_o) := 1\cdot m\cdot C_o\cdot \int_{0.00001\cdot ft}^{20\cdot ft}\int_{0.00001\cdot ft}^{0.5\cdot ft} C''_{silt}(x, y, t)\, dy\, dx$$

$$TTT\left(10\cdot day, 1100\cdot \frac{mg}{L}\right) = 8.065 gm$$

$$\frac{\int_{0.0001\cdot m}^{3\cdot m} Cx''_{sand}(5\cdot m, y, 100\cdot day, 100\cdot day)\, dy}{3\cdot m} = 2.498\times 10^{-3}$$

D.1.1 Estimation of concentration in a well

$$C'_{sand}(x, t) := \frac{\int_{0.0001\cdot m}^{3\cdot m} Cx''_{sand}(x, y, t, 1000\cdot day)\, dy}{3\cdot m}$$

$$t := 1\cdot day, 5\cdot day .. 2000\cdot day$$

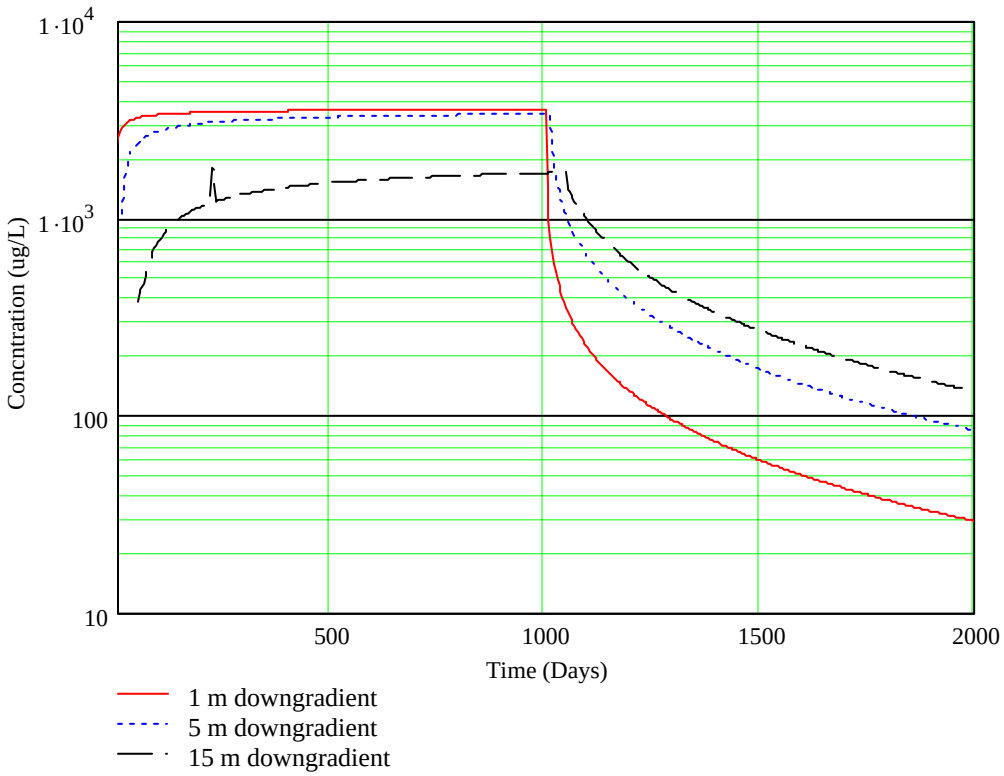
1·10^4
1·10^3
100
10
Concntration (ug/L)
500
1000
1500
2000
Time (Days)
1 m downgradient
5 m downgradient
15 m downgradient

.

APPENDIX E
NUMERICAL MODEL DEVELOPMENTS

APPENDIX E: NUMERICAL MODEL DEVELOPMENTS

LARGE TANK NUMERICAL ANALYSIS

E.1.1 Introduction

The process of numerically modeling NAPL transport has been accomplished in several different domains and realizations. This introduction is by no means meant to be a comprehensive review of all of the numerical models presented, rather it will briefly review three categories of numerical modeling thought to be pertinent to the study of the current research. These three areas include (1) homogeneous domain with a single realization, (2) heterogeneous domain with a single realization and (3) heterogeneous domain with multiple realizations. The sections presents initial modeling work performed prior to the utilization of FEHM.

E.1.2 Homogeneous domain, single realization

Conceptual and mathematical models for multiphase flow in mostly homogeneous porous media in one dimension have been presented by Abriola (1989); Kueper and Frind (1991); Kaluarachchi and Parker (1992). Centimeter scale, first-order rate models in homogeneous porous media have been presented by Miller et al. (1990); Powers et al. (1992, 1994); Imhoff et al. (1994); Imhoff and Miller (1996). These studies support the idea of the establishment of near-equilibrium conditions over short length and time scales.

E.1.3 Heterogeneous domain, single realization

The application of multiphase modeling to heterogeneous formations has been undertaken by Kueper and Frind (1991a and b); Essaid and Hess (1993); and Kueper and Gerhard (1995). These studies highlighted the importance of the variability of permeability and capillary parameters on organic liquid spreading. A better representation of the non-uniform flow field in the NAPL entrapment zone in two dimensions has been investigated by Saba and Illangasekare (2000) and Nambi and Powers (2000). Dekker and Abriola (2000) found that the most critical

factors in modeling organic entrapment in heterogeneous formations included the spill release rate, reliable estimates of the mean, variance, and vertical correlation scale of the formation permeability, and an accurate representation of the correlation between the capillary pressure–saturation function and the permeability. Saenton et al. (2002) found that varying source zone configurations significantly alter the NAPL mass transfer coefficient. Mayer and Miller (1996) observed decreases in dissolution rates in heterogeneous media attainable to the formation of NAPL pools.

E.1.4 Heterogeneous domain, multiple realizations

The conclusions of many heterogeneous NAPL transport simulations identified the necessary implementation of statistics and stochastic modeling to better appreciate the heterogeneity of the subsurface, especially at a field scale. An extensive number of existing studies have addressed the issue of uncertainty in modeling subsurface flow. A more recent approach, as discussed in Sohn et al. (2000), incorporates Bayesian methods to be used to identify both the initial estimate in uncertainty estimates and the uncertainty reduction available compared with the observed field data. This work developed a Bayes Monte Carlo (BMC) method to update the uncertainty of the fate and contaminant transport of a field-scale model.

The present numerical work will continue on the path of the heterogeneous domain and multiple realizations. The tools that will be employed for this task include MODFLOW (McDonald and Harbaugh, 1988; Harbaugh et al., 2000), MT3D (Zheng, 1990; Zheng and Wang, 1999) and SEAM3D (Waddill and Widdowson, 2000). These tools are existing three-dimensional finite difference groundwater flow and contaminant transport codes. These models complement each other to simulate non-equilibrium mass transfer from entrapped NAPL in heterogeneous aquifers.

E.1.5 Code Selection

The first task to development a model framework for the experimental work was to determine the appropriate code for the problem. MODFLOW and MT3D have been used extensively in the literature (Saenton et al., 2002; Sohn et al., 2000) for a similar set of experimental conditions. SEAM3D (Waddill et al., 2000) was chosen as the NAPL dissolution model because: 1) it is integrated within MT3D and 2) it solves the relationship of (taken from Waddill et al., 2000):

$$R_{source,lc}^{NAPL} = max\left[0, k^{NAPL}\left(C_{lc}^{eq} - C_{lc}\right)\right]$$

Using Raoult's Law, C_{lc}^{eq} is calculated (Corapcioglu and Baehr 1987; Parker et al. 1991) as

$$C_{lc}^{eq} = f_{lc} C_{lc}^{sol} \tag{2.44}$$

where f_{lc} is the mole fraction of chlorinated ethene lc in the NAPL [mol_{lc} mol_{NAPL}^{-1}]; and C_{lc}^{sol} is the solubility of pure chlorinated ethene lc in water. During each time step, f_{lc} is computed as

$$f_{lc} = \frac{C_{lc}^{NAPL} / \omega_{lc}}{I^{NAPL} / \omega_I + \sum_{ls=1}^{NS} C_{lc}^{NAPL} / \omega_{lc} + \sum_{lt=1}^{NT} T_{lt}^{NAPL} / \omega_{lt}} \tag{2.45}$$

where C_{lc}^{NAPL} is the NAPL mass of chlorinated ethene lc per unit mass dry soil [M_{lc} M_{solid}^{-1}]; I^{NAPL} is the NAPL concentration of inert (i.e., relatively insoluble constituents) [M_I M_{solid}^{-1}]; T_{lt}^{NAPL} is the NAPL concentration of nonbiodegradable tracer lt [M_{lt} M_{solid}^{-1}], and ω_j is the molecular weight of NAPL constituent j. Equations (2.44) and (2.45) represent the concept that the effective solubility of any NAPL constituent is reduced when other constituents are simultaneously dissolving into the aqueous phase. With each time step, C_{lc}^{NAPL} is updated as

$$\frac{dC_{lc}^{NAPL}}{dt} = -\frac{\theta}{\rho_b} R_{source,lc}^{NAPL} \tag{2.46}$$

where ρ_b is the bulk density of the porous medium [M_{solid} L_{pm}^{-3}]. Thus, dissolution causes the NAPL concentration of chlorinated ethene lc to decrease as the aqueous phase concentration increases.

E.1.6 Grid Size

The numerical dispersion effect that grid size can have on the model domain has been previously discussed in many sources (Zheng and Bennet 1995, Zheng 1999). In order to determine the appropriate grid size for the experimental model, the model domain was continually refined while observing the computational time versus percent change in effluent concentrations. Figure E-1 shows a refinement in grid size from an initial start of 2.5 cm by 2.5 cm by 5.0 cm thick down to the smallest size of 0.5 cm by 0.5 cm by 5.0 cm thick. It can be seen on the figure that only an 8% change in effluent concentration is observed when going from 0.5 cm to 1.0 cm spacing, yet the computational time increase significantly. The figure also illustrates that there is a 57% change when going from a 2.5 cm x 2.5 cm cell size to a 1.0 cm cell size. These results are only valid at this small laboratory scale, and should not be inferred up to a field scale.

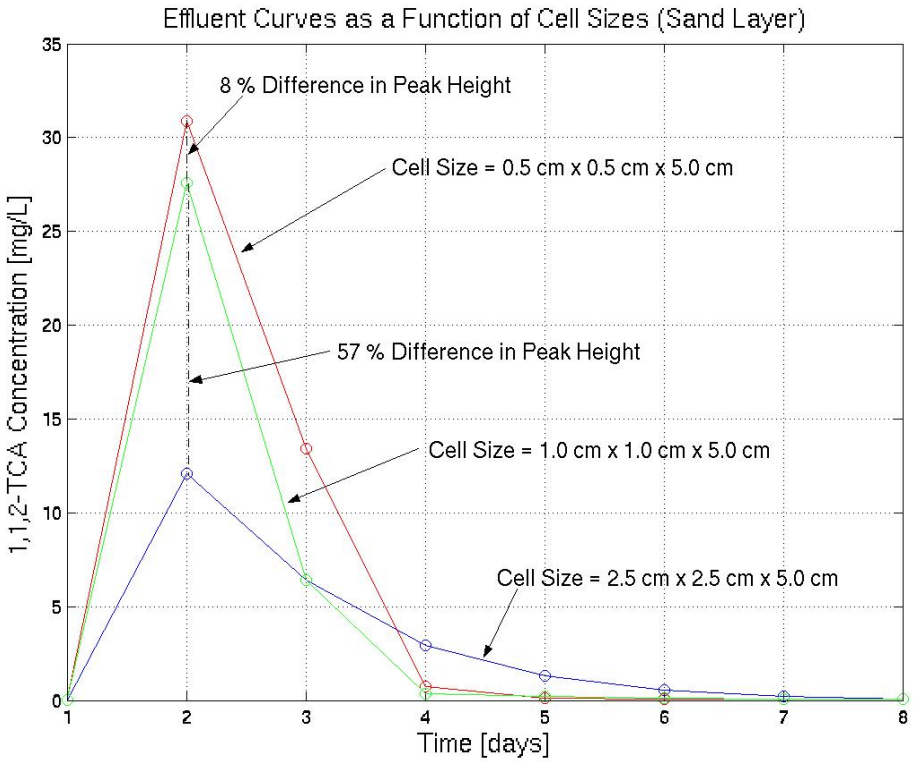

Figure E-1. Effluent curves as a function of cell size.

Based on these findings, a 1.0 cm x 1.0 cm x 5.0 cm cell size was chosen. This gave the accuracy that was needed for the experimental work, but did not require significant computational power. Applying this grid spacing to a 8 ft x 2 ft x 2 in. tank, yielded 244 cells along the 8-ft length, 61 cells along the 2 ft length and (1) 5.0-cm cell was applied to the 2 in. thickness. Based on these the dimensions, the model domain contained 14,884 cells.

E.1.7 Computation Time

Processor limitations at the experimental scale were not found to be a rate-limiting step. With a 1 cm x 1 cm x 5 cm grid spacing, resulting in 14,884 nodes, a Pentium IV class machine had maximum runs times of approximately 60 to 90 minutes. The actual MODFLOW part of the model took only seconds to solve. The majority of the processor iterations were performed in MT3D and SEAM3D.

E.1.8 Parameters

The following tables define the parameters that were used as input to the model.

Table E-1. #30 soil physical properties.

Parameter	Value	Units
horizontal hydraulic conductivity	12500	cm/day
Porosity	0.3	[=]
specific storage	0.007	/cm
longitudinal dispersivity	0.05	cm
bulk density	1542	mg/cm^3
Retardation	1	[=]
Soil layer thickness	38	cm

Table E-2. #140 sand physical properties.

Parameter	Value	Units
horizontal hydraulic conductivity	617	cm/day
Porosity	0.4	[=]
specific storage	.006	/cm
longitudinal dispersivity	0.05	cm
bulk density	1384	mg/cm^3
Retardation	1	[=]
Soil layer thickness	18	cm

Table E-3. MODFLOW parameters.

Parameter	Value	Units
Δx	1	cm
Δy	5	cm
Δz	1	cm
Head Drop	1.6	cm
K_{eff}	9308	cm/day
seepage velocity	210	cm/day

Table E-4. MT3D inputs.

Parameter	Value	Units
ratio of transverse to longitudinal dispersivity	0.1	[=]
ratio of vertical to longitudinal dispersivity	0.1	[=]
effective molecular diffusion coefficient	5e-6	[=]

Table E-5. SEAM3D inputs (all values at 25° C).

Parameter	Value	Units
1,1,2-TCA solubility	4420.0	mg/L
1,1,2-TCA molecular weight	133.0	g/mole
1,1,2 TCA initial concentration	0.3	mass/mass
1,1,2-TCA dissolution rate	0.14	/day
TCE solubility	1100.0	mg/L
TCE molecular weight	131.0	g/mole
TCE initial concentration	0.1	mass/mass
TCE dissolution rate	0.09	/day

E.1.9 Simulations

All the model packages (MODLFOW, MT3D, and SEAM3D) were integrated within the Groundwater Modeling System (GMS) software, version 4.0. GMS allowed rapid display of head gradients in the flow model and kriged concentration data in the transport model. GMS also allowed the feature of observation points within the model domain to observe a particular point within the model domain.

For all simulations, the flow model was solved first using MODFLOW. The model domain was established with constant head cells at each end of the grid. Two soil layers were defined within the grid; the #30 soil at the top and the #140 soil at the bottom. Both soil layers were defined as confined aquifers. Flow was arbitrarily established from left to right of the grid system. The flow model was solved under steady state conditions. Only horizontal flow was established, no vertical flow was defined in the system. The output of the flow model would define cell-to-cell flow values and head, both required inputs for the transport model.

Once the flow model was solved, the transport part of the model was solved, based on a point-source injection point located at [30,43] within the model domain. At this point, the DNAPL parameters were inputted. The MT3D part of the transport model solved the advection/diffusion equation with the appropriate inputted parameters. Outputs of the model presented the DNAPL concentration at every cell for every timestep, or a kriged concentration profile could be displayed. Timesteps were automatically defined within GMS 4.0, at the time of execution, based on satisfying Peclet and Courant number requirements (Zheng and Bennett 1995).

RESULTS

The following figures show the results of the modeling simulations. For all of the figures, the output of the model is based solely on the input of the laboratory-measured data. No calibration or validation was performed. In the case of the data in Figure E-2, the mass removed from the model domain was plotted against the measured effluent data. The model predicts a total mass removal of 3,700 mg, while the experimental data showed approximately 4,300 mg. The actual amount of 1,1,2-TCA injected was 4,240 mg. The resulting mass recovery for the model was 87%.

For Figure E-3, the sum of the model cell concentrations of 1,1,2-TCA of the last column at the effluent end of the model domain (rows 6-61, column 244) was plotted against the measured effluent concentration. The model captures the initial start and endpoint of the breakthrough curve, but does not capture the actual mass seen through the measured data. This is thought to occur because the model is advection dominated and does not accurately capture the diffusion that is occurring in the system. Figures E-4 and E-5 present a breakout of Figure E-3 for the time periods 1 to 10 days and 10 to 60 days. It is also seen in these figures that the model is underestimating the actual processes that are occurring.

Figures E-6 and E-7 present the predicted values of the TCE data, although no experimental data is available. The dissolution rate used in the TCE model was calculated from the X-ray data.

Although the model is not accurately predicting the experimental data, it is showing the dominant features of the system. It is interesting to point out that in the “tails” of the plumes in the modeling simulations, i.e., the downstream plume that has diffused into the silt layer and is now back diffusing into the sand and advectively moving through the silt. The majority of the mass is removed in the first week of simulation (>80%), while the remaining mass (which is still greater than MCL) is still contributing to the system over a large area and time scale. The experimental data provides evidence to this observation.

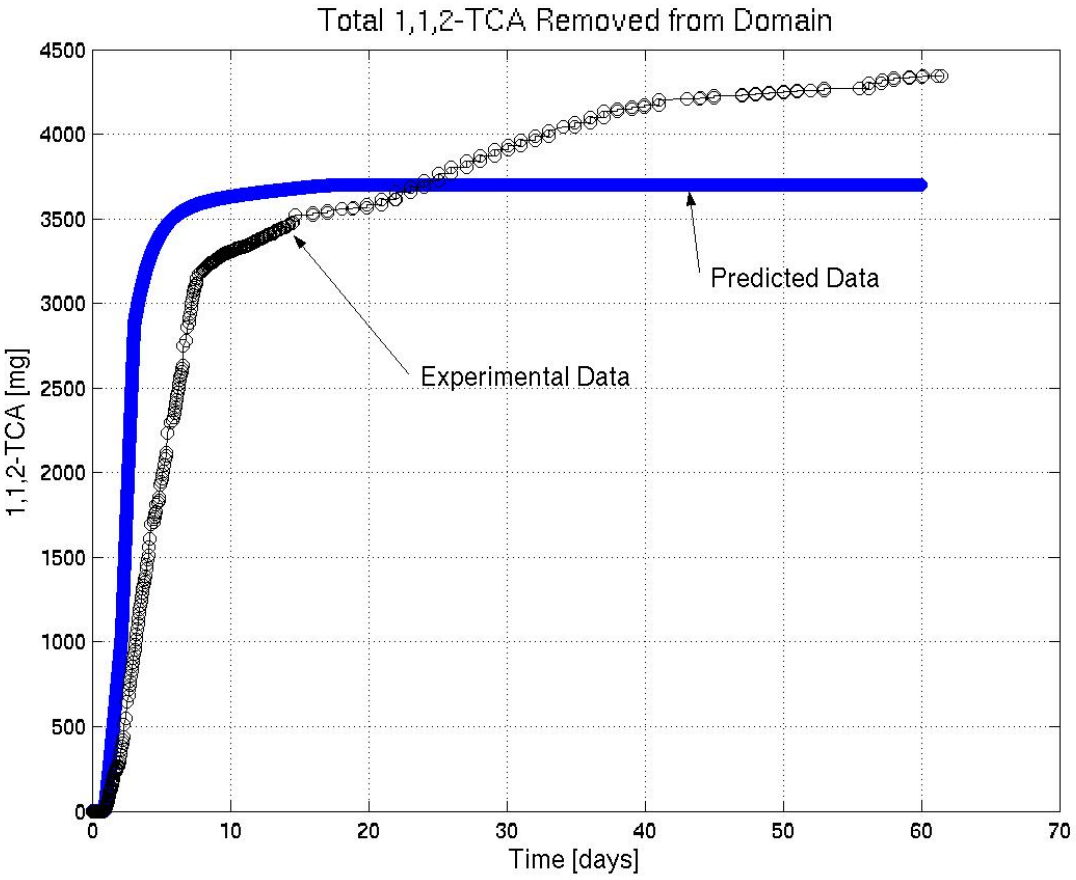

Figure E-2. 1,1,2-TCA-modeled mass remaining in domain vs experimental data.

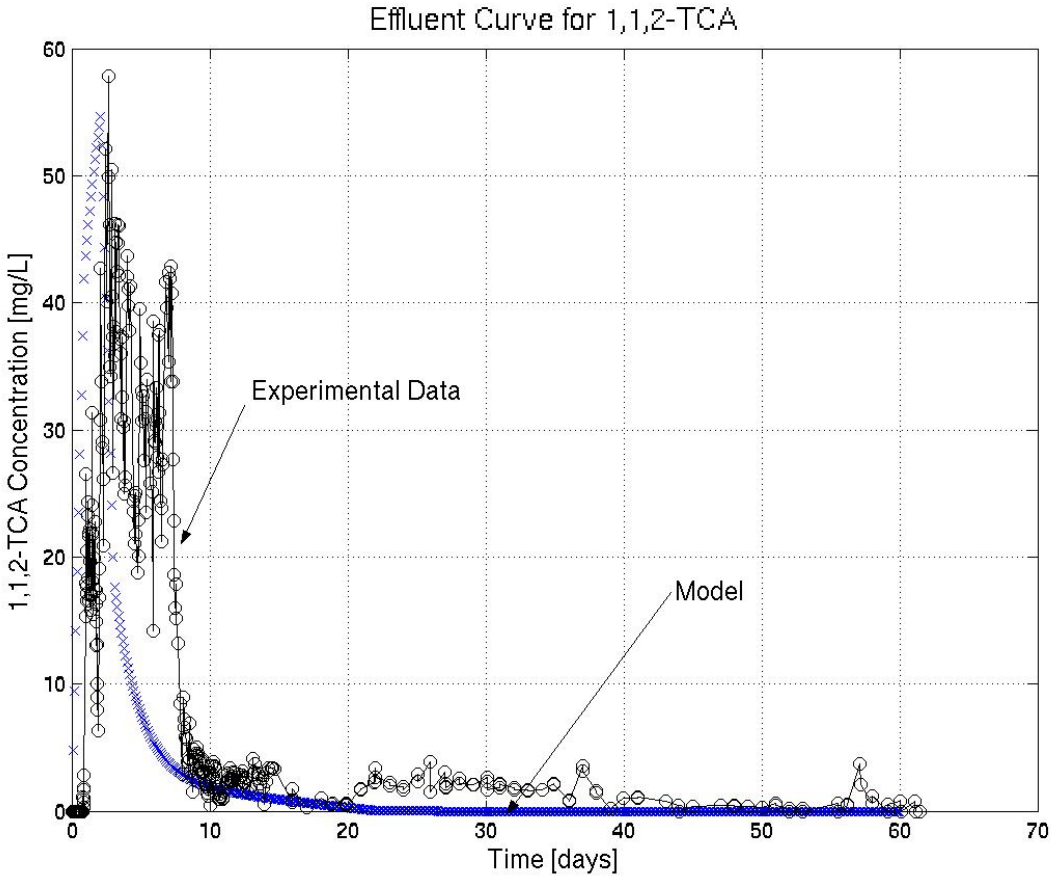

Figure E-3. 1,1-2-TCA modeled effluent curve vs measured effluent data.

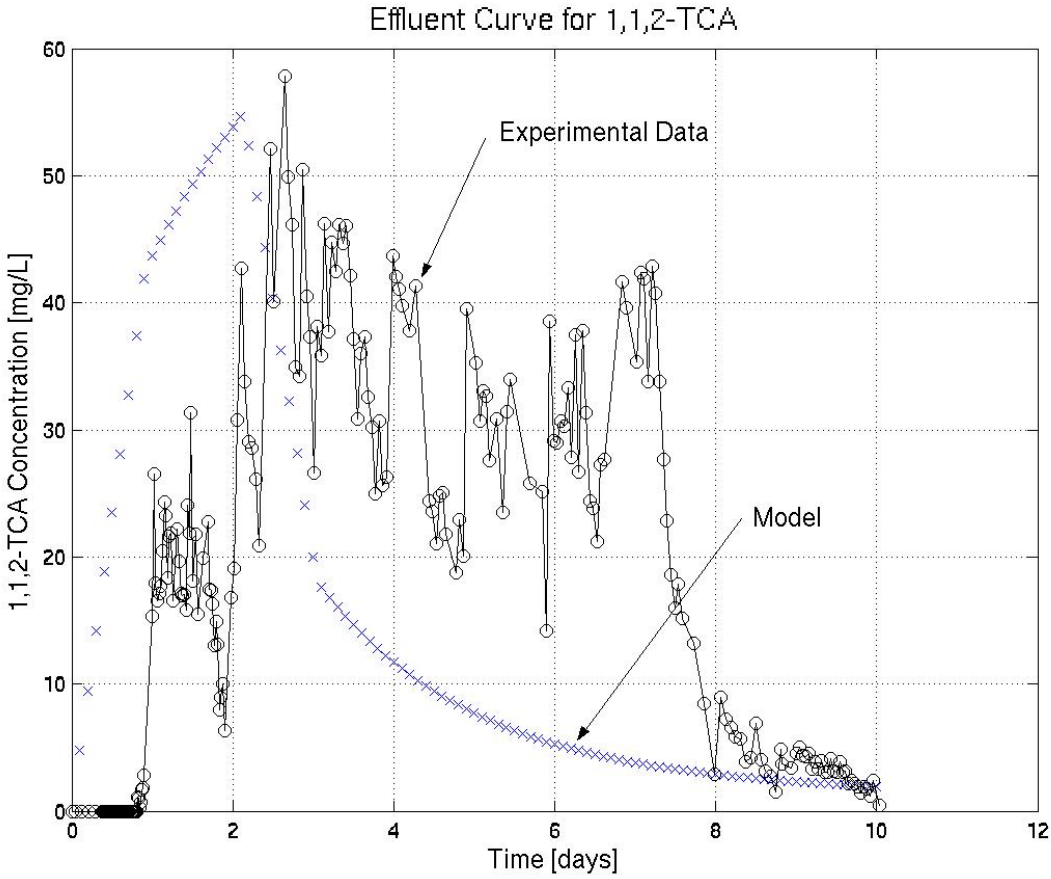

Figure E-4. 1,1-2-TCA modeled effluent curve vs measured effluent data [1 to 10 days].

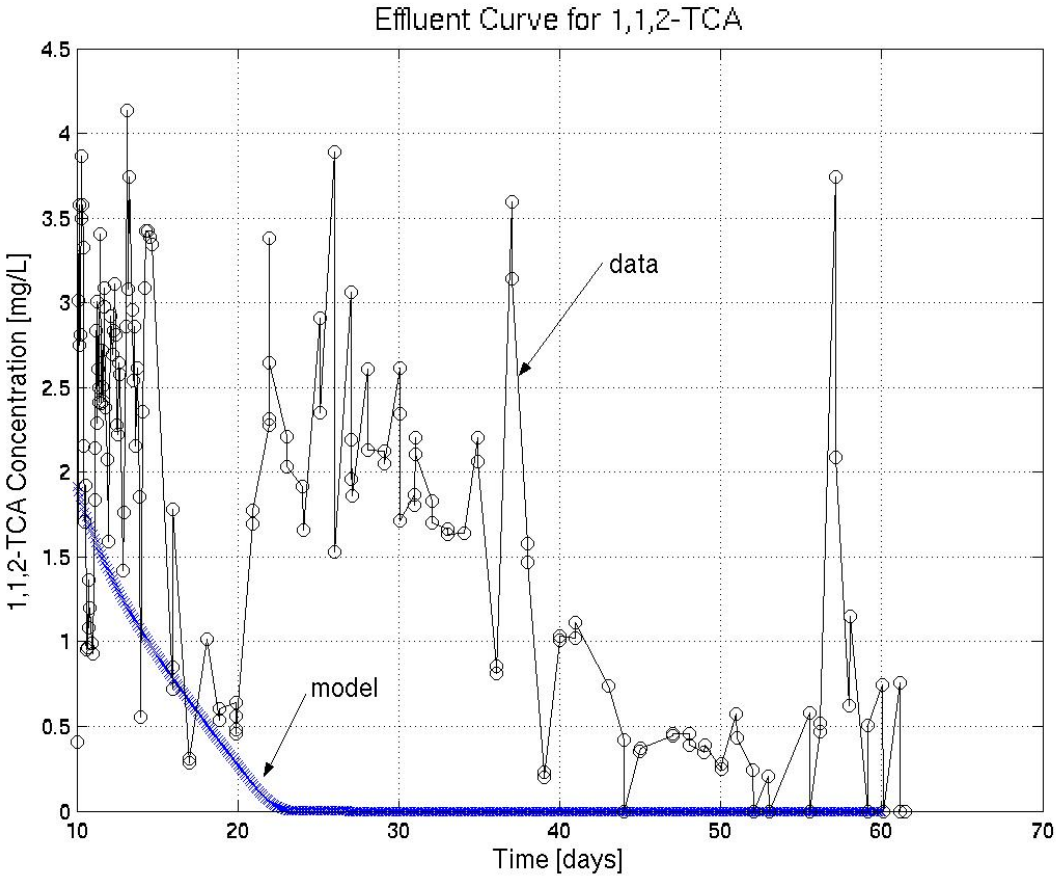

Figure E-5. 1,1-2-TCA modeled effluent curve vs measured effluent data [10 to 60 days].

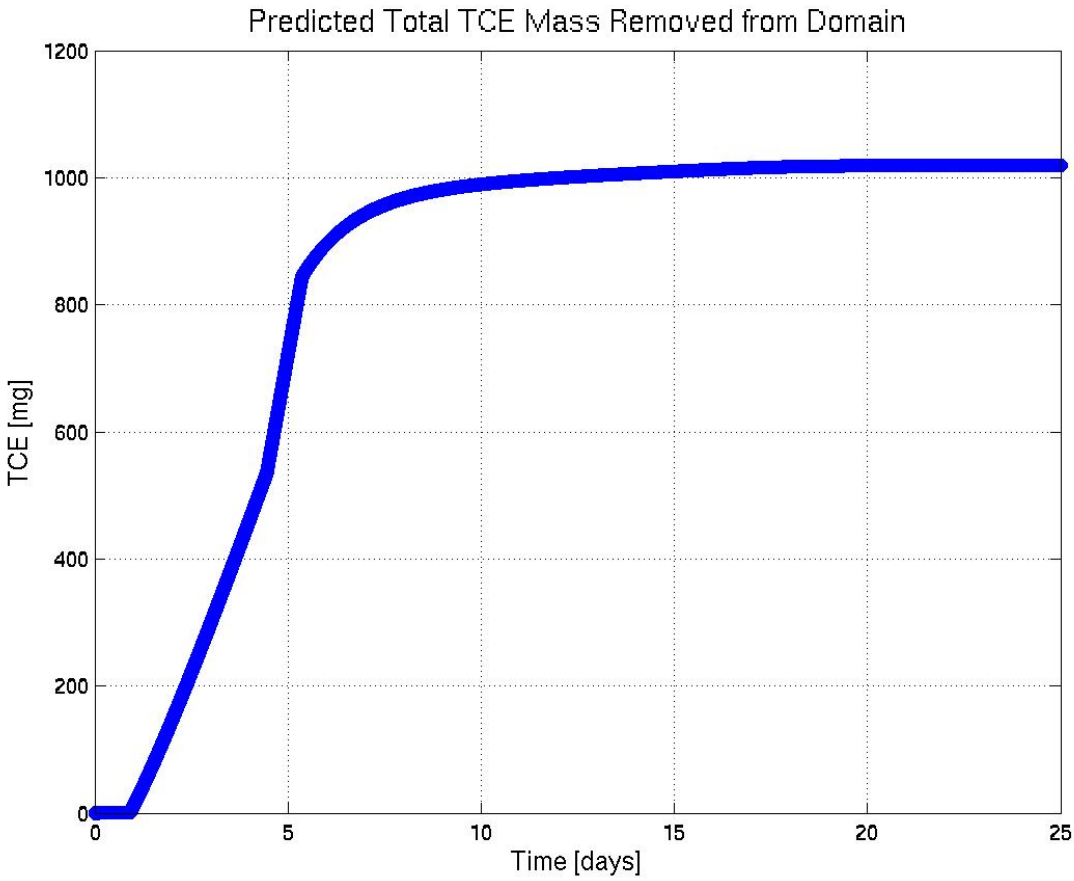

Figure E-6. TCE modeled cumulative mass removed from domain.

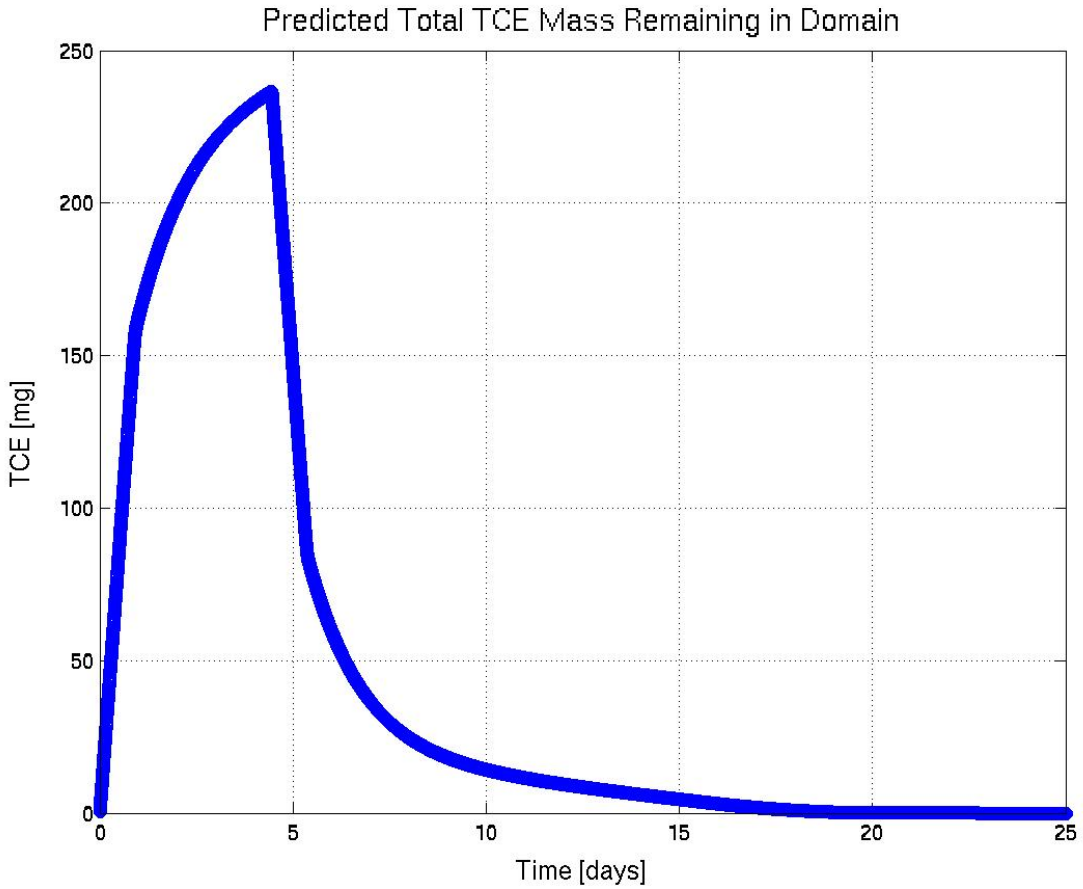

Figure E-7. TCE mass remaining in domain.

E.1.10 Mass Balance

All mass balances errors (numerical) for the both the flow (MODFLOW) and transport (MT3D/SEAM3D) models were near zero according to the mass balance output files of each designated program.

E.1.11 Model Validation

Due to the experimental issues with the TCE experiment, the model was not validated, as the 1,1,2-TCA data set was the only one available. The model will be validated through the 2-ft tank and 16-ft tank experiments.

CONCLUSIONS

The present experimental model captures the advective processes that are occurring, but more work needs to be done to better simulate and predict the diffusive processes of the system. Due to various experimental issues, as described in the body of this report, the model has not been experimentally verified. The model is in the process of being calibrated and validated through the 2 ft-tank experimental work. Work is also in progress to upscale the model for the 16-ft tank experiment. Future simulations for the 16-ft tank model will incorporate the parameters of the field soils, and randomize both the heterogeneity and the architecture of the source zone to better capture the domain of field conditions, and vary the DNAPL saturation of the zone source.

REFERENCES CITED

Abriola, L.M., 1989. “Modeling multiphase migration of organic chemicals in groundwater systems — a review and assessment.” *Environmental Health Perspectives*, 83, 117–143.

Ball, W.P., and P.V. Roberts. 1991. “Long-Term Sorption of Halogenated Organic Chemicals by Aquifer Material 1. Equilibrium,” Environmental Science Technology, Vol. 25(7), pp. 1223-1237.

Dekker, T.J., and L.M. Abriola. 2000. “The influence of field-scale heterogeneity on the infiltration and entrapment of dense nonaqueous phase liquids in saturated formations.” *Journal of Contaminant Hydrology*, Vol. 42, pp. 187–218.

Essaid, H.I. and Hess, K.M., 1993. “Monte Carlo simulations of multiphase flow incorporating spatial variability of hydraulic properties.” *Ground Water*, Vol. 31, No 1, pp. 123–134.

Harbaugh, A.W., E.R Banta, M.C. Hill, and M.G McDonald. 2000. *MODFLOW-2000, The U.S. Geological Survey Modular Ground-Water*

Model—User Guide to Modularization Concepts and the Ground-Water Flow Process. Open file report 00-92. U.S. Geological Survey.

Imhoff, P.T., and C.T. Miller. 1996. “Dissolution fingering during the solubilization of nonaqueous phase liquids in saturated porous media: 2. Experimental observations.” *Water Resources Research*, Vol. 32 (7), pp. 1929–1942.

Illangasekare, T.H. and, E.J. Armbruster, III. 1995. “Non-Aqueous-Phase Fluids in Heterogeneous Aquifers-Experimental Study.” *Journal of Environmental Engineering,* August, Vol. 121, No. 8.

Kaluarachchi, J.J., and J.C. Parker. 1992. “Multiphase flow with a simplified model for oil entrapment.” *Transport in Porous Media*, Vol. 7, pp. 1–14.

Kechavarzi, C., K. Soga, and P. Wiart. 2000. *Multispectral image analysis method to determine dynamic fluid saturation distribution in two-dimensional three-fluid phase flow laboratory experiments.* pp. 46, 265-293.

Kueper, B.H., and E.O Frind. 1991a. “Two-phase flow in heterogeneous porous media 1: model development.” *Water Resources Research.* Vol. 27, No. 6, pp. 1049–1058.

Kueper, B.H., and E.O Frind. 1991b. “Two-phase flow in heterogeneous porous media 2: model application.” *Water Resources Research*, Vol. 27, No 6, pp. 1059–1070.

Kueper, B.H., and J.L. Gerhard. 1995. “Variability of point-source infiltration rates for two-phase flow in heterogeneous porous media.” *Water Resources. Research*, Vol. 31, No. 12, pp. 2971–2980.

Lagrega, M.D., P. Buckingham, and J. Evans. 1994. *Hazardous Waste Management.* New York: McGraw-Hill, Inc.

McDonald, M.G., and A.W. Harbaugh. 1988. “A modular three-dimensional finite-difference ground-water flow model.” *Techniques of Water Resources Investigations*. Book 6, U.S. Geological Survey.

Miller, C.T., M.M Poirier-McNeill, and A.S. Mayer. 1990. “Dissolution of trapped nonaqueous phase liquids: mass transfer characteristics.” *Water Resources. Research*, Vol. 26 (11), pp. 2783– 2793.

Nambi, I.M., and S.E. Powers. 2000. “NAPL dissolution in heterogeneous systems: an experimental investigation in a simple heterogeneous system*.” Journal of Contaminated Hydrology*, Vol. 44, pp. 161– 184.

Powers, S.E., L.M Abriola, W.J Weber, Jr. 1992. An experimental investigation of nonaqueous phase liquid dissolution in saturated subsurface systems: steady state mass transfer rates. *Water Resources Research*, Vol. 28 (10), pp. 2691–2705.

Powers, S.E., L.M Abriola, W.J Weber, Jr. 1994. “An experimental investigation of nonaqueous phase liquid dissolution in saturated subsurface systems: transient mass transfer rate.” *Water Resources Research*, Vol. 30 (2), pp. 321– 332.

Saba, T.A., and T.H. Illangasekare. 2000. “Effect of ground-water flow dimensionality on mass transfer from entrapped nonaqueous phase liquid contaminants.” *Water Resources Research*, Vol. 36 (4), pp. 971– 979.

Saenton S., T.H. Illangasekare, K. Soga, and T.A Saba. 2002. “Effects of source zone heterogeneity on surfactant-enhanced NAPL dissolution and resulting remediation end-points.” *Journal of Contaminant Hydrology*, Vol. 59, 27– 44,

Sohn, Michael D., Mitchell J. Small, and Marina Pantazidou. 2000. “Reducing Uncertainty in Site Characterization Using Bayes Monte Carlo Methods.” *Journal of Environmental Engineering*, October, Vol. 126, No.10.

Sorens, T.S., D.A Sabatini, and J.H Harwell. 1998. “Effect of flow bypassing and non-uniform NAPL distribution on the mass transfer characteristics of NAPL dissolution.” *Water Resources Research*, Vol. 34 (7), pp. 1657–1673.

Waddill, D. W., and M.A. Widdowson. 2000. “SEAM3D: A numerical model for three-dimensional solute transport and sequential electron acceptor-based bioremediation in groundwater” ERDC/EL TR-00-18, prepared for U.S. Army Engineer Research and Development Center, Vicksburg, MS.

Zheng, C. 1990. “MT3D: A modular three-dimensional transport model for simulation of advection, dispersion, and chemical reactions of contaminants in groundwater systems.” Report 74280. U.S. EPA Robert S. Kerr Environmental Research Laboratory, Ada, OK, USA.

Zheng, C., and P.P. Wang. 1999. *MT3DMS: A modular three-dimensional multispecies transport model for simulation of advection, dispersion, and chemical reactions of contaminants in groundwater systems; Documentation and user’s guide.* Contract report SERDP-99-1. U.S. Army Engineer Research and Development Center.

Zheng, C., and G.D Bennett. 1995. *Applied Contaminant Transport Modeling: Theory and Practice.* Van Nostrand Reinhold.

APPENDIX F
FIELD SOILS CHARACTERIZATION

APPENDIX F: FIELD SOILS CHARACTERIZATION

INTRODUCTION

Soils for laboratory studies were collected for FEW and NASFtW. The use of site soils was viewed as critical for the following reasons:

(1) The sorptive capacities of site soils can be significantly greater than typical laboratory sands.

(2) We want our result viewed as representative of field conditions by the parties at FEW and NASFtW.

The following describes soils collection and testing.

FEW SOILS ACQUISITION AND PROPERTIES

Soils were acquired from the vicinity of monitoring well MW38S at F. E. Warren (FEW) AFB, WY. The soils were collected during the excavation of a trench for an electrically driven permeable reactive barrier (PRB). This was done as a part of a CSU-ESTCP demonstration project. Figure F-1 presents: a) the location b) the excavation, c) a geologic cross section and d) a key for the geologic cross section. For detailed discussion, see Section F-4.

Samples were transferred to the CSU lab in Fort Collins, CO. The soil contained coarse and fine constituents as well as considerable moisture and historical contamination. The first step taken was to spread the soil into a thin layer and allow it to air dry. Pebbles were removed and clumps of dirt were crushed. Once dried, the soil was then run through a sieving process separating the coarse and fine fractions. The silt fraction (particle size < 250 μm) was then coned and quartered at least four times to homogenize the sample. The sand fraction (particle size > 450 μm) was washed three times to remove as much of the aggregated silt particles as feasible. The sand was then re-dried, coned and quartered.

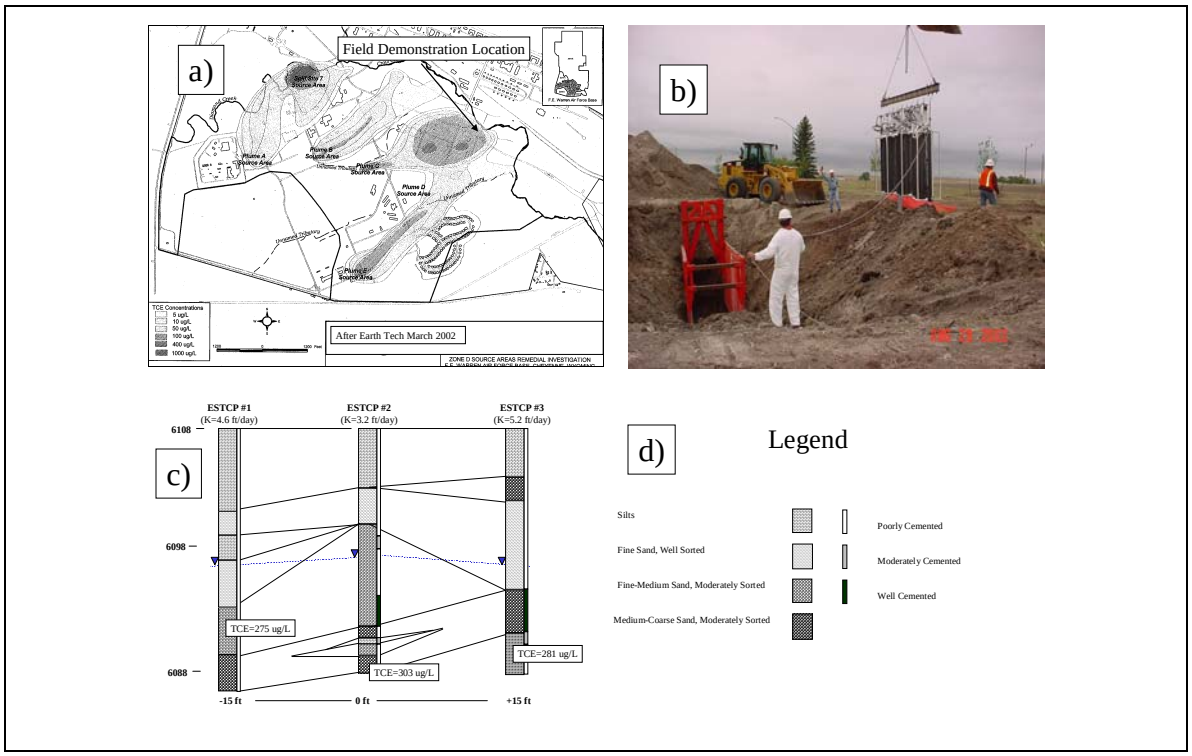

Figure F-1. Map of soil excavation site at F. E. Warren AFB, Cheyenne (top left), Image of barrier installation (top right), Schematic of barrier construction (bottom).

F.1.1 COLUMN STUDIES

The objective of the column studies was to determine the hydraulic conductivity, retardation factor, bulk density, porosity, and diffusivity of sand and silt fractions taken from F.E. Warren AFB, Cheyenne, WY, in relation to TCE, PCE, and MTBE.

F.1.1.1 BACKGROUND

In order to test the effect of stagnant zones on contaminant transport processes, it was necessary to determine some of the physical properties of the soils being used. The mathematical model contains parameters for porosity, ϕ, bulk density, ρb, dispersivity, α, hydraulic conductivity, K, and retardation, R. There are other parameters as well but they are independent of the soil used and will be discussed separately. Retardation is unique in this list in that it depends on the

contaminant. Each soil-contaminant combination will have a unique retardation factor. The others are independent of contaminant and depend only on the soil.

The advective-dispersive equation in one dimension is used to model transport in columns where the source is uniform over the diameter and is given by:

$$R\frac{dc}{dt} = D_L \cdot \frac{d^2c}{dx^2} - V_w \cdot \frac{dc}{dx} \qquad (1)$$

Each of the parameters in this equation can me estimated using the parameters described above and will be explained below. But first, some of the physical parameters of the soil must be determined.

The porosity of the soil is the amount of empty space between the soil grains. In order to calculate the porosity we need to know the volume of the container the soil is held in, the mass of the soil in the container, and the density of each grain. The formula for porosity is then;

$$\phi_{soil} = V_{container} - \frac{M_{soil}}{\rho_{soil\_grain}} \qquad (2)$$

The density of the soil grains is assumed to be 2.65 gram/cm^3 (the published density of quartz). The bulk density is the mass per unit volume of the soil in the container. This is simply

$$\rho_{bulk} = \frac{M_{soil}}{V_{container}} \qquad (3)$$

The dispersivity, α, hydraulic conductivity, k, and retardation, R, are not as easily determined and must be gathered experimentally.

The dispersivity is a measure of the amount of spreading in the transport of material due to the random nature of the path each molecule must take to get around all the soil grains. This is known as tortuosity. Tortuosity, τ, is the ratio of the length of the direct path, divided by the length of the actual path and is always less than one. The paths are not all equally tortuous however so some of the mass will make it through the media very quickly ($\tau \rightarrow 1$) while some will go through very slowly ($\tau << 1$). Rather than try to determine the actual level of tortuosity, we determine what this spreading effect is directly. Total dispersion comes from two sources; dispersivity, and molecular diffusion. Molecular diffusion is similar to dispersivity in that each molecule of contaminant must get around the molecules of water just like they have to get around soil grains. This effect is far smaller than dispersivity for normal flow rates and is sometimes neglected. Total dispersion is given as:

$$D_L = D_m \cdot \phi^{\frac{1}{3}} + \alpha_L \cdot V_w \qquad (4)$$

The molecular diffusion coefficient, Dm, is taken from published values and depends on the two constituents (in this case water and one of three contaminants) and temperature and is on the order of 10^{-10} m^2/s. The ϕ term is a correction factor for tortuosity. A rule of thumb for α is one tenth of the length of the column. Vw is the velocity of the water through the column.

Hydraulic conductivity, K, is a measure of the resistance to pushing a fluid through a porous medium. Conductivity is essential in our assumption that all of the advective transport in the experiment is through the coarse layer. It is calculated by measuring the head loss across a sample, and the total flux through the sample. Flux, or Darcy flux is denoted as q and has units of length per unit time. The total volumetric flux is given as Q and has units of volume per unit time. The Darcy flux is given as:

$$q = \frac{Q}{A} \tag{5}$$

where A is the area of the discharge outlet. The hydraulic conductivity is the proportionality constant of Darcy flux to head loss per unit length of sample and is given by:

$$q = K \cdot \frac{dh}{dx} \tag{6}$$

The head loss can be measured directly with a manometer and the length is just the length of the packed column.

The water velocity, Vw, is the actual speed the water is moving past a given point in the medium. It is calculated simply as:

$$V_w = \frac{Q}{A \cdot \phi} \tag{6a}$$

The retardation factor, R, is a measure of the effect of sorption of a contaminant onto the soil itself. Sorption is generally considered to be proportional to concentration as long as the concentration is low. For our purposes this is largely true. Retardation is then a function of the contaminants affinity to attach to the soil grains as opposed to remaining in the aqueous phase. This affinity is denoted, Kd. As the contaminant is sorbed onto the soil grains it appears to vanish from the aqueous phase. This makes it appear as though the contaminant is moving more slowly through the medium than the water. Retardation is then the ratio of the speed of the water to the speed of the contaminant and is therefore always greater than or equal to one. Retardation, R, is given as:

$$R = 1 + \frac{\rho_{bulk} \cdot K_d}{\phi} \tag{7}$$

The one is added because if the contaminant does not adsorb at all (Kd = 0) then it will move at exactly the same speed as the water (R=1). Kd is often modeled as:

$$K_d = K_{oc} \cdot f_{oc} \tag{8}$$

Where Koc is the organic carbon partitioning coefficient (which is material specific and relatively constant) and foc is the fraction of organic carbon in the soil. For very low organic carbon content this may not be true as other adsorption mechanisms begin to take over.

We now have estimates for each of the parameters in the advective-dispersive equation in one dimension (1). However, not all of the values are known so direct measurements of concentration versus time are taken and the parameters (R and DL) are adjusted to fit the data to the model.

F.1.2 COLUMN DESIGN AND CONSTRUCTION

The columns used were all of similar construction. They are made of plexiglass, 15.1 cm in length total with 1.1 cm liquid head tanks at the top and bottom. The three columns that contained silt were 10.1 cm in diameter; the three columns filled with sand were 5.1 cm in diameter. The different diameters were used in anticipation of the additional head loss in the silt columns. The head tanks are separated from the main body of the columns by plexiglass plates with small diameter apertures throughout. The sand or silt was held in place through the use of a small amount of glass beads at the top and bottom between the soil and the plexiglass perforated plates. Small internal diameter glass tubing was used to connect the feed bottles to the bottom of the columns. Ismatec model 78001-15 positive displacement pumps (or similar) were used to maintain volumetric flow rates. The column effluent was channeled to glass carboys with a bypass at the top of the column for sampling.

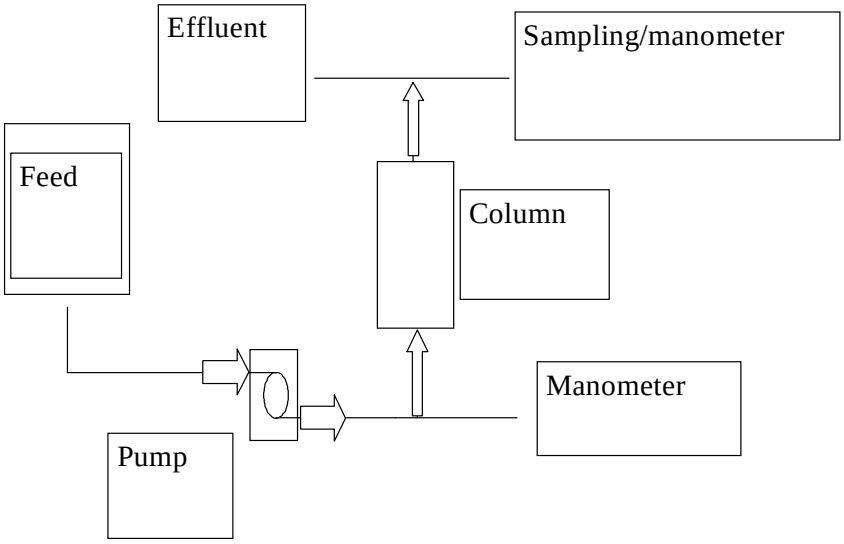

Figure F-2. Column piping diagram.

The columns were first weighed while empty and then again with glass beads sufficient for immobilization. For the silt columns, three types of glass beads were used to keep it from eroding. Large beads were placed next to the perforated caps, medium size beads were placed on top of them, and finally very fine beads were used. A minimum amount of beads were used to keep from affecting hydraulic conductivity (it was assumed in the hydraulic conductivity calculations that the glass beads played no part). For the sand columns, only large beads were used.

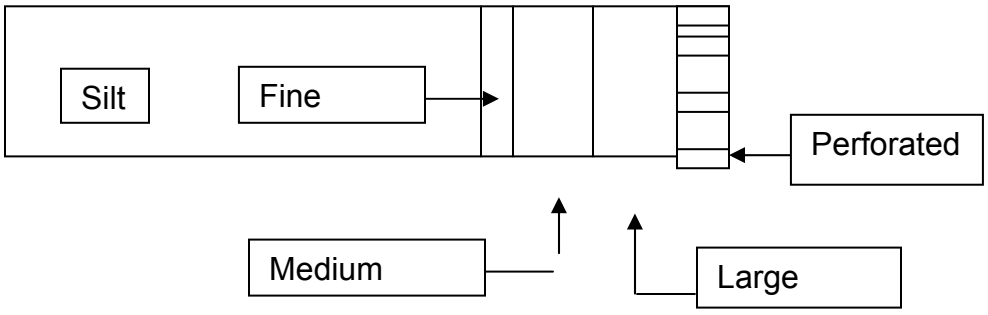

Figure F-3. Cross Section of Column Construction.

Once the bottom layers of beads were in place the columns were filled with soil. In order to achieve as uniform a packing as possible, the soil was dropped through a funnel 38 cm long, and the side of the column was struck approximately 3 times per second. Once the column was nearly full, the second layering of beads was placed on the top of the soil and the columns were capped. The columns were then weighed again to determine the mass of soil added.

De-aired tap water was then flushed through the columns until all of the visible air bubbles were removed. The length of the packed soil was then measured to determine the total volume of packed material.

The sand columns were then connected to water manometers to determine the pressure drop over the column length. The silt columns, due to their greater pressure drops, were connected to mercury manometers.

F.1.3 EXPERIMENT DESIGN

The experiment was run 6 times, three times on sand, three on silt. Each of the two types of soil was run with TCE, PCE, and MTBE.

The first stage of the experiment was to calculate the hydraulic conductivity of the sand and silt. All three of the sand columns were connected to one pump and all three of the silt columns were connected to another pump. Each pump was then set to various levels of volumetric flow rate. This flow rate was measured using a graduated cylinder and stopwatch for each column. Simultaneously, the pressure of each column was read off the manometers. Each time the pump setting was changed, the columns were given several hours to equilibrate.

From information gathered during construction (volume of packing and mass of soil), the porosity of each column was calculated. The total flow rate for each

column was measured at each pump setting, as well as the pressure drop and hydraulic conductivities were calculated.

Based on a “field-like” Darcy flux of one foot per day, the pumps for each set of columns were set and allowed to equilibrate. Slugs of contaminated water were prepared by diluting saturated solutions of each of the three contaminants 95% (5% saturated solution, 95% deionized water). Samples of the dilutions were taken and stored for later analysis.

The feed solution to the columns was then diverted from de-aired water to the dilutions. Both sand and silt columns for each contaminant shared a feed to maintain equal concentrations to each. Effluent samples were then taken at approximate four hour intervals, recorded, and labeled for later analysis.

F.1.4 SAMPLE PREPARATION/ANALYTICAL

Each sample is taken from the port at the top of the column. A 4-mL glass vial is filled to capacity to eliminate any air bubbles. The vial is then capped with a Teflon coated foam rubber septa, labeled and refrigerated. Less than two weeks later, the sample is removed from the refrigerator. One mL gas chromatogram vials are prepared with 4 mm of sodium sulfate crystals and labeled. The sodium sulfate is present in excess guaranteeing that the ionization in the water is constant. One mL of each sample is added to the GC vials. Then a standard quantity of previously prepared internal standard solution of 1,1,1 TCA is added to the vial. The vial is then immediately capped and shaken for 30 seconds. This procedure is repeated for each of the samples taken from one column.

A set of standards is also prepared. Sixteen standards are prepared for each run; two each of four concentrations spanning the upper range of concentrations (ppm range) and two each of four concentrations spanning the lower range (ppb range). For TCE the four concentrations in the upper range are 100, 67, 33, and 1 ppm, and for the lower range are 1000, 667, 333, and 10 ppb. For PCE the values are exactly half those of TCE. For MTBE, the concentrations are 5000,

1875, 703, 264, 99, 37, 14, 5 ppm. For the lower range the values are 1/1000th of those stated. The vials are then run on an Agilent series 1575 gas chromatogram with mass spectrometer.

The first step is to purge the machine of any previous contamination. This is accomplished using a cleaning method that was developed which bakes off any chemical species still present from the previous run. Next a blank air sample is run as a baseline. The next samples run are the fist set of higher concentration standards. This is done to calibrate the machine as well as to insure that the column is not overwhelmed. Once the standards are finished another air sample is run. All of the samples from the columns will be run next, with an air purge after every tenth sample to keep any carryover or buildup to a minimum. Finally, the second set of high concentration standards is run.

Once this has been done, the data is analyzed. Any sample whose concentration was too low to be detected is run a second time with the machine set to a more sensitive configuration. The same procedure is then repeated but only for those samples and lower concentration standards.

Two peaks are detected for each sample. One of the peaks is the internal standard (1,1,1 TCA) the other is the contaminant for that particular column. It is then assumed that the internal standard should be the same for each sample. An average of the readings is taken and each sample is adjusted to that average (i.e. if the standard signal is twice the average then the contaminant signal is divided in half).

F.1.5 RESULTS

Porosities were calculated for each column. The results are displayed in the following table.

The average porosity for the sand columns (A, B, C) is 0.35. The average porosity for the silt columns (AA, BB, CC) is 0.51. The average bulk density of

the sand columns is 1.71 grams/cm^3, while the average for the silt columns is 1.30 gram/cm^3.

Table F-1. Porosity and Bulk Density.

Column Name	Mass Before (kg)	Mass After (kg)	Mass Sand/Silt (g)	Volume Solids (cc)	Diam (cm)	Radius (cm)	Pack Height (cm)	Packing Volume (cc)	Porosity	Bulk Density (g/cc)
A	0.86	1.33	470	177	5.1	2.6	13.5	276	0.36	1.70
B	0.87	1.35	475	179	5.1	2.6	13.5	276	0.35	1.72
C	0.86	1.34	475	179	5.1	2.6	13.5	276	0.35	1.72
AA	3.05	4.15	1100	416	10.2	5.1	11.0	895	0.54	1.23
BB	2.71	4.01	1300	489	10.2	5.1	12.0	986	0.50	1.31
CC	2.69	3.89	1210	456	10.2	5.1	11.0	895	0.49	1.35

The hydraulic conductivities of the columns were calculated and are shown in the following table.

Table F-2. Hydraulic Conductivity

Column	A	B	C	AA	BB	CC
K^* (cm/sec)	0.015	0.012	0.014	0.00020	0.00010	0.00020

The values shown are average values over the life of the experiment. The values were tracked over time and did not show significant drift. It is clear from these results that the conductivity of the sand is nearly 1000 times that of silt. This should be sufficient to maintain the assumption that there is insignificant advective flow in these regions when placed next to a sand layer.

Retardation and dispersivity values are calculated based on the concentration and time data gathered during the experiment. The model described above is used a basis and the parameters are fitted to the data. The solid red line denotes the model fit, the broken blue line represents the actual data gathered.

$\alpha_L := 1.9 \cdot in \qquad R := 1$

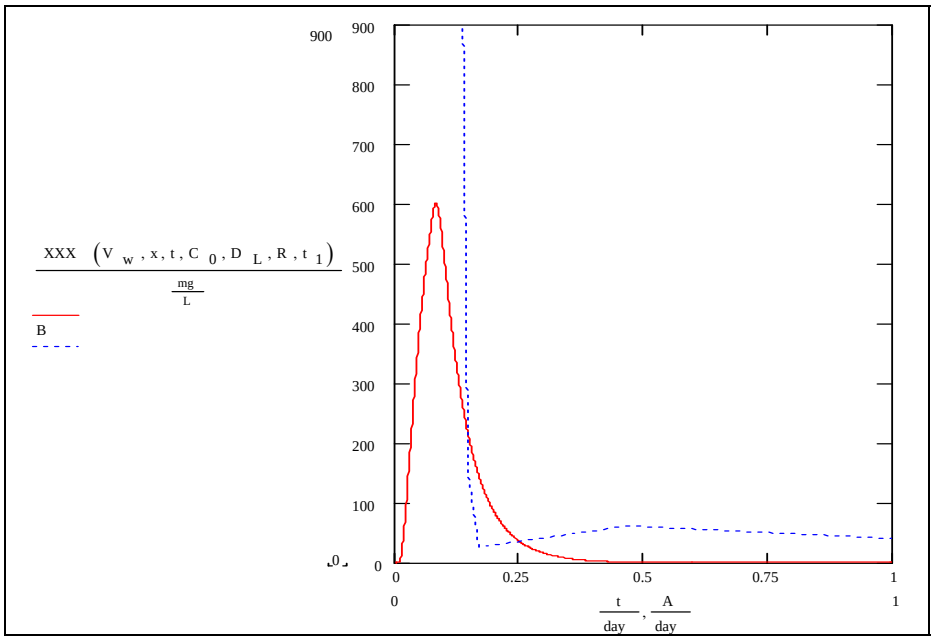

Figure F-4. Retardation and dispersivity calculations for sand column A with 5% solubility solution of MTBE run for 100 minutes.

$\alpha_L := 0.05 \cdot in \qquad R := 1$

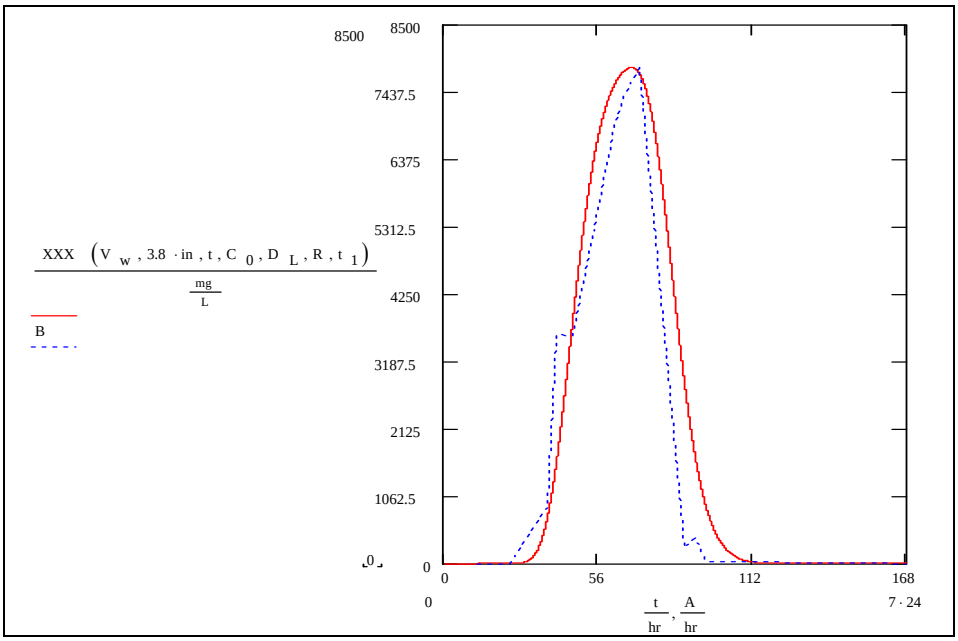

Figure F-5. Retardation and dispersivity calculations for silt column AA with 5% solubility solution of MTBE run for 100 minutes.

$\alpha_L := 0.3 \cdot in \qquad R := 1$

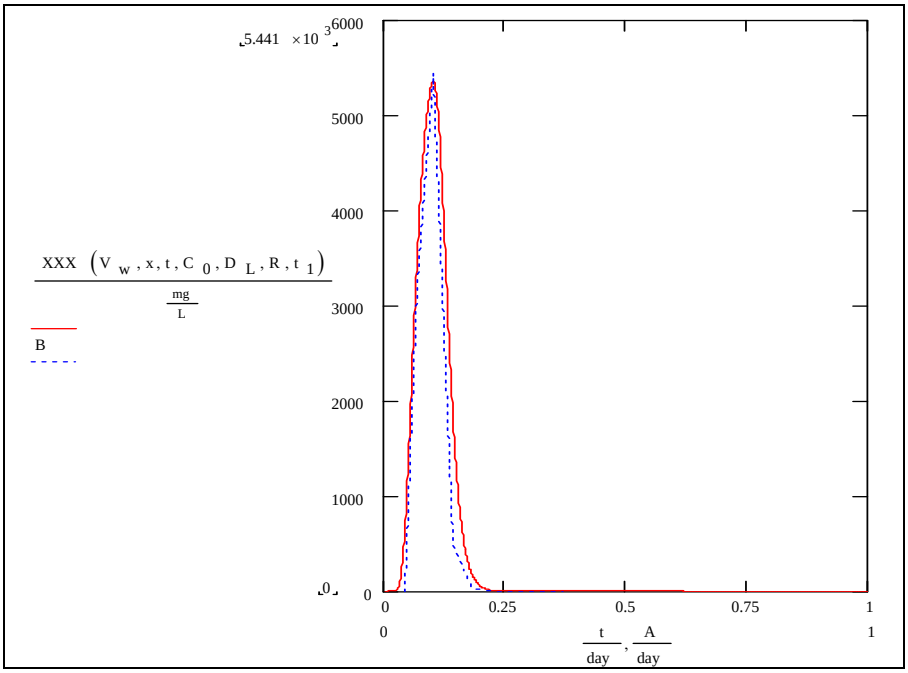

Figure F-6. Retardation and dispersivity calculations for sand column B with 5% solubility solution of MTBE run for 100 minutes.

$\alpha_L := 1.9 \cdot in$ $R := 1.5$

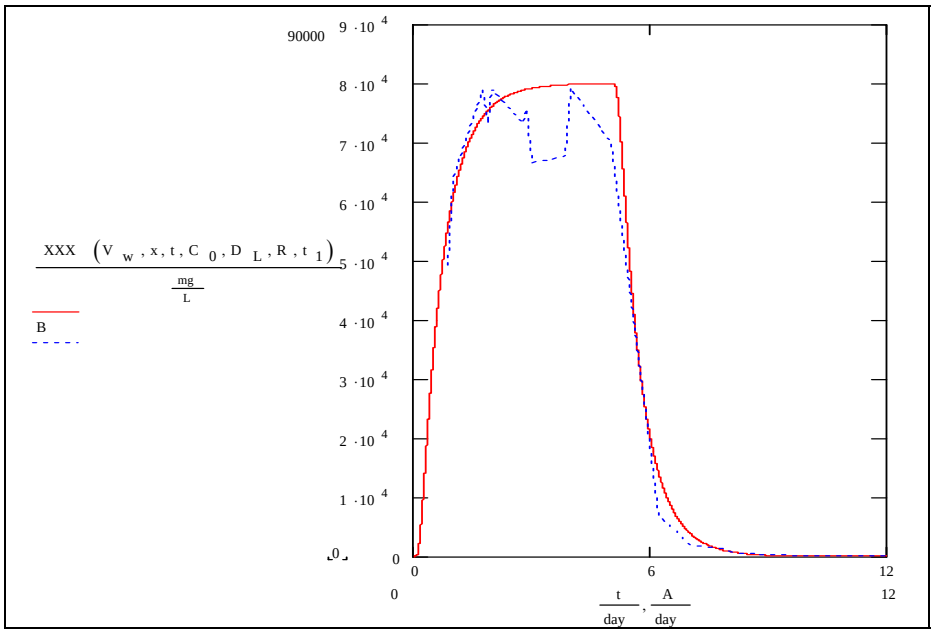

Figure F-7. Retardation and dispersivity calculations for silt column BB with 5% solubility solution of TCE run for 5 days + 30 minutes.

$\alpha_L := 1.7 \cdot in$ $R := 1.7$

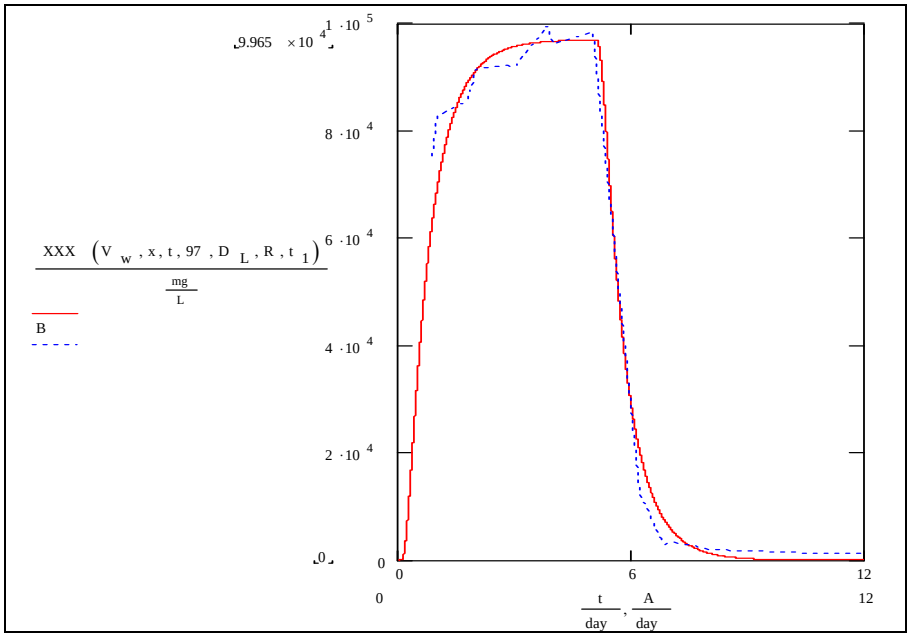

Figure F-8. Retardation and dispersivity calculations for Column C, Sand with a 5% solubility solution of PCE.

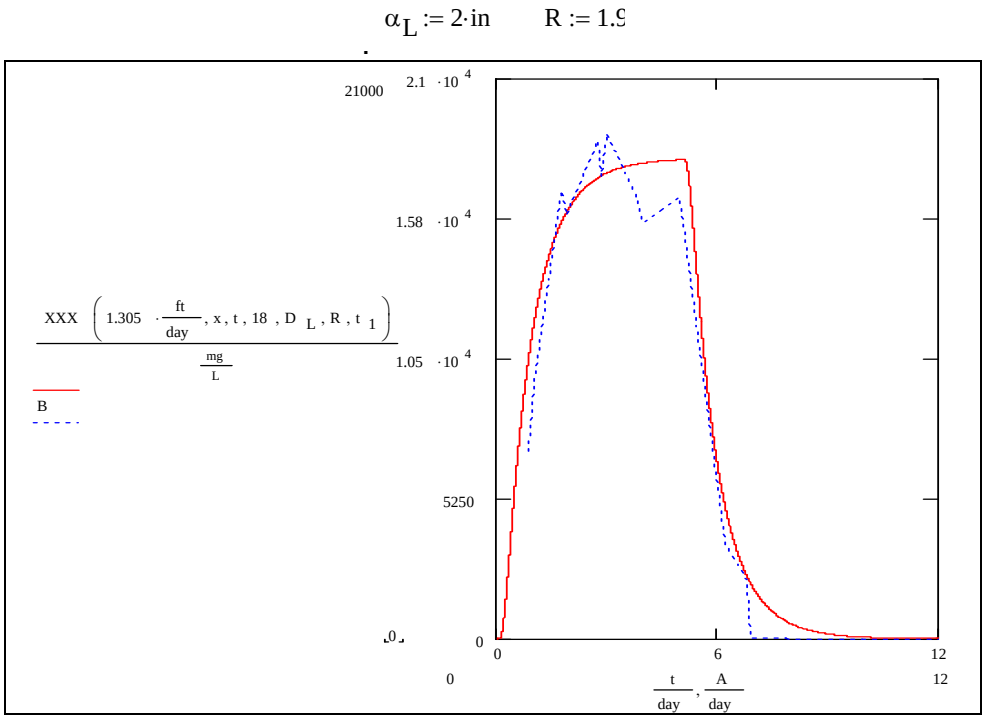

Figure F-9. Retardation and dispersivity calculations for silt column CC with 5% solubility solution of PCE run for 5 days + 30 minutes.

F.1.6 CONCLUSIONS

From the results of these tests, we see that the hydraulic conductivities of the sand samples are nearly three orders of magnitude larger than those of the silt. In the same gradient environment (i.e. the same enclosure) the specific advective flow in the silt areas will be roughly 1/1000th that in the sand layers. The simplification that this value is zero should not affect the results.

The soils themselves are very clean and nearly free of organic matter that, predictably yield very low values for retardation. The values for dispersivity are dependent on the packing method and were well within acceptable limits.

F.1.7 Contaminant Transport Retardation Analysis

In order to calibrate the numerical model based upon the experimental tank studies, values of retardation of the contaminant transport due to soil sorption were obtained. These parameters could not be independently determined based upon tank results alone. A separate study is required to ascertain the retardation properties of the experimental soils.

F.1.8 Hypothesis

The retardation of contaminant transport can be estimated by:

$$R = 1 + (\text{Bulk Density} * K_d)/ \text{Porosity} \qquad (7)$$

where R is the retardation factor and K_d is the sorption coefficient. Porosity can be assumed to be 0.40 for the laboratory soils (F140, F30) and 0.35 for the NASFtW field soils. Bulk density and K_d can be independently determined through batch scale studies that are described below.

F.1.9 Method: Bulk Density Determination

The following procedure was used to obtain the bulk density of each of the four soils used in the AFCEE project at CSM. The procedure was performed in triplicate and was performed on each of the four soils.

Known amounts of soil mass were placed in a vial, and the soil was oven dried for 39 hours at 107°C. After removal from the oven, the soil mass was again recorded. Tap water was added to a replicate vial (empty) until the meniscus reached the same height as the soil in the original vial. The mass of the water was recorded and was assumed to be equivalent to the bulk volume of the soil. Next, the mass of the soil was divided by the volume of the soil to obtain the bulk density. The results are shown in Table F-5.

Table F-3. Summary of results of bulk density study. Values in bold were used as input to the numerical model.

Soil Type	Vial	Mass of Dried Soil (g)	Volume of water to match soil volume (ml)	Bulk Density (kg/L)
F140	a	7.81	5.59	1.40
F140	b	7.12	5.29	1.35
F140	c	7.68	5.55	1.38
F30	a	8.32	5.26	1.58
F30	b	7.79	5.08	1.53
F30	c	7.34	4.76	1.54
NASFtW Mix	a	7.60	5.43	1.40
NASFtW Mix	b	7.31	5.07	1.44
NASFtW Mix	c	7.80	5.46	1.43
NASFtW Silt	a	7.55	5.41	1.40
NASFtW Silt	b	7.17	5.10	1.41
NASFtW Silt	c	7.09	5.10	1.39

F.1.10 Method: Sorption Coefficient Determination

The following methodology was used to perform a 10-day sorption study of aqueous phase 1,1,2-TCA and TCE for each of the four soils that are being utilized in the AFCEE project at the Colorado School of Mines. The protocol is based upon the work of Ball and Roberts (1991). Several deviations from the Ball and Roberts method were made due to equipment and time issues. However, since the goal of this sorption study was to provide a retardation parameter to a numerical model, a close approximation of the actual sorption was satisfactory. Thus, the deviations from Ball and Roberts were deemed to be insignificant in this context.

Known amounts of 1,1,2- TCA and TCE were introduced into a capped glass container with de-aired tap water. The de-aired tap water came from the same source as the experimental tank influent. Next, the container was placed on a shaker table for 10 days to allow for aqueous phase equilibration of the NAPL mixture. During the 10-day equilibration period, several actions were taken to prepare for the ensuing study. Specifically, 75 10-mL centrifuge vials were obtained (15 vials for each of the 4 soils and 15 blanks) and the vial masses were recorded. Then, 12 grams of soil were added to each of the 15 vials for each soil. Next, de-aired tap water was added to the vials with the soil to fully saturate the soil such that the meniscus was approximately 1 mm above top of soil. Finally, the mass and volume of water required for the previous saturating step were recorded and the vials were capped.

After the 10-day equilibration period, 3 samples of the aqueous phase from the 1,1,2-TCA/ TCE solution were taken, and the 1,1,2-TCA and TCE concentrations were measured using the Flame Ionization Detector (FID) on the gas chromatograph (GC). These samples provided a reference point for the expected concentrations in the rest of the vials.

Next, aqueous 1,1,2-TCA/TCE solution and de-aired tap water was added to all 15 vials for each of the four soils such that no headspace remained, and then the vials were capped. The details of each of the 15 vials for one soil type are listed in Table F-6. A range of five concentrations was selected to produce enough data points to fit a sorption coefficient. For each of the five concentrations in the range, sample vials were prepared in triplicate.

Table F-4. The expected TCE and 1,1,2-TCA concentrations added to the NASFtW Silt. The concentrations listed are those that would have been expected if no sorption occurred.

Vial #	TCE Expected Concentration (mg/L)	1,1,2-TCA Expected Concentration (mg/L)
Q1	0.66	2.76
Q2	0.63	2.65
Q3	0.65	2.73
R1	3.00	12.54
R2	2.97	12.45
R3	2.99	12.52
S1	22.98	96.22
S2	27.23	114.02
S3	29.48	123.44
T1	224.68	940.85
T2	232.04	971.67
T3	223.15	934.45

Additionally, de-aired tap water and 1,1,2-TCA/ TCE solution were added to the blanks such that the range of concentrations used in the vials with soil was approximately replicated in triplicate. The blanks were then capped. The vials with soil were placed in a tumbler and tumbled along their longitudinal axis for 10 days at approximately 0.25 rpm. The blanks were not placed in the tumbler. Instead, the blanks were placed on their side to simulate the position of the soil vials during tumbling. This was done to normalize the sorptive effects of the Teflon cap of the vials. Once a period of 10 days had passed, the vials with soil in them were removed from the tumbler. The vials were centrifuged and placed in GC-ready vials.

Using the FID on the GC, aqueous concentrations were obtained. The data were used as input into the following procedure to calculate sorption coefficients.

First, using the data from the blanks, percentage difference between the expected blank concentration based upon the solubility samples and the observed concentrations was determined. This percentage was used to eliminate the effects of the Teflon cap sorption, handling losses, and to allow for calibration issues of the compounds on the GC. Next, the expected soil sample concentrations were multiplied by 1 minus the blank percentage. This step allowed for comparison of the observed concentrations with the expected concentrations such that the only difference should be due to soil sorption.

After the normalization calculations were performed, the observed soil sample concentrations were subtracted from the expected concentrations and multiplied by the bulk density. The result was the sorbed concentration in mg/kg. This data were evaluated to discard any outliers within each group of triplicates. For the remaining data, charts were produced plotting normalized expected aqueous concentration versus observed sorbed concentrations. This was done for each of the four soils and for both 1,1,2-TCA and TCE. The slope of the plots represents the sorption coefficient, K_d.

Sample Plot:

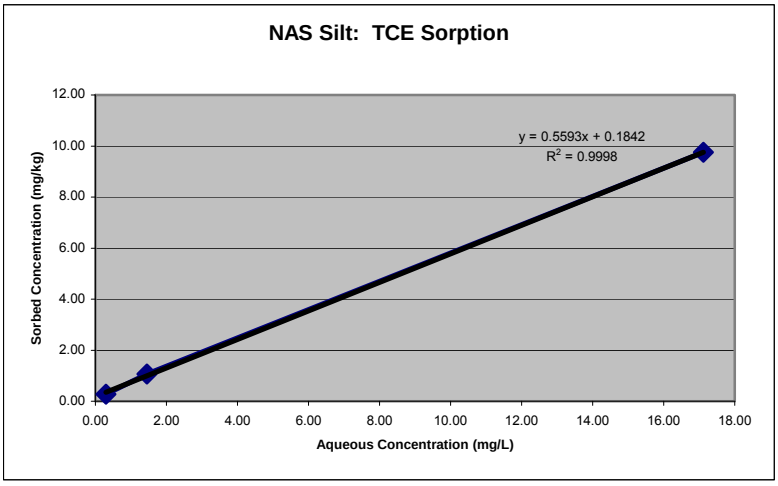

Figure F-10. Sample experimental sorption isotherm.

A linear isotherm was selected. Therefore, K_d values for the soil and contaminant pair were obtained by averaging the K_d from each of the three individual plots provided that the plot represented a linear approximation. If a plot showed a severely non-linear curve, it was discarded. The results of the study are summarized in Table F-7.

Table F-5. Summary of results from 10-day sorption study.

	K_d				Retardation			
	NASFtW Mixed	**NASFtW Silt**	**F140**	**F30**	**NASFtW Mixed**	**NASFtW Silt**	**F140**	**F30**
TCE	0.35	0.6	0.01	0.02	2.43	3.39	1.03	1.08
TCA	0.12	0.19	0.04	0.00	1.49	1.76	1.14	1.00

F.1.11 Conclusions

Based upon these studies, several conclusions were drawn. First, TCE sorbs more strongly to the soils than the 1,1,2-TCA. Second, the laboratory soils (F140, F30) exhibited virtually no sorptive capability. This was expected based upon an assumption that little to no organic carbon existed in these soils. Third, the

NASFtW field soils exhibited stronger sorptive capabilities than the laboratory soils with the NAS Silt being more sorptive than the NASFtW Mixed. This was expected because the NAS Mixed included a sand fraction that was not present in the NASFtW Silt.

BORING LOGS

The soils described in Section F-2 were obtained from four soil borings drilled at FEW. The borings were located at the site of a field demonstration project for a pilot-scale electrolytic barrier at Plume C. The location of the demonstration project is shown on Figure F-13. Attached to this appendix are geologic logs for each of the soil borings.

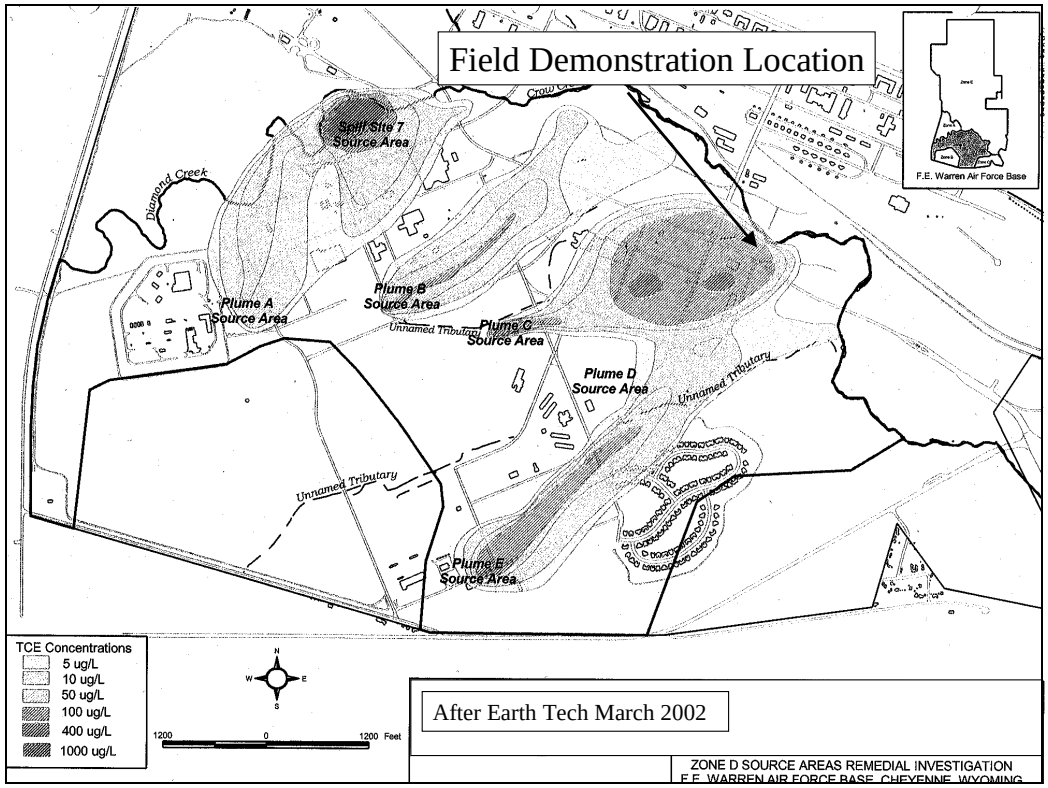

Figure F-11. Location of Electrolytic Barrier Field Demonstration Project at FEW.

Colorado State University **Soil Boring**

Dept of Chemical Engineering

Project Number 532339			**Boring No.** ESTCP #1			Sheet 1 of 1
Project ESTCP e-barrier Demo			**Location** North Lobe Plume C			**Elevation**
Driller Drilling Engineers			**Drilling Equipment** Hollow Stem, Auger - Contiunuous Sampler			
Water Level~10ft bgs		**Start** 10/02/01	**Finish** 10/02/01		**Logger** Tom Sale	
Interval	**Rec.**	**Blow Counts**	**OVM** Avg	Max	**Soil Description** - Soil, Grain size distrib, Mineralogy, Cementation, Color	**Well Completion**
0			0.2	0.2	**Top Soil** - Well sorted silt w/fine sand (sparse pebbles), strong CO3, poorly cemented, black w/roots	
1			0.4	0.4		
2	3 ft Barrel Sample		0.3	0.5		
3			-	-		
4			0.3	0.6	**Silt** - Moderately sorted silt w/fine sand-clay, strong CO3 minor muscovite, Poorly cemented, Black w/ white specs (CO3)	
5			0.4	0.5		
6	4.5 ft Barrel		0.2	0.5	**Silt** - Moderately sorted silt w/fine sand-clay, strong CO3 minor muscovite, Light tan	
7	Sample		0.6	0.6	**Sand** - Poorly sorted fine to medium sand w/silt, Quartz-hornblende-kspar-moderate carbonate, poorly cememted, pink	
8			1.2	2		
9			1.2	1.3	**Silt** - Well sorted silt, weak CO3, Poorly cemented, Brown	
10			1.1	1.3	As above w/ muscovite	
11	4 ft Barrel		1.8	1.9	**Sand** - Well sorted fine sand, Quartz-Muscovite-Biotite-No CO3, Poorly cemmented, Light brown	
12	Sample		-	-		
13			1.8	1.8	As above w/ moderate CO3	
14			-	-		
15			1	1.5	**Sand** - Moderately sorted fine to medium sand, Quartz-Kspar muscovite-low CO3, poorly cemented light brown	
16	3.5 ft Barrel					
17	Sample		1	1		
18						
19			1.8	1.8	**Sand** - Moderately sorted medium to coarse sand, Quartz-Kspar muscovite-low CO3, Poorly cemented, Light pink	
20	2.75 ft Barrel		2.2	2.3		
21	Sample					
22						
23	TD= 21.75 ft					

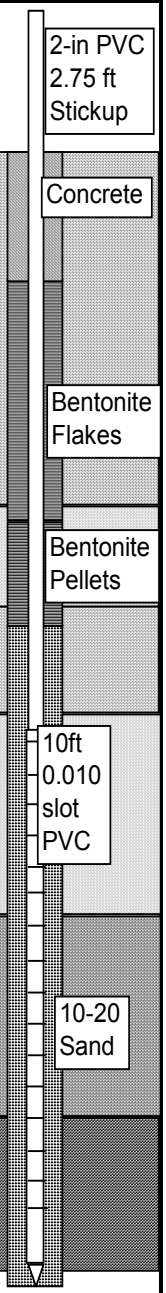

Colorado State University **Soil Boring**

Dept of Chemical Engineering

Project Number 532339				**Boring No.** ESTCP # 2			Sheet 1 of 1
Project ESTCP e-barrier Demo				**Location** North Lobe Plume C			**Elevation**
Driller Drilling Engineers				**Drilling Equipment** Hollow Stem, Auger - Contiunuous Sampler			
Water Level~10ft bgs		**Start** 10/02/01		**Finish** 10/02/01		**Logger** Tom Sale	
Interval	**Rec.**	**Blow Counts**	**OVM** Avg	Max	**Soil Description** - Soil, Grain size distrib, Mineralogy, Cementation, Color		**Well Completion**
3							
2							2-in PVC 2.5 ft Stickup
1							
0			0.6	1.8	**Top Soil** - Well sorted silt w/fine sand (sparse pebbles), strong CO3, poorly cemented, black w/roots		
1			0.5	1.1			Concrete
2	3 ft Barrel Sample						
3			-	-			Bentonite Flakes
4			1	1.1	**Silt** - Moderately sorted silt w/fine sand-clay, strong CO3 minor muscovite, Poorly cemented, Black w/ white specs (CO3)		
5			2.4	5.3	**Sand** - Well sorted fine sand, Quartz-hornblende-Mod CO3, Poorly cemmented, Light brown		
6	4 ft Barrel						Bentonite Pellets
7	Sample		2.5	2.6			
8			2.2	2.4	**Sand** - Moderately sorted fine to medium sand, Quartz-Kspar muscovite-low CO3, poorly cemented light brown		
9			0.2	0.3	As Above moderately cemented		
10			1.5	1.7	**Sand** - Poorly sorted fine to medium sand w/silt, Quartz-Kspar muscovite-low CO3, poorly cemented light brown		
11	4 ft Barrel						10ft 0.010 slot PVC
12	Sample		1	1.3	**Sand** - Moderately sorted fine to medium sand, Quartz-Kspar muscovite-low CO3, poorly cemented light brown		
13							
14			0.4	0.5	As Above - Well Cemented		
15							
16	4.5 ft Barrel		0.2	0.7			
17	Sample		1	1.5	**Sand** - Moderately sorted medium to coarse sand, Quartz-Kspar muscovite-low CO3, Poorly cemented, Light pink		10-20 Sand
			0.1	0.3	**Silt** - Well sorted silt, weak CO3, moderately cemented, Brown		
18			1.9	2	**Sand** - Moderately sorted fine to medium sand, Quartz-Kspar-low CO3, poorly cemented light brown		
19	2 ft Split	14-20-50	0.8	1	**Sand** - Moderately sorted medium to coarse sand, Quartz-Kspar muscovite-low CO3, Poorly cemented, Light pink		
20	Spoon	Lst = 3.5"					
21	TD= 20.5 ft						
22							
23							

Colorado State University **Soil Boring**

Dept of Chemical Engineering

Project Number 532339	**Boring No.** ESTCP # 3		Sheet 1 of 1
Project ESTCP e-barrier Demo	**Location** North Lobe Plume C		**Elevation**
Driller Drilling Engineers	**Drilling Equipment** Hollow Stem, Auger - Contiunuous Sampler		
Water Level~10ft bgs	**Start** 10/03/01	**Finish** 10/03/01	**Logger** Tom Sale

Interval	Rec.	Blow Counts	OVM Avg	OVM Max	Soil Description - Soil, Grain size distrib, Mineralogy, Cementation, Color
0	3 ft Barrel Sample		0.2	0.3	**Top Soil** - Well sorted silt w/fine sand (sparse pebbles), strong CO3, poorly cemented, black w/roots
1			0.3	0.52	
4	4 ft Barrel Sample		0.4	0.4	**Sand** - Poorly sorted fine to coarse sand w/silt, Quartz-hornblende-kspar-moderate carbonate, poorly cememted, pink
6			0.7	0.9	**Sand** - Well sorted fine sand, Quartz-Muscovite-Biotite-No CO3, Poorly cemmented, Light brown
8			1.1	1.2	
9	4 ft Barrel Sample		1.8	2.6	
11			1.4	1.5	
12			1	1.3	
13			1.1	1.4	**Sand** - Moderately sorted medium to coarse sand, Quartz-Kspar
14			1.1	1.5	-low CO3, Well cemented, Pink
16	5 ft Barrel Sample		0.8	1	
17			1.3	1.5	**Sand** - Moderately sorted fine to medium sand, Quartz-Kspar muscovite-low CO3, moderately cemented, Pink
18			2.4	2.5	**Sand** - Moderately sorted fine to medium sand, Quartz-Kspar muscovite-low CO3, poorly cemented light brown
19	2 ft Split Spoon	22-30-50 Last =5"	1.3	1.4	
21	TD= 20.5 ft				

Well Completion

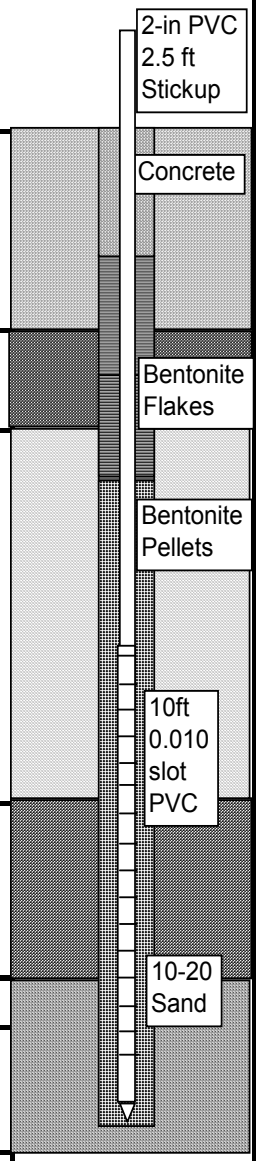

Colorado State University **Soil Boring**

Dept of Chemical Engineering

Project Number 532339			**Boring No.** ESTCP # 4			Sheet 1 of 1
Project ESTCP e-barrier Demo			**Location** North Lobe Plume C			**Elevation**
Driller Drilling Engineers			**Drilling Equipment** Hollow Stem, Auger - Contiunuous Sampler			
Water Level~10ft bgs		**Start** 10/02/01	**Finish** 10/02/01		**Logger** Tom Sale	
Interval	**Rec.**	**Blow Counts**	**OVM** Avg	Max	**Soil Description** - Soil, Grain size distrib, Mineralogy, Cementation, Color	**Well Completion**
0	3 ft Barrel Sample		0	0	**Top Soil** - Well sorted silt w/fine sand (sparse pebbles), strong CO3, poorly cemented, black w/roots	
3			0	0	**Silt** - Moderately sorted silt w/fine sand-clay, strong CO3 minor muscovite, Poorly cemented, Black w/ white specs (CO3)	
4	5 ft Barrel Sample		0	1.7	**Silt** - Moderately sorted silt w/fine sand-clay, strong CO3, Light tan	
5			0.2	0.4	**Sand** - Modertely sorted fine to medium sand, Quartz-hornblende-kspar-strong carbonate, poorly cememted, pink	
7			1.5	1.7	**Sand** - Moderately sorted medium to coarse sand, Quartz-Kspar-moderate CO3, Poorly cemented, Light pink	
9	5 ft Barrel Sample		1.2	1.5	**Sand** - Well sorted fine sand, Quartz-Muscovite-Biotite-moderate CO3, Moderately cemented, Light brown	
11			0.8	1	**Silt** - Moderately sorted silt w/fine sand, Moderate CO3, Light tan	
12			1.5	1.9	**Sand** - Moderately sorted fine to medium sand, Quartz-Kspar-low CO3, poorly cemented light brown w/ interbeds of silts,	
13			0.9	1	**Sand** - Well sorted fine sand, Strong CO3, Moderately cemented, Light brown	
14	2 ft Barrel Sample		1.2	1.3		
15			1	1.9	**Sand** - Moderately sorted fine to medium sand, Quartz-Kspar-moderate CO3, poorly cemented, Light brown	
19	2 ft Split Spoon	18-20-38	1	1.1		
21	TD= 20.5 ft					

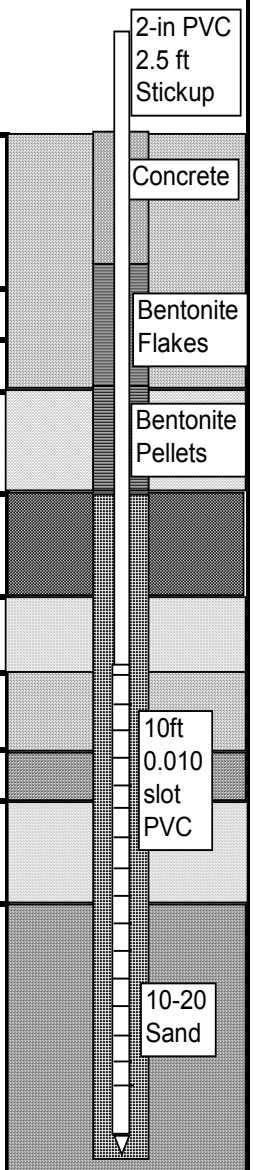

ATTACHMENT

AFP4 DNAPL RECOVERY TECHNICAL PAPER

ENHANCED DNAPL RECOVERY FROM FRACTURED LIMESTONE AFP4, FORT WORTH, TEXAS

Richard B. Wice (rwice@theitgroup.com), John R. Vogeding

(IT Corporation, Pittsburgh, Pennsylvania, USA)

George Walters (United States Air Force, Aeronautical Systems Center

Wright -Patterson Air Force Base, Ohio, USA)

Holmes D. Ficklen (Air Force Center for Environmental Excellence

Brooks Air Force Base, Texas, USA)

ABSTRACT: The U.S. Air Force is recovering dense nonaqueous-phase liquid (DNAPL) from fractured limestone at Air Force Plant No. 4. DNAPL has been detected in the Walnut Formation, a Cretaceous limestone unit with thin interbedded layers of clay. DNAPL is recovered from well W5, which has the maximum measurable DNAPL thickness. DNAPL recovery is conducted utilizing a low-flow bladder pump system. DNAPL is removed at a recovery rate of 3 to 6 gallons per hour, at a frequency of approximately once a week. Groundwater in the well casing above the DNAPL is removed prior to DNAPL pumping. Groundwater removal significantly increases the thickness of recoverable DNAPL in well W5. This is most likely in response to lower hydraulic pressure in the fractures near the well, allowing the DNAPL to flow at a faster rate into the well. A DNAPL recovery program has been implemented by the Air Force.

INTRODUCTION

The U.S. Air Force is removing dense nonaqueous-phase liquids (DNAPL) by direct pumping from the Walnut Formation, a limestone unit at Air Force Plant No. 4 (AFP4) in Fort Worth, Texas. DNAPL recovery from well W5 is enhanced if water in the well casing is bailed off prior to the DNAPL pumping. Removal of the water the day before the DNAPL pumping leads to a significant increase of the recoverable DNAPL thickness in the well. Over time, the recoverable DNAPL thickness in the well has decreased even after water bailing. This may indicate depletion of the free-flowing DNAPL in the Walnut Formation.

SITE DESCRIPTION AND BACKGROUND INFORMATION

AFP4 is a government-owned, contractor-operated, aircraft manufacturing facility located approximately 7 miles west of Fort Worth, Texas. AFP4 occupies 602 acres and is used to manufacture aircraft, aircraft components, missile components, and radar units. AFP4 became operational in 1942 and has been in continuous use up to the present. AFP4 will be in use by the Air Force well into this century for the manufacture of the F-16, F-22 components, and new joint service fighter.

Manufacturing operations at AFP4 have resulted in the generation of various hazardous wastes, including waste oils, fuels, spent solvents, paint residues, and other spent process chemicals. Throughout most of the plant's history, spent chemicals were disposed of in on-site landfills or were burned in fire training areas. Currently, chemical wastes are either disposed off site by a contractor, or treated on site prior to discharge to the sanitary sewer system. AFP4 manufacturing procedures have been modified to replace the wide-scale use of trichloroethene (TCE) with other aqueous cleaning solutions.

The Landfill No. 1 (LF1) and Landfill No. 3 (LF3) areas on the west side of AFP4 were used as waste disposal areas. LF1 covers approximately six acres and was used to dispose of general refuse, construction fill, and potentially hazardous waste. Oils and fuels were also dumped in shallow pits located within LF1 and burned. LF1 was closed in 1966 and the area was graded and paved for a parking area.

In 1983, a portion of LF1, where a former solvent waste disposal pit was located, was excavated down to the top of bedrock. The excavated material, along with several thousand gallons of contaminated groundwater, were sent off site to an approved disposal facility. LF3 was used from 1945 for the disposal of various waste oils and solvents. In 1966 and 1967, fill and rubble were used to grade the LF3 site. Figure 1 shows the location of LF1 and LF3.

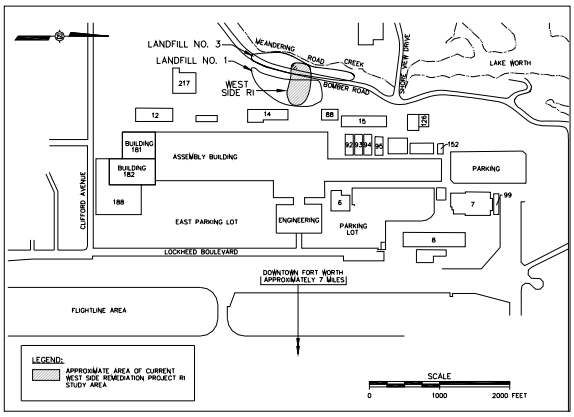

FIGURE 1 LOCATION OF LF1 AND LF3.

SITE CONDITIONS AND INVESTIGATIONS

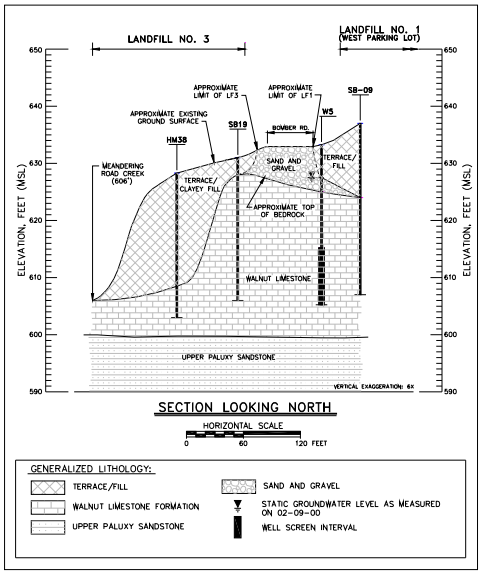

FIGURE 2 CROSS SECTION THROUGH LF1 AND LF3

Volatile organic compounds (VOC), semivolatile organic compounds (SVOC), and fuels are present in groundwater samples collected from monitoring wells screened in the Terrace Alluvium/Fill water table aquifer (Rust Geotech, 1996). The water table aquifer in the LF1 and LF3 areas of AFP4 is composed of fill material, silty clay, and silty sands. In some places, a basal sandy gravel may be present at the top of bedrock. Underlying the Terrace Alluvium and Fill is the Cretaceous Walnut Formation. The Walnut Formation is considered a barrier to vertical migration of contamination. The Walnut Formation is a light gray, 20- to 30-foot-thick fossiliferous limestone with interbedded clay layers. The top of the Walnut is well cemented and appears to prevent the downward migration of groundwater and DNAPL to the underlying Paluxy Formation, a regional aquifer. Figure 2 presents a cross section of the geology on the west side of AFP4.

During a 1996 drilling program to install groundwater monitoring and recovery wells in the deeper Paluxy Formation, water and DNAPL were encountered during the installation of well casings in the Walnut Formation. The Air Force conducted several follow-up site investigation projects from June 1998 through February 2001 to characterize the site (IT, 2001). Figure 3 presents the location of Walnut wells and piezometers and field observations from the Walnut Formation borings in the LF1 and LF3 areas. During the field investigation, water level measurements and well W2 aquifer pumping test drawdown indicated an area of the Walnut with interconnected drainage along fractures or clayey bedding planes. Figure 4 shows the drawdown at 505 minutes into the aquifer test, indicating areas where water and DNAPL are in communication along bedding planes and fractures.

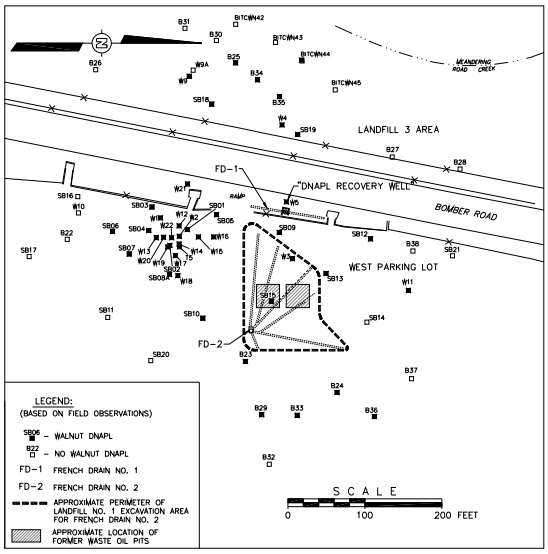

FIGURE 3 WALNUT WELLS AND BORINGS.

DNAPL RECOVERY

During June 2000, the Air Force conducted a series of DNAPL recovery tests in well W5. Well 5 had 11 to 16 feet of DNAPL in the well screen and casing. Well W5 is a 4-inch-diameter stainless steel well with a total depth of 27 feet. The top of the Walnut in well W5 is at a depth of 8 feet below grade. The wire-wrapped stainless steel well screen was installed from 17 to 27 feet below grade.

DNAPL Recovery Procedure. The DNAPL pumping was done using a standard off-the-shelf Clean Environment Equipment (CEE) Model SPT 15 slow purge, bottom filling, bladder pump. The SPT 15 is manufactured with stainless steel and Teflon components. DNAPL recovery testing was done using the following procedure.

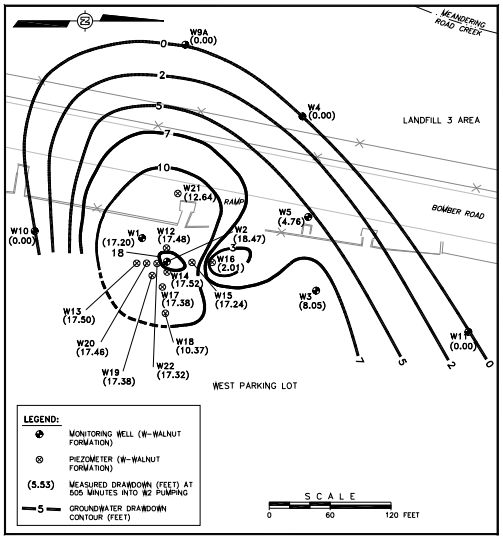

FIGURE 4 WALNUT GROUNDWATER DRAWDOWN AT 505 MINUTES INTO W2 PUMPING.

The bladder pump and controls, and several 5-gallon buckets were set up near W5. For secondary containment, 5-gallon buckets were placed in a plastic mortar mixing box. Static water and DNAPL levels were measured in well W5 (the recovery well) and nearest offset Walnut wells (W3, W4, and W21). The CEE bladder pump inlet was set at a depth of approximately 26 feet below the top of the well casing, approximately 1 foot off the bottom of the well. The bladder pump air lines were connected to the compressor and controller. The product discharge line was set in a 5-gallon bucket and was secured to the inside of the bucket with a clamp or clip.

The bladder pump lift pressure was initially set at 20 pounds per square inch (psi); pump discharge timer at 10 seconds; recharge timer at 10 seconds. Based on pump instructions, 20 psi was the pressure necessary to lift water from the depth at which the pump was set. This pressure also worked well for the DNAPL. Pumping rates were adjusted when there was significant drawdown to maximize DNAPL flow without pumping water. Periodically during the test, the depth to water and DNAPL thickness were measured in wells W5, W3, W4, and W21.

June 6, 2000 Test. During the first test on June 6, 2000, approximately 22 gallons of DNAPL were pumped from the well. The average DNAPL recovery rate was 2 to 3.6 gph. At these flow rates, the water/DNAPL interface was slowly drawn down. The initial bladder pump lift pressure setting was 20 psi, 10-second discharge, and 10-second recharge. As the DNAPL thickness decreased, the flow rate of DNAPL into the bladder pump also decreased. To compensate and maintain optimal pump performance, the pump recharge time interval was increased from 10 seconds to 20 to 30 seconds.

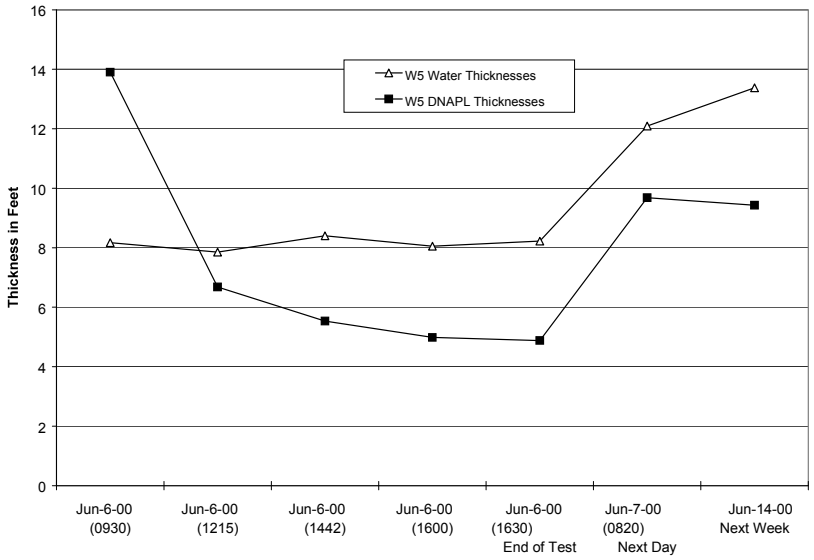

FIGURE 5 W5 WATER AND DNAPL THICKNESSES, JUNE 6, 2000 DNAPL PUMPING.

Figure 5 shows the water and DNAPL thicknesses in well W5 during the recovery test. At the start of the well W5 DNAPL pumping test on June 6, 2000 (0930 hours), the water thickness in the well was 8.17 feet. Approximately 13.9 feet of DNAPL were measured in the well prior to pumping. At the end of the June 6 test, the water thickness was 8.22 feet and the DNAPL thickness was 4.88 feet. On June 7, 2000 (0830 hours), the water thickness recovered to 12.09 feet and the DNAPL thickness recovered to 9.7 feet. As the amount of water in the well increased from June 7 to June 19, 2002, the DNAPL thickness decreased.

During the June 6, 2000 test, water level and depth to DNAPL measurements were collected in Walnut wells W4, W3, and W21. Wells W3 and W4 exhibited water level decreases during the test. Small amounts of DNAPL appeared in W4 and the DNAPL layer increased by 0.37 foot in W21.

June 26 and 27, 2000. On June 26 and 27, 2000, a second DNAPL recovery test was conducted. The setup and procedures for this test were similar to the June 6, 2000 test. The major difference during this test was the pumping of the water out of the well casing prior to DNAPL pumping. The CEE bladder pump was used to pump the water from well W5. The bladder pump inlet was set above the water/DNAPL interface.

As water and DNAPL flow into the well, the DNAPL settles to the well bottom and water rises up the casing into the solid well riser pipe. By reducing the water column in the well by pumping or bailing, the hydrostatic pressure in the Walnut is reduced. The reduction in water pressure leads to an increased capillary pressure at the base of DNAPL pools, allowing for DNAPL migration (Kueper and McWhorter, 1996), in this case, towards and into well W5.

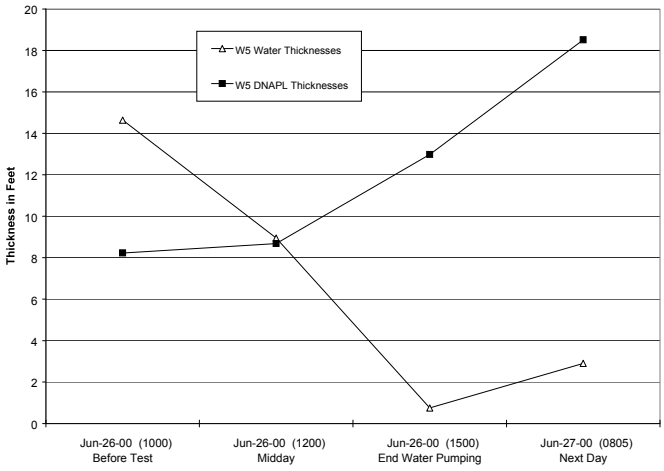

FIGURE 6 W5 WATER AND DNAPL THICKNESSES, JUNE 26, 2000 WATER REMOVAL.

Water above the DNAPL was pumped at a slow rate over a 6-hour period on June 26, 2000. Figure 6 shows how the DNAPL thickness increased from 8 to over 18 feet due to water removal from the well W5 casing. Approximately 15 gallons of water was removed from the well casing. After pumping water out of the casing in well W5, the DNAPL thickness increased over 10 feet. During the well W5 water pumping, water and DNAPL levels were monitored in Walnut wells W4, W3, and W21. Well W3 had a trace of DNAPL after the water was pumped out of well W5. The DNAPL thickness in wells W4 and W21 exhibited a slight increase after water pumping in well W5.

On June 27, 2000, the CEE pump was lowered to near the bottom of well W5 and DNAPL pumping was initiated. During this test, the average CEE pump recovery rate was 6 gph. Approximately 35 gallons of DNAPL were recovered on June 27, 2000.

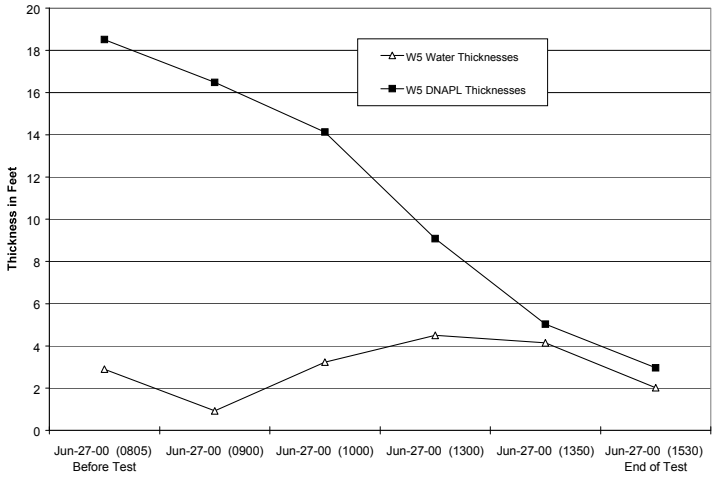

FIGURE 7 W5 WATER AND DNAPL THICKNESSES, JUNE 27, 2000 DNAPL PUMPING.

Figure 7 shows the drop in DNAPL thickness during pumping. Slight changes in DNAPL thickness were observed in offset wells W3, W4, and W21 during the June 26 to 27, 2001 tests. Wells W3 and W21 are located within the drawdown (Figure 4) area created during the well W2 pumping test. Well W4 across Bomber Road was impacted by the DNAPL removal even though it is outside the area drained by the W2 aquifer pumping test. The removal of water or DNAPL from the Walnut appears to have an impact on DNAPL thickness in offset wells.

DNAPL Removal. In July 2001, a DNAPL recovery program was started in well W5. The first step is to bail water out of the well casing. The next day, DNAPL is pumped from the well. Figure 8 presents the water and DNAPL thicknesses before and after water bailing prior to DNAPL recovery pumping. As shown in Figure 8, bailing water off prior to DNAPL recovery increased the DNAPL thickness in well W5. The DNAPL thickness before and after water removal decreased from July to December. After October 31, 2001, DNAPL pumping was suspended for one month to see if recoverable DNAPL thickness would increase under static conditions. The thickness showed a slight increase in early December and then quickly decreased during December 2001. Water thickness increased in the well, indicating possible depletion of the free-flowing DNAPL flowing into well W5 from the Walnut Formation.

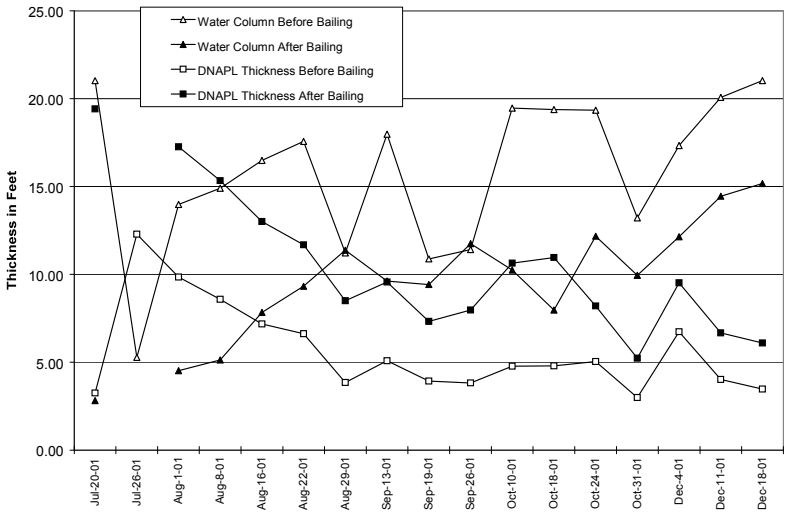

FIGURE 8 W5 WATER AND DNAPL THICKNESSES BEFORE AND AFTER WATER BAILING.

CONCLUSION

Figure 9 shows cumulative recovery of groundwater and DNAPL from well W5. At the end of December 2001, 274 gallons (approximately 3,562 pounds of TCE) of DNAPL and 289 gallons of water were recovered from well W5. The cost to recover each pound of DNAPL ranged from $10 to $20 per pound. Weekly DNAPL recovery was done using simple, off-the-shelf equipment, a field technician for one 8-hour shift per week (to do water removal, DNAPL recovery, and thickness measurements), and disposal of one drum of waste per month by incineration. This compares well to enhanced recovery projects where recovery costs may exceed $1,000 per pound. DNAPL thickness should be measured in offset wells to determine if DNAPL is mobilized during pumping. DNAPL and groundwater removal may cause uncontrolled migration of DNAPL. Initial direct DNAPL removal from the Walnut has resulted in an inexpensive mass removal. Additional enhanced source area removal activities are not anticipated at this time.

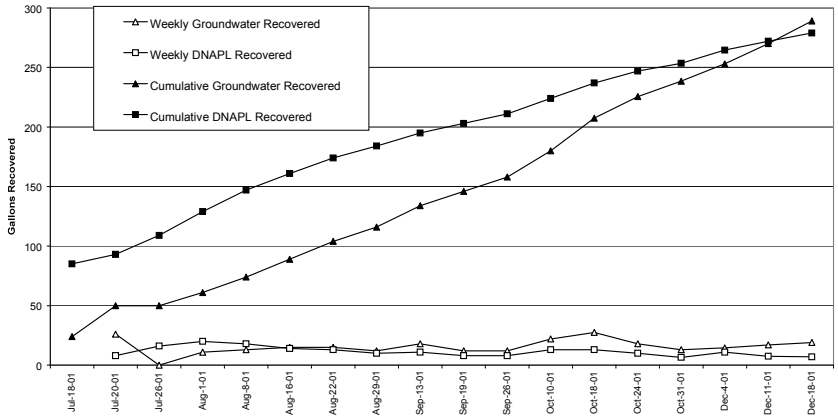

FIGURE 9 GROUNDWATER AND DNAPL RECOVERY FROM WALNUT WELL W5.

ACKNOWLEDGEMENTS

Funding for the DNAPL recovery project was provided by the U.S Air Force Center for Environmental Excellence (AFCEE) under contract No. F41624-00-D-8026, Delivery Order No. 0022. Mr. Randal McDaniel of IT Corporation provided technical and field support for this project.

REFERENCES

IT Corporation. 2001. "West Side Site Investigation Report, Final." Prepared for U.S. Air Force Aeronautical Systems Center, Wright-Paterson Air Force Base, Ohio.

Kueper and McWhorter. 1995. "Physics Covering the Migration of Dense Non-Aqueous Phase Liquids (DNAPL) in Fractured Media." In J. Pankow and J. Cherry (Eds.), Dense Chlorinated Solvents, pp. 337-353.

Rust Geotech. 1996. "Record of Decision, Final." Prepared for U.S. Air Force Aeronautical Systems Center, Wright-Patterson Air Force Base, Ohio.

APPENDIX G
NAS AND FEW CONCEPTUAL MODELS

INTRODUCTION

This appendix presents conceptual models for the NASFtW and FEW sites. The objective of a conceptual model is to integrate all pertinent aspects of the site into a holistic statement that allows for evaluation of processes affecting chemical transport. The conceptual model also provides a basis for assessing the effects of source depletion and plume control. Each conceptual model is a work in progress, and will evolve as additional data are collected.

NASFtW CONCEPTUAL MODEL

The following is a conceptual description of soil and groundwater contamination for an area that includes NASFtW and AFP4 (referred to as the Site). The general setting of the site and historical land use are pertinent, and are discussed below. It is known that multiple release areas existed and that the main contaminants of concern are chlorinated solvents. Owing to standard practices of the era of operation and currently active industrial land use, the exact locations of all release areas are difficult to determine. Relevant aspects of the geologic setting are briefly discussed, including definition of surface and subsurface units and their pertinent features. This is followed by a discussion of site hydrology, which is important in that occurrence and transport of contaminants in groundwater has created the need for corrective action. Where solvents are present as separate phase liquids, they are described as Dense Nonaqueous Phase Liquids (DNAPLs). Mechanisms associated with DNAPL migration and distribution are discussed in Section 2 of the main text. Also discussed are mechanisms controlling chemical diffusion into and out of stagnant zones. These mechanisms are superimposed on the site setting to evaluate the site-specific aspects of contaminant migration.

G.1.1 PHYSICAL SETTING AND LAND USE

The Site is located along the border of two physiographic provinces. The southeastern portion of the Site is situated within the Grand Prairie Section of the Central Lowlands Physiographic Province. The northwest portion of the Site is

within the Western Cross Timbers Physiographic Province. The Site is characterized by rolling topography and broad sloping terrace surfaces. Perennial and intermittent streams drain the area. The main water bodies are Lake Worth to the north, the West Fork Trinity River to the east, and Farmers Branch Creek. The climate is sub-humid with long hot summers and short dry winters. The average annual rainfall is estimated to be 32 in.

G.1.2 BACKGROUND AND PROBLEM

Consistent with aircraft manufacturing and maintenance during the period of operation, chlorinated solvents, mainly trichloroethene (TCE) were used in large quantities. Storage of fresh solvents, degreasing operations, washing (small and large-scale), storage of used solvents, and disposal of used solvents also were common. Areas of known or likely releases include, but are not limited to:

- West Parking Lot Area: a land disposal site west of AFP4
- South AFP4 Area including Building 181: spills and leaks that migrated below the concrete floor

As commonly practiced at other Air Force facilities and aircraft manufacturing facilities, common release areas include industrial sewer systems, deactivated landfills, drum storage areas, and parking areas where waste oil were used to suppress dust. Both land use and the presence of extensive plumes suggest that additional release areas were likely present. Because of the obstructed access in many parts of the facility and the difficulty of locating DNAPLs in the subsurface, the locations of all release areas are uncertain.

G.1.3 GEOLOGIC SETTING

The physical and geologic components important to this conceptual site model are those that affect the hydrology and hydraulics of the Site. The geologic setting of the site basically consists of:

- Fill
- Terrace Alluvium
- Bedrock.

These are discussed below.

G.1.3.1 Fill

The Site contains a large amount of fill and debris. At land surface, the natural soil has been cut, reworked, and used as fill to accommodate buildings, roads, and similar structures. Other fill material has been imported from offsite sources. The thickness of fill materials ranges from zero to about 10 feet.

G.1.3.2 Terrace Alluvium

This geologic unit consists of interbedded gravels, sands, silts, and clays deposited by the Trinity River. The unit is heterogeneous with material variations in both the vertical and horizontal directions. It is generally difficult to correlate individual strata between boreholes. The thickness of the Terrace Alluvium ranges from zero to about 60 feet.

G.1.3.3 Bedrock

The uppermost bedrock units are the Goodland Formation and the Walnut Formation. These generally consist of interbedded limestone siltstone and shale. The limestone can be fractured.

G.1.4 SURFACE WATER

The main surface-water features within and adjacent to the Site include the following:

- Lake Worth: a large manmade reservoir with a surface area of 2500 acres that bounds the site to the north

- West Fork Trinity River: a perennial stream that bounds the site to the east
- Farmers Branch Creek: a perennial stream that flows from west to east across the Site

Groundwater discharges to each of these surface-water bodies.

G.1.5 GROUNDWATER

For this conceptualization, groundwater is considered to occur in two hydrogeologic units. Groundwater occurs under water-table conditions within the Terrace Alluvium. Groundwater also occurs in the underlying limestone bedrock, and is under water-table and/or confined conditions. The heterogeneous (layered) nature of bedrock is interpreted to provide a restriction to vertical flow between Terrace Alluvium and deeper bedrock units. However, the degree of hydraulic communication may be locally enhanced by the presence of bedrock fracturing or erosional features caused by abandoned paleochannels of the ancient West Fork Trinity River.

The occurrence and flow of groundwater within the Terrace Alluvium is generally from west to east. Due to its heterogeneous nature, most flow occurs within the gravel and sand units. The silt and clay units have much lower hydraulic conductivity and can be considered zones of stagnant or nearly stagnant groundwater.

The occurrence and flow of groundwater within the bedrock is generally within fractures. Where fractures are not prevalent or permeable, the bulk hydraulic conductivity is very low, so that groundwater flow is minimal. The presence of siltstone and shale layers in bedrock restricts vertical flow between the Terrace Alluvium and deeper bedrock aquifers. An exception to this occurs in the “window area” below AFP4, where the Terrace Alluvium is in direct contact with the Paluxy Formation, a deeper moderately permeable bedrock unit and primary drinking-water aquifer for this region.

Recharge is attributable to infiltration of rainfall and anthropogenic sources of water (e.g., sewers, potable water-supply lines). It is assumed to be more or less uniformly distributed across the site, with the exception of paved and roof areas where no infiltration occurs. About 10% of the average annual rainfall, or 3 in. per year, recharges the water-bearing zones. This is equivalent to about 100 gpm of recharge per square mile.

Groundwater generally moves from west to east within gravel/sand layers of the Terrace Alluvium. The general east-west flow direction is modified by the horizontal geometry of the sand layers, which may follow old stream channels. The groundwater flow direction may also be modified by the presence of perennial streams.

Groundwater discharge occurs mainly by effluent seepage into perennial streams and other large surface-water bodies. The primary surface-water body that receives groundwater discharge is the West Fork Trinity River that bounds the eastern portion of the Site. Less significant groundwater discharge occurs into Lake Worth and local discharge occurs into Farmers Branch Creek.

Table G-1 presents estimates of average seepage velocity and groundwater discharge from the hydrogeologic units based on estimated hydraulic parameters. These results are based on limited data and should not be viewed as rigorously correct. An important aspect of ongoing investigations is to further characterize the hydraulic parameters presented in Table G-1. Despite the uncertainties in the parameters, the data in Table G-1 provides several useful insights:

- Relatively high flow rates and velocities in sand layers within the Terrace Alluvium

- Low flow rates and velocities within silts and clays of the Terrace Alluvium, and also for unfractured bedrock. Groundwater within these units can be considered essentially stagnant.

- Moderate flow rates, but relatively high velocities in fractured bedrock owing to its low effective porosity

Table G-1. Estimates of Groundwater Velocities and Discharge by Hydrogeologic Unit.

Hydrogeologic Parameter	Terrace Alluvium		Bedrock	
	Sand Layers	Silt/Clay Layers	Fractured	Unfractured
Hydraulic Conductivity (ft/day)	100	0.1	1	0.01
Hydraulic Conductivity (cm/sec)	3.5×10^{-2}	3.5×10^{-5}	3.5×10^{-4}	3.5×10^{-6}
Effective Porosity	0.25	0.25	0.01	0.1
Horizontal Hydraulic Gradient (ft/ft)	0.01	0.01	0.01	0.01
Saturated Thickness (ft)	10	10	50	50
Transmissivity (ft^2/day)	1000	1	5	5
Average Seepage Velocity (ft/day)	4.0	0.004	1.0	0.001
Discharge/ 100 ft of plume width (gal/day)	7480	7.48	374	3.74

G.1.6 CHEMICAL MIGRATION

As discussed in Section 2 of the main text, two mechanisms that can potentially provide chemicals to a dissolved chemical plume are: (1) slow dissolution of DNAPL in the original spill area and (2) diffusion of dissolved compounds from stagnant groundwater zones into zones with active flow. The latter process can occur in the original spill area and also downgradient of this area. In fact, diffusion can be operative in any portion of the plume where, historically, there have been relatively high dissolved concentrations. This implies that currently active chemical sources can exist in areas far removed from the original DNAPL spill site(s).

G.1.6.1 Spill Areas

DNAPL definitely exists in the West Parking Lot Area at AFP4, the site of two former landfills. The immiscible product resides within fractured Walnut Limestone. There currently exists a DNAPL recovery project that extracts DNAPL from a single well. Between June 2000 and December 2002, approximately 470 gallons of chlorinated solvents were extracted. It is apparent, that despite recovery efforts, DNAPL continues to exist below the West Parking Lot, and that this area will continue to operate a chemical source to groundwater. Dissolved chemicals in groundwater may be derived from (1) slow dissolution of the DNAPL present in fractures and (2) diffusion of dissolved compounds from the matrix between fractures into groundwater flowing within the fractures. In subsequent phases of this research project, site data will be evaluated to determine if DNAPL extraction has resulted in a demonstrable decrease in dissolved groundwater concentrations.

DNAPL has not been detected below the South AFP4 Area. It is possible that DNAPL is present, but due to its sparse distribution, has not been encountered during drilling. It is also possible that all DNAPL has been depleted (by dissolution) and that the source is operating by slow diffusion of dissolved constituents from stagnant groundwater zones into zones with active flow. The stagnant zones could include clay/silt layers of the Terrace Alluvium and matrix blocks between fractures in bedrock. It is assumed that active groundwater flow takes place only within sand and gravel layers of the Terrace Alluvium.

The degree to which NASFtW Landfills operate as chemical sources is uncertain, and DNAPL has not been detected in geologic materials within this area. However, the TCE distribution map could be interpreted to indicate that chemicals are being added to a dissolved plume that originates in the South AFP4 Area. If NASFtW Landfills are chemical sources, and if DNAPL is not present, then the mechanism for adding chemicals to groundwater would likely

be the diffusion process with chemical migration from stagnant zones (clay/silt layers) into zones of active flow (sand layers).

G.1.7 NASFTW PRB

The NASFtW PRB is interpreted to be downgradient of any current or past occurrences of DNAPL. Thus, if this area behaves as a chemical source, a likely mechanism may be the diffusion process. The Terrace Alluvium in this area is heterogeneous with sand layers and interbedded silt/clay layers.

The PRB effectively creates a near-zero concentration boundary within the alluvial aquifer that extends across most of the groundwater contaminant plume. Over time, groundwater concentrations downgradient of the PRB should decrease as the area is flushed with non-impacted groundwater (that is, water "created" within the PRB). As shown on Figure G-1, TCE concentrations have decreased (in some cases, dramatically) at wells downgradient of the PRB.

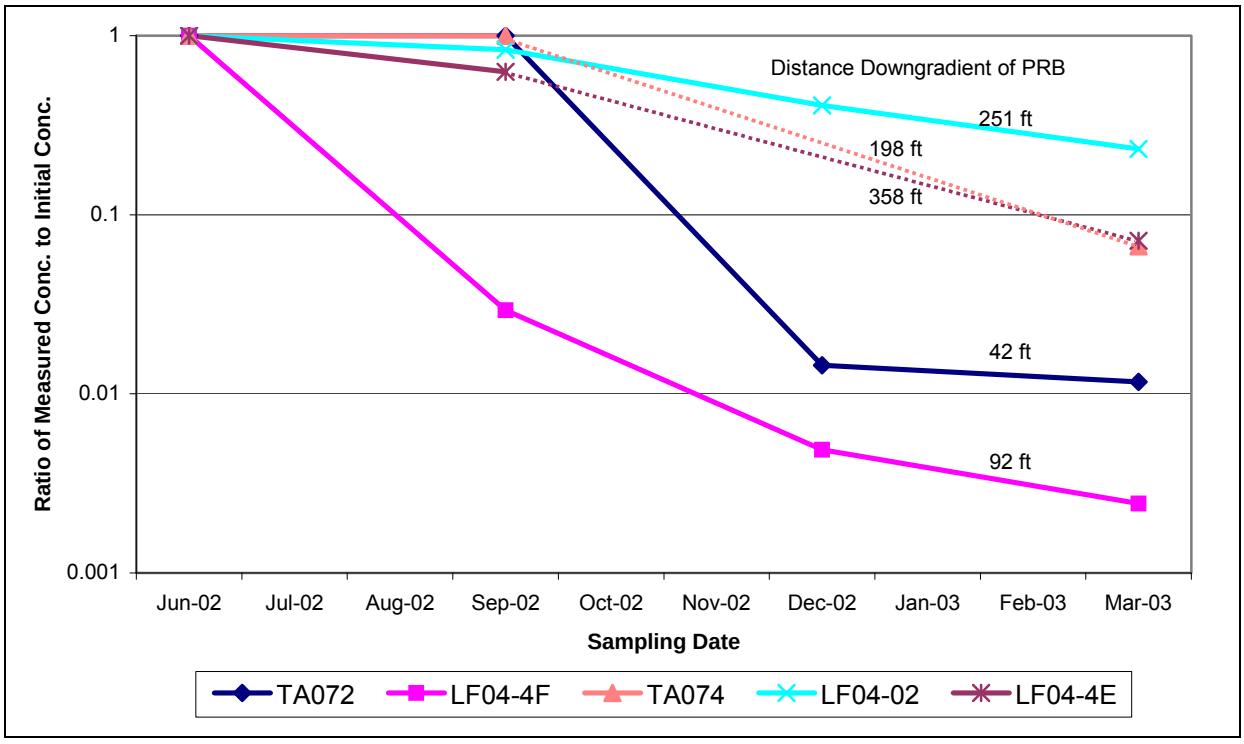

Figure G-1. Relative Concentrations in Selected Wells Downgradient of NAS PRB.

Since the PRB was recently installed, the decreases are more pronounced at wells relatively close to the PRB. Two of these wells, located within 100 feet of the PRB, have experienced a two order-of-magnitude decrease in TCE concentration and appear to be approaching plateau values. Three wells located further from the PRB have decreasing TCE concentrations but have not yet exhibited plateau behavior. More complete evaluation of temporal concentrations in these wells will require future chemical sampling. The plateau behavior would not be predicted if chemical migration included only advection, dispersion, and adsorption. It is interpreted that the lower stabilized concentrations result from diffusive chemical flux from stagnant zones (silt/clay layers) into groundwater migrating within active flow zones (sand layers). This diffusion process supplies chemicals into groundwater that was previously non-impacted; that is, after passing through the PRB. The diffusive process therefore behaves as a chemical source capable of re-contaminating clean groundwater. This source behavior may occur far from the chemical spill sites that originally created the chemical plume.

FEW CONCEPTUAL MODEL

The following is a conceptual description of soil and groundwater contamination for an area known as Spill Site 7 (Site), which is located within F. E. Warren (FEW) Air Force Base. The general setting of the site and historical land use are pertinent, and are discussed below. It is known that multiple release areas existed and that the main contaminants of concern are chlorinated solvents. Owing to standard practices of the era of operation and currently active industrial land use, the exact locations of all release areas are difficult to determine. Relevant aspects of the geologic setting are briefly discussed, including definition of surface and subsurface units and their pertinent features. This is followed by a discussion of site hydrology, which is important in that the occurrence and transport of contaminants in groundwater has created the need for corrective action. Where solvents are present as separate phase liquids they are described as Dense Nonaqueous Phase Liquids (DNAPLs). Mechanisms associated with

DNAPL migration and distribution are discussed in Section 2 of the main text. Also discussed are mechanisms controlling chemical diffusion into and out of stagnant zones. These mechanisms are superimposed on the site setting to evaluate the site-specific aspects of contaminant migration.

G.1.8 PHYSICAL SETTING

FEW is located in the western portion of the High Plains section of the Great Plains physiographic province. The general area characterized as a relatively uniform flat plain that slopes to the east with a gradient of several tens of feet per mile. Perennial and intermittent streams drain the area. The main water body at the Site is Diamond Creek, a perennial stream that flows north along the western site boundary and then east-southeast along the north boundary. The climate is semiarid with moderately warm summers and cold winters. The average annual rainfall is estimated to be 15.3 in. Rainfall generally occurs as thunderstorms during the summer months. Average snowfall is 56 in. per year with greatest accumulations in late winter and early spring.

G.1.9 BACKGROUND AND PROBLEM

Activities conducted at FEW included industrial operations and aircraft maintenance. Consistent with aircraft operations, chlorinated solvents, mainly trichloroethene (TCE) were used in large quantities. Storage of fresh solvents, degreasing operations, washing (small and large-scale), storage of used solvents, and disposal of used solvents also were common. One area of release is referred to as Spill Site 7, an apparent chemical disposal site. Two other chemical release sites are identified upgradient of SS-7 (Spill Site 4 and an area near well MW-146). These upgradient sites appear to provide less chemical mass to the groundwater system compared to SS-7.

G.1.10 GEOLOGIC SETTING

The physical and geologic components important to this conceptual site model are those that affect the hydrology and hydraulics of the Site. The geologic setting of the site basically consists of:

- Alluvium
- Ogallala Formation

These are discussed below.

G.1.10.1 Alluvium

Alluvium, the upper-most geologic unit, is composed of alternating layers of clay, silt, and sand. Individual layers have variable thickness and are laterally discontinuous. It is generally difficult to correlate individual layers between boreholes. Gravel and occasional boulders also exist within the unit. Some of the sand and silt layers are weakly to moderately cemented with calcium carbonate. The thickness of Alluvium varies with location, but is generally less than 70 feet.

G.1.10.2 Ogallala Formation

Underlying Alluvium is the Tertiary age Ogallala Formation which has an estimated thickness of about 300 feet. This fluvial (and locally eolian) deposit consists of a heterogeneous mixture of clay, silt, poorly sorted sand, and gravel layers.

G.1.11 SURFACE WATER

The main surface-water feature at the Site is Diamond Creek, which is a perennial stream located west and north of SS-7. Contaminated groundwater discharges to the creek as indicated by detections of TCE in the surface water.

G.1.12 GROUNDWATER

For this conceptualization, groundwater is considered to occur in two hydrogeologic units. Groundwater occurs under water-table conditions within Alluvium. Groundwater also occurs in the underlying Ogallala Formation under unconfined and locally semi-confined conditions. There are no pervasive low permeability confining units between the Alluvium and the Ogalalla. Thus, it is assumed that the two hydrogeologic units are hydraulically connected.

Within the Alluvium, groundwater flow is generally to the north and northeast. Due to its heterogeneous nature, most flow occurs within the gravel and sand units. The silt and clay units have much lower hydraulic conductivity and can be considered zones of stagnant or nearly stagnant groundwater.

The occurrence and flow of groundwater within the Ogallala is not specifically addressed in this conceptual model because it does not appear to contain contaminated groundwater and or significantly to affect flow in the Alluvium.

Recharge is attributed to infiltration of rainfall, and is assumed to be more or less uniformly distributed across the site. About 10% of the average annual rainfall, or 1.5 in. per year, recharges the water-bearing zones. This is equivalent to about 50 gpm of recharge per square mile.

Groundwater generally moves from south to north within gravel/sand layers of the Alluvium. The general flow direction is modified by the horizontal geometry of the sand layers, which may follow old stream channels. The groundwater flow direction may also be modified by the location of Diamond Creek.

Groundwater discharge occurs mainly by effluent seepage into perennial streams. The primary surface water body that receives groundwater discharge is Diamond Creek, which bounds the north and western portion of the Site. Because contaminated groundwater has been identified north of the creek, it appears that some groundwater flows under the creek without discharging.

Table G-2 presents estimates of average seepage velocity and groundwater discharge from the hydrogeologic units based on estimated hydraulic parameters. These results are based on limited data and should not be viewed as rigorously correct. An important aspect of ongoing investigations is to further characterize the hydraulic parameters presented in Table G-2. Despite the uncertainties in the parameters, the information in Table G-2 provides useful insights:

- Relatively high flow rates and velocities in sand layers within the Alluvium
- Low flow rates and velocities within silts and clays. Groundwater within these units can be considered essentially stagnant.

Table G-2. Estimates of Groundwater Velocities and Discharge by Geologic Material Type.

Hydrogeologic Parameter	Terrace Alluvium	
	Sand Layers	Silt/Clay Layers
Hydraulic Conductivity (ft/day)	100	0.1
Hydraulic Conductivity (cm/sec)	3.5×10^{-2}	3.5×10^{-5}
Effective Porosity	0.25	0.25
Horizontal Hydraulic Gradient (ft/ft)	0.015	0.015
Saturated Thickness (ft)	10	10
Transmissivity (ft^2/day)	1,000	1
Average Seepage Velocity (ft/day)	6.0	0.006
Discharge/ 100 ft of plume width (gal/day)	11,200	11.2

G.1.13 CHEMICAL MIGRATION

As discussed in Section 2 of the main text, two mechanisms that can potentially provide chemicals to a dissolved chemical plume are: (1) slow dissolution of

DNAPL in the original spill area and (2) diffusion of dissolved compounds from stagnant groundwater zones into zones with active flow. The latter process can occur in the original spill area and also downgradient of this area. In fact, diffusion can be operative in any portion of the plume where, historically, there have been relatively high dissolved concentrations. This implies that currently active chemical sources can exist in areas far removed from the original DNAPL spill site(s).

G.1.13.1 Spill Areas

DNAPL has not been identified at SS-7 or at any other potential chemical source areas that could affect the contaminant plume. It is possible that DNAPL is present, but due to its sparse distribution, has not been encountered during drilling. It is also possible that all DNAPL has been depleted (by dissolution) and that the source areas are operating by slow diffusion of dissolved constituents from stagnant groundwater zones into zones with active flow. The stagnant zones likely include clay/silt layers. It is assumed that active groundwater flow takes place only within sand and gravel layers.

G.1.14 FEW PRB

The FEW PRB is interpreted to be downgradient of any current or past occurrences of DNAPL. Thus, if this area behaves as a chemical source, a likely mechanism may be the diffusion process. As discussed previously, the alluvium in this area is heterogeneous with sand layers and interbedded silt/clay layers.

The PRB effectively creates a near-zero concentration boundary within the alluvial aquifer that extends across most of the groundwater contaminant plume. However, because the PRB only penetrates the upper portion (15 feet) of the saturated alluvium, there is some groundwater that flows under the PRB and is not subject to in situ treatment. Over time, groundwater concentrations downgradient of the PRB should decrease as the area is flushed with non-impacted groundwater (that is, “created” within the PRB). TCE

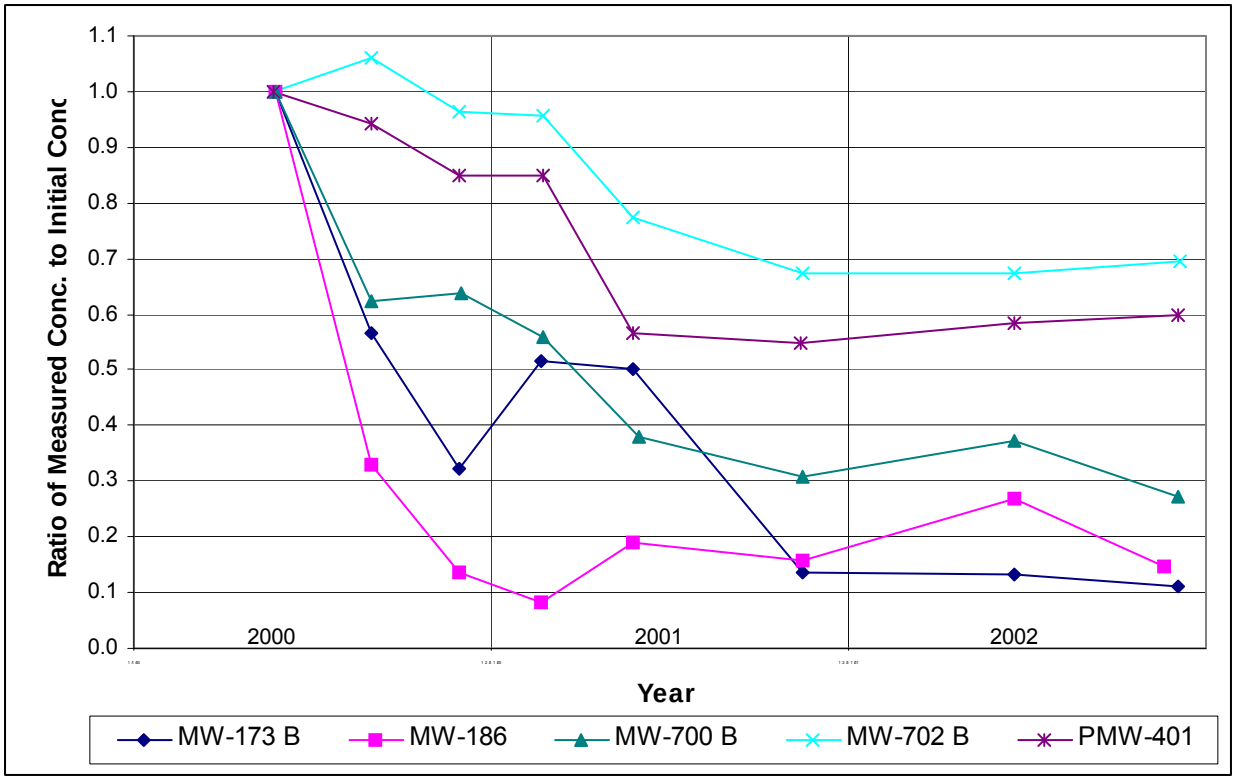

Figure G-2. Relative Concentrations in Selected Wells Downgradient of FEW PRB.

concentrations have decreased in most monitoring wells located downgradient of the PRB. A common behavior was for TCE concentrations to decrease by 30 to 90 percent after the PRB was installed. However, there was also a tendency for the concentrations to plateau and become somewhat stable at a lower value. This is shown on Figure H-2 for selected downgradient wells.

It is interpreted that the lower stabilized concentrations result from diffusive chemical flux from stagnant zones (silt/clay layers) into groundwater migrating within active flow zones (sand layers). This diffusion process supplies chemicals into groundwater that was previously not impacted; that is, after passing through the PRB. The diffusive process therefore behaves as a chemical source capable of ***re-contaminating*** clean groundwater. This source behavior may occur far from the chemical spill sites that originally created the chemical plume.

It is possible that the plateau behavior may also result in part from affected groundwater that flows under the PRB and thus bypasses the treatment system. Site data indicate that deeper groundwater is generally uncontaminated or has relatively low chemical concentrations. While by-pass may be a factor contributing to downstream chemical concentrations, it does not appear to be the sole process that is operating.